



Phytoplankton and turbulence at selected scales

by

Rudi Herbert Regel

Limnology Group
School of Earth and Environmental Sciences
The University of Adelaide

A thesis submitted to The University of Adelaide
for the degree of Doctor of Philosophy

February 2003



CRC for Water Quality
and Treatment

“There is no life without water, and there is no life in water without turbulence in water”

Ambühl (1960)

“One does not discover new lands without consenting to lose sight of the shore for a very long time”

André Gide
Do it! (1992)

Contents

Contents.....	iii
List of figures.....	ix
List of tables.....	xiii
Summary.....	xiv
Declaration.....	xvi
Acknowledgements.....	xvii
Chapter 1. Introduction.....	1
1.1 A question of scale.....	1
1.2 Limnological progress.....	3
1.3 Biological techniques.....	4
1.3.1 Flow cytometry and fluorescent probes.....	4
1.3.2 Fluorometry, photosynthesis and chlorophyll fluorescence.....	6
1.4 Turbulence.....	8
1.4.1 Turbulence theory and energy spectrum.....	9
1.4.2 Turbulence generation.....	11
1.4.3 Turbulence length scales.....	11
1.5 Phytoplankton- turbulence relations.....	14
1.5.1 Large-scale turbulence, phytoplankton entrainment- photosynthesis.....	14
1.5.2 Small-scale turbulence and phytoplankton.....	17
1.6 Cyanobacteria, water quality and artificial mixing.....	20
1.7 Lake management and project study sites.....	22
Chapter 2. Testing the procedural protocols.....	34
2.1 Introduction.....	34
2.1.1 Fluorescent probes and flow cytometry.....	35
2.1.2 Fluorometry and variable fluorescence.....	37
2.1.3 Objectives.....	37
2.2 Experimental designs and methods.....	38
2.2.1 Phytoplankton cultures.....	38
2.2.2 Probe assay development.....	39
2.2.2.1 Flow cytometry.....	39
2.2.2.2 Fluorescein diacetate staining and esterase activity.....	39
2.2.2.3 Sytox staining and cell viability.....	40
2.2.3 Microscopy.....	41
2.2.4 Testing probe assays.....	41
2.2.4.1 Estimation of the number of viable & nonviable cells in a population....	41
2.2.4.2 Detection of nutrient limitation and repletion.....	42
2.2.4.3 Detection of copper toxicity.....	42
2.2.5 PAM fluorometry and phytoplankton photo-physiology.....	43
2.2.5.1 Photochemical quenching.....	43
2.2.5.2 Maximum quantum yield of photosystem 2.....	45
2.2.5.3 Effective absorption cross-section.....	46

2.2.5.4	Photosynthetic rate.....	46
2.2.6	Influence of light intensity and nutrients on photo-physiology.....	47
2.2.7	F_v/F_m depression and recovery kinetics.....	47
2.2.8	Measurement and modeling of photosynthesis in a natural population.....	48
2.2.9	Statistical analysis.....	50
2.3	Results.....	51
2.3.1	Optimisation of FDA staining.....	51
2.3.2	Optimisation of Sytox staining.....	52
2.3.3	Estimation of the number of viable & nonviable cells in a population.....	53
2.3.4	Detection of nutrient limitation and repletion.....	53
2.3.5	Detection of copper toxicity.....	55
2.3.6	Influence of light intensity and nutrients on photo-physiology.....	56
2.3.7	F_v/F_m depression and recovery kinetics.....	57
2.3.8	Measurement and modeling of photosynthesis in a natural population.....	58
2.4	Discussion.....	59
2.4.1	Fluorescent probes and flow cytometry.....	59
2.4.2	Fluorometry.....	62
2.4.3	Conclusions.....	66
 Chapter 3. Vertical migration, entrainment and photosynthesis of the freshwater dinoflagellates, <i>Peridinium cinctum</i> in a shallow urban lake.....		87
3.1	Introduction.....	87
3.2	Methods.....	89
3.2.1	Site description.....	89
3.2.2	Field experiment.....	89
3.2.2.1	Shear velocity, <i>P. cinctum</i> swimming velocity and entrainment.....	90
3.2.2.2	F_v/F_m photo-physiology measurements.....	91
3.2.2.3	Integral photosynthesis.....	92
3.2.3	Laboratory experiments.....	92
3.2.4	Photo-physiology measurements.....	93
3.3	Results.....	94
3.3.1	Field experiment.....	94
3.3.1.1	Meteorology and thermal stratification.....	94
3.3.1.2	Entrainment versus disentrainment.....	95
3.3.1.2.1	Chlorophyll fluorescence.....	95
3.3.1.2.2	<i>Peridinium cinctum</i> cell number.....	96
3.3.1.2.3	Maximum quantum yield, F_v/F_m	96
3.3.1.2.3.1	Bottle F_v/F_m	97
3.3.1.2.3.2	Lake F_v/F_m	97
3.3.1.2.3.3	Ratios of bottle to lake F_v/F_m	98
3.3.1.3	Entrainment criterion.....	98
3.3.1.4	Depth-time integral of photosynthesis.....	99
3.3.2	Laboratory experiments.....	99
3.4	Discussion.....	100

Chapter 4. Changes in the photochemistry of <i>M. aeruginosa</i> in response to light and mixing.....	116
4.1 Introduction.....	116
4.2 Methods.....	119
4.2.1 Field measurements.....	119
4.2.1.1 Field site description.....	119
4.2.1.2 Evidence of photoinhibition in natural populations.....	119
4.2.1.3 Measurement of maximum quantum yield, F_v/F_m	120
4.2.1.4 Meteorological station instrumentation.....	120
4.2.1.5 Calculating the rate of inhibition and recovery.....	121
4.2.2 Modeling.....	121
4.2.2.1 Model validation.....	121
4.2.2.2 Modeling photoinhibition.....	122
4.2.2.2.1 Scenario 1 A stratified water body with no motion and no vertical migration.....	122
4.2.2.2.2 Scenario 2 A cell circulating within the surface mixed layer.....	122
4.2.2.2.3 Scenario 3 A nocturnally mixed water column, which stratifies at dawn.....	123
4.2.2.2.4 Scenario 4 Langmuir circulation.....	123
4.2.2.2.5 Scenario 5 A simulation of turbulent water motion.....	124
4.3 Results.....	125
4.3.1 Field experiments.....	125
4.3.1.1 Evidence of depressed F_v/F_m in natural populations.....	125
4.3.1.2 Entrainment of <i>M. aeruginosa</i> colonies.....	125
4.3.1.3 The rate of depression and recovery of F_v/F_m in <i>M. aeruginosa</i>	126
4.3.2 Modeling.....	128
4.3.2.1 Model validation.....	128
4.3.2.2 Modeling photoinhibition.....	129
4.3.2.2.1 Scenario 1 A stratified water body with no motion.....	129
4.3.2.2.2 Scenario 2 A cell circulating within the surface mixed layer.....	129
4.3.2.2.3 Scenario 3 A nocturnally mixed water column.....	130
4.3.2.2.4 Scenario 4 Langmuir circulation.....	130
4.3.2.2.5 Scenario 5 A simulation of turbulent water motion.....	132
4.4 Discussion.....	133
4.4.1 Evidence of depressed F_v/F_m in natural populations.....	133
4.4.2 Simulation of photoinhibition in natural populations.....	133
4.4.3 Entrainment of <i>M. aeruginosa</i> colonies.....	134
4.4.4 Size distribution of colonies and its impact on photoinhibition.....	135
4.4.5 The scale of light penetration, turbulent transport and photoinhibition.....	136
 Chapter 5. The measurement of flow and small-scale turbulence around artificial mixing systems in a deep reservoir and shallow lake.....	 152
5.1 Introduction.....	152
5.2 Materials and methods.....	156
5.2.1 Field sites and artificial mixing systems.....	156
5.2.2 Myponga Reservoir experiments.....	156
5.2.2.1 Surface mixer flow characteristics.....	156

5.2.2.2	Phytoplankton transport through draft tube.....	157
5.2.2.3	Phytoplankton adjacent to and 70 m from surface mixer.....	157
5.2.2.4	Phytoplankton and flow cytometry analysis.....	158
5.2.2.4.1	Metabolic activity and FDA staining technique.....	158
5.2.2.4.2	Cell viability and Sytox staining technique.....	159
5.2.2.4.3	Flow cytometry.....	159
5.2.2.4.4	Statistical analysis of phytoplankton measurements.....	159
5.2.3	Torrens Lake experiments.....	160
5.2.3.1	Bubble plume aerator.....	160
5.2.3.2	Submerged aspirator and high volume surface aerator.....	160
5.2.3.3	Wind versus mixer generated circulation.....	161
5.2.4	Flow velocity and turbulence measurements and analysis.....	161
5.2.5	Wind generated turbulent kinetic energy dissipation rates.....	163
5.3	Results.....	164
5.3.1	Turbulence analysis.....	164
5.3.2	Myponga Reservoir experiments.....	165
5.3.2.1	Surface mixer flow characteristics.....	165
5.3.2.1.1	Meteorological conditions.....	165
5.3.2.1.2	Flow velocities below the mixer.....	165
5.3.2.1.3	Turbulent intensity, shear velocity and turbulent kinetic energy dissipation.....	165
5.3.2.2	Phytoplankton transport through mixer and draft tube.....	166
5.3.2.3	Phytoplankton adjacent to and 70 m from surface mixer.....	166
5.3.3	Torrens Lake experiments.....	168
5.3.3.1	Bubble plume aerator.....	168
5.3.3.1.1	Meteorological conditions.....	168
5.3.3.1.2	Temperature and flow velocities.....	168
5.3.3.1.3	Turbulent intensity, shear velocity and turbulent kinetic energy dissipation.....	169
5.3.3.2	Submerged aspirator.....	170
5.3.3.2.1	Meteorological conditions.....	170
5.3.3.2.2	Temperature and velocity profiles.....	170
5.3.3.2.3	Turbulent intensity, shear velocity and turbulent kinetic energy dissipation.....	172
5.3.3.3	High volume surface aerator.....	173
5.3.3.3.1	Meteorological conditions.....	173
5.3.3.3.2	Temperature and velocities.....	174
5.3.3.3.3	Turbulent intensity, shear velocity and turbulent kinetic energy dissipation.....	175
5.3.4	Wind-generated turbulence.....	176
5.4	Discussion.....	176
5.4.1	Measurement of turbulence.....	177
5.4.2	Myponga mixer flow and turbulence analysis.....	178
5.4.3	Torrens Lake bubble plume aerator flow and turbulence analysis.....	180
5.4.4	Torrens Lake aspirator and aerator flow and turbulence analysis.....	181
5.4.5	Comparisons between artificial and naturally generated turbulence.....	182
5.4.6	Conclusions.....	185

Chapter 6. The influence of small-scale turbulence on <i>Microcystis aeruginosa</i>.....	216
6.1 Introduction.....	216
6.2 Methods.....	218
6.2.1 Test organism and experimental design.....	218
6.2.2 Vertically oscillating grid system.....	219
6.2.3 Flow and turbulence measurement.....	220
6.2.4 Statistical analysis.....	221
6.3 Results.....	221
6.3.1 Turbulent intensity.....	221
6.3.2 Responses of <i>M. aeruginosa</i>	221
6.3.2.1 Cell esterase activity.....	222
6.3.2.2 Cell viability.....	222
6.3.2.3 Cell division.....	223
6.3.2.4 Cell chlorophyll fluorescence.....	223
6.3.2.5 Cell size and granularity.....	223
6.4 Discussion.....	224
Chapter 7. Spatial and temporal heterogeneity of phytoplankton in a shallow urban lake.....	239
7.1 Introduction.....	239
7.2 Materials and methods.....	242
7.2.1 The Torrens Lake and study sites.....	242
7.2.2 The monitoring program.....	244
7.2.3 Statistical analysis.....	245
7.3 Results.....	246
7.3.1 Torrens Lake limnological characteristics.....	246
7.3.1.1 Hydrological and meteorological conditions.....	246
7.3.1.2 Water column stability.....	247
7.3.1.3 Nutrients.....	248
7.3.1.4 Dissolved oxygen.....	249
7.3.1.5 Water clarity.....	249
7.3.1.6 Ratio of euphotic to mixed depth.....	249
7.3.2 General description of phytoplankton.....	250
7.3.2.1 Chlorophyll <i>a</i> concentration.....	250
7.3.2.2 Cell volume.....	250
7.3.2.3 Phytoplankton species composition.....	250
7.3.3 Phytoplankton richness and diversity.....	255
7.3.4 Phytoplankton community change.....	256
7.3.5 Sample date groupings- identification of major change in phytoplankton....	257
7.3.6 Relationship between phytoplankton composition and major environmental changes.....	260
7.4 Discussion.....	261
7.4.1 Allogenic factors.....	261
7.4.2 Phytoplankton composition and diversity.....	263
7.4.3 Effects of disturbances on phytoplankton.....	265
7.4.4 Implications for phytoplankton control and monitoring.....	266
7.4.5 Conclusions.....	267

Chapter 8. General summary and discussion.....	300
8.1 Phytoplankton and turbulence.....	300
8.2 Biological techniques and field studies.....	300
8.3 Phytoplankton entrainment and implications.....	305
8.4 Turbulent intensity and phytoplankton.....	306
8.5 Lake management.....	307
Bibliography.....	309
Appendix 1.....	327

List of figures

Chapter 1.

1.1	Time-space diagrams to define scales of physical processes & phytoplankton response.....	26
1.2	Interaction of cell with a flow cytometer laser beam.....	27
1.3	Model of the relationship between light, ETC & variable yield of chlorophyll fluorescence.....	28
1.4	Sketch illustrating common turbulence sources within a lake.....	29
1.5	Conceptual model of the entrainment criterion for phytoplankton.....	30
1.6	Location of project study sites within South Australia, Australia.....	31
1.7	FRP- <i>Microcystis</i> during 1998/99 & 2000/01 summers in the Torrens Lake.....	32
1.8	Seasonal variation in FRP and chlorophyll <i>a</i> concentrations in Myponga Reservoir.....	33

Chapter 2.

2.1	Illustration of the measurements involved in variable chlorophyll fluorescence.....	68
2.2	Time course for FDA conversion to fluorescein for several phytoplankton.....	69
2.3	Microscopic analysis of fluorescein fluorescence for 50: 50 % living: dead mixtures.....	70
2.4	Time course of Sytox fluorescence for several phytoplankton.....	71
2.5	Microscopic analysis of Sytox fluorescence for 50: 50 % living: dead mixtures.....	72
2.6	Estimation of the number of viable & nonviable cells using Sytox and FDA.....	73
2.7	Monitoring the response of <i>M. aeruginosa</i> to nutrient limitation & repletion.....	74
2.8	Affect of copper on <i>S. quadricauda</i> growth, esterase activity & viability.....	77
2.9	Influence of light intensity on <i>M. aeruginosa</i> photo-physiology.....	78
2.10	Influence of light intensity on <i>C. pyrenoidosa</i> , <i>A. circinalis</i> and <i>A. granulata</i>	79
2.11	Influence of nutrient status on <i>M. aeruginosa</i> photo-physiology.....	80
2.12	<i>A. circinalis</i> F_v/F_m depression and recovery kinetics.....	81
2.13	Influence of high light exposure time on F_v/F_m depression & recovery kinetics of <i>A. circinalis</i>	82
2.14	Meteorological conditions, phytoplankton physiology & modelled photosynthesis in Myponga.....	83

Chapter 3.

3.1	Meteorological conditions at the Torrens Lake on 11 Jan 2001.....	104
3.2	Vertical temperature structure of the Torrens Lake on 11 Jan 2001.....	105
3.3	Variation in surface mixed layer depth and turbulent intensity on 11 Jan 2001...	106
3.4	Chlorophyll fluorescence profiles for the Torrens Lake on 11 Jan 2001.....	107
3.5	<i>P. cinctum</i> cell concentrations for the Torrens Lake on 11 Jan 2001.....	108
3.6	Changes in F_v/F_m of <i>P. cinctum</i> of bottle and lake samples on the 11 Jan 2001..	109
3.7	<i>P. cinctum</i> entrainment & relationship between swimming velocity & shear	

	velocity.....	110
3.8	Photosynthetic-irradiance curve for an integrated Torrens Lake sample.....	111
3.9	Modeled chlorophyll distribution within the Torrens Lakes on 11 Jan 2001.....	112
3.10	Photosynthetic production for <i>P. cinctum</i> population within the Torrens Lakes on 11 Jan 2001.....	113
3.11	Photosynthetic production for a homogenously distributed <i>P. cinctum</i> population.....	114
3.12	<i>P. cinctum</i> concentration & F_v/F_m with respect to depth and time in an artificial water column.....	115

Chapter 4.

4.1	Photosynthetic active irradiance incident on the Torrens Lake on 3 Feb 2000....	137
4.2	F_v/F_m of <i>M. aeruginosa</i> in bottle and lake sample on 3 Feb 2000.....	138
4.3	Vertical temperature structure of the Torrens Lake on 3 Feb 2000.....	139
4.4	Wind speed and shear velocity at the Torrens Lake on 3 Feb 2000.....	140
4.5	F_v/F_m of <i>M. aeruginosa</i> collected from Torrens Lake & exposed to constant light intensities.....	141
4.6	Numerical simulation of F_v/F_m of <i>M. aeruginosa</i> maintained at constant light intensities.....	142
4.7	Numerical simulation of F_v/F_m of <i>M. aeruginosa</i> maintained at discrete depths in Torrens Lake.....	143
4.8	Surface mixed layer depth, simulated photosynthetic irradiance and F_v/F_m of a <i>M. aeruginosa</i> colony.....	144
4.9	Particle trajectory of buoyant 53 and 200- μm radius <i>M. aeruginosa</i> colonies....	145
4.10	Velocity field and streamlines following the Buranathanitt <i>et al.</i> (1982) Langmuir cell model.....	147
4.11	Trajectory of neutrally buoyant <i>M. aeruginosa</i> colonies in Langmuir circulation.....	148
4.12	Trajectory of buoyant 53- μm radius <i>M. aeruginosa</i> colonies in Langmuir circulation.....	149
4.13	Trajectory of buoyant 200- μm radius <i>M. aeruginosa</i> colonies in Langmuir circulation.....	150
4.14	Trajectory of <i>M. aeruginosa</i> in a turbulent water column.....	151

Chapter 5.

5.1	Schematic diagram of flow by bubble plume aeration & surface mounted mechanical mixing.....	186
5.2	Schematic diagram of the surface mounted mechanical mixer in Myponga Reservoir.....	187
5.3	Photographs of the surface mounted mechanical mixer in the Myponga Reservoir.....	188
5.4	Map of Myponga Reservoir showing the location of surface mixers.....	189
5.5	Location of water velocity profiling sites around Albert Street Bridge bubble plume aerator	190
5.6	Location of submerged aspirator and high volume surface aerator within the Torrens Lake.....	191
5.7	Current velocity profiling and boat set up.....	192

5.8	Energy spectra estimated from acoustic Doppler velocimetry velocity data.....	193
5.9	Meteorological conditions at the Myponga Reservoir on the 5 February 2002....	194
5.10	Radial, vertical & sum of velocity components below surface mixer draft tube in Myponga Reservoir.....	195
5.11	Surface mixer turbulent intensities, shear & turbulent kinetic energy dissipation	196
5.12	Effect of transport through surface mixer draft tube on Myponga phytoplankton characteristics.....	197
5.13	Comparison of phytoplankton characteristics adjacent to surface mixer & 70 m away.....	198
5.14	Meteorological conditions at the Torrens Lake on the 22 February 2001.....	199
5.15	Temperature & velocity profiles around Albert Street Bridge bubble plume aerator.....	200
5.16	Bubble-plume turbulent intensities, shear & turbulent kinetic energy dissipation	201
5.17	Meteorological conditions at the Torrens Lake on the 23 Mar 2002.....	202
5.18	Meteorological conditions at the Torrens Lake on the 2 Apr 2002.....	203
5.19	Temperature profiles around the aspirator.....	204
5.20	Radial velocities around the submerged aspirator.....	205
5.21	Vertical velocities around the submerged aspirator.....	206
5.22	190° N transect of aspirator turbulent intensities, shear & turbulent kinetic energy dissipation..	207
5.23	270° N transect of aspirator turbulent intensities, shear & turbulent kinetic energy dissipation.....	208
5.24	Temperature profiles around the high volume surface aerator.....	209
5.25	Radial velocities around the high volume surface aerator.....	210
5.26	Vertical velocities around the surface aerator.....	211
5.27	150° N transect of aerator turbulent intensities, shear & turbulent kinetic energy dissipation.....	212
5.28	270° N transect of aerator turbulent intensities, shear & turbulent kinetic energy dissipation....	213
5.29	Influence of wind speed on turbulent intensity, shear & turbulent kinetic energy dissipation.....	214
5.30	Map of shear velocity values with respect to bed gradient, water column height & wind speed.....	215

Chapter 6.

6.1	Schematic diagram of the turbulence generating oscillating grid.....	230
6.2	Relationship between grid oscillation frequency and turbulent intensity	231
6.3	Influence of grid-generated turbulence on <i>M. aeruginosa</i> mean esterase activity	232
6.4	Influence of grid-generated turbulence on <i>M. aeruginosa</i> esterase activity (low activity state).....	233
6.5	Influence of grid-generated turbulence on <i>M. aeruginosa</i> cell viability.....	234
6.6	Influence of grid-generated turbulence on <i>M. aeruginosa</i> cell growth.....	235
6.7	Influence of grid-generated turbulence on <i>M. aeruginosa</i> cell chlorophyll fluorescence.....	236
6.8	Influence of grid-generated turbulence on <i>M. aeruginosa</i> cell size.....	237
6.9	Influence of grid-generated turbulence on <i>M. aeruginosa</i> cell granularity.....	238

Chapter 7.

7.1	Phytoplankton C-S-R life history classification after Reynolds (1997).....	268
7.2	Map of sampling sites, A ₁ to L in the lower Torrens Lake.....	269
7.3	Photographs of sampling sites.....	270
7.4	24 h rainfall and discharge at Holbrookes Road during the study period.....	273
7.5	Meteorological conditions at site L in the Torrens Lake during the study period.	274
7.6	Vertical temperature structure at site L in the Torrens Lake during the study period.....	275
7.7	Vertical temperature structure at site B in the Torrens Lake during the study period.....	277
7.8	Daily surface mixed layer at site L during the study period.....	278
7.9	Total and filterable reactive phosphorous at sites A ₂ , E, H and L in the Torrens Lake.....	279
7.10	Total Kjeldahl and inorganic nitrogen at sites A ₂ , E, H and L in the Torrens Lake.....	280
7.11	Dissolved oxygen concentrations at site L in the Torrens Lake.....	281
7.12	Temporal changes in light attenuation coefficient, euphotic depth and Z_{eu}/Z_{mix} .	283
7.13	Temporal changes in chlorophyll a and biovolume at selected sites.....	284
7.14	Phytoplankton species composition at site A ₂	285
7.15	Phytoplankton species composition at site B.....	286
7.16	Phytoplankton species composition at site D.....	287
7.17	Phytoplankton species composition at site E.....	288
7.18	Phytoplankton species composition at site H.....	289
7.19	Phytoplankton species composition at site L.....	290
7.20	Summed difference index for phytoplankton community at sites A ₂ , B, D, E, H, and L.....	291
7.21	Sample date groupings for sites A ₂ , B, D, E, H, and L in the Torrens Lake.....	292
7.22	Ordination of autogenic factors and phytoplankton community composition.....	294
7.23	Ordination of phytoplankton community composition and cardinal points.....	297

List of tables

Chapter 2.

2.1	Summary of photochemistry nomenclature used throughout the thesis.....	44
-----	--	----

Chapter 5.

5.1	Radial & vertical direction of water movement below a surface mixer in the Myponga Reservoir.....	167
5.2	Radial and vertical direction of water movement around the submerged aspirator in the Torrens Lake.....	173
5.3	Radial and vertical direction of water movement around the surface aerator in the Torrens Lake.....	175
5.4	Summary of the range of shear velocities, turbulent kinetic energy dissipation rates and Kolmogorov eddy sizes reported in nature.....	184

Chapter 6.

6.1	Summary of phytoplankton and small-scale turbulence experiments.....	229
-----	--	-----

Chapter 7.

7.1	Morphometric data for the Torrens Lake.....	243
7.2	Summary of all recorded genera within the Torrens Lake.....	253
7.3	Torrens Lake site groupings based on phytoplankton composition.....	254

Summary

Water motion strongly influences phytoplankton access to sunlight and nutrients, which ultimately govern primary production. The motion predominantly takes the form of turbulence. Understanding primary production and the ecology of phytoplankton including harmful algal blooms (HAB) and their control requires an understanding of the relevant physical processes and the scales of their interaction. The interaction between phytoplankton and physical processes are diverse and occur at a range of spatial and temporal scales. The main objective of this thesis is to contribute to the understanding of how turbulence affects phytoplankton in freshwater systems. The major focus is the temporal and spatial scales in phytoplankton dynamics ranging from photochemistry in the surface mixed layer to small-scale shear and growth to intra-seasonal changes in community composition in a lake subject to high disturbances.

A major requirement in studying the relationship between environmental variability and physiological processes is the ability to sample and analyse biological components at appropriate temporal and spatial scales. The reliability of flow cytometry in combination with fluorescent stains (FDA, Sytox) and PAM fluorometry were tested to detect the response of phytoplankton to environmental variability. Staining protocols with FDA and Sytox were optimised for their ability to quantify cell metabolic activity and viability, respectively. 'Activity' and 'viability' states were established for 3 phytoplankton species subjected to heat treatment, nutrient limitation and replenishment and copper toxicity.

PAM fluorometry was used to investigate the influence of light intensity, duration of exposure and nutrient status on phytoplankton photo-physiology. Measurements of photochemical quenching, maximum change quantum yield of photosystem 2 (F_v/F_m) and effective absorption cross-section were made on both laboratory cultures and field populations. Each characteristic was found to be sensitive to light and nutrients for the different species examined. In particular, the magnitude of F_v/F_m was dependent upon light intensity and dose and provided a feature of phytoplankton that could be traced to assess the impacts of turbulent mixing and thermal stratification on cell entrainment and distribution. An experiment in the Myponga Reservoir (South Australia) demonstrated that F_v/F_m in combination with the other photo-physiology characteristics enables the calculation of photosynthesis with greater temporal and spatial resolution compared with traditional methods.

The interplay between wind mixing, thermal stratification and cell motility on phytoplankton distribution was investigated in the Torrens Lake (South Australia) with measurements carried out on the dinoflagellate, *Peridinium cinctum*. *In situ* profiles of chlorophyll fluorescence and cell counts, revealed the vertical migration of *P. cinctum*, ascending in the morning and descending in the afternoon. Swimming velocity reached $2.35 \times 10^{-4} \text{ m s}^{-1}$. Cell distribution was a function of wind speed and swimming velocity and reflected the entrainment model of Humphries and Imberger (1982). When $\psi < 1$, distribution was dominated by wind speed and when $\psi > 1$, distribution was dominated by swimming velocity. Measurements of F_v/F_m of *P. cinctum* cells through time and depth revealed minimal photo-inhibition although cells actively avoided high irradiance. A depression in F_v/F_m was observed in surface samples however, this recovered to initial values later in the day. A comparison between modeled daily photosynthetic rates of a migrating ($2,574.1 \text{ mg O}_2 \text{ m}^{-2}$) and a homogeneous population ($3,120 \text{ mg O}_2 \text{ m}^{-2}$) revealed that migration would not increase photosynthetic rates within the Torrens Lake. In addition to

phototaxis, it was postulated that dinoflagellates move deeper in the water column to avoid small-scale shear stress generated by turbulence in the surface mixed layer.

The maximum quantum yield (F_v/F_m) was also used to determine the light history of *Microcystis aeruginosa* colonies in the Torrens Lake. As insolation increased the lake stratified and colonies displayed a depression in F_v/F_m , which became less severe with depth. In the afternoon, wind speed increased entraining colonies and disrupting the discrete depth variable F_v/F_m response. The point where the photochemical response became homogenized allowed the determination of the shear velocity necessary to entrain colonies ($u^* = 0.003 \text{ m s}^{-1}$). This fits the entrainment model proposed by Humphries and Lyne (1988). Rates of F_v/F_m depression were light intensity dependent whereas recovery was dependent upon light dose. A model is presented which examined the influence of five mixing scenarios on the F_v/F_m of *M. aeruginosa*.

Field experiments examined the current flow around several artificial mixing devices including a surface mechanical mixer/draft tube system in the Myponga Reservoir (South Australia) and bubble plume aerators and aspirators within the Torrens Lake. An acoustic Doppler velocimeter was used to measure current velocity, which also enabled the calculation of turbulent intensity, shear velocity and the turbulent kinetic energy dissipation rate (determined using spectral analysis). Turbulent intensities, shear velocities, and turbulent kinetic energy dissipation rates were found to be high around the mixing devices relative to turbulence generated by wind. Turbulent kinetic energy dissipation rates ranged from $5 \times 10^{-7} \text{ m}^2 \text{ s}^{-3}$ to $3.4 \times 10^{-4} \text{ m}^2 \text{ s}^{-3}$, while shear velocity in the immediate vicinity of the devices was of a magnitude ($>5.9 \times 10^{-3} \text{ m s}^{-1}$) to entrain most phytoplankton. Measurements of metabolic activity and viability of phytoplankton above and below the Myponga Reservoir surface mixer/ draft tube revealed that transport and subsequent exposure to small-scale shear had no impact on the population. Current velocity measurements enable the zone of influence of artificial mixing devices to be determined which assists in the assessment of their performance.

A vertically oscillating grid-tank system was used to simulate observed turbulence levels around the artificial mixing devices. Turbulent intensity increased with an increase in oscillation frequency (1-5 Hz). Grid-generated turbulence affected *Microcystis aeruginosa* metabolic activity, viability and growth. At 4 Hz metabolic activity, viability and growth decreased which was most evident after 96 hours. Small-scale shear was postulated to be insignificant in *M. aeruginosa* ecology but may have a role in regulating colony size and may contribute to bloom decline under stressed conditions.

A field study examined the spatial and temporal heterogeneity in phytoplankton community composition within the lower Torrens Lake. Twenty-eight genera were identified during the 5-month sampling period representing phytoplankton with C-S-R (Grime, 1979) traits. Although, no single factor could be identified to affect species succession, summer rainfall events acted as a major disturbance by flushing and diluting the populations and reintroducing nutrients. Often C-S-R species coexisted in the lake verifying the intermediate disturbance hypothesis of Connell (1978). It is difficult to predict and manage phytoplankton community composition in small-shallow urban lakes such as the Torrens Lake due to the unpredictability of summer rainfall and the short time scale of events such as storm water runoff from the surrounding catchment.

Declaration

This thesis contains no material which has been accepted for the award of any other degree or diploma in any university or other tertiary institution and to the best of my knowledge and belief, contains no material previously published or written by no other person, except where due reference has been made in the text. I consent to the thesis being made available for photocopying and loan if accepted for the award of the degree.

Rudi H. Regel

26 February 2003

Acknowledgements

I would like to express my sincere thanks to the following people:

Firstly, my supervisors Associate Professor George Ganf and Dr Justin Brookes who have both encouraged, tested and most of all inspired me in the field of Limnology. George, thank you for being an outstanding university supervisor and scientist. Justin, thank you for your enthusiasm towards research, particularly phytoplankton and help in the field, which has contributed to chapters 2-5 and 7.

I would also like to acknowledge the Cooperative Research Centre for Water Quality and Treatment and specifically Mike Burch, Dennis Steffensen, Dennis Mulcahy and Don Bursill for supporting and sponsoring my research and also to AWQC staff, Peter Baker and Peter Hobson.

David Cenzato - for being a great colleague and your help with computing, technical problems, sampling, boating, flow cytometry and the list goes on. I have greatly enjoyed our discussions on the 'Benham' steps over the years.

David Lewis, thank you for your help in the field and providing technical advice and most of all those memorable 'marron' moments. Specifically, thank you for your assistance in the fieldwork associated with chapter 5.

To my fellow Limnology students (in no order): Jason Nicol, Mark Siebentritt, Ben Taylor, Todd Wallace, Leon Linden, Paul van Ruth, Karen Westwood, Kay Morris, Kerri Muller and Sean White. Thank you for your encouragement and the 'good old' limno support! A special cheers to my office mate, Kane Aldridge- I have thoroughly enjoyed our chats and jokes.

I must also acknowledge the friendly and helpful staff of the Environmental Biology Department and in particular Marilyn Saxon who has always greeted me with a smile.

During my study I have also visited several institutions and would like to thank the following people for their time: Francisc Peters, Luuc Mur, Petra Visser, and Anthony Walsby.

I would like to acknowledge the financial support of the Australian Water Association, The University of Adelaide and the Department of Environmental Biology for attending the World Water Congress in Berlin (2001) and the visit to the CSIC in Barcelona.

The *Microcystis*-small-scale shear work in chapter 6 would not have been possible without the lending of the oscillating grid by Ross Griffiths of the University of Canberra.

Thanks also to the University of Adelaide Civil Engineering Department who have assisted with equipment and John Vitkovsky for your help in developing the turbulence program.

The fieldwork on Myponga Reservoir would not possible without the technical, laboratory, boating and accommodation support of Allen Brown and Rod Boothey of SA Water.

Special thanks to my Grandpa, George Flint, for support, love and chit chats- a great landlord.

My parents, Eileen and Herbert for love, support, encouragement, a roof over my head and the ability to believe in myself, and that life holds no bounds. I certainly cannot forget Cello – a mans true friend.

Last, but certainly not least, Anne-Sophie Morvan. Since we met in disguise at a Halloween, life has only got better. Thank you for your love, patience, support and encouragement – a gros bisous to you!

Chapter 1

Introduction

1.1 A question of scale

Aquatic ecosystems are driven by the flow of energy from sunlight through primary production of phytoplankton to higher trophic levels. Water motion is a driver which strongly influences phytoplankton access to sunlight, nutrients and ultimately primary production. The water motion predominantly takes the form of turbulence, which has long been recognised as a source of 'auxiliary' or external energy to pelagic systems compared to the internal energy of cell metabolism (Margalef, 1978). Turbulence is the mechanism by which large-scale motions of winds and waves couples to the viscous small-scale environment of the phytoplankton (Thomas *et al.*, 1997). Consequently, understanding primary production and the ecology of phytoplankton including harmful algal blooms (HAB) requires an understanding of the relevant physical processes (Spigel and Imberger, 1987) and the scales of their interaction.

The modes of interaction between phytoplankton and physical processes are diverse and occur at a range of spatial and temporal scales. Physical processes create the structure of the pelagic environment and affect the rate of biological processes within the phytoplankton. A continuum of scales exists for water motion from laminar basin flows to turbulent mixed layers with eddies of all sizes and velocities down to small-scale turbulence and molecular motion. At each level, there are consequences for the transport and distribution of phytoplankton and their exposure to light, their access to nutrients and for their contact with zooplankton (Reynolds, 1994a) and their interaction with small-scale shear stress. Phytoplankton cells are generally smaller than the smallest eddy in a turbulent spectrum and subsequently occupy a viscous medium. However, with sufficient turbulence they are entrained and transported over large spatial distances. At large scales, turbulence affects whole populations and communities, whereas at small scales turbulence directly affects individual cells.

Harris (1986) pointed out that the vast number of scales could be simplified if they were viewed from the point of phytoplankton. He defined the scales of biological interest as those, which elicit a response in phytoplankton. Reynolds (1994a) compared the scales of physical processes to the

levels of biological response of phytoplankton. He highlighted the important physical processes that occur in the turbulent to viscous range of motion, which elicit a biological response in seconds, such as photochemical fluorescence, to months, such as seasonal periodicity in community composition (figure 1.1). Consequently, physical structures generated by water motion determine the spatial scale of phytoplankton processes and it is the phytoplankton that determines the temporal scales (Mann and Lazier, 1991).

The temporal scales for biological processes are centred on the generation time of individual species. At short time scales (seconds to days), phytoplankton respond to environmental variability via physiological adjustments (physiological scale). Variability at time scales longer than the generation time (growth rate scale) influence population dynamics, species competition and community composition. Species suited to the new physical and/or chemical conditions will grow and divide while those less suited may grow too slowly to maintain a presence and or be vulnerable to sedimentation or grazing (Harris, 1986).

The main objective of this thesis is to contribute to the understanding of how turbulence affects phytoplankton in freshwater systems. The major focus is the temporal and spatial scales in phytoplankton dynamics ranging from photochemistry in the surface mixed layer to small-scale shear and growth to intra-seasonal changes in community composition in a lake subject to high disturbances. This has been accomplished through:

- Testing of flow cytometry/ fluorescent probes and active fluorometry techniques for rapidly measuring phytoplankton metabolic activity and viability (chapter 2).
- Increasing the understanding between the interplay of dinoflagellate migration, entrainment, large-scale wind mixing and photosynthesis (chapter 3).
- Increasing the understanding of the influence of wind mixing on cyanobacterial photochemistry (chapter 4).
- Determining turbulence levels faced by phytoplankton in managed water bodies by measuring flow, turbulent intensities and dissipation rates around artificial mixing systems (chapter 5).
- Simulating turbulence using a vertically oscillating grid under controlled conditions and discerning an impact of small-scale shear on a cyanobacterial species (chapter 6).
- At a larger scale, investigating the spatial and temporal heterogeneity of phytoplankton in a shallow urban lake and testing of the intermediate distance hypothesis (chapter 7).

1.2 Limnological Progress

Traditionally, phytoplankton ecology has focused on describing macroscale processes such as the effects of physical and or chemical conditions on phytoplankton at the population or community level typically at weekly or seasonal scales (Spigel and Imberger, 1987). Physical processes have often been considered in the context of whether the water column is mixed or thermally stratified and the ramifications on the light and nutrient resources of the phytoplankton. The ratio of euphotic depth to mixed depth (Z_{eu}/Z_{mix}) ratio has been widely appreciated to influence phytoplankton photosynthesis and species competition and community dynamics. In particular, the affect of mixing, and thermal stratification in seasonal succession in temperate lakes is well understood (Reynolds, 1994b). Moreover, the seasonal alternation between mixed and thermally stratified conditions is also acknowledged to influence the initiation of phytoplankton blooms as a result of the replenishment of nutrients to the euphotic zone (Legendre, 1981; Koseff *et al.*, 1993; Taylor and Stephens, 1993). The presence and absence of species and their respective functional morphologies has enabled the classification of phytoplankton into C_{invasive}-S_{acquisitive}-R_{acclimative} life strategies (Reynolds, 1988a).

Furthermore, water quality monitoring programs have often involved the determination of either species composition or phytoplankton biomass (i.e. chlorophyll) over a weekly period generally without the consideration of time scales of 'events', which may influence phytoplankton dynamics (i.e. rainfall, mixing, stratification). Often, phytoplankton growth has been measured as a whole community response with chlorophyll *a* used as an index of abundance against which rate process such as photosynthesis are normalized (Smayda, 1997). When individual species dynamics have been investigated, population based parameters, such as cell yield, mask concurring processes such as cell death or lysis. Cell lysis is increasingly being recognized as an important loss process along with sedimentation and grazing in population budgets (Veldhuis *et al.*, 1997).

Phytoplankton research now has a renewed emphasis on microscale processes attempting to resolve spatial and temporal variations in phytoplankton processes in relation to environmental fluctuations. Harris (1986) concluded organisms 'track' fluctuations in the environment brought about by physical processes by physiological and behavioural (e.g. vertical migration) adjustments so that function and growth are maintained. Smayda (1997) states "community

growth is the least significant, masking eco-physiological processes whose resolution is essential for proper understanding of harmful algal bloom dynamics". Physiological information contributes to cellular growth and growth rates determine population size and community structure (Harris, 1986). Although phytoplankton growth is the net result of all environmental fluctuations, examination of physiological processes at small scales may be able to provide further insights into phytoplankton ecology.

A major requirement in studying microscale processes is to be able to more accurately and rapidly assess phytoplankton physiology at scales equivalent to environmental fluctuations. Sophisticated instrumentation has enabled physical limnologists to rapidly describe physical processes, using microstructure profilers and thermistor probes with data logger recording devices. In contrast, biological technology has been slower to develop. Although advances in technologies such as chlorophyll fluorescence profilers, active fluorometry, flow cytometry and fluorescent dyes are useful tools in phytoplankton research to overcome experimental problems, associated with temporal and spatial resolution in field studies such as speed of measurement, replication and heterogeneity in phytoplankton activity. In chapter 2, the use of flow cytometry and fluorescent dyes are explored as measures of phytoplankton metabolic activity and viability, and active fluorometry to assess phytoplankton photo-physiology in relation to wind mixing. It is therefore appropriate to give a brief overview of flow cytometry, fluorescent probes and active fluorometry.

1.3 Biological techniques

1.3.1 Flow cytometry and fluorescent probes

Flow cytometry (FCM) is a general term for the rapid measurement of particles in a moving fluid (Yentsch *et al.*, 1983). Flow cytometers measure multiple optically expressed features of single cells. Measured parameters may include the fluorescent signal and light scatter of individual particles (i.e. cells) as they pass a laser beam of pre-determined wavelength at flow rates of 1000 cells per 30 seconds (figure 1.2). The fluorescent signal originates from either *in vivo* chlorophyll fluorescence or a stain. Chlorophyll fluorescence, measured as red fluorescence, is the maximum fluorescence when photosystem 2 reaction centers are closed and photochemical quenching is minimal (Xu *et al.*, 1990) and is linearly related to cellular chlorophyll concentrations (Veldhuis

and Kray, 2000). In addition to fluorescent signals, morphological information is simultaneously obtained from scattered light. Forward and side scatter provide information on cell size and granularity, respectively.

There are a range of fluorescent stains that can be used to label structural and biochemical cellular components and quantify the physiological activity of phytoplankton cells. The stains or probes can be classified as either static or kinetic. Static components include DNA, proteins or other chemicals within or on the surface of cells whose staining, once achieved, remains stable. In kinetic measurements, the staining result or fluorescence yield depends on the time of analysis and quantifies relative activity.

Static probes such as propidium iodide, PicoGreen, SYBR Green, DAPI, TOTO-1 and Sytox stain DNA and are traditionally used for cell cycle analysis and increasingly to assess cell viability. The nucleic acid probes only penetrate cells with a compromised membrane but will not cross membranes of living cells. Consequently, the DNA in viable cells does not stain whereas, DNA in non-viable cells does. New stains, such as Sytox green, have major advantages over previous dyes such as propidium iodide because they can be excited at 488 nm, the standard laser wavelength in a flow cytometer and fluoresce green, which exerts little interference with chlorophyll-red fluorescence. FCM can distinguish between labeled and non-labeled cells and provide a quantitative measure of the percentage of viable/ nonviable cells within a sample.

The principle of kinetic measurement is the addition of non-fluorescent substrates that are metabolically processed within cells, cleaving the substrate and releasing a strong fluorogen. The cleavage of the non-fluorescent substrate results in accumulation of fluorescent compound within the cell that initially increases until saturation. FCM can distinguish between labeled and non-labeled cells and provide a quantitative measure of the rate at which cells process the substrate.

Fluorescein diacetate (FDA) is a lipophilic, non-polar, non-fluorescent stain that diffuses freely into intact cells (Rotman and Papermaster, 1966). Inside viable cells, non-specific esterases (e.g. lipase, acetylcholinesterase), cleave the ester bonds, producing fluorescent fluorescein and two acetate molecules. Fluorescein is hydrophilic and does not leak readily out of intact cells. FDA conversion does not occur in dead cells, but maximum esterase activity and subsequently maximum fluorescence is evident in log-phase cell cultures (Bentley-Mowat, 1982). Esterase

function is involved in phospholipid turnover in membranes, which occur on a time scale of several hours (Yentsch *et al.*, 1988). Consequently, the technique is useful to detect subtle changes in metabolic activity ranging from sub-daily to daily.

1.3.2 Fluorometry, photosynthesis and chlorophyll fluorescence

Active fluorometry involves probing phytoplankton with defined light intensities and measuring the chlorophyll fluorescent yield. The yield of chlorophyll fluorescence is sensitive and variable in intact cells and depends on their history (particularly light) and environment. In order to demonstrate the use of active fluorometry it is necessary to provide a brief overview of photosynthesis and chlorophyll fluorescence.

The light reactions of photosynthesis comprise of two electron regulated photochemical systems, photosystems 1 and 2 (PS1 and PS2), which are connected by an electron transport chain (ETC). The first step in photosynthesis requires the capture of light by chlorophyll and the funneling of energy to reaction centers (RCs) at the core of each photo-system. In PS2, the energy of the photons raises electrons from water in P680 molecules in the RCs from their ground state to an excited state (charge separation), and each electron is passed singly towards PS1 with pheophytin via quinone acceptors, Q_a , Q_b and plastoquinone (PQ). Quinone (Q_a) is the primary acceptor molecule at the start of the electron transport chain. Once Q_a accepts an electron it is reduced to Q_a^- , P680 becomes $P680^+$ and another electron from water re-reduces it based upon a separate donor system (tyrosine protein). The RC is unable to accept further electrons and remains closed until re-oxidation of Q_a clears the pathway for the next electron.

From Q_a , electrons are transferred to Q_b acceptor and once two electrons have been accepted, Q_b disassociates into a pool of plastoquinone (PQ). Reduced PQH_2 is then oxidized by cytochrome *b/f*. Simultaneously, the P700 chlorophyll molecule of PS1 is excited and its acceptor, allows passage of electrons beyond PQH_2 pool to CO_2 via the reduction of nicotinamide adenine dinucleotide phosphate (NADP to $NADPH_2$) and the generation of adenosine triphosphate (ATP) from phosphate ions and adenosine diphosphate (ADP). The equation of photosynthesis: $2H_2O + CO_2 \ggg \text{photons} \ggg CH_2O + H_2O + O_2$, requires 4 electrons to transfer through each photo-system to fix each carbon atom (alternatively 0.125 mol of carbon is produced per one mol of photon absorbed). The rate of transfer of electrons from PQH_2 to PS1 is rate limiting and takes

between 2 and 15 ms, and thus PQH₂ acts as a capacitor and restricts sudden “bursts” of electrons going to PS1.

The processing of light energy into chemical energy is dependent upon the redox state of the electron transport chain. Light energy captured by chlorophyll molecules can be dissipated via three pathways; it can be used in photosynthesis when the ETC is oxidized, lost through heat or be re-emitted as chlorophyll fluorescence. The majority of chlorophyll fluorescence comes from PS2 (Krause and Weis, 1991) when the ETC is reduced when charge separation does not occur (figure 1.3).

In darkness when chlorophyll molecules are reduced (P680⁻), Q_a is oxidized and the reaction center is said to be open (trap is open). In this state it is able to carry out photosynthesis and fluorescence would be minimal, F_o (figure 1.3a). Conversely, maximum chlorophyll fluorescence occurs when the chlorophyll molecules capture a photon while Q_a is still reduced from a previous photon and the reaction is said to be “closed” or “shut” (figure 1.3b). The energy from the second photon cannot be transferred to Q_a and it is released giving a maximum fluorescence signal, F_m . Under ambient light the fluorescence yield, F increases as Q_a becomes reduced, reaching a maximum, F_m when all reaction centers are closed.

Since each cell contains many photosynthetic units, the intensity of the fluorescent signal is dependent upon the relative number of open and closed traps and chlorophyll fluorescence is therefore variable. Variable fluorescence, F_v is the difference between F_m and F_o . The relative change in the quantum yield of fluorescence reflects the level of reduction of Q_a and theoretically an inverse relationship exists between photochemistry and fluorescence without the affect of quenching. The variable fluorescence is standardized to F_m . The ratio (F_v/F_m) is termed the maximum change in quantum yield and provides an estimate of the number of functional reaction centers in photo-system 2 and is indicative of the photosynthetic capability of the cell (Falkowski and Kolber, 1995). In laboratory cultures of phytoplankton grown under optimal conditions the maximum change in quantum yield is 0.65 for most species and it is generally assumed that when $F_v/F_m = 0.65$, 100% of reaction centers are functional (Kolber and Falkowski, 1993). Under sub-optimal conditions F_v/F_m and maximum photosynthesis (P_m) decline (Kolber *et al.*, 1988).

A reduction in fluorescence due to photosynthesis (photochemistry) is termed photochemical quenching (q_p). The magnitude of fluorescence can also be affected by mechanisms not related to the redox state of Q_a and are termed non-photochemical quenching processes (q_N) and may be the result of trans-membrane electrochemical potentials and pH gradients within chloroplasts, photo-degradation of PS2 reaction centers (Owens, 1991), state 1 and 2 transitions and photo-inhibition due to excessive radiation (Oliver and Whittington, 1998).

Because F_v/F_m is sensitive to light it has potential as a parameter to offer insight into the immediate past history of phytoplankton and provides a feature of phytoplankton which can be used to link physical mixing processes to light climates and cell distribution, activity and photosynthesis (Kroon, 1992; Oliver and Whittington, 1998). An additional parameter measurable by active fluorometry is the effective absorption cross-section (σ) which is a measure of the relative size of the light harvesting antennae in PS2 and is the product of the light harvesting capability of the pigments and the efficiency of electron transfer to the reaction center (Dubinsky, 1992). Together F_v/F_m , σ and photochemical quenching can be combined to determine the photosynthetic rate of a sample (Falkowski and Kolber, 1993).

1.4 Turbulence

Water bodies are nearly always turbulent, however, turbulence in experimental ecosystem studies is often ignored, inadequately characterized or unreported (Thomas and Gibson, 1990; Sanford, 1997). A notable exception is the study of physical and phytoplankton processes in large lakes which have progressed the understanding of spatial and temporal variability of turbulence and its ramifications on phytoplankton circulation, mixing times and sediment re-suspension in fluid dynamic terms (Spigel and Imberger, 1987; MacIntyre, 1993; MacIntyre and Melack, 1995; MacIntyre, 1996; MacIntyre, 1998). However, the lack of reporting of turbulence in phytoplankton studies is probably attributable not only to costs associated with sophisticated instrumentation but also a lack of understanding of physical processes by biologically oriented limnologists (Straskraba, 1998).

At large scales, turbulence plays a fundamental role in governing the vertical and horizontal distribution of phytoplankton and scalars such as nutrients. The vertical transport of phytoplankton through light gradients influences the intensities of light to which phytoplankton

are exposed and therefore the rate of photosynthesis, “the frequency of cell generation”- growth and the selection of species. At small scales, turbulence can directly affect phytoplankton growth through shear or nutrient uptake, increase encounter rates between phytoplankton and zooplankton and enhance particle aggregation and disaggregation (Rothschild and Osborn, 1988; Kiorboe *et al.*, 1990; Thomas and Gibson, 1990; Berdalet, 1992, Kiorboe, 1993; Hondzo and Lyn, 1999). To gain an appreciation of the role of turbulence and mixing processes in phytoplankton ecology a brief overview is provided of the factors that govern turbulence generation and its intensity and distribution.

Turbulence is the result of unstable excess physical energy and is a property of the motion not of the fluid (Gargett, 1997). An exact definition of turbulence is difficult since all flows are highly individualistic. However, turbulent flows share a number of common characteristics such as being random in space and time, homogenous in velocity at small-scales (statistically independent in all directions), dissipative of energy and diffusive of properties, which exceed molecular values associated with laminar flows and lastly are a threshold phenomenon (Tennekes and Lumley, 1972).

Flow can be described using the Reynolds decomposition equation ($u = U + u'$), where flow velocity (u) over time at a given point in space consists of a mean component (U) and a fluctuating component of accelerations and decelerations (u'). The fluctuating component represents the random turbulent nature of a flow. In laminar flow, the fluctuation component is small and the flow is ordered and predictable by the mean flow. However, if additional energy is put into the flow, molecules become sheared and the laminar flow breaks into a complex series of recoiling and interacting eddies with various velocities ($U \pm u'$) and sizes. Summation of positive and negative terms squared, defines turbulent intensity (u^{*2} , $m^2 s^{-2}$). The turbulent intensity includes horizontal (u') and vertical (w') velocity fluctuations components. The square root of the turbulent intensity (u^*) is known as the shear or friction velocity ($m s^{-1}$) and is important to describe phytoplankton cell entrainment and distribution.

1.4.1 Turbulence theory and energy spectrum

Turbulence is generated by unstable excess physical energy at large scale motions through mechanisms such as wind forcing, breaking waves, heat transfer, internal waves and tides in

marine systems. Turbulence theory outlines that the energy is extracted into large eddies and is progressively dissipated through successively smaller eddies by shear until the smallest eddies are overcome by viscosity and the energy is dissipated as heat. The break down of large eddies into smaller eddies is known as the cascade of turbulent kinetic energy (Richardson, 1922). The cascading process whereby energy is transferred from large slow, to small fast scales is rapid. Shear occurs when one eddy tears into another and the interaction between eddies results in a cascade of eddies and energy from large to small (Ozmidov, 1965) and is the reason for rapid diffusion and mixing of heat, nutrients, particles and phytoplankton. Large eddies are not homogeneous and anisotropic, reflecting the generating mechanism. They tend to stir the water when the inertial forces are about equal to the buoyancy forces. However, as the energy cascades to smaller and smaller eddies the turbulence becomes more homogenous, isotropic, and is independent of the generating mechanism.

Once turbulence has been generated it can be described statistically by the *Homogenous Isotropic Theory* (Batchelor, 1967), which distributes the turbulent energy in eddies of different sizes in terms of wave numbers or frequencies. The theory predicts that a region known as the *equilibrium range* will define the turbulent energy spectrum. In this range, there is no direct external input of energy and the rate of transfer equals the rate of extraction from the mean flow by the large eddies which equals the rate of energy dissipation by viscosity at the smallest scales. This rate is referred to as the *turbulent kinetic energy dissipation rate* and is constant. It is equivalent to the product of the turbulent intensity and velocity gradients in unconfined turbulence. The smallest scale or eddy size of turbulence of the equilibrium range is defined as the *Kolmogorov microscale* and below this viscosity dominates. Kolmogorov (1941) showed that the energy at each scale follows a $k^{-5/3}$ law where k is the wave number (i.e. scale) of the eddies. The isotropic turbulence theory also predicts that the scalar (e.g. nutrient) spectrum in the inertial subrange will equal the velocity spectrum, but there is also an additional spectrum and the smallest size for scalar fluctuations is known as the *Batchelor microscale* (Sanford, 1997). Larger turbulent motion is less subject to dissipation than smaller motion and in small-scale homogenous turbulence, the turbulent intensity is uniquely determined by the kinetic energy dissipation rate.

1.4.2 Turbulence generation

There exist many sources of turbulence generation within lakes and the likelihood and intensity of turbulence can be expressed in terms of ratios (e.g. Reynolds, Richardson, Rayleigh numbers) between destabilizing (shear or buoyancy generated) and stabilising forces (mainly temperature stratification). Figure 1.4 illustrates the most common turbulent and transport mechanisms within a lake. The intensity of turbulence is extremely variable in time and patchy in space as a result of the fluctuations in mechanical energy (e.g. wind speed, differential cooling), the dissipation rate, the thermal properties and the morphometry of the water body. The variability influences the mixed layer depth and phytoplankton entrainment and circulation, exposure to light, nutrient concentrations and availability. Turbulence is generally most intense in the surface mixed layer, boundary layers and in plunging river flow (Reynolds, 1998). Without artificial mixing, the interior of a lake is largely quiescent with currents in laminar flow and turbulence suppressed by buoyancy forces as a result of thermal stratification (Spigel and Imberger, 1987).

In an unconstrained turbulence field driven by wind forcing, turbulence is highest in the thin surface layer and decreases with depth as the large eddies propagate into smaller eddies downwards in the water column weakening to the base of the turbulent layer. In stratified or shallow lakes, where the water column is unable to accommodate the downward eddy propagation, the energy is more intense creating smaller eddies (Reynolds, 1994a). If the energy is not contained it can be forced out as wave splash or the structure enlarged as in bank erosion. Moreover, in shallow lakes, energy dissipation is confined to the absolute depth of the water column, and mixing may be more vigorous, and a consequence of a greater shear stress on sediments, is the potential for increased sediment and nutrient re-suspension, for sustained entrainment of particles and phytoplankton (Reynolds, 1994a).

1.4.3 Turbulence length scales

The cascading processes inherent to 3-dimensional turbulence, whereby energy is transferred from larger (slow) to the small (fast) scales are rapid. In the period of a few eddy turnover times the spectrum is filled with eddies of all sizes down to the Kolmogorov scale and consequently shear mixes scalars quickly as opposed to molecular diffusion. The length scale (size) of eddies varies vertically and horizontally in the water column as a result of complex interactions between

the generating mechanism, lake depth, morphometry and thermal structure. Large-scale turbulent eddies are those considered greater than cm to m, whereas small-scale turbulent eddies are those considered from the Kolmogorov microscale to mm. The smallest Kolmogorov microscale is a function of the turbulent kinetic energy dissipation rate and the kinematic viscosity of the fluid (Spigel and Imberger, 1987). The more energetic the turbulence, the greater the dissipation rate, the finer grained will be the straining motions and eddy sizes necessary to achieve the dissipation. Below the Kolmogorov microscale, fluid viscosity dominates and the velocity shear is the same at all scales although it varies randomly in strength and direction (Lazier and Mann, 1989). There is increasing evidence that small-scale turbulence may be an important factor in phytoplankton ecology (Hondzo *et al.*, 1998; Hondzo and Lyn, 1999; Paerl, 2000; Peters and Marrase, 2000; Moisander *et al.*, 2002), which will be discussed below and explored in chapters 5 and 6.

At the other end of the spectrum, the largest eddies are strongly influenced by thermal stratification. In an unstratified water body, the size of the largest turbulent eddies approximates the overall size of the flow such as the depth of the mixed layer or water column or thickness of the bottom layer. In a thermally stratified water body, the largest eddies are smaller than the overall flow due to substantial energy being lost working against the stratification (Turner, 1973). The length scale for the largest eddy in a stratified turbulence field is known as the *Ozmidov length*. The buoyancy of the warmer water resists the downward propagation of eddies so that a new layer of reduced thickness floats on a deeper colder layer. The depth of the surface mixed layer is determined by a balance between the rate at which turbulence is produced and the buoyancy created by surface heat exchange.

The depth of mixing can vary substantially during a day and a water body continuing to gain heat is often extremely difficult to mix (MacIntyre, 1998). Measurements using microstructure profilers have shown that despite its name the upper mixed layer is not always mixing (Spigel and Imberger, 1987). Imberger (1985) and Shay and Gregg (1986) found that only a small temperature difference (0.02 °C) could separate regions with different eddy intensities and overturns. However, without biological measurements whether these small gradients cause heterogeneity in phytoplankton activity is difficult to ascertain. If the turbulence is insufficient to penetrate to the seasonal thermocline, a diurnal thermocline will form below the surface layer with a subsurface layer extending to the seasonal thermocline. The extent of these layers will

vary diurnally and seasonally and influence phytoplankton photosynthesis, growth and competition.

Often thermoclines will break up in the evening which would enable eddies to propagate deeper into the water column. For example, MacIntyre (1998) found that the surface mixed layer depth varied diurnally from 1 m in the day to 6 m at night. During the day, most of the turbulence generated by the wind worked against the strong stratification in the upper 2 m. However, at night, heat loss at the surface generated turbulence and deepened the surface mixed layer (i.e. nocturnal mixing). Nocturnal mixing may influence phytoplankton-nutrient dynamics, particularly in shallow water bodies, which stratify during the day. If mixing penetrates to the thermocline or hypolimnion, nutrient rich water may be entrained and brought to the surface for phytoplankton growth. This process is why turbulence and associated mixing can often “trigger” phytoplankton blooms after periods of stratification and are important for competition between species and maintaining community diversity.

Furthermore, the presence of density gradients (temperature or salinity) may restrict the size of eddies that turnover vertically so that mixing is greater in the horizontal than in the vertical direction (Reynolds, 1994a). Furthermore, the depth of mixing may vary substantially in the horizontal direction as a result of differences in water depth, degree of stratification and subsurface processes. For example, in Lake Biwa, the depth of overturns varied from 4 m to 10 m in a distance of 1.4 km as a result of differential stratification due to differential cooling and subsurface processes (MacIntyre, 1993). MacIntyre (1993) found that mixing could be divided into two regions with different dynamics, one in which turbulence was active and one in which it was constrained by buoyancy. This affected phytoplankton circulation as in the deep basin; cells would experience a greater range of light intensities, whereas in shallow regions only part of the population would be circulated (MacIntyre, 1998). This situation is not so evident in other water bodies such as the Myponga Reservoir in South Australia, because large basin scale motions tend to homogenise water properties and phytoplankton.

1.5 Phytoplankton-turbulence relations

1.5.1 Large-scale turbulence, phytoplankton entrainment-photosynthesis

At large scales, turbulence governs the vertical and horizontal distribution of phytoplankton depending upon its intensity, extent and the degree of cell entrainment. Entrainment is dependent upon the cells morphological characteristics and associated intrinsic velocity relative to the turbulent velocity of the fluid motion. Reynolds (1987) proposed that for a cell to be entrained the turbulent velocity would need to be 1 to 2 orders greater than the intrinsic velocity of the phytoplankton. Alternatively, based on studies at Burrinjuck Reservoir (New South Wales), Humphries and Imberger (1982) proposed ψ as the extent of cell (or particle) entrainment, where $\psi = 15|w_s|/u$ and $|w_s|$ = modulus of the intrinsic velocity of the organisms and u = turbulent velocity. If $\psi < 1$, the cell will be entrained in the motion, subsequently controlling cell distribution. However, if $\psi > 1$, the cell will be disentrained and its own sinking, swimming or floating velocities will determine its position. Reynolds (1994a) expanded the entrainment concept and provided a model of the sinking or floating velocities of common freshwater phytoplankton and the shear velocities necessary to entrain them (figure 1.5).

The turbulent extent or depth of mixing is an additional factor governing cell distribution. The interface between the mixed and the boundary layer is less turbulent than within the mixed layer and consequently as cells are circulated towards the interface, there is greater potential for disentrainment. Consequently, species such as diatoms are likely to be disentrained and their sedimentation rate increased in a shallow mixed layer compared to a deeply mixed surface layer.

Wind mixing that fully entrains a phytoplankton community will homogenize its vertical distribution being dispersed and diluted throughout the surface mixed layer and transported at approximately the same velocities as the turbulent eddies. Depending upon the mixing time and depth, mixing has major ramifications on the light intensities and doses experienced by cells generally causing increased light intensity variability and decreasing average light dose. MacIntyre (1993) reported that the light received by phytoplankton in a 1.5 m overturn would change from 85 % to 3 % of incident light in 3-4 minutes. Even on a calm day, phytoplankton

can experience fluctuations of 20% while circulating within eddies that were only 10% of the euphotic depth (MacIntyre, 1998).

Where turbulence and mixing weakens in time or space, due to either increased heating of the surface layers or weakening of winds, the sinking, swimming or floating velocities will influence cell distribution and photosynthesis and population and community dynamics. Under stratified conditions, the morphological and/or mobility characteristics of the cell will influence the species ability to remain suspended in the surface layers with sufficient light. The differential capacities of species to harvest light will in the short-term influence photosynthesis and in the long-term influence species composition. It is generally assumed that phytoplankton will be entrained under turbulent conditions. However, the entrainment function, ψ becomes more critical to phytoplankton photosynthesis in water bodies that are shallow, exposed to intermittent wind forcing or undergo diurnal stratification. Under these conditions, there is potential for temporal variability between the interplay of species migration, entrainment and photosynthesis and production. In particular, 'bloom forming' cyanobacteria and dinoflagellates are able to persist through brief periods of mixing until stratification resumes (Ganf, 1974; Reynolds, 1994a).

Despite the significance of the entrainment criterion there are few empirical field studies supporting it or testing whether the factor $\psi >/< 1$ is correct (Oliver and Ganf, 2000). In chapters 3 and 4 the entrainment criterion is investigated for a dinoflagellate, *Peridinium cinctum* and a cyanobacterium, *Microcystis aeruginosa*, respectively.

The influence of large-scale turbulence in creating a fluctuating light climate, and as a function of euphotic to mixed depth ratios, has been extensively explored in relation to photosynthesis, photo-adaptation, species competition and succession (see Prezelin *et al.*, 1991; Ferris and Christian, 1991; Ibelings *et al.*, 1994; Reynolds, 1994b for reviews). Several studies have shown that mixing is a strong determinant of photosynthetic rates (Lewis *et al.*, 1984a, b; Schubert *et al.*, 1995) and that in the short term phytoplankton meet the demands of variable light by showing extreme plasticity in their photosynthetic apparatus (Flameling and Kromkamp, 1997). The processes involved in photosynthesis are complex and readjust or photo-adapt at different time scales as a cell moves through a light gradient depending upon whether the intensities are in the light-limited, light saturated or photo-inhibited portion of the photosynthesis curve. In low light, cells attempt to maximize photosynthesis by increasing their light harvesting ability. Conversely,

under high light intensities, cells attempt to avoid photo-inhibition by either reducing the amount of light absorbed, dissipating the light energy, self shading or physically moving away from the light.

Characterization of the light climate of cells is a key step in distinguishing the ways in which different species respond to turbulence and fluctuating light in water bodies. There have been numerous investigations simulating mixing and fluctuating light regimes and the role of maximum light intensities and photoperiods on photosynthesis and growth. Some studies have reported on the affect of light fluctuations, while keeping the total daily light dose (TDL) constant (Marra, 1978; Kroon *et al.*, 1992; Kromkamp and Limbeek, 1993; Flameling and Kromkamp, 1997; Nicklisch, 1998). Other studies have varied TDL while keeping the light intensity constant (Zevenboom and Mur, 1984; Ibelings *et al.*, 1994). However, *in situ* measurements of photosynthesis and growth in response to turbulence and fluctuating light intensities are far more difficult due to limitations with techniques and associated bottle effects with the measurement of photosynthesis (Kolber and Falkowski, 1993).

Since the processes involved in photosynthesis readjust at different rates during circulation, the possibility exists that vertical mixing rates and cell light history could be deduced from the vertical distribution of measurable photosynthetic properties. Cell properties that adapt rapidly to variable light intensities would show differences between samples taken from the top and bottom of the mixed layer, and properties that would adapt slowly would display minor differences between surface and depth. Conversely, if the time scale of mixing were shorter than the fastest photo-adaptation mechanism, phytoplankton at all depths would display similar properties and appear homogenous. However, in stratified water, phytoplankton would exhibit depth-dependent heterogeneity in their properties. In a pioneering study, describing turbulence in terms of fluid dynamic terms (i.e. turbulent kinetic energy dissipation rate), Lewis *et al.* (1984b) showed that mixing rate determines photosynthetic rate in the upper mixed layer in Bedford Basin. When turbulent intensity was high, there was minor variation in maximum photosynthesis (P_m), but on days when the turbulent intensity was low, surface samples displayed higher values of P_m compared to depth.

Originally, Harris (1980) identified a "fluorescence ratio" which was sensitive and displayed a vertical gradient under stratified conditions. More recently, a review has demonstrated the

potential of active fluorometry in linking turbulent mixing regimes to cell activity through adjustments in photo-physiology parameters associated with variable chlorophyll fluorescence (Oliver and Whittington, 1998). The chlorophyll fluorescence yield is a sensitive feature of phytoplankton to light and responds at time scales similar to those of turbulent mixing (Denman and Gargett, 1983). When a cell moves upwards from a sub-saturating photon flux, it will experience two concurrent processes (Reynolds, 1998). The greater bombardment of light harvesting complexes by photons, means that some now arrive to reaction centers that are still closed, while accumulation of PQH₂ in the PQ pool limits the reduction of Q_a and re-activation of the LHC's. The energy from the absorbed unused photons arriving at P680 is reradiated as chlorophyll fluorescence (figure 1.3). Conversely, a cell moving from high light to low light will receive less photon flux and reduced bombardment of photons at the reaction centers in PS2. The probability of the reaction centers being open increases as previous photons are utilized and the ETC is oxidized. Subsequently, the light energy is converted into chemical energy and there is less energy re-radiated as chlorophyll fluorescence. Consequently, the F_v/F_m of cells at each depth may vary depending upon the mixing time of the eddy. Moreover, the 'tracking' of the F_v/F_m feature of phytoplankton samples will enable the assessment of whether samples are entrained or disentrained and together with other photo-physiology measurements determine the photosynthetic rate of the phytoplankton.

1.5.2 Small-scale turbulence and phytoplankton

Recent research has indicated that turbulence may have profound ecological affects at small-scales as it does at large scales. There are essentially four interrelated areas including predator-prey interactions, particle aggregation/ disaggregation, small-scale patchiness and phytoplankton species-specific growth (Fogg, 1991). A European Union funded project titled 'NTAP' is currently investigating the nutrient dynamics mediated through turbulence and plankton interactions. Small-scale turbulence is associated with eddy sizes at the mm-Kolmogorov microscale, where turbulence is homogeneous. The term micro-scale turbulence has often been referred to and includes the processes on scales in the transition between turbulence and molecular diffusion and only covers the smallest scales of small-scale turbulence. In this study small-scale turbulence will refer to turbulence affects that are on individual phytoplankton cells.

Small-scale turbulence has been a relatively neglected factor in phytoplankton physiology, ecology and mass culture (Thomas and Gibson, 1990), despite advances in studies of phytoplankton-zooplankton interactions as a result of pioneering work by Rothschild and Osborn (1988). Although, there are a few empirical observations showing that turbulence can be important for the growth and survival of species (Savidge, 1981; Pollinger and Zemel, 1981). The degree to which the physical environment is experienced or 'felt' by a cell remains controversial (Hondzo and Lyn, 1999). Cells typically range in size from 10^{-6} to 10^{-4} m, which is smaller than the Kolmogorov scale of approximately 10^{-3} m in lakes and rivers (Reynolds, 1994a). Hence there is a gap between the scale of water motion and the size of the majority of species and it has been suggested that the Kolmogorov scale places an upper limit on the size of phytoplankton in general (Reynolds, 1998). However, the diffusion layer around each phytoplankton extends out to 10 times the radius of the cell (Lazier and Mann, 1989). It is therefore likely that strong levels of turbulence will affect larger phytoplankton. The velocity field in the vicinity of a cell would approximate a linear velocity gradient or shear varying randomly in time. The shear environment depends upon the turbulent kinetic energy dissipation rate and cell size, which will determine the length scales of the velocity gradients relevant to the cell. The shear is proportional to the rate of strain and represents the magnitude of the deformation rate due to mean velocity gradients.

The interactions between phytoplankton and small-scale turbulence are poorly understood. Low turbulent intensities have been reported to enhance the growth of phytoplankton, particularly diatom cultures through removing boundary layers and increasing nutrient uptake (Savidge, 1981), but moderate intensities have inhibited growth rates or caused cell damage and high intensities have caused mechanical damage (Thomas and Gibson, 1990). The sensitivity of phytoplankton appears to be species-specific with dinoflagellates being deleteriously affected and diatoms benefiting from increased turbulence, although a recent review indicated that turbulent shear generally decreases growth (Peters and Marrase, 2000). Peters and Marrase (2000) found that the statistical analysis within the literature review was highly biased due to the number of studies carried out on dinoflagellates (particularly marine species). If dinoflagellates were excluded from the statistical analysis, turbulence increased growth rates. Progress in the field will require the wider testing of small-scale turbulence on different phytoplankton species (Thomas *et al.*, 1997). Thomas and Gibson (1990) proposed a ranking of the sensitivity of different species to turbulence as dinoflagellates > diatoms > cyanobacteria > green algae, but this has not been

adequately assessed (Thomas *et al.*, 1997) and may or may not be consistent with seasonal pattern of phytoplankton succession.

A major challenge in assessing the affects of small-scale turbulence on phytoplankton is simulating conditions that are representative of the environment of phytoplankton. There currently exists a degree of uncertainty as to whether the deleterious affects of turbulence in laboratory results are realistic or whether the 'degrees of agitation' are excessive and would not occur under natural conditions (Peters and Marrasé, 2000). Furthermore, there is still considerable uncertainty as to the intensities of turbulence which organisms face under natural conditions (Peters and Marrasé, 2000), particularly in the surface layer. Further progress in the field will require greater characterization of the physical conditions of the environment and phytoplankton response at the same scales. A great deal has been learnt from measurements of turbulence in the ocean in terms of intensity and generating mechanisms, but more attention is needed in freshwater systems. Further complexity is added when considering freshwater systems, which are either constrained (e.g. shallow) and exposed to high wind forcing or water bodies which employ artificial mixing devices to stir the water column to improve water quality. Artificial mixing systems are widely installed to attempt to control cyanobacterial growth by inducing light-limitation, but the significance of small-scale shear through either growth inhibition, or increased nutrient uptake affects are unknown. Recent research is indicating that small-scale shear is significant in cyanobacterial ecology (Kucera, 1996; Paerl, 2000, Moisander *et al.*, 2002, O'Brien *et al.*, *in review*) and consequently artificial mixing may have not only large scale mixing affects through influencing the cell light climate, but also small-scale affects through shear stress.

Despite the numerous postulations involving physical damage and inhibition of physiological processes in relation to small-scale turbulence, few studies have measured the activity of enzymes (e.g. esterases) and/or quantified cell viability. Fluorescent stains in combination with flow cytometry offer the opportunity to assess the physiological condition of cells on an individual cell basis in real time. In chapter 5, the flow and turbulent intensities are characterized below and around several contrasting artificial mixing devices in the Myponga Reservoir and Torrens Lake in South Australia, while in chapter 6, the significance of small-scale shear in phytoplankton ecology is explored by investigating the effect of grid-generated turbulence on

Microcystis aeruginosa using cell growth, metabolic activity (esterase activity) and cell viability as biological responses.

1.6 Cyanobacteria, water quality and artificial mixing

Freshwater blooms consisting of cyanobacterial species continue to pose a problem to fisheries, drinking water supplies and recreational water bodies within Australia and around the world (Morse *et al.*, 1993; Heath, 1997). The major concerns of cyanobacterial blooms include undesirable tastes, odours and toxins in water supplies. Depending upon the type of toxin, human health effects range from minor skin irritations to gastroenteritis (Teixera *et al.*, 1993) to liver injury (Falconer *et al.*, 1994; Jochimsen *et al.*, 1998) and death (Teixera *et al.*, 1993). For water companies, there are also considerable costs to find alternative water supplies, install/ upgrade facilities and treat the problems associated with cyanobacteria. Freshwater and estuarine food webs can be negatively impacted due to poor palatability of toxic cyanobacterial strains (Lampert, 1987; Matveev *et al.*, 1994). It has been demonstrated that the selective feeding of zooplankton for eukaryotic phytoplankton, provides cyanobacteria with less competition and more nutrients, thus leading to a reduction in phytoplankton and zooplankton diversity (Nicholls, 1980).

Water column stability is recognized as a major factor favouring the growth of several 'bloom forming' cyanobacterial species, such as *Microcystis*, *Anabaena* and *Nodularia* (Ganf and Oliver, 1982; Visser, 1995). The development and persistence of thermal stratification in summer favours the growth of several (but not all) cyanobacterial species, which are able to regulate their buoyancy and poise themselves in optimal positions for light harvesting and nutrient acquisition. Conversely, non-motile species are unable to remain in the illuminated layers and sink leaving cyanobacteria with less competition for the remaining nutrients (Reynolds and Walsby, 1975; Paerl, 1988). The observations of seasonal succession and the strong negative correlation between bloom forming cyanobacteria and turbulent mixing in large water bodies have led to the development of techniques that either reverse or prevent the onset of thermal stratification by increasing the degree of mixing.

Artificial mixing is an in-reservoir technique that refers to the use of mechanical mixers or bubble plume aerators to add energy to a water body to break down existing stratification or prevent the

onset of stratification by creating turbulent conditions. The objective of cyanobacterial control using artificial mixing is to reduce the light dose received by the cyanobacterial population by increasing the $Z_{\text{mix}}:Z_{\text{eu}}$ ratio, thereby increasing their respiration: photosynthesis ratio. Additionally, increasing dissolved oxygen (DO) concentrations by reducing the density difference between the epilimnion and hypolimnion or by hypolimnetic oxygenation are also techniques aimed at reducing the carrying capacity of the water body by preventing nutrient release from sediments.

The relative success of artificial mixing depends on a number of factors such as the water quality problem (e.g. DO or cyanobacteria), nutrient/ light status of the phytoplankton, proposed mixing system, size and depth of the water body, trophic status and mixing rate. A review of 50 destratification projects in Australia found that only 24% were successful in improving total water quality (McAuliffe and Rosich, 1990). The review revealed that artificial mixing was the least successful in controlling phytoplankton, including cyanobacteria.

The response of phytoplankton communities to artificial mixing can be highly variable and attributable to multiple factors (Pastorok *et al.*, 1980) such as species composition, trophic status and mixing rate or duration. The different outcomes of the phytoplankton community in the literature can be categorised as: 1) a decrease in biomass including cyanobacteria (Steinberg, 1983; Rybak, 1985; Steinberg and Zimmerman, 1988; Steinberg and Tille-Backhaus, 1990; Daldorph, 1998; Simmons, 1998), 2) a reversal of seasonal succession in phytoplankton from cyanobacteria to green algae/ diatoms (Toetz, 1981; Reynolds *et al.*, 1983; Rybak, 1985; Hawkins and Griffiths, 1993), 3) an increase or persistence of cyanobacteria (Pastorok *et al.*, 1980) and 4) an increase or no change in biomass (Hawkins and Griffiths, 1993).

On the basis of artificial mixing experiments in Blelham Tarn, Reynolds *et al.* (1983) distinguished four groups of phytoplankton dependent upon their response to mixing: 1) favoured by mixing (*Asterionella*, *Fragilaria*, *Staurastrum*, *Oscillatoria*), 2) favoured by stability but whose increase stimulates zooplankton grazing (*Cryptomonas*, *Rhodomonas*, *Ankyra*), 3) abruptly reversed by deep episodes of deep mixing (*Sphaerocystis*, *Eudorina*) and 4) merely arrested by episodes of deep mixing (*Anabaena*, *Ceratium*, *Volvox*, *Microcystis*).

According to Visser *et al.* (1996), to be successful, artificial mixing must satisfy three conditions: 1) at least 80% of the water volume should be mixed, 2) the mixing rate must be higher than the vertical movement of cyanobacterial colonies and 3), a large part of water body must be sufficiently deep or mixing in shallow water bodies will be unable to induce light limitation (depth > 20 m). The degree of mixing experienced by the water column and the bearing this has on the growth of individual phytoplankton cells needs to be understood before one can accurately predict the response of the phytoplankton community to artificial mixing (McAuliffe and Rosich, 1990). According to the McAuliffe and Rosich (1990) review, there is a need to better understand: energy input and the movement of water, the movement of water and the movement of phytoplankton cells, the movement of cells and the amount of light they receive and the amount of light received and the effect on growth.

1.7 Lake management and project study sites

Presently, within Australia there is renewed interest in the study of biological components of inland waters. This stems from both increasing urbanization and the associated responsibilities of catchment authorities to assess change and improvements in aquatic systems and secondly the water industry is moving towards a multi-barrier approach to ensuring water quality. Regarding cyanobacteria, in-reservoir techniques, which either reduce nutrient supply or promote light limitation such as artificial mixing, are being explored to prevent the sole reliance on water treatment for removing cells and or toxins.

The management of lakes and reservoirs, and the application of techniques such as artificial mixing, requires an appreciation of the time and spatial scales at which external and internal physical, chemical and biological 'events' or processes occur and affect water quality. Temporal scales range from short (e.g. wind mixing with the surface mixed layer and cell entrainment/ photosynthesis) to sub-daily/ daily (e.g. rain events) to seasonal (e.g. water temperature) and to inter-annual (e.g. rainfall and internal nutrient load). Spatial scales range from microzones (e.g. cell boundary layers) to euphotic depths to the whole water body or entire catchment. Time scales relevant to cyanobacterial growth are the rate of change of nutrient supply and the rate of change of physical conditions. The requirements for growth are firstly that soluble nitrogen and filterable reactive phosphorus (FRP) exceed 0.1 and 0.01 mg L⁻¹, respectively (Sas, 1989) and secondly that there is sufficient light (Reynolds, 1984).

The Torrens Lake and the Myponga Reservoir are two water bodies in South Australia, which are vulnerable to cyanobacterial blooms and are the field sites within this project (figure 1.6). Artificial mixing systems have been installed in both water bodies without a full appreciation of the time scales of 'events' influencing cyanobacterial growth. The Torrens Lake (138° 35' E 34° 55' S) is a shallow urban artificial recreational lake adjacent to the central business district of Adelaide, South Australia. The Lake is fed by the River Torrens that drains the western Mount Lofty Ranges via six creeks and storm water draining the local urban catchment. The physical conditions ($Z_{\text{mix}} \sim Z_{\text{eu}}$) through late spring and summer are often suitable for cyanobacterial growth, but growth is suppressed by nutrient limitation. Summer rainfall replenishes nutrient supply ($\text{FRP} \gg 0.025 \text{ mg L}^{-1}$) and initiates the growth of the cyanobacterium, *Microcystis* (figure 1.7). In the 1998/99 and 2000/01 summers, rapid *Microcystis* growth occurred approximately one week after rainfall.

The Myponga Reservoir (138° 25' E 35° 24' S) is a large deep supply reservoir consisting of a main basin (35 m deep) and a long side arm (17 m deep). The Myponga Creek drains the surrounding rural catchment before entering the side arm. Seasonal winter rain (July to November) provides a suitable nutrient load ($\text{FRP} > 0.01 \text{ mg L}^{-1}$) for future phytoplankton growth in summer- January to March (Linden, 2000). Phytoplankton growth as represented by chlorophyll *a* follows a seasonal inverse relationship with FRP (figure 1.8). Cyanobacterial growth, specifically *Anabaena*, within the community is restricted due to the prevailing physical conditions during summer. For the majority of summer, Z_{mix} exceeds Z_{eu} and consequently the time *Anabaena* spends in light is insufficient to satisfy growth requirements (Lewis *et al.*, *in press*).

Cyanobacterial growth within the Torrens Lake and Myponga Reservoir results from events, which occur over different time scales. The Torrens Lake has the appropriate physical environment (sub/daily scale), but requires an injection of nutrients (daily scale) to initiate cyanobacterial growth. Conversely, the Myponga Reservoir has a favourable nutrient environment (seasonal scale) but rarely a favorable physical environment for cyanobacteria due to daily transport in the surface mixed layers.

The phytoplankton composition of shallow urban lakes is far less predictable compared to stratified temperate lakes, which undergo clear stages of seasonal succession (e.g. Reynolds, 1982). Meteorological forcing through rainfall and or wind mixing may constitute major disturbances to the community. For example, rainfall events and associated storm water runoff in summer may affect phytoplankton composition by flushing and diluting the populations, re-introducing nutrients, re-suspending nutrients from sediment, or by increasing turbulence levels and the depth of the mixed layer.

The reaction of the phytoplankton to a disturbance will depend upon the type of disturbance, its intensity, duration and frequency. Based upon Reynold's (1997) phytoplankton C-S-R life strategies, if the frequency of disturbances is high relative to the generation time of species, the lake will be more suited to C strategists, which can grow quickly and establish populations between perturbations (Sommer, 1981). For example, the greater the rate of flushing the more important it is for a phytoplankton to grow rapidly and colonise new habitat. Conversely, if the frequency of disturbance is low, S strategists will proliferate due to the constant conditions and gradual nutrient limitation. In both situations, phytoplankton diversity can remain low. If the disturbance is of insufficient intensity, duration or frequency to completely eliminate the existing phytoplankton, coexistence of C and S strategists may result leading to higher diversity. The intermediate disturbance hypothesis proposed by Connell (1978) attempts to explain the impact of disturbance on species composition and diversity. In chapter 7, the spatial and temporal heterogeneity of phytoplankton composition is investigated in the Torrens Lake within the summer season. An objective of the investigation was to explore the intermediate disturbance hypothesis in relation to phytoplankton composition within urban lakes.

“Understanding patterns in terms of processes that produce them is the essence of science” (Levin, 1992). Both pattern and process are wedded by scale, which has a characteristic magnitude either in space or time. To understand the behaviour of aquatic systems and specifically pelagic ecosystems requires an appreciation of the spatial and temporal interactions of organisms and the primary driving force, water motion. Physical processes give rise to patterns in the distribution of organisms and their access to resources and consequently their respective rates of change. Moreover, the water column with its interaction with atmospheric factors such as wind, solar radiation and rainfall introduces variability into the system. These may constitute a disturbance and depend upon the timing and or magnitude of the physical forces. The scales at

which phytoplankton respond are strongly influenced by physical processes. Species respond differentially at the biochemical and physiological time scale, which is reflected by variations in the growth of populations and leads to changes in the floristic composition of the community. Conversely, at the spatial scale, phytoplankton cells are either imbedded in turbulent motion or are governed by their own motion. The 'switch' between the two extremes is governed by the entrainment criterion. 'Phytoplankton and turbulence, at selected scales' examines the influence of turbulence on phytoplankton at the physiological scale in relation to the spatial scale of the surface mixed layer depth, the cell spatial scale through small-scale shear and the cell growth (generation) scale in relation to physical forcing and disturbance at the lake scale. Integrating physical and biological processes will further our understanding of aquatic systems.

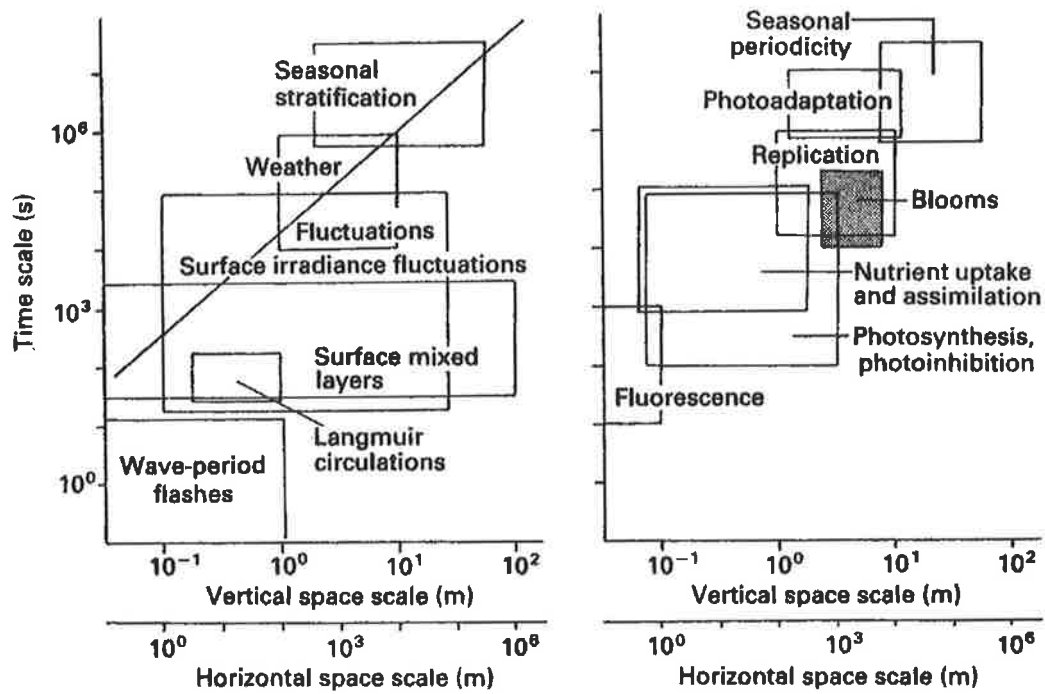


Figure 1.1 Time-space diagrams to a) define the scales of physical processes affecting phytoplankton and b) the levels of biological response (after, Reynolds 1994a, figure 6.1 page 144).

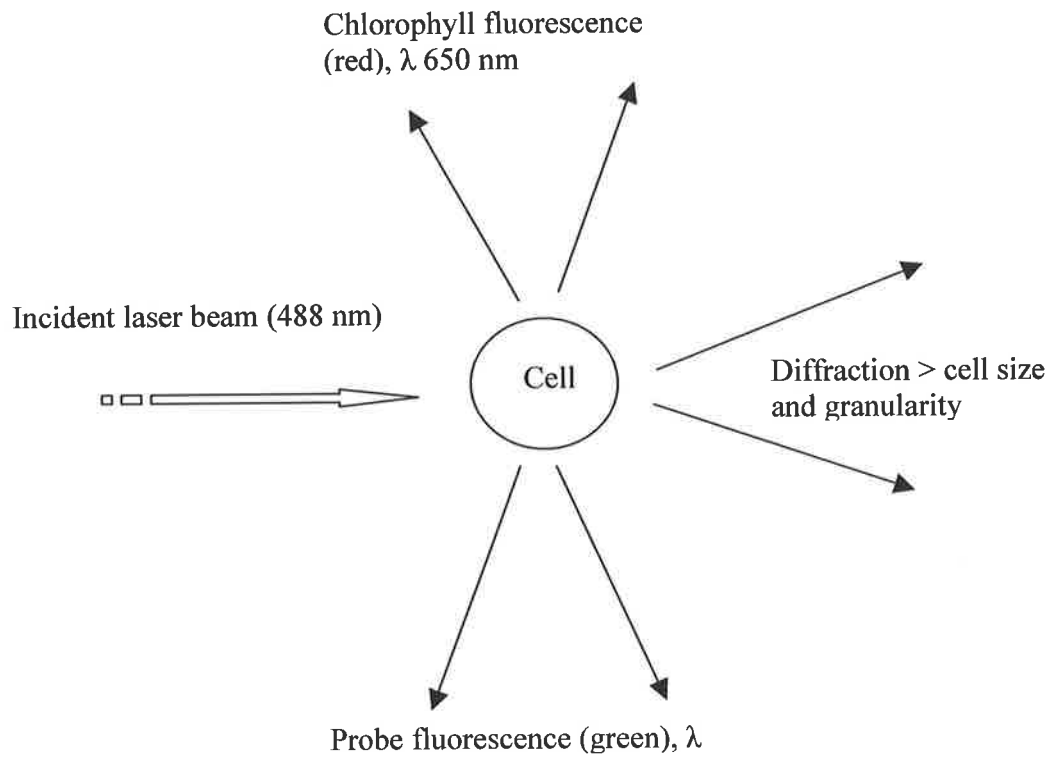


Figure 1.2 Interaction of a cell with a flow cytometer laser beam (adapted from Premazzi *et al.*, 1989; Arsenault *et al.*, 1993). Cells are passed through a laser beam and the resulting light scatter or fluorescence signals are detecting at a prescribed wavelength.

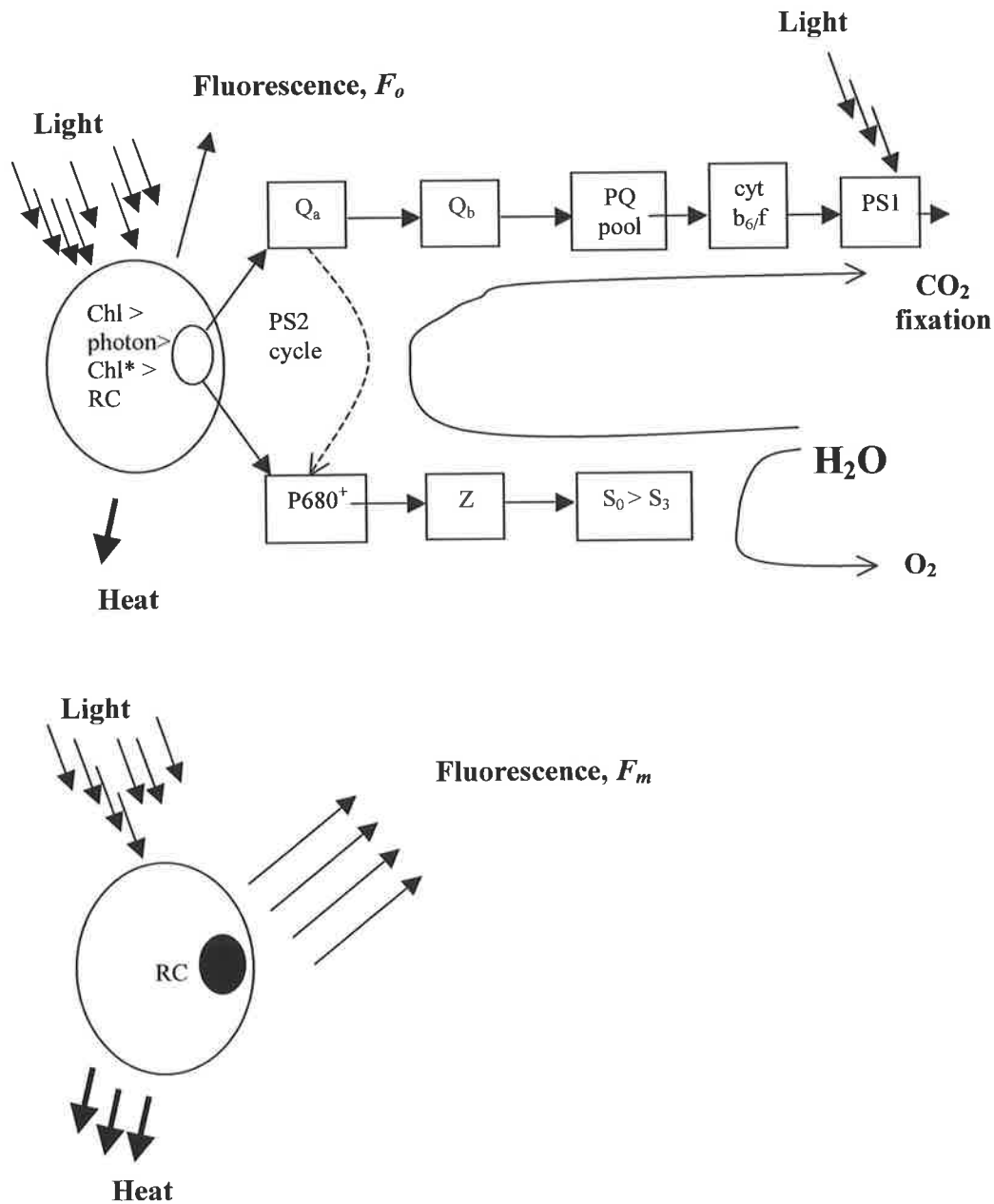


Figure 1.3 A simple model of the relationship between light, electron transport chain (ETC) and the variable yield of chlorophyll fluorescence (adapted from Kolber and Falkowski, 1993). Light energy absorbed by the antenna molecules of PS2 (P680), can be dissipated as photosynthesis, heat or fluorescence. When the ETC is oxidized (trap open, Q_a), minimum fluorescence (F_o) is measured. However, when the ETC is reduced (trap is shut, Q_a^-), maximum fluorescence (F_m) is obtained. The maximum quantum yield of photosystem 2, $F_v/F_m = (F_m - F_o) / F_m$.

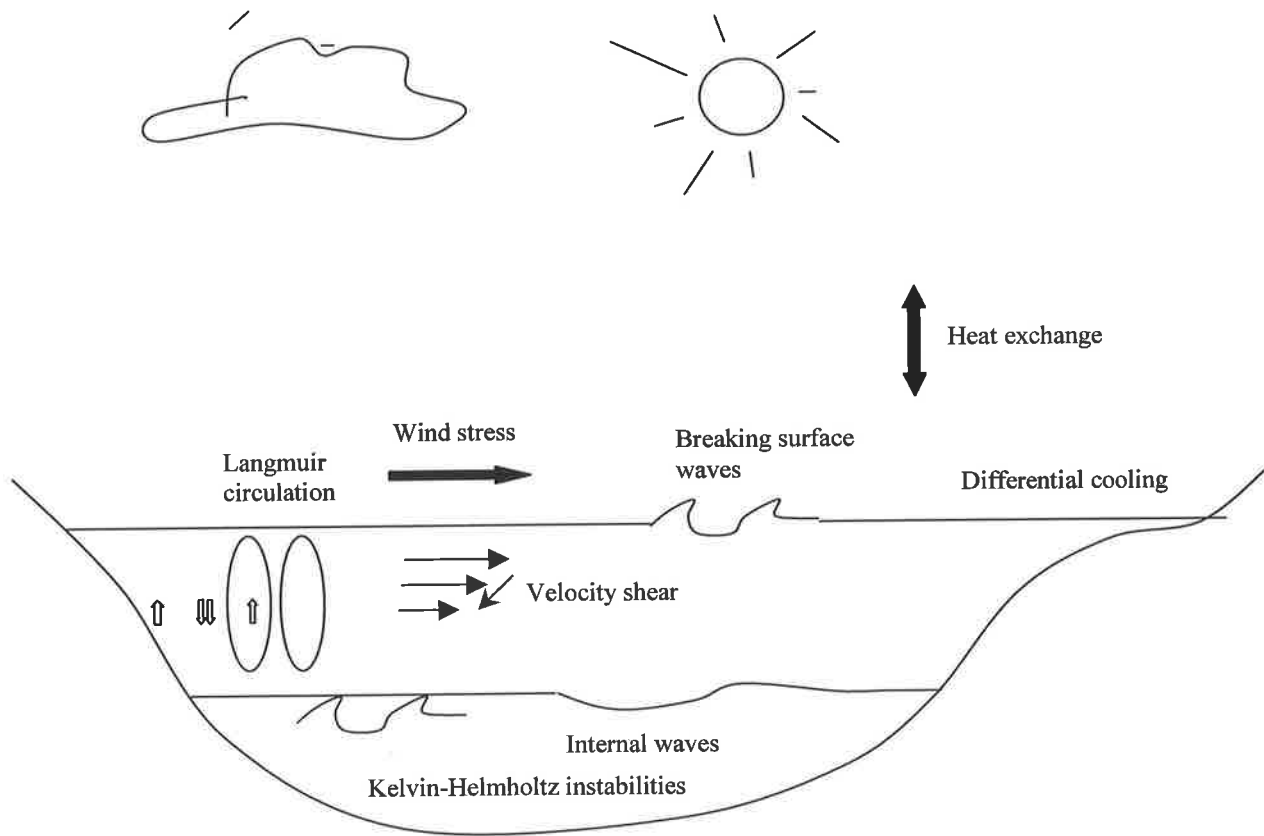


Figure 1.4 Sketch illustrating the most common turbulence sources and factors influencing turbulent intensity and extent (adapted from Spiegel and Imberger, 1987).

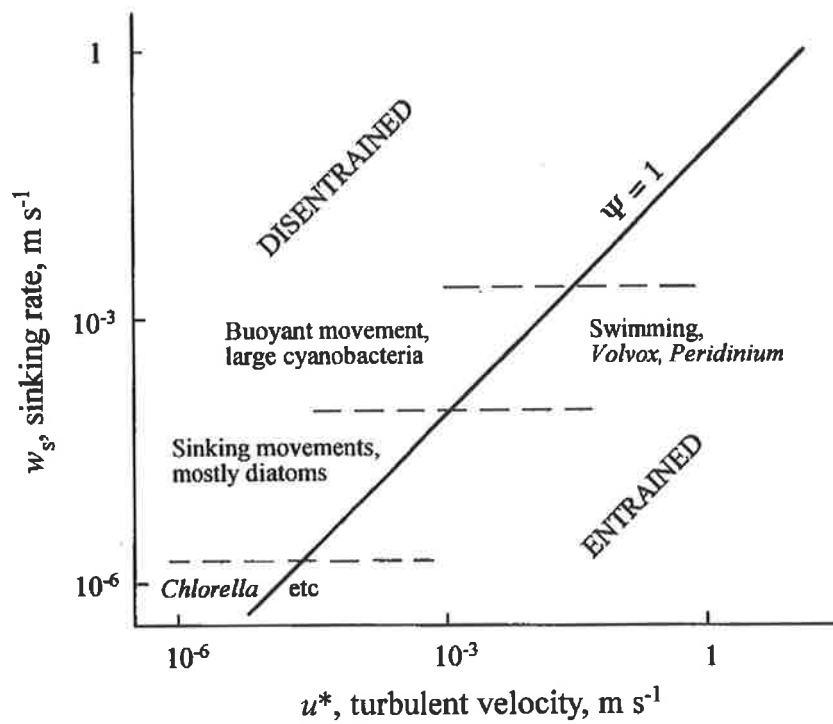


Figure 1.5 Conceptual model of the entrainment criterion for different kinds of phytoplankton (after Reynolds 1994a, figure 6.2a, page 153). When turbulent (shear) velocity (u^*) exceeds intrinsic velocity (w_s), the phytoplankton cells are entrained ($\psi < 1$). Conversely, if phytoplankton sinking or swimming speed exceeds turbulent velocity then the phytoplankton cells are disentrained ($\psi > 1$).

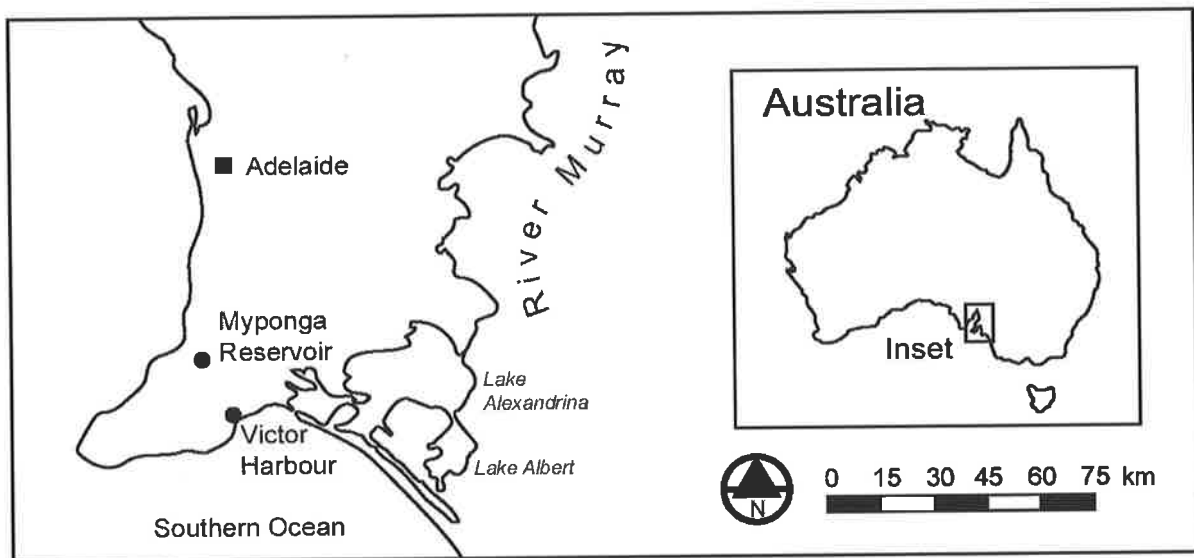


Figure 1.6 Location of project study sites, the Torrens Lake adjacent to the central business district of Adelaide and Myponga Reservoir.

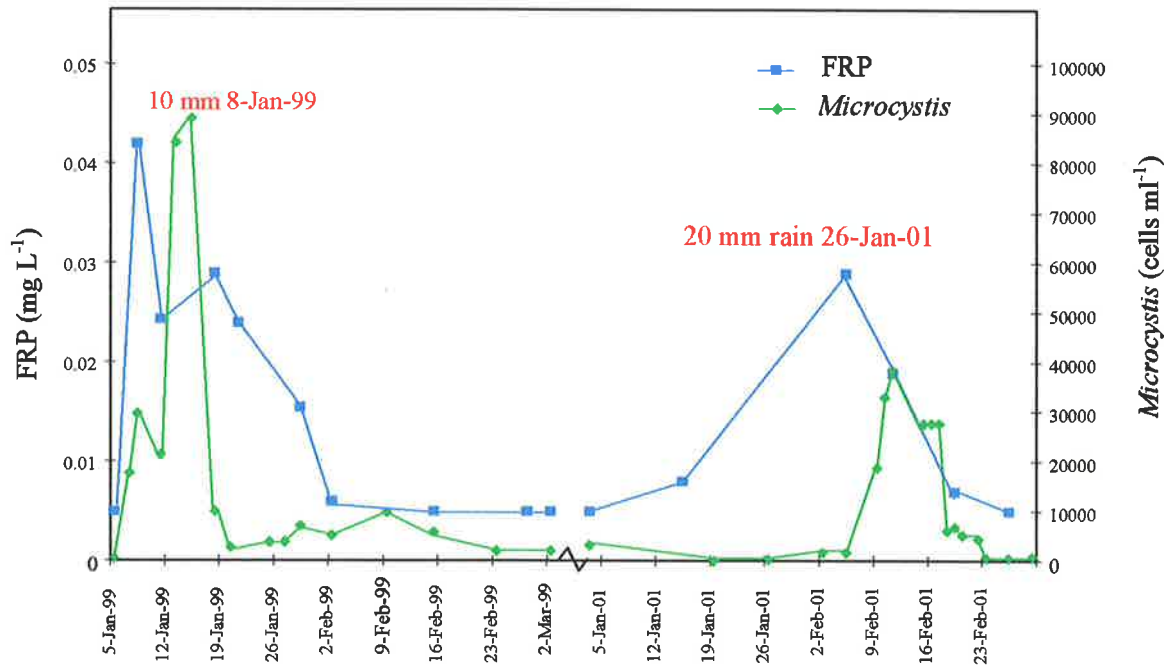


Figure 1.7 Variation in filterable reactive phosphorus (FRP) and *Microcystis aeruginosa* cell numbers in response to rainfall during 1998/99 and 2000/01 summers in the Torrens Lake, South Australia. Cyanobacterial growth occurred during periods of thermal stratification when $Z_{\text{mix}} < Z_{\text{eu}}$.

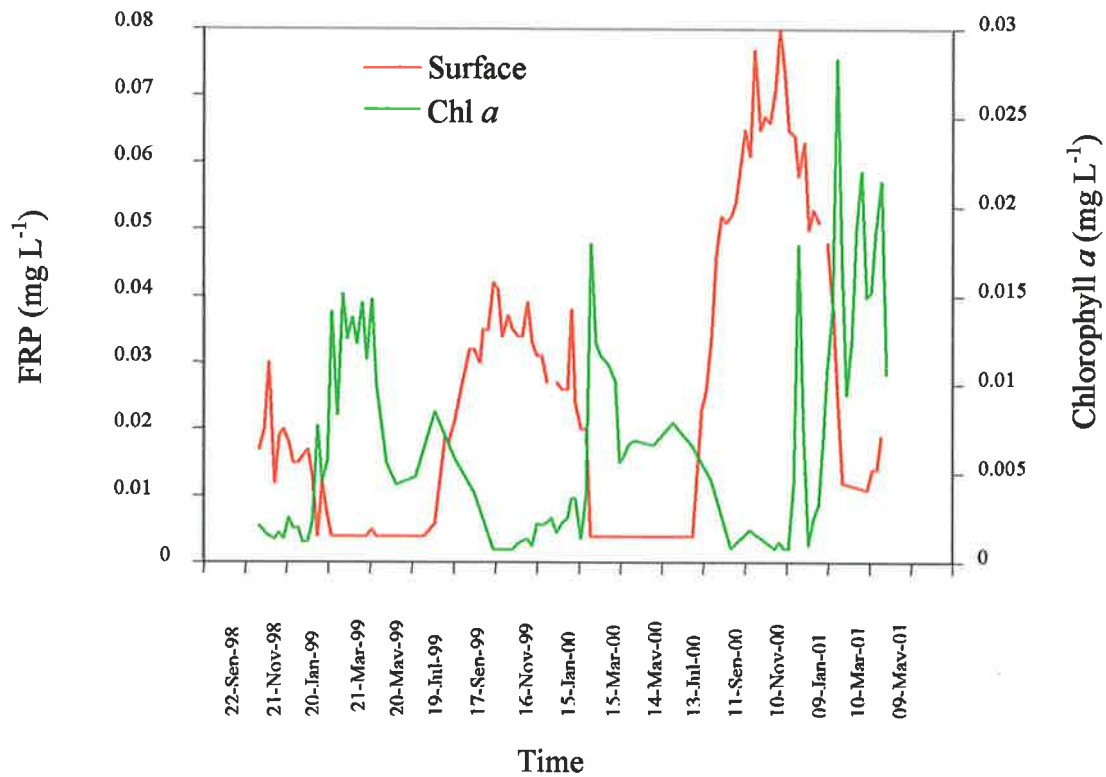


Figure 1.8 Seasonal variations in filterable reactive phosphorus, FRP and chlorophyll *a* concentrations in Myponga Reservoir, South Australia. Cyanobacterial growth within the phytoplankton population is restricted to one or two weeks per year when the surface mixed layer approximates the euphotic depth ($Z_{\text{mix}} \sim Z_{\text{eu}}$).

Chapter 2

Testing the procedural protocols – measurement of phytoplankton metabolic activity and viability

2.1 Introduction

Phytoplankton exhibit a wide range of scales of variability in both time and space. This variability can only be explained through an understanding of the interactions between different physical and biological processes. A requirement is the ability to sample and analyze the physical, chemical and biological components of lakes at appropriate time and space scales. Chemical and physical components can be readily and accurately measured and recorded using sensors (e.g. thermistors) and data loggers. However, the measurement of biological variables is far more difficult and often involves isolating phytoplankton from critical processes to which they are responding (Brookes *et al.*, 2000a).

The ultimate parameter for monitoring phytoplankton and their responses to environmental conditions is the *in situ* growth rate, as this integrates the numerous variables impacting on growth. However, growth rates and other population-based parameters such as cell yield and total chlorophyll *a* have several inherent limitations. Apart from problems associated with replication, speed of measurement, and ‘bottle effects’ they do not yield information on the immediate physiological activity or heterogeneity of responses within a population or community. Within a single population there is a large degree of heterogeneity (Yarmolinsky, 1995) and cells may be metabolically active, dying or dead. Quantification of population-based parameters may not detect simultaneous changes in growth and death, but assume the population is uniform in size and activity. Furthermore, there is increasing evidence that ‘automortality’ may be a significant process in population dynamics (Van Bleijswijk *et al.*, 1994; Brussard *et al.*, 1995; Agusti *et al.*, 1998; Berges and Falkowski, 1998; Veldhuis *et al.*, 2001).

Traditional methods of measuring primary productivity using inorganic carbon incorporation or O₂ production are also vexed by problems with temporal and spatial limitation, long incubation times and associated bottle effects. Measurements of photosynthesis and bioassays generally

involve the isolation and bottling of a phytoplankton sample and or filtration of the test solution to remove bacteria and debris. Long incubation times can cause pH drift due to phytoplankton metabolism (Nyholm and Kallqvist, 1989), alteration of synthetic media and release of heavy metal complexing organics (Xue and Sigg, 1990). These limitations are somewhat dependent upon current techniques. Microscopy is unsurpassed for species identification but there are drawbacks with speed and quantitative power. Furthermore, cell counts alone give no indication of the metabolic activity or vitality of individual cells. Cell counters may also be flawed because living cells, cell fragments, dead cells and other particles, which may have formed during an assay, interfere with the accuracy of measurement.

2.1.1 Fluorescent probes and flow cytometry

Advances in the fields of flow cytometry, fluorescent stain technology and active fluorometry offer the opportunity to develop biological sampling methodologies that can solve spatio-temporal variability and enable the more accurate assessment of phytoplankton dynamics including heterogeneity under different environmental conditions. Fluorescein diacetate (FDA) and Sytox green are two such fluorescent stains, which are useful in quantifying phytoplankton enzyme (esterase) activity and cell viability, respectively. FDA is a non-fluorescent substrate which diffuses freely into intact cells (Rotman and Papermaster, 1966) and once inside, ubiquitous esterases cleave the ester bonds producing fluorescent fluorescein. The fluorescein does not easily leak out of cells but increases over time depending upon the metabolic activity of esterases and substrate concentration. FDA conversion does not occur in dead cells, but maximum esterase activity and subsequently maximum fluorescence is evident in log-phase cell cultures (Bentley-Mowat, 1982), consequently the probe is useful in determining cell viability (Dorsey *et al.*, 1989).

The rate of FDA conversion to fluorescein is correlated with photosynthesis (Brookes *et al.*, 2000b) and nutrient limited growth (Brookes *et al.*, 2000a), which validates the use of the assay to assess the metabolic activity of phytoplankton cells (Dorsey *et al.*, 1989). The phytoplankton FDA assay has been used in aquatic toxicology (Arsenault *et al.*, 1993; Gala and Giesey, 1994; Leszczynska and Oleszkiewicz, 1996; Regel, 1997; Franklin *et al.*, 2001; Regel *et al.*, 2002) and studies into phytoplankton ecology (Geary *et al.*, 1997; Brookes *et al.*, 2000a, b), survivorship (Selvin *et al.*, 1989; Jochem, 1999) and cell lysis (Agusti and Duarte, 2000; Linden, 2000; Agusti

and Sanchez, 2002) studies.

Sytox green is a nucleic acid probe that only diffuses freely into cells with compromised membranes but will not cross membranes of living cells. The staining of nucleic acid results in green fluorescence of a high intensity and consequently non-viable fluorescent cells can be easily differentiated from viable, non-fluorescent cells. Sytox green has had limited use compared to FDA and has been applied to quantify viability in bacteria (Langsrud and Sundheim, 1996; Lebaron *et al.*, 1998) and in marine phytoplankton (Veldhuis *et al.*, 1997; Veldhuis *et al.*, 2001; Brussard *et al.*, 2001).

The applications of FDA (Dorsey *et al.*, 1989; Minier *et al.*, 1993; Selvin *et al.*, 1989; Agusti and Duarte, 2000, Agusti and Sanchez (2002) and Sytox green (Veldhuis *et al.*, 1997, Veldhuis *et al.*, 2001; Brussard *et al.*, 2001) assays have predominantly focused on marine phytoplankton and other marine organisms (Cachot *et al.*, 1994; Moffat and Snell, 1995) and have been used sparingly in the study of freshwater phytoplankton. Progress in the field will require development of protocols and greater application of fluorescent probe techniques to freshwater phytoplankton and under different environmental conditions. There exist a number of published techniques for staining phytoplankton with FDA (Dorsey *et al.*, 1989; Geary *et al.*, 1997; Franklin *et al.*, 2001) and Sytox green (Veldhuis *et al.*, 2001), but each species requires well-defined protocols such as stain concentration and loading time to ensure optimal measurement of the response to the environmental condition.

Cell fluorescence whether due to fluorescein or Sytox can be easily detected using either epifluorescence microscopy (Bentley-Mowat, 1982) or flow cytometry (Regel, 1997; Geary *et al.*, 1997; Brookes *et al.*, 2000a, b; Regel *et al.*, 2002). As discussed in several reviews (Premazzi *et al.*, 1989; Maftah *et al.*, 1993; Reckermann and Colijn, 2000 and references therein; Brookes *et al.*, 2002) flow cytometry has a number of attributes such as being able to rapidly and accurately measure the fluorescence and morphological characteristics of cells simultaneously and on an individual basis.

2.1.2 Fluorometry and variable fluorescence

Active PAM fluorometry (Schreiber *et al.*, 1994) involves probing phytoplankton with defined light intensities and measuring the chlorophyll fluorescence yield (response). The yield of chlorophyll fluorescence is sensitive and variable in intact cells and depends on their history and environment. The yield provides information on the major processes in light capture and electron transport including photosynthetic efficiency (F_v/F_m), photochemical quenching, and effective absorption cross-section. In combination, the parameters provide an estimate of photosynthesis (Kolber and Falkowski, 1993). The major advantages of the technique are that measurements can be undertaken quickly (< 2 min sample⁻¹), no incubation time is required and the technique is non-invasive. F_v/F_m has been widely used in a range of species and responds rapidly to fluctuations in the light field and less dramatically to the nutrient field (Geider *et al.*, 1993; La Roche *et al.*, 1993; Kolber and Falkowski, 1993; Ibelings *et al.*, 1994; Greene *et al.*, 1994; Falkowski and Kolber, 1995; Schubert *et al.*, 1995; Oliver and Whittington, 1998; Lippemeier *et al.*, 1999; Beardall *et al.*, 2001a; Parkhill *et al.*, 2001; Bergman *et al.*, 2002; Villareal and Morton, 2002).

2.1.3 Objectives

The primary purpose of this study was to ensure that a good understanding of the procedures involved in the methods of fluorescent stains and fluorometry was obtained for application in later chapters. The study consisted of two components. The first component involved the further development and testing of the FDA and Sytox green probe-flow cytometer assays on freshwater phytoplankton to ensure that they could be used confidently to determine cell metabolic activity and viability, respectively. FDA was chosen as the metabolic stain because of its fast absorbency into cells, low cost and green emission fluorescence, which does not interfere with chlorophyll *a* red auto fluorescence. Similarly, Sytox green was chosen as the cell viability stain due to its green fluorescence emission spectrum. The first aim was to optimise the staining protocols for each probe by adjusting stain concentrations and stain-cell loading times. The second aim was to determine whether or not the two stains demonstrate a response that is consistent with reduced metabolic activity and death. To address this question, the dyes were used to measure metabolic activity and viability of phytoplankton cultures subject to death (heat treatment), nutrient depletion / repletion and copper toxicity. An additional aim was to ascertain the time for a

response to occur as a result of these treatments.

The second component of this chapter involved investigation into the usefulness of photochemistry parameters as tracers in linking biological and physical processes at relevant time scales. Using active PAM fluorometry, a number of experiments involving both field populations and laboratory-cultured phytoplankton were carried out to assess the affect of light intensity and nutrients on photochemical quenching, maximum change in quantum yield and effective absorption cross-section. The final aim was to outline the use of PAM fluorometry in combination with an integral photosynthesis model (Walsby, 1997) in determining primary production within a water column, at an appropriate temporal and spatial resolution for vertical mixing studies.

2.2 Experimental designs and methods

2.2.1 Phytoplankton cultures

All phytoplankton species used in either of the flow cytometry or PAM fluorometry experiments were maintained as batch cultures using WC media (Guillard and Lorenzen, 1972). Stock cultures were generally grown in 250 mL Erlenmeyer flasks, containing 150 mL of media and maintained in exponential growth phase at 22 °C and $50 \mu\text{mol m}^{-2} \text{s}^{-1}$ with a light dark cycle of 12:12 hours, unless otherwise indicated. All glassware was acid washed. Seven freshwater species were used in the development of probe assays. *Anabaena circinalis* (strain 271 B) *Microcystis aeruginosa* (strain Mash01), *Chlorella pyrenoidosa*, *Chlamydomonas reinhardtii* and *Selenastrum capricornutum* were obtained from the Australian Water Quality Centre collection, Adelaide, Australia. *Scenedesmus quadricauda* (strain UTEX) was originally obtained from the University of Austin collection, Texas, USA. *Aulocoseira granulata* was obtained from the Murray Darling Basin Research Centre, Albury, Australia. Silica was added at 45.4 mg L^{-1} to WC media for the maintenance of *Aulocoseira* cultures. *Anabaena circinalis* (strain 271B), *Microcystis aeruginosa* (strain Mash01), *Chlorella pyrenoidosa* and *Aulocoseira granulata* were used for the PAM fluorometry experiments.

2.2.2 Probe assay development

2.2.2.1 Flow cytometry

A FACStrak flow cytometer, FCM (Becton Dickinson) equipped with a 15-mW, 488 nm air-cooled argon ion laser and 70 μm nozzle was used to measure phytoplankton cells fluorescence and light scatter characteristics. Operation involves a sample being channeled into a narrow laminar stream of sheath fluid that carries the cells in single file at high speed. The cells cross the laser beam and short flashes of their fluorescence and of their scattered light refractivity are cast through a system of filters onto photo-multipliers (PMT) and photo-iododes. Fluorescein and Sytox green fluorescence was measured in channel 1 (FL1, 530 nm) and short pass filters separated green fluorescence from the red fluorescence of chlorophyll a in channel 2 (FL2, 630 nm).

The FCM was interfaced with a Hewlett Packard 9000 series computer with LYSIS II software (Becton Dickinson). Phytoplankton cells were distinguished from other particles by gating on two-parameter plots of forward scatter (FSC) versus positive chlorophyll fluorescence (FL2). The photo-multiplier tube (PMT) voltage of FL1 was adjusted to obtain sufficient probe fluorescence for each species. Approximately 1500 events over a period of 30 seconds (depending upon cell concentration) were recorded with the FCM.

Probe fluorescence, chlorophyll fluorescence, forward scatter (cell size) and side scatter (cell granularity) data were collected and displayed in logarithmic one-dimensional histograms. The 'HSTATS' mode was used to obtain mean values of the histograms. In addition to mean values, the percentage of cells falling into marker defined 'states' were recorded for probe fluorescence histograms. Markers were applied to histograms to define either 'metabolic' states associated with fluorescein diacetate or nonviable/ viable states associated with Sytox green (see below).

2.2.2.2 Fluorescein diacetate staining and esterase activity

Kinetic stains such as FDA require defined concentrations and staining times with cells to minimise error during flow cytometric measurement. For each phytoplankton species, the staining protocol involved optimizing the FDA incubation time and final concentration with cells.

The incubation time and concentration was determined by manipulating the FDA incubation time and stock concentration in the protocol developed by Geary *et al.* (1997). Incubation times of 1-60 minutes and final FDA concentrations of 1, 10, 40 μM were tested. FDA ($\text{C}_{24}\text{H}_{11}\text{O}_7$) stock solutions were prepared by dissolving FDA, (Sigma, Cat. No. F-7378) in reagent grade acetone and maintained in darkness at $-20\text{ }^\circ\text{C}$. Stock solutions were made on the day of measurement. Working solutions were prepared by adding 40 μL of stock solution to 10 mL of deionised water and were discarded after 30 minutes to prevent flocculation. Esterase activity was determined by adding 300 μL of FDA working solution to 400 μL of the phytoplankton sample in a Falcon polystyrene tube (12 x 75 mm) and maintained at room temperature prior to flow cytometric measurement. Final FDA concentrations were varied by manipulation of the volumes of FDA working solutions to algal solution.

Esterase activity was interpreted as the mean rate of FDA conversion to fluorescein, FDAC ($\text{cell}^{-1}\text{min}^{-1}$), calculated by dividing the mean fluorescence of cells by the incubation time. In addition, esterase activity states were defined on the basis of fluorescein fluorescence histograms. Three states were defined: a low activity state, $S1_{\text{fda}}$, corresponded to the activity of heat treated cells (microwaved for 90 s), a normal state, $S2_{\text{fda}}$, corresponded to the activity distribution of an exponentially growing population in WC media and a stimulated activity state, $S3_{\text{fda}}$, corresponded to activity above the normal range.

2.2.2.3 Sytox staining and cell viability

The Sytox green nucleic acid stain ($\text{C}_2\text{H}_6\text{OS}$, Molecular probes, S-7020) was used to determine the percentage of viable to nonviable cells in a sample. Protocol development involved optimizing dye incubation time and concentration. Incubation times of 1-60 minutes and final Sytox concentrations of 0.1, 1.0 and 10 μM were tested. The supplied Sytox was diluted in DMSO to a final stock concentration of 100 μM and stored in darkness at $-20\text{ }^\circ\text{C}$. The stock solution was diluted in deionised water to give a working solution of Sytox at 50 μM . Cell viability was determined by adding small volumes ($<0.1\text{ mL}$) of the working solution to approximately 1 mL of algal sample (depending on desired concentration) in a Falcon polystyrene tube (12 x 75 mm) and maintained in darkness at room temperature prior to flow cytometric measurement. For example, a final concentration of 1 μM was achieved by adding 0.02 mL of Sytox to 0.98 mL of algal solution.

The number of viable or dead cells was interpreted as the percentage of cells falling into the viable or nonviable state, $S1_{\text{syt}}$ and $S2_{\text{syt}}$, respectively. These two states were defined from Sytox fluorescence histograms using the marker function in the HSTATS mode of the flow cytometer. The viable state, $S1_{\text{syt}}$ was defined from the Sytox fluorescence histogram of a normal exponentially growing sample in WC media, the nonviable state, $S2_{\text{syt}}$ was defined from a Sytox fluorescence histogram of heat-treated cells (microwaved for 90 s) which gave maximum fluorescence emission.

A comparison between the percentages of cells in $S2_{\text{syt}}$ from the Sytox assay versus the percentage of cells in $S1_{\text{fda}}$ from the FDA assay allows evaluation of whether or not the two techniques compliment each other.

2.2.3 Microscopy

Microscopy was undertaken to confirm whether or not FDA and Sytox penetrated living and dead cells, respectively. An Olympus BX 51 microscope fitted with a reflective fluorescence systems, BX RFA and Olympus DP/10 digital camera was used in combination with an Olympus fluorescence mirror unit, UMWIB 2 consisting of an excitation wavelength of 460-490 nm and a barrier filter of 510 nm to measure probe fluorescence. In other experiments, cell counts and growth rates were determined after preservation with Lugol's iodine, using either a Neubauer haemocytometer, or a Sedgewick Rafter cell and a Zeiss microscope.

2.2.4 Testing probe assays

2.2.4.1 Estimation of the number of viable and nonviable cells in a population

To evaluate the ability of Sytox and FDA to differentiate between viable and dead cells within a population, the optimized protocols for each species were applied to pre-determined combinations of viable and nonviable cells with ratios ranging from 0:100. Species used as test organisms included *Scenedesmus*, *Anabaena* and *Microcystis*. Nonviable cells were prepared by heating an exponentially growing culture in a microwave for 5 minutes. The culture was allowed

to cool to room temperature before being mixed with a viable/ normal population of the respective species to achieve the desired ratio.

2.2.4.2 Detection of nutrient limitation and repletion

To determine whether or not the two probes demonstrate a response that is consistent with reduced metabolic activity and or death as a result of nutrient limitation, *Microcystis* was grown in batch cultures of WC media without nitrogen (N), phosphorus (P) or nitrogen and phosphorus (N, P) under optimal light conditions ($80 \mu\text{mol m}^{-2} \text{s}^{-1}$). It was postulated that in batch cultures starved of an essential nutrient, *Microcystis* would firstly respond physiologically by decreasing esterase activity (reduced fluorescein fluorescence) followed by a decrease in cell growth eventually leading to cell death (increased Sytox fluorescence). Conversely, replenishment of the limiting nutrient would enable esterase activity to recover and the cell to continue with growth until further nutrient limitation. An aliquot from a culture was washed 3 times with N free, P free or N and P free WC media and placed back into WC media deplete of the relevant nutrient(s) [N, P or N & P]. Final cell concentration after washing approximated 1×10^4 cells mL^{-1} . The experiments were performed in batch culture, and therefore the initial concentrations were depleted with time – inducing nutrient limitation over 19 days. The cells were starved of key nutrients for 19 days. After 19 days, N and P and C were spiked to the nutrient deplete cultures. Esterase activity, viability, chlorophyll fluorescence, FSC, SSC, F'_v/F'_m (see 2.3.1.b) and cell growth were monitored during the limitation and replenishment of nutrients for a total of 27 days.

2.2.4.3 Detection of copper toxicity

To assess the ability of FDA and Sytox to detect chronic and lethal toxicity, *Scenedesmus* was exposed to various concentrations of copper. It was postulated that if copper is toxic to *Scenedesmus*, cell esterase activity will firstly decrease and if it causes mortality the number of nonviable cells will increase as detected by an increase in the number of cells in $S2_{\text{syt}}$. Copper was chosen as a reference toxicant as it is one of the most common pollutants from urban, industrial and mining inputs into aquatic ecosystems (Guanzon *et al.*, 1994). The experiment involved placing a 4 mL aliquot of an exponentially growing *Scenedesmus* stock culture into fresh WC media (50 mL) with the addition of copper sulfate, in a 100 mL conical flask. EDTA was excluded from the WC media. Copper sulfate concentrations tested included 0.01, 0.1, 0.5, 2,

and 5 mg L⁻¹ and the control consisted of WC media. The initial and final pH was measured and was found not to vary beyond 6.5-7 units. The flasks were maintained in a constant temperature (21 °C) and light (45-50 μmol m⁻² s⁻¹) controlled room, with a light dark cycle of 12:12 h. The bioassay was run for 72 hours and measurements of cell esterase activity and viability and cell counts were taken at 1, 24, 48 and 72 hours.

2.2.5 PAM fluorometry and phytoplankton photo-physiology

A Walz Xenon Pulse Amplitude Modulated (Xe-PAM with BG39 excitation filter, R65 and RG645 emission filters, Walz, Effeltrich, Germany) fluorometer was used to measure photochemistry characteristics throughout the study. The PAM fluorometry technique involves probing the status of the photo-system using a pulsed beam of light and higher intensities of light, which can saturate the photo-system. The weak flash provides enough photons only to enable minimum photochemistry and does not change the state of PS2. When the cells have been dark-adapted, the photochemical quenching is maximal and consequently the light pulse only induces a minimum fluorescence signal (F_o). The proportion of shut traps can be increased by pre-conditioning cells with a flash of light before the response to the weak light. By increasing the preconditioning flash intensity the number of shut traps is increased giving fluorescence F , until photochemical quenching is minimal ($q_p = 0$) and fluorescence reaches a maximum (F_m). The maximum fluorescence was measured when all reaction centers were closed following a 600 ms pulse of saturating light (Schreiber *et al.*, 1986). A summary of the nomenclature used throughout the thesis for fluorometry measurements is provided in table 2.1, following Van Kooten and Snel (1990).

2.2.5.1 Photochemical quenching (q_p)

Photochemical quenching (q_p) was determined from the change in yield of probe flashes preceding and following a saturating pump flash at any ambient light intensity (figure 2.1). Photochemical quenching was calculated using:

$$q_p = (F'_m - F) / (F'_m - F'_o) \quad (1)$$

where F'_o is the fluorescent signal in background (actinic light). F'_m is the maximum fluorescent

Table 2.1 A summary of the photochemistry nomenclature used throughout the thesis. Adapted from Van Kooten and Snel (1990).

Symbol	Parameter	Definition
<i>Fluorescence intensity indicators</i>		
F	Fluorescence intensity	Fluorescence intensity at any time under any conditions.
F_o	Minimum fluorescence (dark)	Fluorescence intensity with all reaction centers of PS2 open in a dark or low light adapted state ($q_P = 1$ and $q_N = 0$).
F_m	Maximum fluorescence (dark)	Fluorescence intensity with all reaction centers of PS2 closed ($q_P = 1$ and $q_N = 0$) in a dark or low light adapted state.
F'_o	Minimal fluorescence (light)	Fluorescence intensity with all reaction centers of PS2 open in any light adapted state, when $q_P = 0$ and $q_N \geq 0$.
F'_m	Maximum fluorescence (light)	Fluorescence intensity with all reaction centers of PS2 closed in any light adapted state, when $q_P = 0$ and $q_N \geq 0$.
F_v	Variable fluorescence (dark)	Maximum variable fluorescence in the state when all non-photochemical processes are at a minimum ($F_m - F_o$).
F'_v	Variable fluorescence (light)	Maximum variable fluorescence in any light adapted state ($F'_m - F'_o$).
F_v/F_m	Maximum photosynthetic efficiency (dark)	Maximum quantum yield of PS2 when all non-photochemical processes are at a minimum ($F_m - F_o$)/ F_m .
F'_v/F'_m	Photosynthetic efficiency (light)	Maximum quantum yield of PS2 in any light adapted state ($F'_m - F'_o$)/ F'_m .
<i>Fluorescence quenching parameters</i>		
q_P	Photochemical quenching	$(F'_m - F)/(F'_m - F'_o)$
q_N	Non-photochemical quenching	$1 - (F'_m - F'_o)/(F_m - F_o)$

signal by the saturating flash and is measured in conjunction with a conditioning flash of sufficient intensity to saturate and close all the open reaction centers so that photochemical quenching is at a minimum. F is the variable fluorescence stimulated by the weak probe when the sample is under continuous actinic irradiance (the proportion of closed reaction centers depends on the intensity of actinic light), preceding the pump flash.

Unfortunately, the degree of non-photochemical quenching (q_N) was not measured due to limitations with the set up and lack of a far red light source with the PAM fluorometer.

2.2.5.2 The maximum quantum yield of photosystem 2 (F_v/F_m)

To measure the maximum change quantum yield (often referred to as the potential yield or the variable to maximum fluorescence), the phytoplankton sample was dark adapted for 15 minutes before analysis. After dark adaptation, the cells were subjected to a weak probe flash to induce F_o , preceding a saturating flash to induce F_m . The maximum quantum yield was calculating using:

$$F_v/F_m \text{ (dark-adapted)} = (F_m - F_o) / F_m \quad (2)$$

When the phytoplankton sample is removed from ambient irradiance conditions or has been exposed to light the maximum change quantum yield is said to be light-adapted (i.e. *in situ* sampling)

$$F'_v/F'_m \text{ (light-adapted)} = (F'_m - F'_o) / F'_m \quad (3)$$

where F'_o is the fluorescence intensity with all reaction centers of PS2 open in any light adapted state, and $q_P = 0$ and $q_N = 0$. F'_m is the fluorescence intensity with all reaction centers of PS2 closed in any light adapted state $q_P = 0$ and $q_N \geq 0$.

2.2.5.3 Effective absorption cross-section (σ_{ps2})

The effective absorption cross-section of photo-system 2 (PS2) reaction centers was measured using the PAM fluorometer with single turnover excitation flashes controlled by a series of

neutral density filters. σ_{ps2} was measured by the pump and probe method by gradually increasing the intensity of the pump flash and following the flash- intensity saturation curve of variable fluorescence (F_v). The saturation curve fits a cumulative single hit Poisson function (Falkowski and Kolber, 1995):

$$(F - F_o) / (F_m - F_o) = 1 - e^{-\sigma I} \quad (4)$$

where I is the flash intensity in quanta $^{-2}$ flash $^{-1}$ and σ is the effective absorption cross section in \AA^{-2} quanta $^{-1}$, F_o is the fluorescence yield preceding the pump flash of light energy I and F is the fluorescence yield following the pump flash. Flash intensity was increased step wise from 0.000576 to 0.064816 mol m^{-2} s^{-1} . The absorption cross section was determined by solving the Poisson distribution model using JMP Inc. software.

2.2.5.4 Photosynthetic rate

For any phytoplankton sample, determination of photosynthetic rate (P) using PAM fluorometry was based on combining the measurements of q_p , F_v/F_m and absorption cross section using an equation proposed by Falkowski and Kolber (1993)

$$P = I \sigma q_p (F_v/F_m / 0.65) \Phi \eta_{ps2} \quad (5)$$

where P is the photosynthetic rate (mol O_2 mol $\text{chl}a^{-1}$ h^{-1}), I is the light intensity (mol photons m^{-2} h^{-1}), σ is the effective absorption cross section (m^2 mol quanta $^{-1}$), $F_v/F_m / 0.65$ = fraction of effective reaction centres, Φ = mol of O_2 evolved per photon processed by the reaction centers and was assumed to be constant at 0.25 mol e mol photons $^{-1}$ (Kolber and Falkowski, 1995) and η_{ps2} is the number of photons processed per mol of $\text{Ch}la$ and was assumed to be constant at 545 $^{-1}$ for eukaryotes (Oliver and Whittington, 1998) and 345 $^{-1}$ for cyanobacteria (Kolber and Falkowski, 1993). The equation is applicable to all light intensities experienced by phytoplankton (Kolber and Falkowski, 1993). A combination of filters in conjunction with the fluorometer actinic light source were used to generate a range of I from 29.5 to 1840 $\mu\text{mol m}^{-2}$ s^{-1} and F_v/F_m was measured at each light intensity.

2.2.6 Influence of light intensity and nutrients on photo-physiology

To investigate the affect of light intensity on phytoplankton photo-physiology, *Microcystis* was grown at a range of light intensities (10, 25, 50, 75, 125 and 250 $\mu\text{mol m}^{-2} \text{s}^{-1}$) for 6 days in nutrient replete WC media. The experiment was carried out in triplicate in a temperature (25 °C) controlled room with a light dark cycle of 12:12 h. Initial stock cultures of *Microcystis* were grown at 50 $\mu\text{mol m}^{-2} \text{s}^{-1}$ and were in exponential growth phase. Photochemical quenching (q_p), the maximum quantum yield (F'_{ν}/F'_m), the effective absorption cross-section (σ) and cell growth were monitored daily.

A similar experiment examined the affect of three light intensities (10, 100 and 400 $\mu\text{mol m}^{-2} \text{s}^{-1}$) on *Chlorella pyrenoidosa*, *Aulocoseira granulata* and *Anabaena circinalis* photo-physiology. The three species were grown in WC media and placed at the three light intensities in triplicate for 5 days at a temperature of 25 °C with a light dark cycle 12:12 hours. F'_{ν}/F'_m and σ were measured on day 5 for each of the species.

To investigate the effects of nutrients on phytoplankton photo-physiology, *Microcystis* was used as a test organism and was firstly grown in N-deplete WC media with various nitrate additions (0, 2, 5, 10, 25, 50 and 100 μM and secondly subjected to N, P and N/P depletion and repletion. For the first nitrate limitation experiment an exponentially growing stock culture was washed 3 times with N-deplete WC media prior to being added to fresh WC media with various nitrate additions. The experiment was carried out in triplicate in a controlled light (50 $\mu\text{mol m}^{-2} \text{s}^{-1}$) and temperature (25 °C) room. For details of the nutrient depletion/ repletion experiment, refer to the 'detection of nutrient limitation/ repletion experiment' (2.2.4.2).

2.2.7 F'_{ν}/F'_m depression and recovery kinetics

Two experiments were conducted using *Anabaena circinalis* to investigate the effect of light intensity and duration of exposure on F'_{ν}/F'_m kinetics. The first experiment involved using *Anabaena* grown in batch culture at a light intensity of 20 $\mu\text{mol m}^{-2} \text{s}^{-1}$, exposing it to a range of light intensities (0, 120, 250, 350, 570 and 1500 $\mu\text{mol m}^{-2} \text{s}^{-1}$) for 20 minutes. The light intensities were obtained using the PAM fluorometer actinic light source. F'_{ν}/F'_m was measured before,

during, and after exposure to each light intensity. The second experiment involved subjecting *Anabaena* to a light intensity of $1500 \mu\text{mol m}^{-2} \text{s}^{-1}$ for either 5, 20, 30 or 60 minutes before being returned to conditions of $20 \mu\text{mol m}^{-2} \text{s}^{-1}$ of light. F'_v/F'_m was measured 10 minutes before, during, and up to 30 minutes after exposure to $1500 \mu\text{mol m}^{-2} \text{s}^{-1}$.

2.2.8 Measurement and modeling of photosynthesis in a natural population

The objective of this experiment was twofold. Firstly, to use F_v/F_m and effective absorption cross-sections to calculate photosynthetic rates over the time course of one day in Myponga Reservoir. Secondly, to determine the total productivity at meteorological station 1 using the PAM-calculated productivity rates, phytoplankton distribution (expressed as chlorophyll concentration) and the photosynthesis model and procedure of Walsby (1997).

Triplicate water samples were taken from 0.25, 0.5, 1, 2 and 3.6 m depth, corresponding to 70, 50, 30, 10 and 1% of surface irradiance every 2 hours from 0:700 h to 19:00 h on 10 January 2000. At each depth-time interval, F_v/F_m (15 minutes of dark adaptation) and light intensity was measured and water samples were filtered for chlorophyll *a* concentration according to the method of Talling and Driver (1963). Sampling was undertaken adjacent to meteorological station 1 (see below) so that the physical conditions (temperature, wind speed) of the site were precisely known.

The daily integral of photosynthesis model by Walsby (1997) was used to determine the total productivity of the site. The model incorporates photosynthetic rates, the vertical concentration of phytoplankton, vertical profiles of irradiance and temperature and underwater light climate and interpolates all the data over time and depth.

Photosynthetic rate

Measurements of photosynthetic rate ($\text{mol O}_2 \text{ mol Chl}a^{-1} \text{ h}^{-1}$) were made following the PAM fluorometry procedure and that of Falkowski and Kolber (1993) for a range of light intensities (equation 5). Measurements were made in triplicate for surface samples taken from the Myponga

Reservoir at 07:30 h. The data were entered into the Walsby model and photosynthetic rates were determined according to:

$$P_c = P_m (1 - \exp(-\alpha I / P_m)) + R + \beta I \quad (6)$$

where P_m is the maximum photosynthetic rate, R is the rate of respiration, α is the slope of P/I observed at light limiting irradiances and β is the slope due to photo-inhibition at high irradiances. Using the least squares method and 'Solver' software the values of P_m , α , β which gave minimum $(\Sigma'(P-P_c)^2)^{0.5}$ values are used for calculation of photosynthetic integrals.

Phytoplankton concentration

Chlorophyll a concentration was determined using the ethanol / spectrophotometer method and following Talling and Driver (1963):

$$\text{Chl } a \text{ } (\mu\text{g L}^{-1} = \text{mg m}^{-3}) = 13.9 (A_{665} - A_{750}) V_1 \times 10^3 / V_2 d \quad (7)$$

where A_{665} and A_{750} are the absorptions at 665 and 750 nm, respectively; V_1 is the volume of ethanol added in mL; V_2 is the volume of reservoir sample filtered (mL) and d is the path length of the cell (cm).

The data was incorporated into the Walsby model and interpolated at intervals of 0.25 m from 0 to 4 m depth. Concentrations at intermediate depths and time intervals were interpolated by assuming a linear change in concentration between measurements of adjacent intervals.

Irradiance and light field

The under water irradiance at meteorological station 1 was accurately characterized, correcting for light attenuation, wind speed (U_w) and surface irradiance (E). Wind speed at 10 minute intervals and surface irradiance were obtained from meteorological station 1, to determine the amount of reflectance caused by time of year, solar elevation, zenith angle and the southern hemisphere. The equations of Kirk (1994) were used to calculate reflectance in the Walsby (1997) model.

Integrals of PAR, phytoplankton concentration and photosynthesis

The net photosynthesis in this study was obtained by trapezoidal integration (Walsby, 1997), by summing all values divided by the increments of time (1 step h^{-1}) and depth (4 steps m^{-1}).

To compare the photosynthesis-irradiance curves of each of the depth-time samples obtained from the PAM fluorometry technique with the modeled values obtained using Walsby (1997), an additional table was established within the Walsby model which summarized only the corresponding depths (0.25... 3.6 m) and times (07:00...19:00 h) of phytoplankton sampling.

Meteorological measurements – station 1

For Myponga Reservoir experiments, meteorological variables were measured at station 1 deployed in the main basin. Wind speed and direction (Climatronics WM-111) measured 2 m above the water surface, down welling short wave radiation (300–3000 nm, Middleton EP08) and upwelling and down welling long wave radiation (0.3–60 μm , Middleton CN1-R) were measured and logged every 10 minutes. Temperature was recorded every 2 minutes by thermistors spanning the water column over 35 m (Betatherm, resolution ± 0.01 $^{\circ}\text{C}$).

A LICOR underwater quantum sensor (LI 192SA) was used for all underwater light measurements. Light intensities at 0.1 m intervals were loge transformed and regressed against depth to calculate the vertical attenuation coefficient according to the Beer Lambert law.

2.2.9 Statistical analysis

All experiments were carried out in triplicate and results were presented as a mean \pm standard deviation. A one-way analysis of variance (ANOVA) was used to determine if there were significant differences between treatments ($\alpha = 0.05$) and a Welch ANOVA was used when variances were unequal.

2.3 Results

2.3.1 Optimisation of FDA staining

The time course of FDA conversion to fluorescein at 1, 10 and 40 μM for each of the phytoplankton is shown in figure 2.2. Fluorescein fluorescence is a function of cell uptake, esterase activity and fluorescein leakage from cells. For all four species a final concentration of 1 μM resulted in minor fluorescein fluorescence indicating that there was insufficient FDA substrate to evaluate esterase activity. An increase in FDA substrate concentration to 10 and 40 μM resulted in significant increases in fluorescein fluorescence. For all species, the conversion of FDA to fluorescein was near linear in the first 10-15 minutes, indicating that there was no substrate limitation and sufficient fluorescence. Maximum fluorescence tended to plateau or decrease after 20 minutes suggesting either FDA substrate limitation or leakage of fluorescein from cells.

Fluorescein fluorescence varied between species with *Scenedesmus* displaying the highest intensities for all FDA concentrations (figure 2.2a). This implies that uptake and conversion of FDA to fluorescein occurs rapidly and efficiently in this species. In contrast, *Aulocoseira* displayed the smallest fluorescent signal probably due to cell morphology and silica wall structures, which may limit the uptake of FDA (figure 2.2d).

For subsequent assays, the optimal FDA concentration was chosen to be 40 μM for all species. To ensure that fluorescence was governed by esterase activity not substrate limitation, staining times of 7 minutes for *Microcystis*, 10 minutes for *Anabaena* and 8 minutes for *Scenedesmus* were chosen. Overlays of fluorescein fluorescence histograms for exponentially and heat-treated cells for each respective species enabled the identification of metabolic states. Microscopic analysis of 50:50 live dead mixtures of *Scenedesmus*, *Anabaena* and *Microcystis* demonstrated that at a FDA concentration of 40 μM , metabolically active cells could be differentiated on the basis of positive fluorescence versus no fluorescence for heat-treated dead cells (figure 2.3). It should be noted that due to limitations with microscope barrier filters, the red chlorophyll auto-fluorescence of the green alga, *Scenedesmus* tended to overshadow the green fluorescence of FDA.

2.3.2 Optimisation of Sytox staining

The optimal concentration and staining time of Sytox green was determined with concentrations of 0.1, 1 and 10 μM over a 60-minute period using exponentially growing and nonviable (heat-treated) cells (figure 2.4). Large differences between the fluorescence of viable and nonviable cells were evident. However, these differences were concentration and species dependent. At the lowest Sytox concentration tested (0.1 μM), heat-treated cells were not reliably stained and differentiable from viable cells. The fluorescence of nonviable cells did not increase immediately and the magnitude of fluorescence was not high, indicating probe limitation in staining DNA. For *Scenedesmus* (figure 2.4a) both viable and non-viable cells fluoresce at 50 units, whereas *Anabaena* (figure 2.4b) and *Microcystis* (figure 2.4c) fluorescence increased approximately 6 fold for nonviable cells compared to viable cells.

An increase in Sytox concentration to 1 μM resulted in clear differences in mean cell or event fluorescence between viable and nonviable cells for all three species. The fluorescence of nonviable cells occurred within 1 minute of incubation. In addition, the fluorescence of viable cells remained at a relatively constant value for 60 minutes, which indicates that at this concentration, Sytox was not inducing cell death. Fluorescence of *Scenedesmus*, increased from 50 units for viable cells and 500 units for non-viable cells, after 10 minutes (figure 2.4a). For *Anabaena*, the difference in fluorescence ranged from 100 units for viable cells to 1100 units for nonviable cells (figure 2.4b), while *Microcystis* fluorescence increased from 175 to 900 units for viable and nonviable cells, respectively (figure 2.4c).

At the highest concentration (10 μM), Sytox induced cell death and consequently viable cells that should show minimal fluorescence displayed high fluorescence similar to levels of heat-treated cells. Furthermore, mean Sytox fluorescence of viable cells tended to increase with time. After 7 minutes, the mean fluorescence of viable *Anabaena* cells was 300 compared to 400 for nonviable cells (figure 2.4b). Similarly, for *Microcystis* after 8 minutes, mean viable cell fluorescence approximated 400 units compared to 700 units for nonviable cells (figure 2.4c).

To avoid limitation of Sytox staining DNA and toxicity at high concentrations, 1 μM Sytox displayed separation between viable and nonviable cells and was chosen for all species in future assays. An optimal staining time of 10 minutes was chosen for all species. An overlay of Sytox fluorescence histograms for viable and nonviable cells for each respective species enabled the identification of viability states. Microscopic analysis of 50: 50 live: dead mixtures for all species

demonstrated that at a concentration of 1 μM and staining time of 10 minutes, viable and nonviable cells could be clearly differentiated on the basis of Sytox green nucleic acid staining and subsequent bright fluorescence (figure 2.5).

2.3.3 Estimation of the number of viable and nonviable cells in a population

To evaluate the ability of Sytox and FDA to differentiate between viable and nonviable cells within a population, the optimized staining protocols were applied to predetermined combinations of viable and heat-treated nonviable cells. Sytox differentiated between viable and nonviable cells within mixed populations for all species with less than 5% error (figure 2.6a-c). As the percentage of viable cells increased within the population, the number of cells increased in $S1_{\text{syt}}$ and conversely decreased in $S2_{\text{syt}}$. For *Scenedesmus*, *Anabaena* and *Microcystis*, there was 5, 2 and 3 % disagreement, respectively. For example a *Microcystis* population containing a 50:50 mixture of viable and non-viable cells was shown flow cytometrically to have only 38 % of viable cells falling into $S2_{\text{fda}}$ (figure 2.6c). In contrast the FDA assay was less accurate and tended to underestimate the number of viable *Microcystis* cells within a population by approximately 10- 15 % (figure 2.6d).

2.3.4 Detection of nutrient limitation and repletion

Microcystis growth, activity, morphology and viability were affected by the nitrogen and or phosphorus concentration in WC media. Cell counts revealed that with sufficient N and P, the culture was in an exponential growth phase (figure 2.7a). Conversely, all other treatments of -N and or -P resulted in reduced growth, which became evident after 8 days. Between day 8 and day 19, cell numbers generally did not change. However, the spiking of N and P to respective replete treatments on day 19 resulted in significant increases in cell numbers on days 25 and 27 compared to ongoing N and P free treatments. The lowest cell count recorded was for -N and -P treatments for the entire 27 days, although there were no significant differences with either of the -N-N or -P-P treatments.

Microcystis metabolic activity was less predictable than cell counts in responding to N and P concentration (figure 2.7b). With the exception of an initial increase, metabolic activity as expressed as the FDA conversion rate to fluorescein per cell per minute generally decreased over

time for all treatments and there was little difference in activity among treatments until day 22. On day 22 (3 days after N and P spiking), the metabolic activity of the +P treatment was significantly higher than the ongoing -P treatment. In terms of cell counts, this pattern was not consistent on day 22, but was on days 25 and 27 (figure 2.7a). In contrast, the addition of N on day 19 had no effect on metabolic activity compared to the N deplete treatment. Interestingly, the FDA conversion rate of the N and P deplete treatment was higher than the N and P replete treatment after day 22, indicating potential limitation in another unidentifiable nutrient in the latter treatment.

The number of *Microcystis* cells in the low metabolic activity state; $S1_{fda}$ followed a similar pattern to the mean FDA conversion rate (figure 2.7c). For the first 6 days, less than 10% of cells were in $S1_{fda}$ for all treatments. However, within 2 days, the numbers of P deplete cells increased to 40% in $S1_{fda}$ and continued to increase to approximately 85% on day 27. The addition of P on day 19 significantly decreased the number of cells in $S1_{fda}$ for 6 days (until day 25), although this was only temporary as the number of low activity cells doubled on day 27. Interestingly, the number of cells in $S1_{fda}$ was generally less for N deplete than P deplete cultures. The addition of N on day 19, temporarily decreased the number of low activity cells by 10%, but by day 27, there were 20% more low activity cells. Consistent with mean FDA conversion rates, the number of cells in $S1_{fda}$ was less in the N and P deplete treatment compared to the N and P replete treatment after day 22. The number of *Microcystis* cells in the normal activity state; $S2_{fda}$ followed a similar pattern to the FDA conversion rate and was the inverse of the $S1_{fda}$ pattern (figure 2.7d). As cell numbers increased in the low metabolic state, they decreased in the normal metabolic state and visa versa.

Microcystis cell viability as determined by the number of cells with high Sytox fluorescence in state, $S2_{syt}$, was dependent upon the N and P treatment (figure 2.7e). For the first 19 days, the number of nonviable cells was generally less than 10%, although the N and P deplete treatment displayed the lowest viability. Nutrient addition decreased cell viability in both N and P deplete and replete treatments compared to individual N or P treatments. Cell viability in all other treatments including the P deplete treatment remained below 10%. On day 22, 25% of cells were nonviable in the N and P replete culture compared to 15% in the N and P deplete culture, suggesting that another nutrient maybe limiting apart from N and P as identified with the FDA assay.

Flow cytometrically measured chlorophyll fluorescence per cell decreased over time for all treatments, until nutrient spiking on day 19 (figure 2.7f). Reflective of cell counts, chlorophyll fluorescence per cell was highest in the N and P replete treatment. Nutrient spiking tended to increase chlorophyll fluorescence per cell either within 3 days (+N treatment) or gradually until day 27 (+P treatment). The addition of N or P increased chlorophyll fluorescence per cell relative to each respective nutrient deplete treatment. Population growth followed a similar trend.

Forward light scatter, FSC indicative of cell size ranged from 180 to 500 units cell⁻¹ (figure 2.7g). FSC decreased from approximately 400 units per cell on day 1 to less than 300 units on day 4, indicating a decrease in cell size probably as a result of cell division/ growth, reflected in cell counts. The FSC of the N and P replete and deplete culture generally approximated 300 units per cell. The N deplete cultures had significantly higher FSC values compared to all other treatments on day 19, averaging 450 units. N addition decreased cell size to 250 units, suggesting that the high FSC of N deplete cultures is due to a lack of cell division. Although to a lesser degree, this pattern was also evident in the +P cultures. Cell side scatter or granularity ranged between 500 and 1050 units cell⁻¹ over 27 days.

2.3.5 Detection of copper toxicity

Copper sulphate toxicity was detected by changes in *Scenedesmus* cell number, and the number of cells, in either the low metabolic activity, S1_{fda} or the nonviable state, S2_{syt} relative to the control (0 mg L⁻¹ copper sulphate). There were no significant differences ($p > 0.05$) between the control and 0.01 or 0.1 mg L⁻¹ copper additions over 72 hours for either cell growth, metabolic activity or cell viability measurements (figure 2.8a, b, c). However, an increase in copper concentration (0.5 to 5 mg L⁻¹) caused a decrease in growth rate relative to the control cultures after 72 hours (figure 2.8a). FDA measurements revealed that the number of low metabolically active cells (%S1_{fda}) tended to increase with copper concentration (0.5 > 5 mg L⁻¹) and over time (figure 2.8b). A gradient was evident after 72 hours with 5 mg L⁻¹ of copper inducing 60% of cells into the low active state compared to only 5% for the control culture. Measurements of cell viability using Sytox mirrored FDA measurements (figure 2.8c). As copper concentration increased from 0.5 to 5 mg L⁻¹, the number of nonviable cells (%S2_{syt}) increased over time. A

plot of the number of cells in $S2_{\text{synt}}$ versus the number of cells in $S1_{\text{fda}}$, revealed a linear relationship with an r^2 value of 0.78, suggesting that both fluorescent probes are useful in toxicity assays (figure 2.8d).

2.3.6 Influence of light intensity and nutrients on photo-physiology

Varying light intensity ($10 - 250 \mu\text{mol m}^{-2} \text{s}^{-1}$) significantly affected the photochemistry of *Microcystis* (figure 2.9a, b). After 6 days of acclimation, *Microcystis* cells grown at $250 \mu\text{mol m}^{-2} \text{s}^{-1}$ had higher levels of photochemical quenching (more reaction centers open) than cultures grown in lower irradiance (figure 2.9). Cells grown in low light ($10 \mu\text{mol m}^{-2} \text{s}^{-1}$) displayed a rapid decline in photochemical quenching with increasing irradiance. High light grown cells were more efficient in processing electrons through the electron transport chain and consequently had a greater capacity for photosynthesis. F'_v/F'_m increased with light intensity from 10 to $250 \mu\text{mol m}^{-2} \text{s}^{-1}$ (figure 2.9b). Although consistent among treatments, the degree of F'_v/F'_m was dependent upon the time of experimental light exposure on day 6 of measurement. F'_v/F'_m increased with a longer exposure time for light intensities up to $125 \mu\text{mol m}^{-2} \text{s}^{-1}$ (i.e. F'_v/F'_m 12 h > 0 h). However, at $250 \mu\text{mol m}^{-2} \text{s}^{-1}$, the number of effective reaction-centers was independent of the time of measurement ($p > 0.05$). Light intensity had no significant ($p > 0.05$) effect on *Microcystis* effective absorption cross-section (figure 2.9c). The average measured cross-section was $57.04 \text{ \AA}^2 \text{ quanta}^{-1}$ (s.d. = 2.29). Patterns in photo-physiology parameters were consistent with *Microcystis* growth. Cell growth increased exponentially from 10 to $125 \mu\text{mol m}^{-2} \text{s}^{-1}$ reaching a maximum of 0.65 between 125 and $250 \mu\text{mol m}^{-2} \text{s}^{-1}$ (figure 2.9d).

A further increase in light intensity to $400 \mu\text{mol m}^{-2} \text{s}^{-1}$ tended to decrease the number of effective reaction centers for exponentially growing *Chlorella pyrenoidosa*, *Anabaena circinalis* and *Aulocoseira granulata* cultures (figure 2.10a). After 6 days in batch culture, F'_v/F'_m was diminished by 30% for all three species when grown at $400 \mu\text{mol m}^{-2} \text{s}^{-1}$ compared to $10 \mu\text{mol m}^{-2} \text{s}^{-1}$ ($p < 0.05$). There were no significant differences between 10 and $100 \mu\text{mol m}^{-2} \text{s}^{-1}$ or 100 and $400 \mu\text{mol m}^{-2} \text{s}^{-1}$ treatments ($p > 0.05$). In contrast to F'_v/F'_m , the response of effective absorption cross-section to light intensity was species dependent (figure 2.10b). The size of the effective absorption cross-section (σ) of *Chlorella* did not change between light treatments. In contrast, σ

tended to increase for *Aulocoseira* and decrease with *Anabaena* cultures grown at the higher light intensities.

The addition of various concentrations of nitrate to N-deplete WC media affected *Microcystis* F_v/F_m and effective absorption cross-section (figure 2.11). After 3 and 6 days, the nitrate free starved (no added nitrate) and 2 μM treatments significantly decreased F_v/F_m compared to nitrate additions of $> 5 \mu\text{M}$, indicating that the cultures were nutrient-limited (figure 2.11a). There were no differences in F_v/F_m for nitrate additions from 5 to 100 μM . After 3 days, the nitrate deplete (no added nitrate) and 2 μM treatments significantly decreased *Microcystis* absorption cross-section ($\sim 45 \text{ \AA}^2 \text{ quanta}^{-1}$) relative to $> 5 \mu\text{M}$ treatments ($\sim 55 \text{ \AA}^2 \text{ quanta}^{-1}$) [figure 2.11b]. However, after 6 days the absorption cross-section of the N deplete culture approached that of the 5 μM treatments ($\sim 52 \text{ \AA}^2 \text{ quanta}^{-1}$). Interestingly, the absorption cross-section of the 2- μM treatment remained small at $42 \text{ \AA}^2 \text{ quanta}^{-1}$.

Similarly, *Microcystis* F_v/F_m was sensitive to changes in the N or P status of WC media (figure 2.11c). For the first 4 days, F_v/F_m ranged between 0.4 and 0.5 before progressively decreasing for the entire nutrient-deplete treatments (-N, -P or -N & -P). After 19 days, F_v/F_m was lower for -P cultures compared to -N cultures, which was also evident with esterase activity measurements (figure 2.7b). On day 19, F_v/F_m responded to both P and N addition. P addition increased F_v/F_m from 0.15 on day 19 to 0.5 on day 27. N addition increased F_v/F_m from 0.3 on day 19 to 0.5 on day 27. The F_v/F_m of the N and P replete treatment remained at approximately 0.38 for 27 days. In contrast the N and P deplete treatment fell to 0.15 from day 19 to day 27.

2.3.7 F'_v/F'_m depression and recovery kinetics

Anabaena grown at a light intensity of $20 \mu\text{mol m}^{-2} \text{ s}^{-1}$ and subsequent exposure to various low to high light intensities for 20 minutes demonstrated that the degree of F'_v/F'_m depression and recovery time was dependent upon light intensity (figure 2.12a). Exposure to $1500 \mu\text{mol m}^{-2} \text{ s}^{-1}$ resulted in maximum depression (~ 0.03) and the longest recovery time to reach 95 % of original value (~ 35 minutes). In contrast, exposure to only $120 \mu\text{mol m}^{-2} \text{ s}^{-1}$ resulted in only a 50% reduction and an immediate recovery to the original F'_v/F'_m value. For this particular species

grown at low irradiance and an exposure time of 20 minutes, the recovery time of F_v/F_m increased linearly with light intensity (figure 2.12b).

However, changes in exposure time with a fixed high light intensity of $1500 \mu\text{mol m}^{-2} \text{s}^{-1}$ revealed that F_v/F_m recovery time was not always linear (figure 2.13a-d).

2.3.8 Measurement and modeling of photosynthesis in a natural population

On the day of sampling, Myponga Reservoir became thermally stratified until wind induced mixing at 16:00 h (figure 2.14a). Between 07:00 and 13:00 h the average wind velocity was below 4 m s^{-1} and the surface mixed layer depth was less than 0.6 m. At 11:00 h, the surface mixed layer depth approximated 0.2 m. After 13:00 h, average wind velocity increased leading to the progressive deepening of the surface mixed (figure 2.14b). Irradiance at each sampling depth followed a typical sinusoidal pattern except for a brief cloudy period at 11:00 h (figure 2.14c). Maximum photosynthetically active irradiance was approximately $2500 \mu\text{mol m}^{-2} \text{s}^{-1}$ at the surface.

The F_v/F_m of the natural population ranged between 0.24 and 0.34 during the course of the day (figure 2.14d). At 07:00 h, F_v/F_m approximated 0.32 units before decreasing at all depths at 09:00 h. At 11:00 h as irradiance increased, a gradient in F_v/F_m was evident, with depression in surface samples. The 0.25 m samples fell to a minimum of 0.25 compared to 2 and 3.6 m samples both approximately 0.32. The light intensity at 0.25 m was approximately 10 fold higher than at 2 m (figure 2.14c). At 13:00 h, the surface mixed layer deepened to 1.5 m enabling surface samples at 0.25 m to recover, resulting in similar F_v/F_m with depth of 1.0 m. The F_v/F_m of the 2.0 m sample remained high at 0.32. Interestingly, the F_v/F_m of the 3.6 m sample decreased to 0.24. At 15:00 and 17:00 h, there were no significant differences in F_v/F_m with depth as the surface mixed layer deepened to at least 3.0 m. The final measurement indicated that the 0.25 m sample had the highest F_v/F_m value when irradiance approximated $250 \mu\text{mol m}^{-2} \text{s}^{-1}$.

Exposure and subsequent measurement of quantum yield at actinic light intensities clearly demonstrated that surface samples had fewer functional reaction centres than samples taken from either 2 or 3.6 m under ambient conditions (figure 2.14e). Phytoplankton chlorophyll *a*

concentration tended to decrease with depth and during the course of the sampling period (figure 2.14f). Chlorophyll *a* concentrations were low and ranged from 4 to 6 $\mu\text{g L}^{-1}$. The depth-time integration of chlorophyll *a* concentration is shown in figure 2.14g. Phytoplankton photosynthetic rates ranged between 0.1 and 6.5 $\text{mg O}_2 \text{ mg Chl } a^{-1} \text{ h}^{-1}$, reaching a maximum at 13:00 h and decreasing with depth (figure 2.14h). Similarly, oxygen productivity tended to reach maxima at 13:00 h and decrease with sampling depth (figure 2.14i). At 13:00 h and 0.25 m depth, 0.033 $\text{mg O}_2 \text{ L}^{-1} \text{ h}^{-1}$ was produced. For each sampling depth, modeled productivity tended to overestimate O_2 rates by 0.01 $\text{mg O}_2 \text{ L}^{-1} \text{ h}^{-1}$ (figure 2.14i versus j).

Actual and calculated photosynthesis-irradiance curves of a surface sample are shown in figure 2.14k. The calculated curve closely approximated actual PAM determined data. The depth-time integration of photosynthesis is shown in figure 2.14l. Productivity increased in the middle of the day and in surface layers. As a result of low chlorophyll *a* concentrations, the total productivity equated to only 800 $\text{mg O}_2 \text{ m}^{-3}$ (or 0.8 $\text{mg O}_2 \text{ L}^{-1}$) for 24 hours and only 830 $\text{mg O}_2 \text{ m}^{-3}$ (or 0.83 $\text{mg O}_2 \text{ L}^{-1}$) for the daylight period.

2.4 Discussion

2.4.1 Fluorescent probes and flow cytometry

In order to utilise flow cytometry and fluorescent probes in phytoplankton studies it was important to optimise the staining protocol for each test species and stain to yield maximum staining between viable, metabolically active and nonviable cells. The combination of FDA and flow cytometry enabled the degree of fluorescein fluorescence to be quantified, which relates to the relative physiological activity of cells. In contrast, the Sytox assay differentiates only between living and nonviable cells, and there is no continuous spectra fluorescence.

The FDA assay detected esterase activity in all living species grown in standard WC media at pH 7. Conversely, heat treatment killed cells inactivating esterases resulting in minor or no fluorescein fluorescence as reported previously for *Microcystis* (Regel, 1997) and *Hymenomonas elongata* (Bently-Mowat, 1982). The expression of esterase activity as fluorescein fluorescence was dependent upon FDA substrate concentration and staining time. Generally, the degree of

fluorescein fluorescence was limited by esterase activity rather than substrate limitation over the first 15 minutes of staining. An optimal staining time within this period was chosen to ensure that expression of esterase activity was not influenced by substrate concentration or fluorescein leakage from cells, which may occur after 30 minutes (Brookes, 1997). The different shapes or cell types (prokaryote vs eukaryote) of the test species did not hinder the FDA assay and fluorescence characteristics. Microscopy indicated that the cells in the filaments of *Anabaena* and cells within *Scenedesmus* clusters stained equally as would be expected with unicellular cells such as *Microcystis*. However, caution should be used with the interpretation of results with filamentous or colonial phytoplankton. Unlike *Microcystis*, whereby mean esterase activity represents the activity of each cell, mean fluorescence data for *Anabaena* and *Scenedesmus* represents the whole event or filament or cluster. Regardless of these limitations, differential fluorescence was reliably measured under different stain concentrations and times.

A major advantage of flow cytometry is the ability to explore heterogeneity of responses within a population. Most studies using FDA have measured the test species' response to a specific treatment as a mean value of esterase activity (Berglund and Eversman, 1988; Geary *et al.*, 1997; Brookes *et al.*, 2000a, b) even though the discrimination of the cell responses may be non-normal. Moreover, mean values may mask subtle changes such as the depression or recovery of cells within a population. The representation of fluorescence data in terms of metabolic states using markers on histograms negates the problems associated with non-normal data. The definition of a low metabolic state using heat-treated cells has proven useful in toxicity bioassays (Regel, 1997; Regel *et al.*, 2002). Regel (1997) using plots of mean esterase activity, mean chlorophyll fluorescence cell^{-1} and cell number versus the number of cells in $S1_{\text{fda}}$ revealed that esterase activity was linearly related to the number of unhealthy cells.

The Sytox assay differentiated between viable and dead cells for all three species, but was dependent upon concentration and staining time. Insufficient substrate ($0.1 \mu\text{M}$) did not allow enough DNA to be stained in dead cells whereas higher stain ($10 \mu\text{M}$) concentrations resulted in false staining of viable living cells. False staining of healthy cells has also been reported using propidium iodide at high concentrations for freshwater phytoplankton (Franklin *et al.*, 2001) and bacteria (Williams *et al.*, 1998).

However, a final Sytox concentration of 1 μM reliably stained dead cells, resulting in high fluorescence. Conversely, living cells excluded Sytox resulting in minor fluorescence, which was also reported for numerous marine phytoplankton representing all groups except Eustigmatophyceae (Veldhuis *et al.*, 1997). Microscopy highlighted a difference between prokaryote cells and eukaryote cells in which only the nucleus is stained compared to the whole cell in the former (figure 2.5a vs. b, c).

The strong fluorescence signal of nonviable cells compared to living cells enabled the establishment of viability states ($S1_{\text{sytx}}$, $S2_{\text{sytx}}$). These states enabled the accuracy of the assay to be tested with mixed combinations of dead and living cells. A previous study by Lebaron *et al.* (1998) reported that Sytox underestimated the number of nonviable bacterial cells. This problem was not encountered and Sytox despite being developed for bacterial cells, accurately differentiated between viable and dead cells for both the eukaryote and prokaryote species with less than 10 % error. In contrast, the FDA assay was less accurate and results with *Microcystis* showed an underestimation of dead cells. Moreover detection of dead cells improves as viability decreases with Sytox as opposed to esterase activity in which the response declines with reducing viability (Jochem, 1999). The Sytox stain was regarded to be superior for cell viability assays in agreement with Langsrud and Sundheim (1996).

Esterase activity in phytoplankton has been shown to be a sensitive endpoint capable of detecting subtle differences in temperature, light, salinity, nutrient status and growth phase (Minier *et al.*, 1993; Geary *et al.*, 1997; Brookes *et al.*, 2000a, b) and also in toxicity assays involving heavy metals and storm water (Regel, 1997) and acid mine drainage (Regel *et al.*, 2002). In this study, *Microcystis* esterase activities reflected the nutrient status of cells in either N or P replete or deplete WC media and were relatively consistent with cell growth as determined by cell counts. As cells became nutrient limited, their metabolic activity decreased resulting in less FDA conversion to fluorescein and more cells classified into the low metabolically active state. Esterase activity appeared to be more affected by P deficiency than N deficiency. Nutrient repletion resulted in a recovery in esterase activity consistent with cell division. Geary *et al.* (1997) also reported an increased FDA conversion rate for *Microcystis* after 2 days with the addition of P, but not N into P deficient ASM media. In natural populations, Brookes *et al.* (2000a) detected N-limitation in the lower River Murray and co-limitation of N and P in Wachtel's Lagoon using the FDA assay. Nutrient limitation was detected within 24 hours which

avoided problems associated with long incubation times and growth as an endpoint (Brookes *et al.*, 2000a).

In contrast to the experiments by Geary *et al.* (1997) and Brookes *et al.* (2000a, b), the present study demonstrated that with nutrient limitation and repletion the number of cells in $S1_{\text{fda}}$ increased and decreased, respectively. The recovery of low activity cells also suggests that cells can persist in a low activity state before dying. It was initially postulated that these cells would die and be detectable using Sytox. However, for 27 days, no such pattern was evident and the number of nonviable cells remained relatively low or compatible with nutrient replete cultures. Although, one exception was the treatment, involving the repletion of both N and P. This treatment resulted in increased esterase activity and growth, which is likely to have led to the depletion of other essential nutrient (s). This second step of limitation induced cell death, as detected by a 25% increase in the number of cells in $S2_{\text{sytx}}$, after 27 days.

Esterase activity was also a sensitive indicator of copper toxicity in *Scenedesmus*. As copper concentrations increased, esterase activity reduced in a concentration-dependent manner. Toxicity caused a decrease in mean esterase activity and an increase in the number of low activity cells ($S1_{\text{fda}}$), which was also reported by Regel (1997) for *Microcystis aeruginosa* and *Selenastrum capricornutum* by Franklin *et al.* (2001). The concentration threshold for a no observable effect (NOEC) was 0.1 mg L^{-1} . A copper concentration of 0.5 mg L^{-1} decreased esterase activity within 24 hours, although Arsenault *et al.* (1993) reported an 80 % shift of the population into a low esterase activity state after 3 hours. Copper toxicity initially induced a decrease in esterase activity followed by cell death at 2 and 5 mg L^{-1} . The Sytox assay detected an increase in the number of nonviable cells at high copper concentrations which increased with time and consequently, the assay is suitable for detecting lethal effects of a toxicant.

2.4.2 Fluorometry

Several small experiments with cultured and natural phytoplankton demonstrated the use and potential of PAM fluorometry in measuring photochemistry and its response to light and nutrients. Cells responded to both light and nutrients by altering components of their photosystem, which is reflected in the variable chlorophyll fluorescence yield. Experiments with *Microcystis* grown at light intensities ranging between 10 and $250 \mu\text{mol m}^{-2} \text{ s}^{-1}$ demonstrated that

cells grown at higher light intensities had higher levels of photochemical quenching indicating that they were more capable in processing electrons through the electron transport chain than cells grown in low light. Similarly, the maximum quantum yield, F_v/F_m was found to increase with irradiance, but measurement was dependent upon exposure time to light, increasing during the day cycle. This indicates that in the case of bioassays, the time of measurement of F_v/F_m should be consistent for all treatments (e.g. half way into the light cycle).

The response of F_v/F_m to irradiance is dependent upon the balance between photochemical and non-photochemical processes, which are related to the intensity of irradiance, and the duration of exposure. Medium light intensities of $400 \mu\text{mol m}^{-2} \text{s}^{-1}$ depressed F_v/F_m for *Chlorella*, *Anabaena* and *Aulocoseira* compared to $10 \mu\text{mol m}^{-2} \text{s}^{-1}$, demonstrating that non-photochemical quenching becomes more significant in quenching fluorescence as irradiance exceeds optimal intensities. The influence of irradiance on photosynthetic efficiency was demonstrated using cultured *Anabaena circinalis* and monitoring F'_v/F'_m kinetics before, during and after exposure to high light. The degree of F'_v/F'_m depression was dependent upon light intensity, and secondly that upon return to low light, rate of recovery increased with light intensity due to the continued relaxation of non-photochemical quenching. Recovery time was also dependent upon the exposure time to high light (figure 2.13). A short exposure time (5 min) resulted in a faster recovery rate than a long exposure time (60 min) to high light.

Phosphorus, nitrogen and iron play critical roles in cellular metabolism as part of membranes and in energy transduction and therefore limitations of these nutrients have major effects on photosynthetic efficiency. Consequently, photosynthetic efficiency has been commonly used to assess the nutrient status of phytoplankton as part of bioassays. Depression in F_v/F_m has been observed for numerous phytoplankton groups predominantly in the ocean when the water column has been deficient of N, P, Fe or silica (Kolber *et al.*, 1988; Geider *et al.*, 1993; La Roche *et al.*, 1993; Greene *et al.*, 1992; Lippemeier *et al.*, 1999). Experiments with *Microcystis* showed that, F_v/F_m was affected by nitrate limitation decreasing by approximately 30% after 3 and 6 days. Similarly, F_v/F_m decreased from 0.4 to 0.1 with N, P or N and P limitation after 27 days. F_v/F_m followed a similar pattern to measurements of esterase activity with FDA as would be expected when FDA conversion rate is a function of photosynthesis (Geary *et al.*, 1997). Replenishment of the limiting nutrient results in a recovery in F_v/F_m as has been reported for natural populations (Geider *et al.*, 1993).

The sensitive and rapid response of F_v/F_m to changes in light intensity and duration of exposure and to nutrient conditions provides a feature of phytoplankton which can be traced to assess the impacts of mixing and stratification on cell distribution, entrainment and or photosynthesis in lakes and reservoirs. Under stratified nutrient replete conditions, given a reasonably low light attenuation coefficient, with minimal vertical mixing, a gradient in F_v/F_m increasing with depth would be expected. Conversely, wind mixing would be expected to entrain and circulate cells through the same light climate resulting in homogeneity of F_v/F_m to the depth of the mixed layer. The Myponga Reservoir study, despite periods of cloud cover which influenced surface layer F_v/F_m levels, demonstrated that the F_v/F_m of phytoplankton in the water column matched that of bottled phytoplankton at each respective light intensity, indicating minimal vertical cell movement and the dependency of F_v/F_m on irradiance. Oliver and Whittington (1998) showed that in Chaffey Dam (Australia), during periods of stratification, there was maximum depression of F_v/F_m for phytoplankton dominated by *Oocystis* species in surface samples and progressively smaller changes with depth until a maximum at 1.8 m, where the light intensity was 10 % of surface irradiance. The depression was consistent with the effects of non-photochemical quenching and photo-inhibition. Wind mixing events in the afternoon, indicated by isotherms corresponded to an increase in F_v/F_m of near surface samples.

Ibelings and Mur (1992) and Ibelings and de Windner (1994) reported depressed F'_v/F'_m in surface blooms of *Microcystis* attributable to photo-inhibition, which resulted in reduced rates of gross photosynthesis. Ibelings *et al.* (1994) using *Microcystis* and *Scenedesmus* in laboratory experiments demonstrated strong depression in F'_v/F'_m with a sinusoidal light regime, which reflected natural light without wind mixing. They found that oscillations of light within the sinusoidal regime reflective of wind mixing mitigated photo-inhibition. Vincent *et al.* (1984) also reported shifts in photochemistry closely followed the diel cycle of stratification and mixing in Lake Titicaca, while Lewis *et al.* (1984a) reported that turbulent intensity (turbulent kinetic energy dissipation rate) was a strong determinant of photosynthetic rate in Bedford Basin. Consequently, changes in F_v/F_m in relation to light dose can be used to estimate phytoplankton-mixing trajectories at time scales similar to physical processes, resulting in accurate estimates of productivity.

The effective absorption cross-section of the light-harvesting antenna of phytoplankton can change in response to irradiance and or nutrient conditions, but the degree of plasticity tends to be

species dependent (Oliver and Whittington, 1998). *Microcystis* cross-sections did not vary when grown at light intensities ranging between 10 and 250 $\mu\text{mol m}^{-2} \text{s}^{-1}$ and approximated 55 $\text{\AA}^2 \text{quanta}^{-1}$ which is within the range (31-63 $\text{\AA}^2 \text{quanta}^{-1}$) reported by Oliver and Whittington (1998) for laboratory cultures. Oliver and Whittington (1998) suggest that the size of the absorption cross-section is indicative of the light conditions to which a cell is best suited. Consistent with F_v/F_m measurements, the absorption cross-section of *Anabaena* decreased when grown at 400 $\mu\text{mol m}^{-2} \text{s}^{-1}$ compared to 100 $\mu\text{mol m}^{-2} \text{s}^{-1}$, indicating that cells are acclimating to higher light intensities by decreasing the size of the light harvesting complex. However, there were no changes in *Chlorella* effective cross-sections and *Aulocoseira* sections tended to increase when grown at 10, 100 or 400 $\mu\text{mol m}^{-2} \text{s}^{-1}$.

The effective absorption cross-section is also affected by nutrient limitation (Kolber *et al.*, 1988). The *Microcystis*-nitrate repletion experiment (figure 2.11b) indicated that after 3 days, the absorption cross-section of 0 and 2 μM nitrate treatments decreased slightly relative to nutrient replete cultures ($> 5 \mu\text{M}$). Interestingly, after 6 days, the absorption cross-section of the 'no added' nitrate treatment (0 μM) recovered to levels equivalent to nitrate sufficient treatments. The effective absorption cross-section has been observed to increase due to nutrient limitation and has been attributed to an increased number of inactive reaction centers, allowing the antennae to serve fewer reaction centers leading to an increase in the effective absorption cross-section (Kolber *et al.*, 1988). It is possible that the recovery in cross section after 6 days is due to the inactivation of reaction centers and associated energy transfer.

The fluorometry technique has a number of advantages over the traditional techniques of inorganic carbon incorporation or O_2 evolution in a fluid vessel. Both traditional methods require confinement of the phytoplankton sample, which firstly introduces 'bottle effects' and associated problems such as differentiating between net and gross photosynthesis and changes in community structure due to shock and grazing (Eppley, 1980). There are also problems with reproducing natural irradiance and matching the time scale of photosynthesis to turbulent mixing. In contrast, fluorescence measurements are not only sensitive and nondestructive but can be made rapidly; therefore limiting bottle effects and have temporal advantages in studies of turbulent mixing, high frequency light fluctuation due to cloud cover or surface waves. Moreover, the rapidity of measurement enables greater replication, spatial assessment and improved accuracy of photosynthesis and productivity in lakes and reservoirs.

The monitoring of photochemistry of phytoplankton in Myponga Reservoir (figure 2.14) demonstrated the usefulness of the fluorescence technique combined with a depth-time photosynthesis model. Measurements of F_v/F_m throughout the day enabled the affects of stratification or wind mixing to be assessed on the population. In combination with the effective absorption cross-section of samples from each depth, the photosynthetic rate could be calculated. With the inclusion of meteorological data such as wind speed and irradiance and chlorophyll distribution, the primary productivity was determined for each depth and modeled over the day. It was found that as a result of low chlorophyll *a* concentrations the total productivity of Myponga Reservoir was low at approximately $800 \text{ mg O}_2 \text{ m}^{-3} \text{ d}^{-1}$. The depth-integral photosynthesis model offers the opportunity to investigate the impact of wind mixing and or vertical migration of species such as gas vacuolated cyanobacteria or swimming dinoflagellates.

2.4.3 Conclusions

The FDA and Sytox probes in combination with flow cytometry reliably and rapidly measured the metabolic activity and viability of *Scenedesmus*, *Anabaena* and *Microcystis*. The two probes accurately monitored the activity and viability of cultures subjected to heat treatment, nutrient limitation and replenishment and copper toxicity. Advantages of the two stains are that they firstly compliment each other; FDA assesses relative metabolic activity while Sytox quantifies the number of dead cells. Advantages of the dyes are firstly since the fluorescence of both stains does not interfere with chlorophyll fluorescence they can be used with basic single laser flow cytometers. Furthermore, the chlorophyll fluorescence signal can be used verify the analysis of intact cells and be used to gate out bacteria and debris. Additional advantages include the minimal preparation of the stains with the samples, only small volumes are needed and that results are acquired quickly within 10 minutes. Besides bioassays, the two assays are ideal in ecological studies investigating heterogeneity within populations including the succession of species and or programmed cell death. The ability of flow cytometers to simultaneously measure chlorophyll fluorescence, cell size and side scatter enable further insight into phytoplankton physiology and population variability (Brookes *et al.*, 2002).

Measurements of variable chlorophyll fluorescence using active fluorometry were found to be useful in assessing the affect of irradiance and nutrients on phytoplankton photochemistry. The

measurement of fluorescence is fast, non destructive and enables changes in photochemistry to be monitored at time scales equal to irradiance fluctuations of cells *in situ* (Kroon, 1992, Oliver and Whittington, 1998). The two fluorescent probes, flow cytometry and fluorometry are useful tools in phytoplankton studies where biological processes relating to metabolic activity and viability need to be linked at the same temporal and spatial scales of chemical and physical processes.

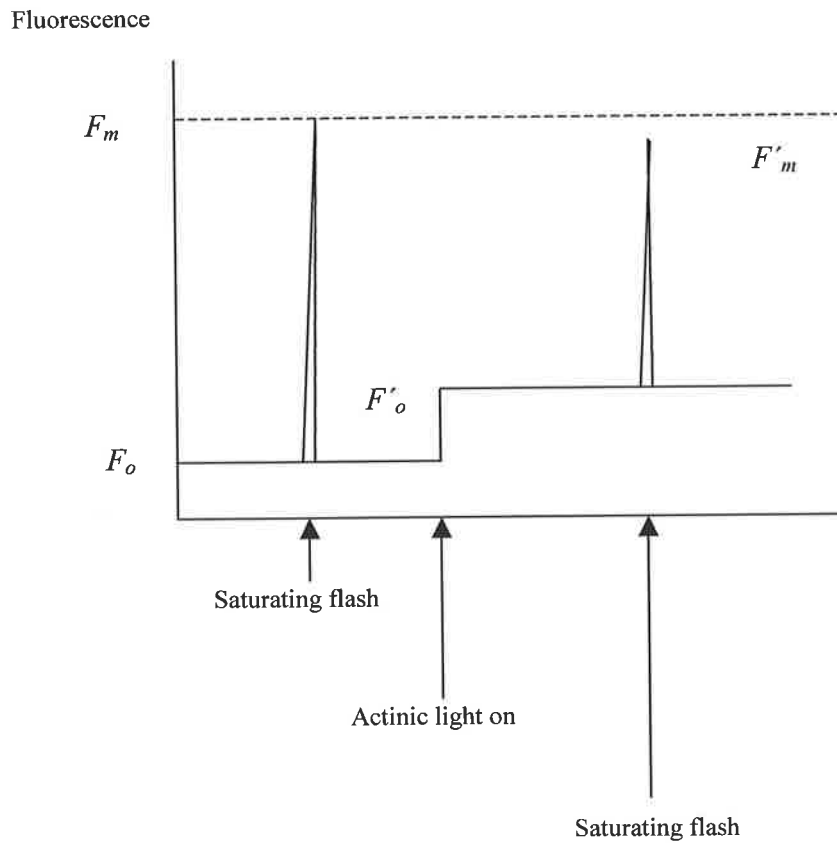


Figure 2.1 Illustration of the measurements involved in variable chlorophyll fluorescence (adapted from Oliver and Whittington, 1998). In dark-adapted cells (15 min), the minimum fluorescence generated by the probe is F_o and without inducing non-photochemical quenching the maximum fluorescence signal generated by a saturating light flash is F_m . In the presence of actinic light, the steady state fluorescence signal F is generated by the proportion of reaction centers closed by the probe at the actinic light intensity. Following a saturating flash of light is F'_m , which is smaller than F_m due to non-photochemical quenching. Under light adaptation, the maximum quantum yield is classified as $F'_m - F'_o$ (light-adapted) = $(F'_m - F'_o) / F'_m$

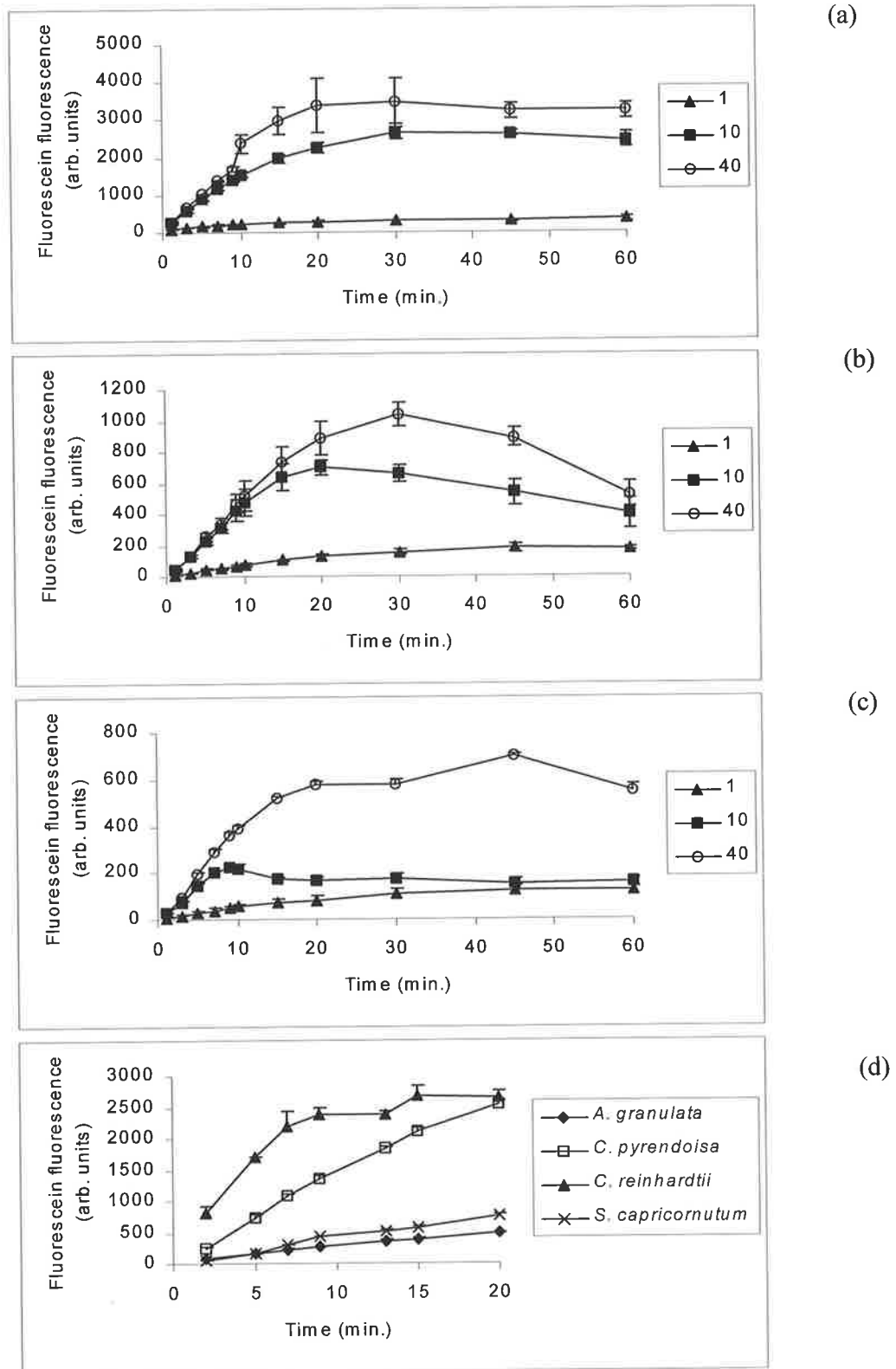


Figure 2.2 Time course for FDA conversion to fluorescein fluorescence at 1, 10 and 40 μM for a) *Scenedesmus quadricauda*, b) *Anabaena circinalis*, c) *Microcystis aeruginosa* and d) various species at a final FDA concentration of 40 μM .

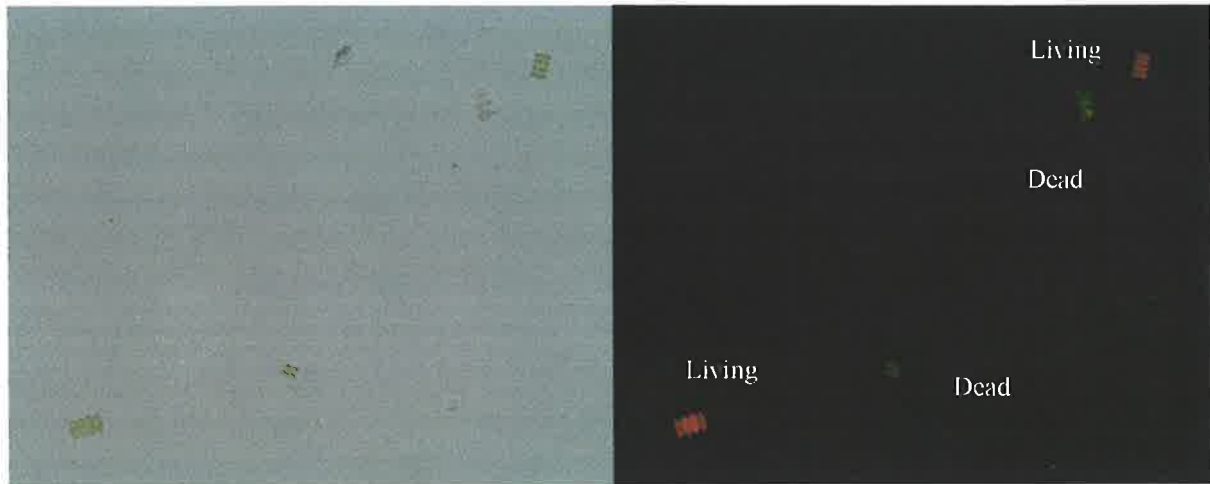
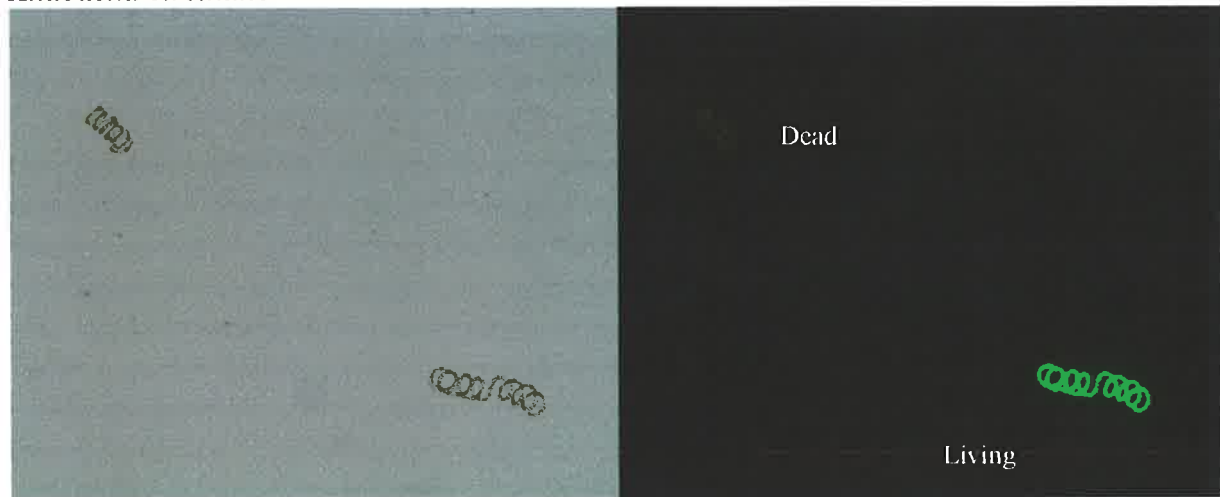
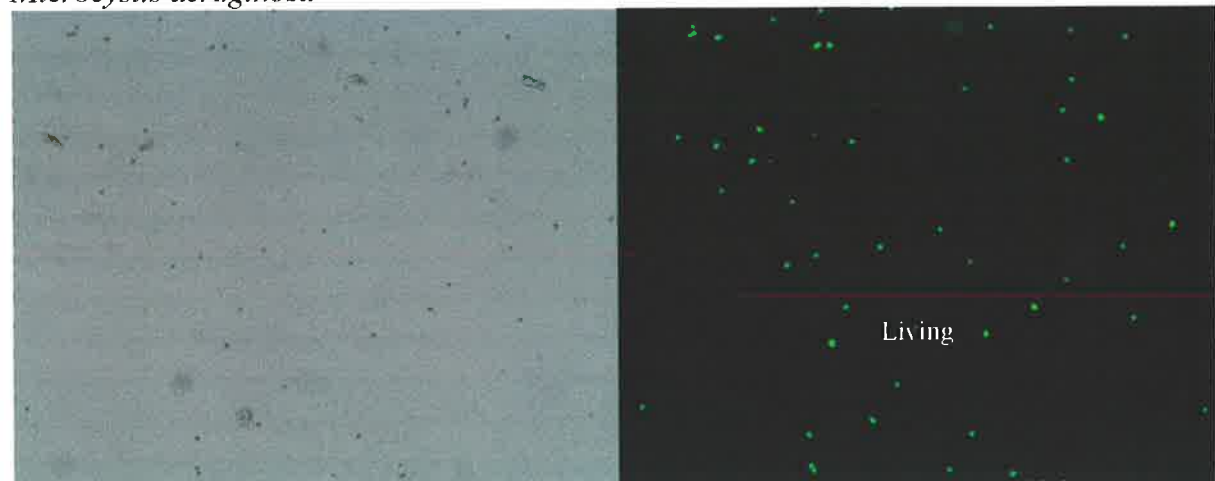
Scenedesmus quadricauda*Anabaena circinalis**Microcystis aeruginosa*

Figure 2.3 Microscopic analysis of fluorescein fluorescence for 50:50 % living: dead mixtures of *Scenedesmus quadricauda*, *Anabaena circinalis* and *Microcystis aeruginosa* with a 40 μM final FDA concentration and respective optimal staining times. Note the lack of green fluorescein fluorescence of metabolically active *Scenedesmus* cells due to high chlorophyll.

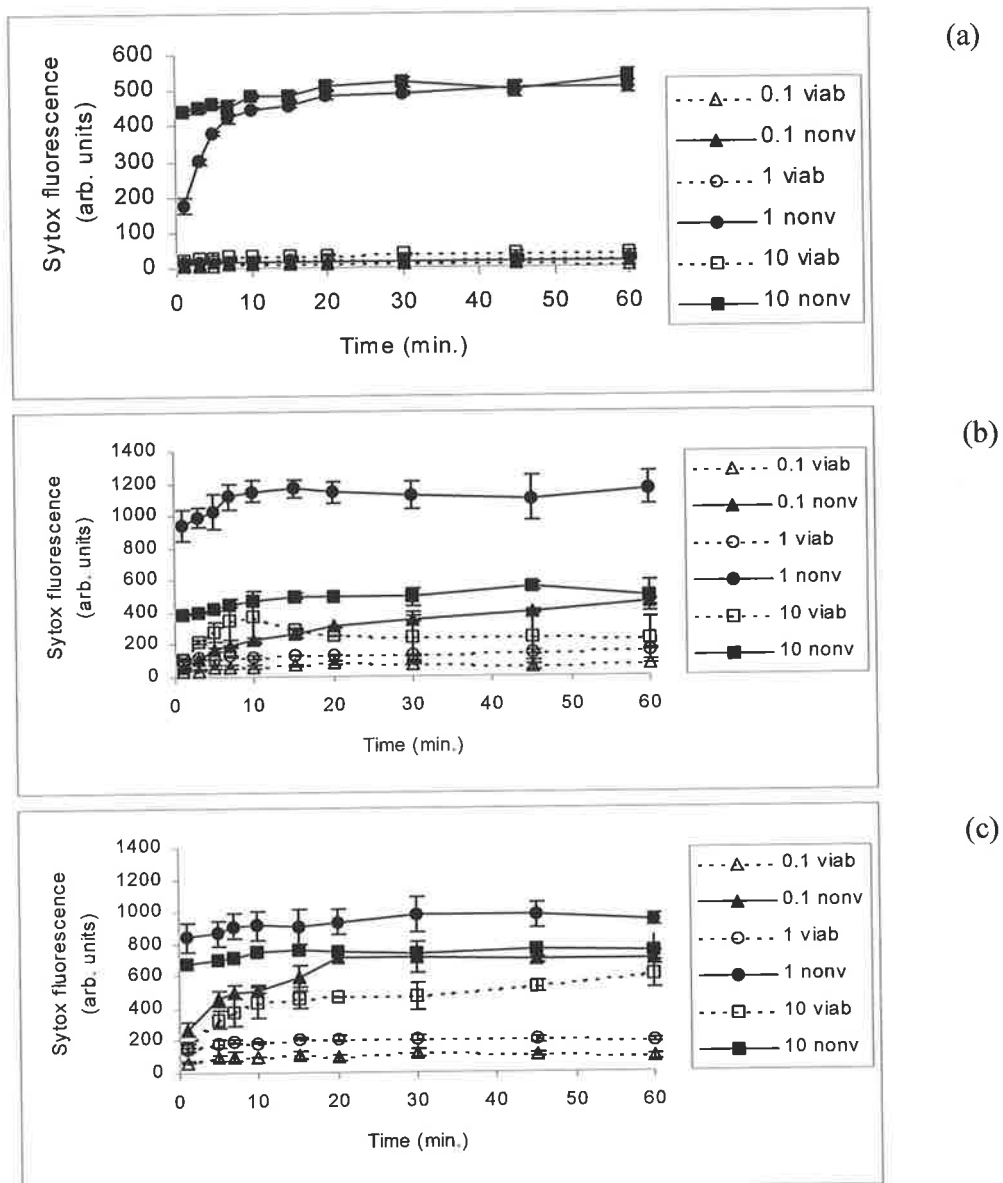


Figure 2.4 Time course (min.) of Sytox fluorescence of living and nonviable (heat-treated) cells for *Scenedesmus quadricauda* (a), *Anabaena circinalis* (b) and *Microcystis aeruginosa* (c) using final stain concentrations of 0.1, 1.0 and 10.0 μM . Sytox only penetrates permeable or compromised membranes and stains DNA resulting in maximum fluorescence. Impermeable living cells are not stained resulting in minimal fluorescence. Fluorescence was measured with a flow cytometer and all units are arbitrary. Note, viab = viable cells and nonv = nonviable cells.

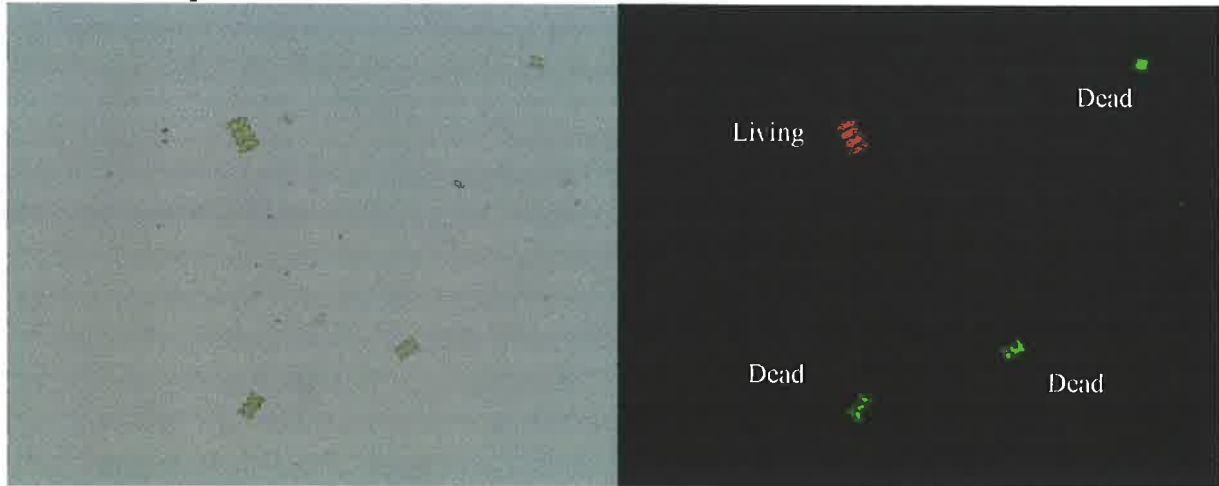
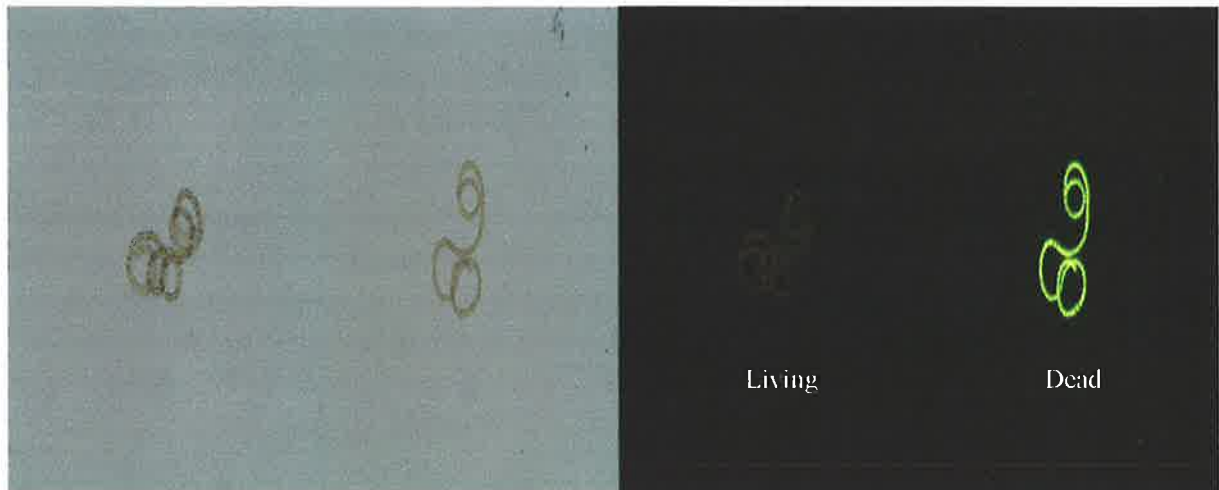
Scenedesmus quadricauda*Anabaena circinalis**Microcystis aeruginosa*

Figure 2.5 Microscopic analysis of Sytox fluorescence for 50:50 % living: dead mixtures of *Scenedesmus quadricauda*, *Anabaena circinalis* and *Microcystis aeruginosa* with a 1- μ M final Sytox concentration and respective optimal staining times.

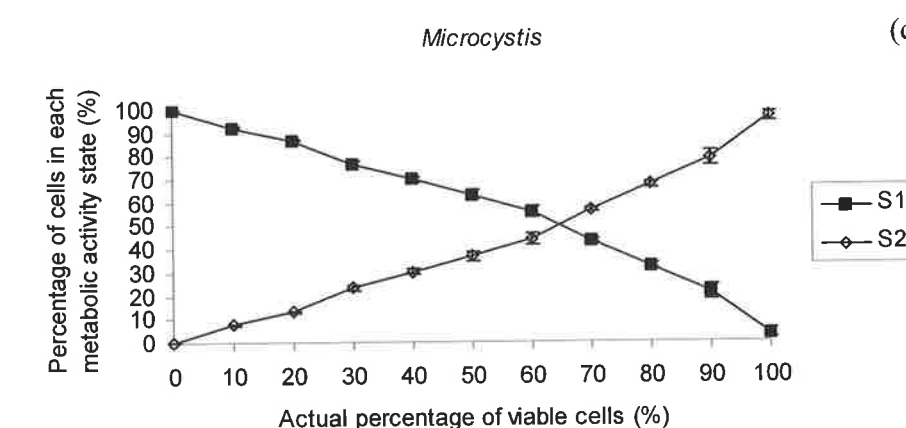
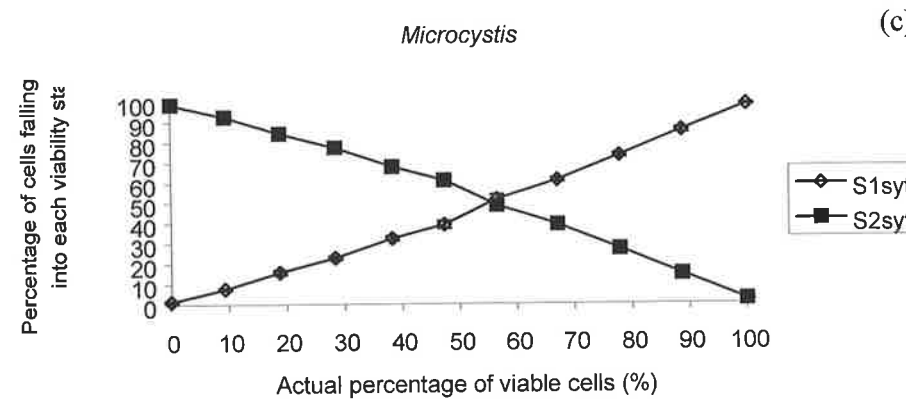
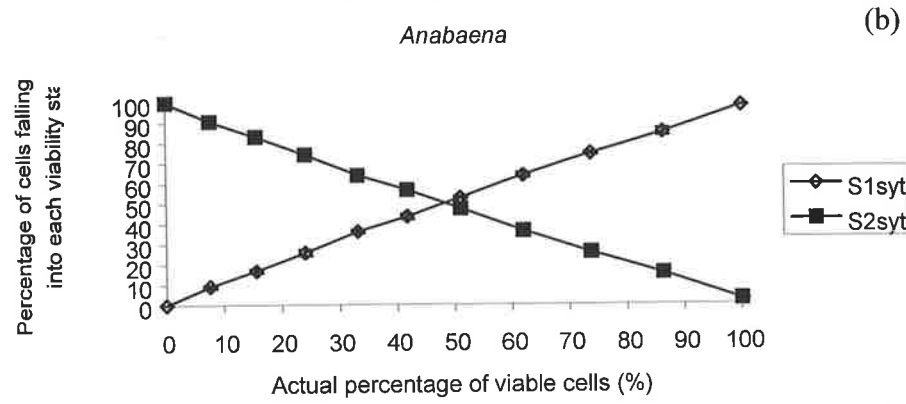
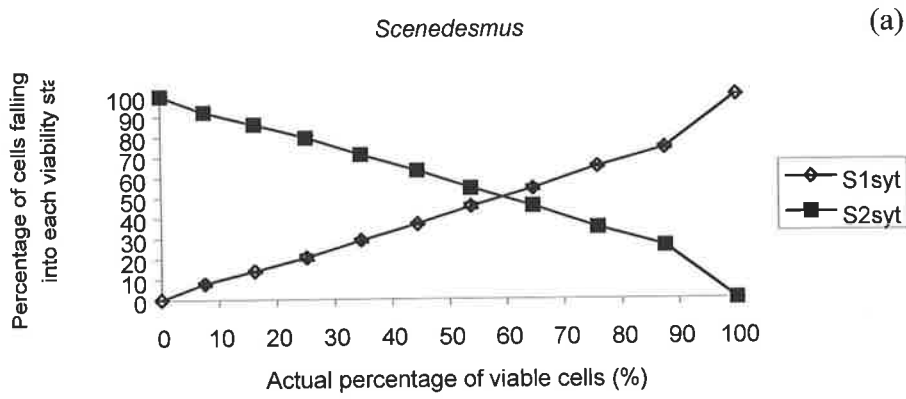


Figure 2.6 Estimation of the number of viable and nonviable cells in living/ dead cell mixtures of *Scenedesmus quadricauda* (a), *Anabaena circinalis* (b) and *Microcystis aeruginosa* (c) using Sytox and of *Microcystis* using FDA (d).

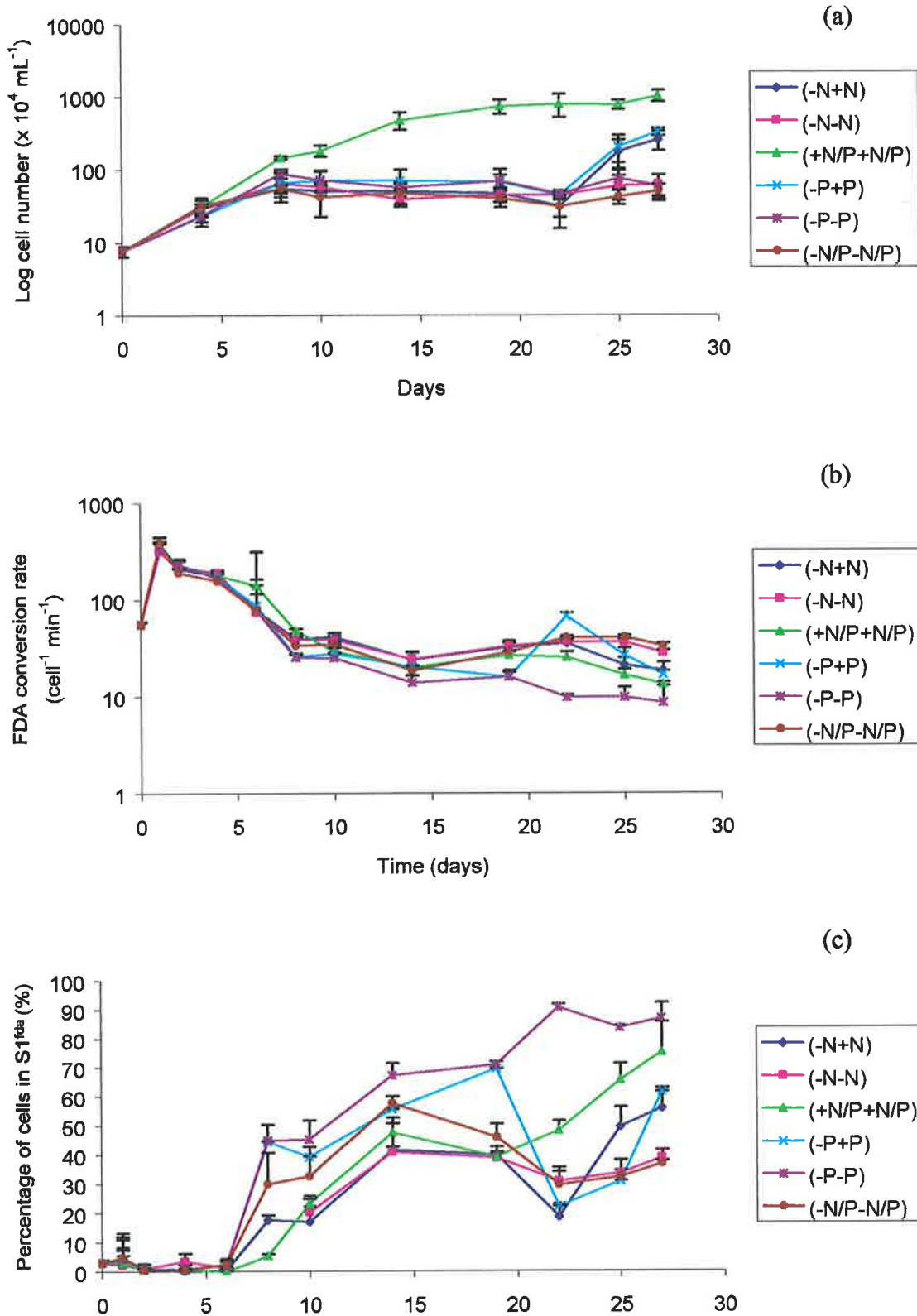


Figure 2.7 Monitoring the response of *Microcystis* cell numbers (a), mean esterase activity, FDAC $\text{cell}^{-1} \text{ min}^{-1}$ (b) and number of cells in low esterase activity state, $S1_{\text{fda}}$ (c) to nutrient limitation and repletion of limiting nutrient (s) over time. Note: nutrient repletion occurred on Day 19.

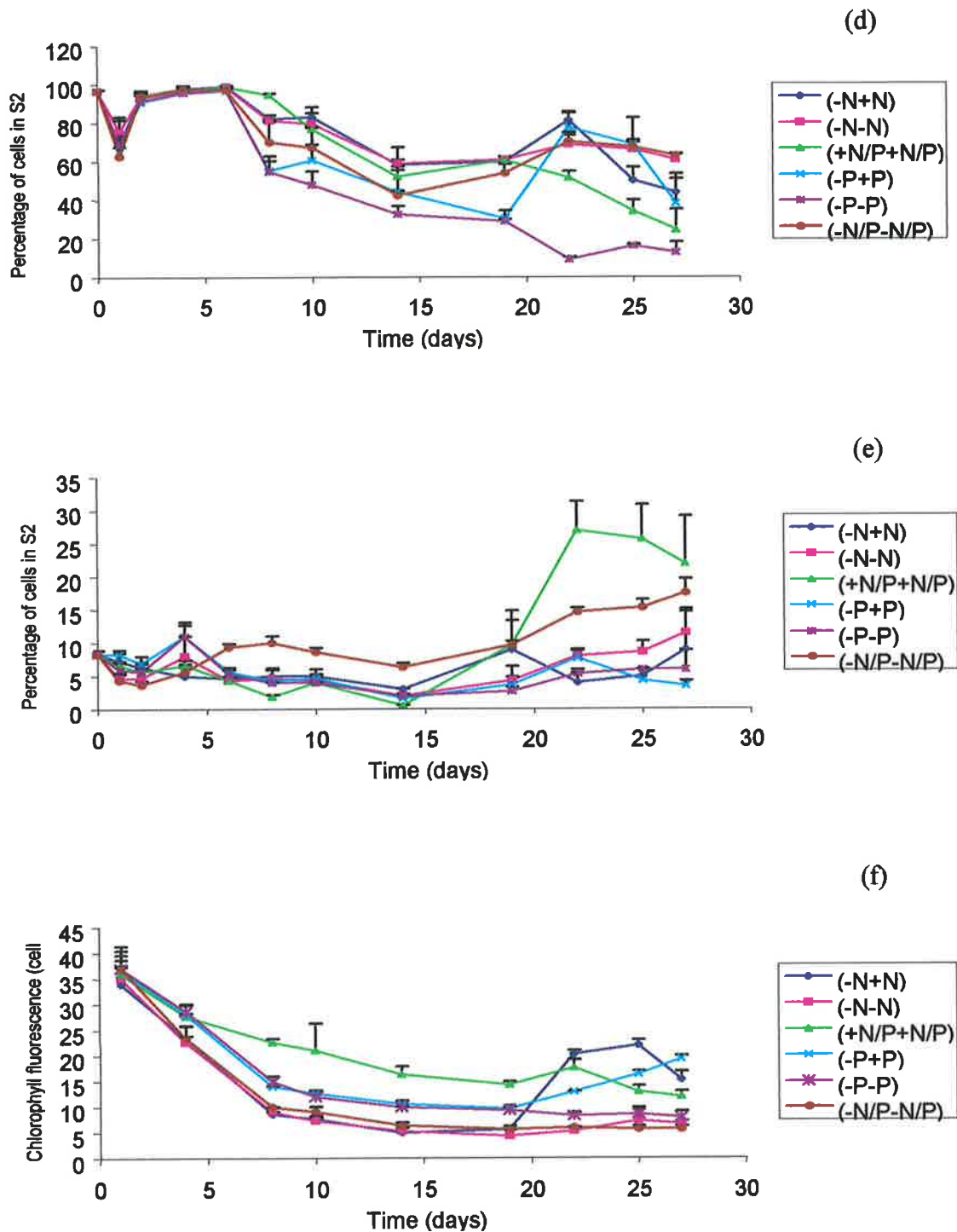


Figure 2.7 Monitoring the response of *Microcystis* number of cells in the normal esterase activity state, $S2_{fda}$ (d), number of cells in nonviability state, $S2_{syt}$ (e) and chlorophyll fluorescence $cell^{-1}$ (f) to nutrient limitation and repletion of limiting nutrient (s) over time. Note: nutrient repletion occurred on day 19.

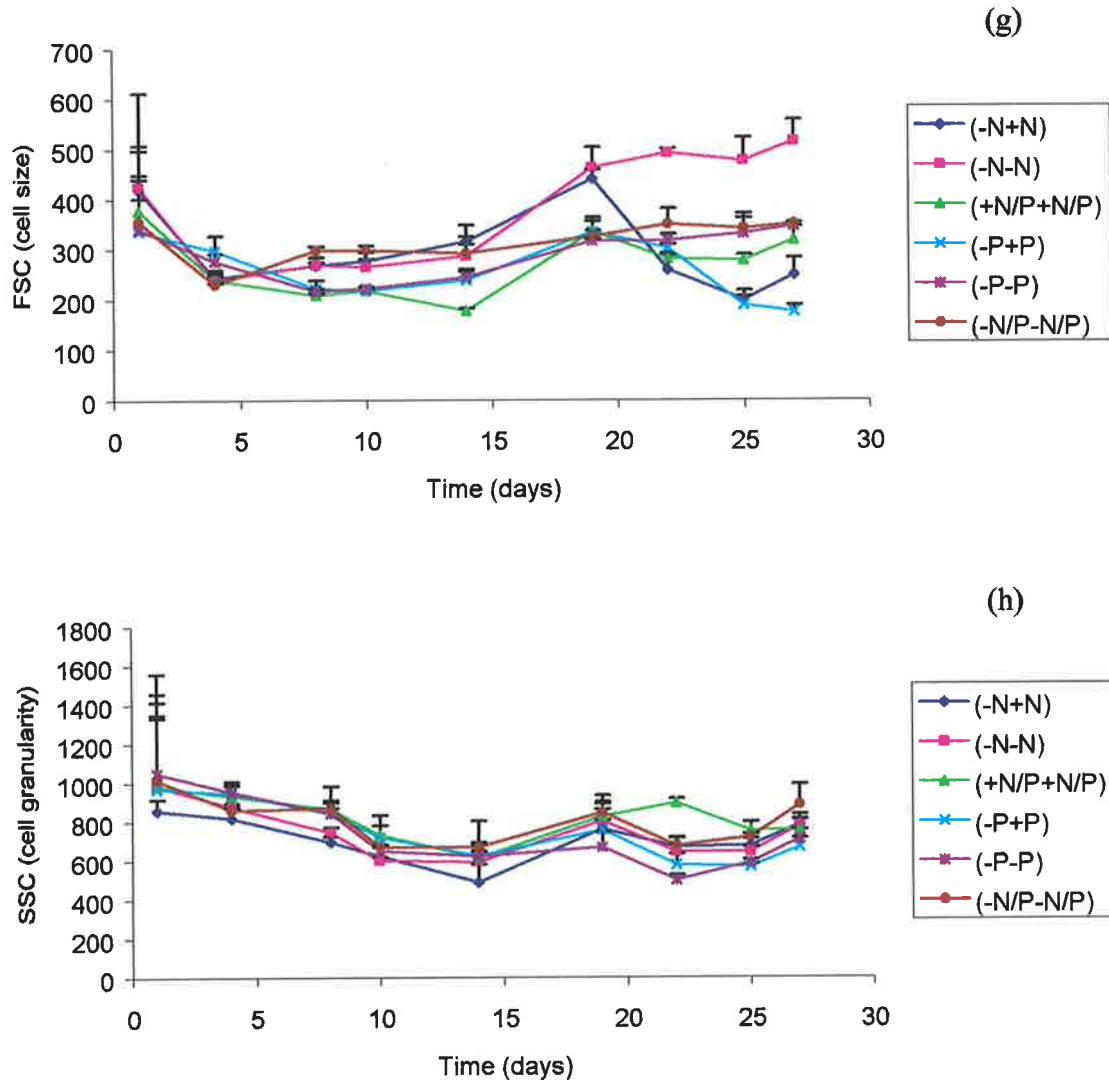


Figure 2.7 Monitoring the response of *Microcystis* cell size, FSC scatter (g) and cell granularity, SSC scatter (h) to nutrient limitation and repletion of limiting nutrient (s) over time. Note: nutrient repletion occurred on day 19.

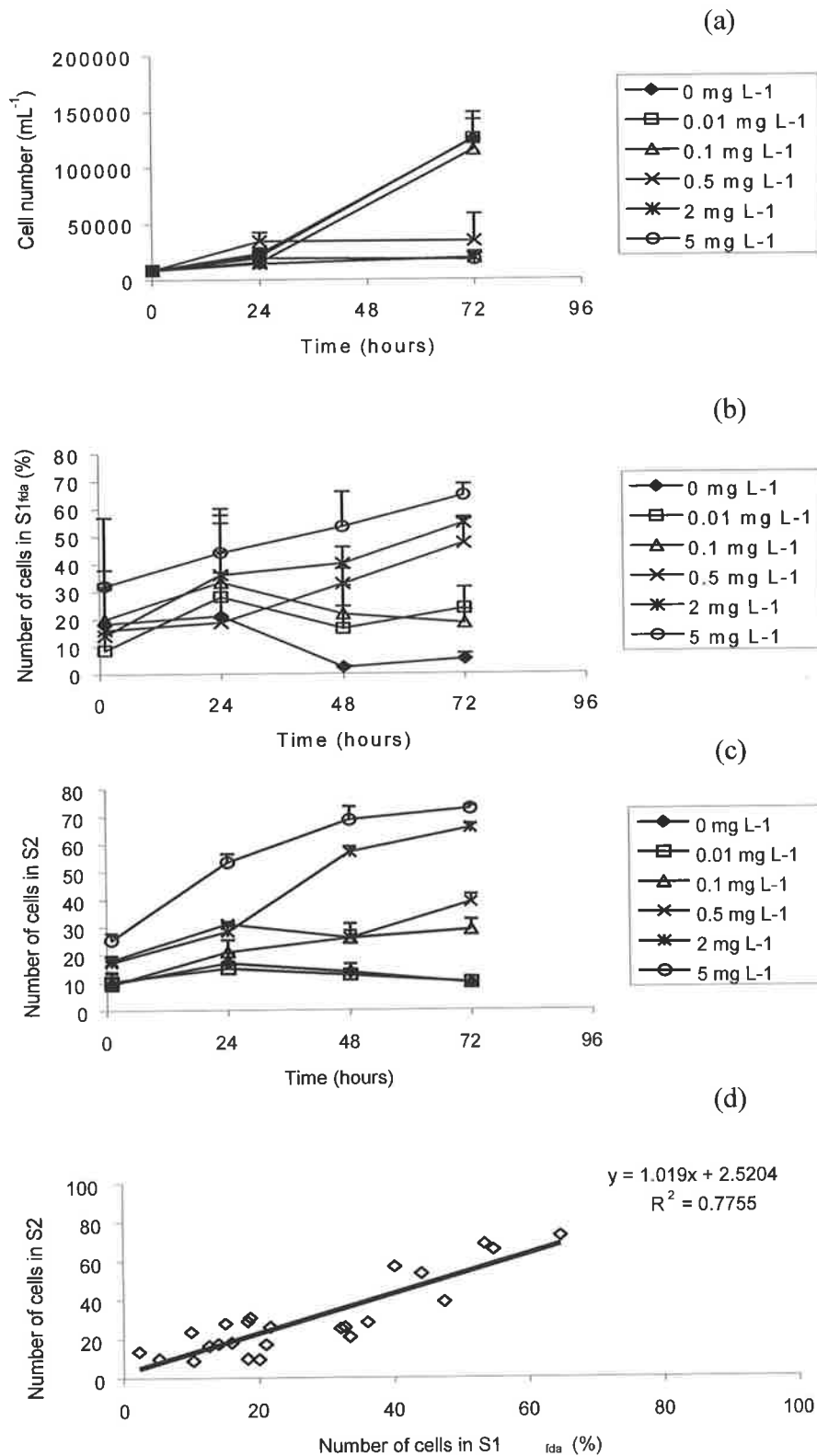


Figure 2.8 Effect of copper at concentrations from 0.01 to 5 mg L⁻¹ on *Scenedesmus quadricauda* growth expressed as cell numbers mL⁻¹ (a), esterase activity expressed as the number of cells in low activity state, S1_{fda} (b) cell viability expressed as number of cells in state, S2_{syt} (c) and the resultant relationship between S1_{fda} and S2_{syt} (d).

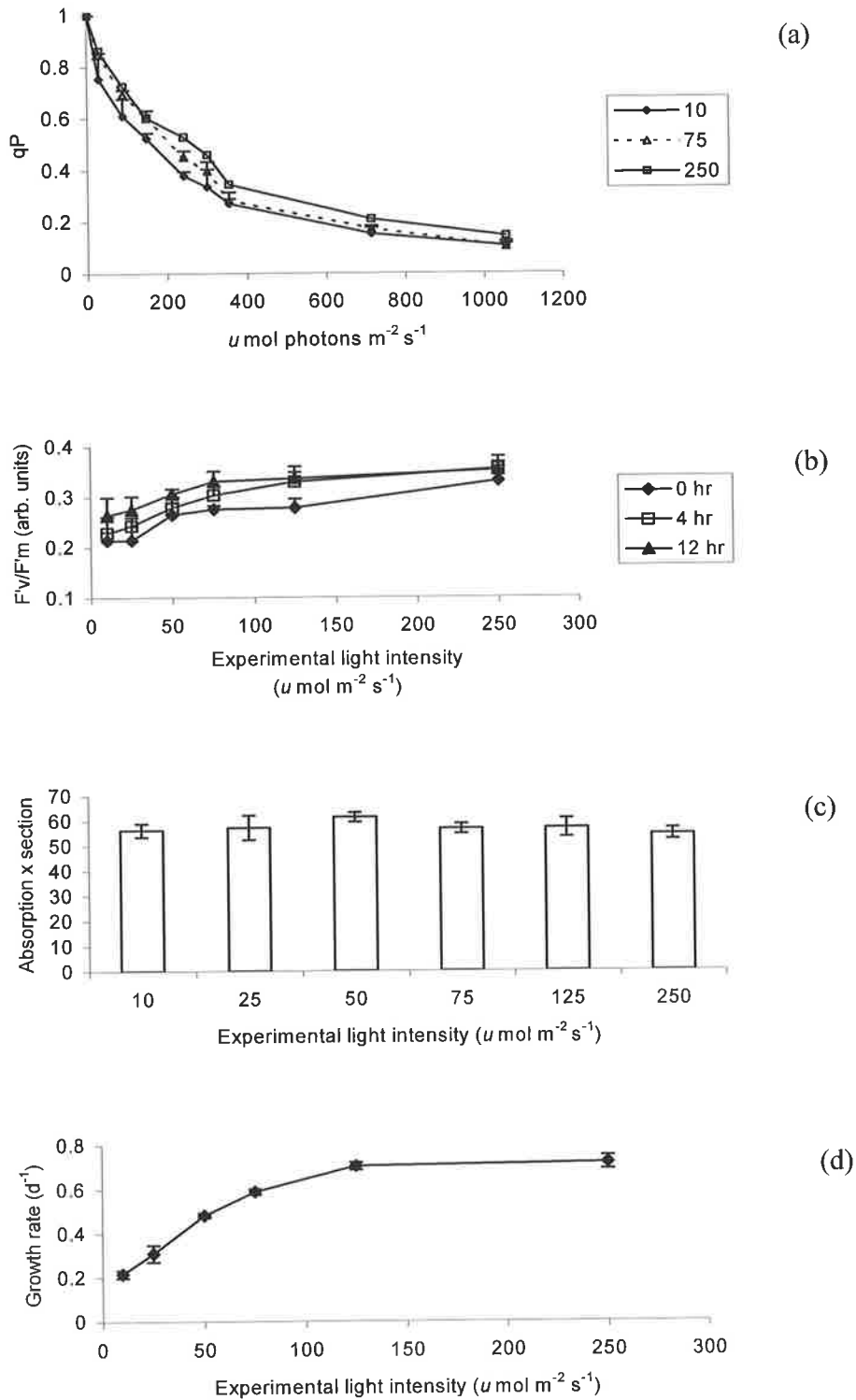


Figure 2.9 Influence of light intensity on *Microcystis aeruginosa* photochemical quenching (a), maximum quantum yield, F'_v/F'_m (b), effective absorption cross-section (c) and growth rate (d) after 6 days at each light intensity. Variable chlorophyll fluorescence measurements were made with a PAM fluorometer.

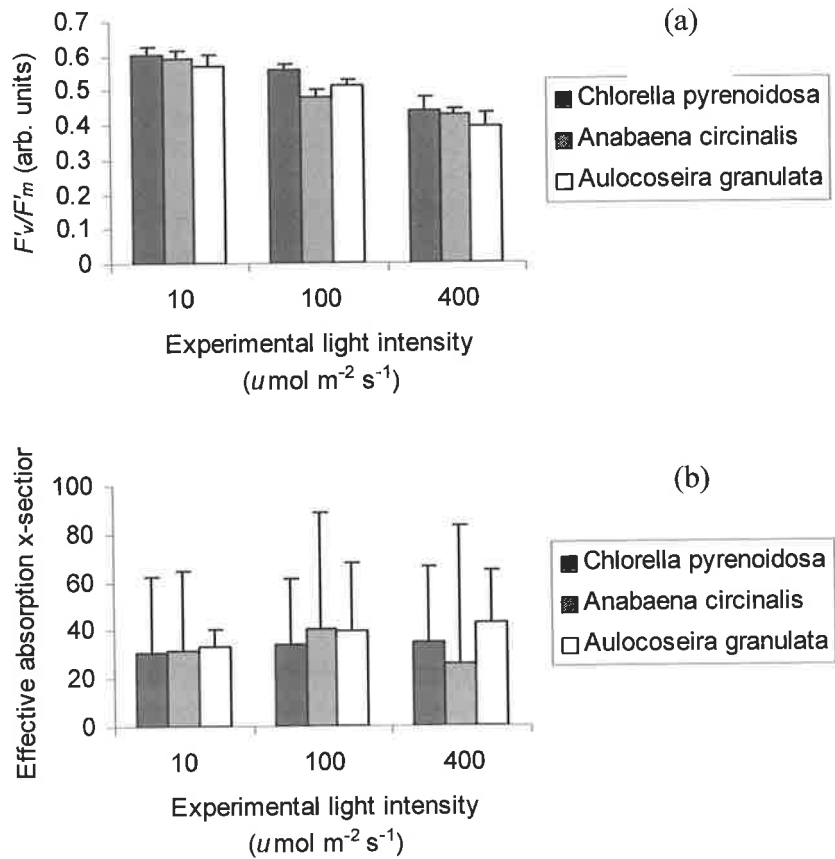


Figure 2.10 Influence of light intensity on the maximum quantum yield, F_v/F_m (a) and effective absorption cross-section (b) after 5 days of incubation for *Chlorella pyrenoidosa*, *Anabaena circinalis* and *Aulocoseira granulata*. Note: effective absorption cross-section units are $\text{\AA}^2 \text{ quanta}^{-1}$.

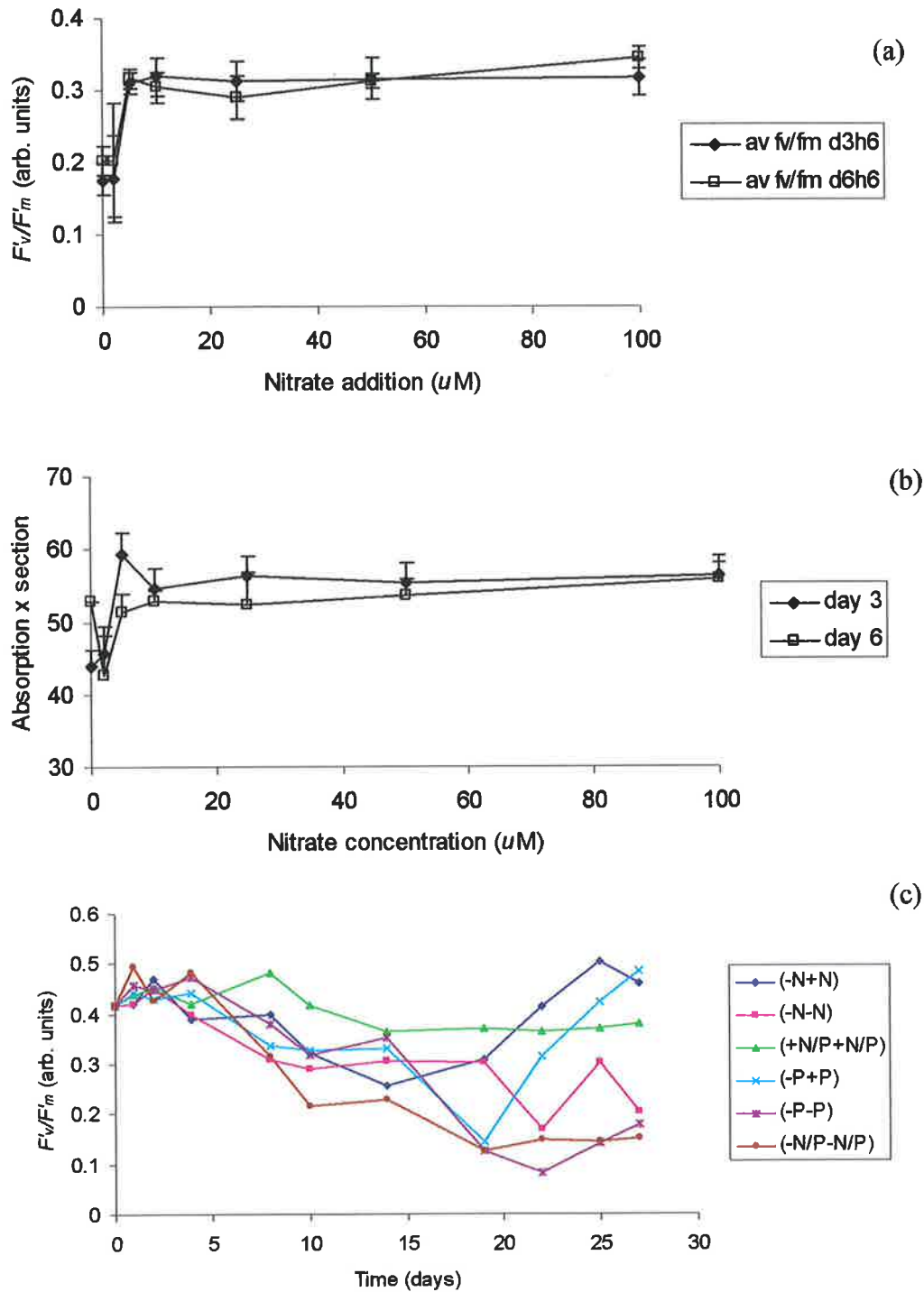


Figure 2.11 Influence of nutrient status on *Microcystis aeruginosa* photophysiology – nitrate addition to N-deplete WC media and maximum quantum yield, F_v/F_m (a), effective absorption cross-section (b) and the influence of -N or -P or -N/-P limitation repletion on maximum quantum yield (c). Note for (c), nutrient repletion occurred on day 19 and units for effective absorption cross section are $\text{\AA}^2 \text{ quanta}^{-1}$.

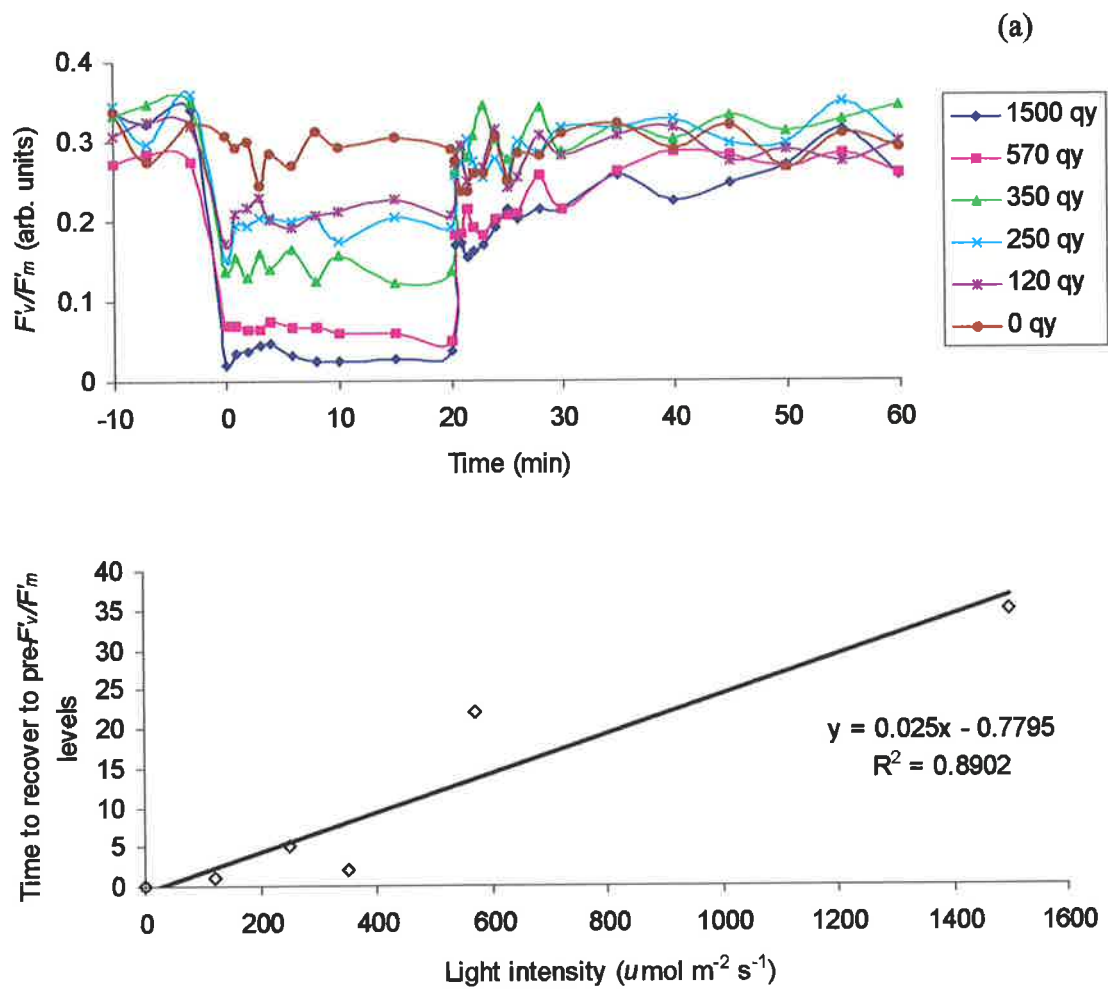


Figure 2.12 F_v/F_m depression and recovery kinetics of cultured *Anabaena circinalis* to various low and high light intensities (a) and the relationship between light intensity and recovery time of F_v/F_m to original levels before light exposure (b).

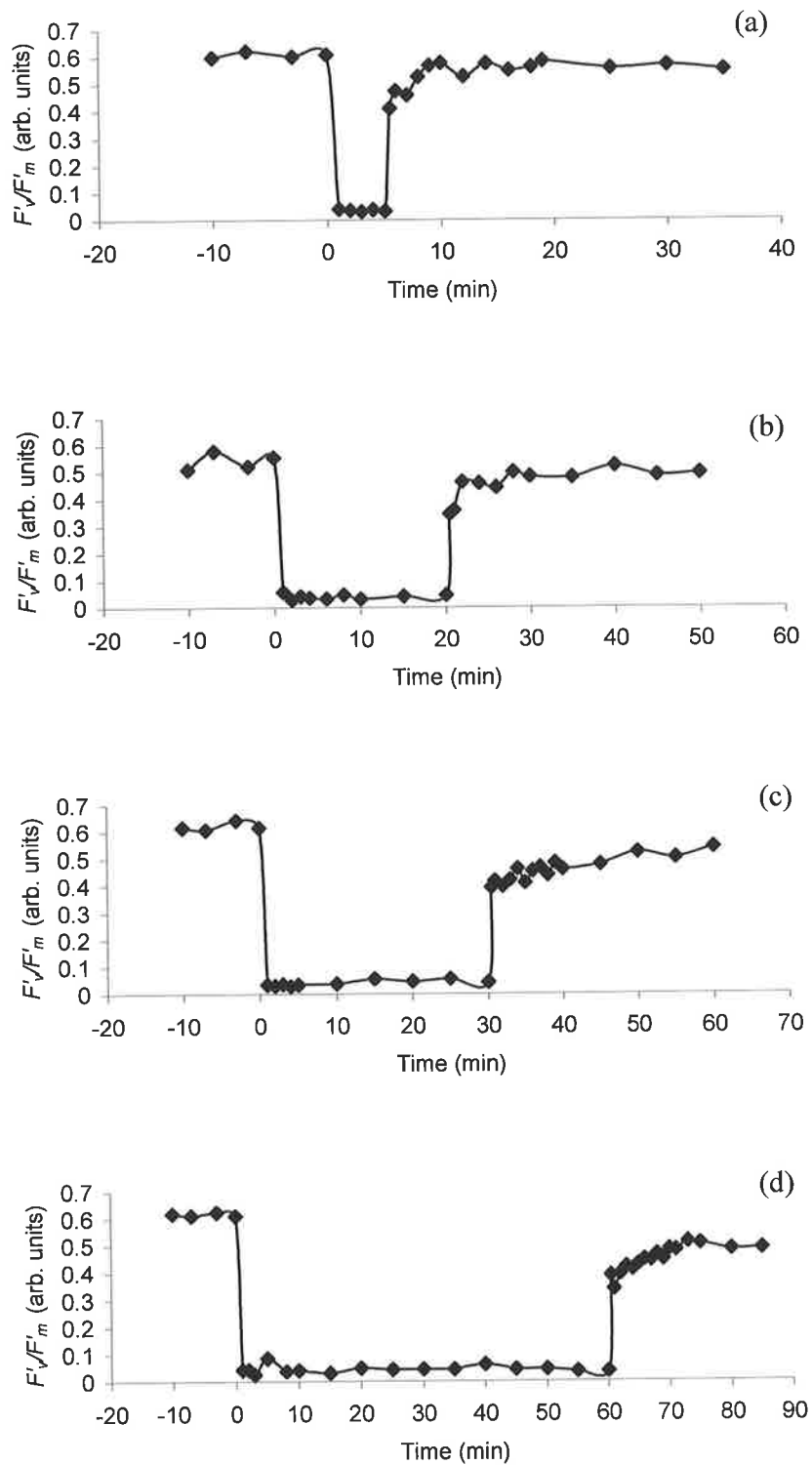


Figure 2.13 Influence of high light ($1500 \mu\text{mol m}^{-2} \text{s}^{-1}$) exposure time ranging from 5 min. (a), 20 min. (b), 30 min. (c) and 60 min. (d) on F_v/F_m depression and recovery of cultured *Anabaena circinalis* grown at $20 \mu\text{mol m}^{-2} \text{s}^{-1}$.

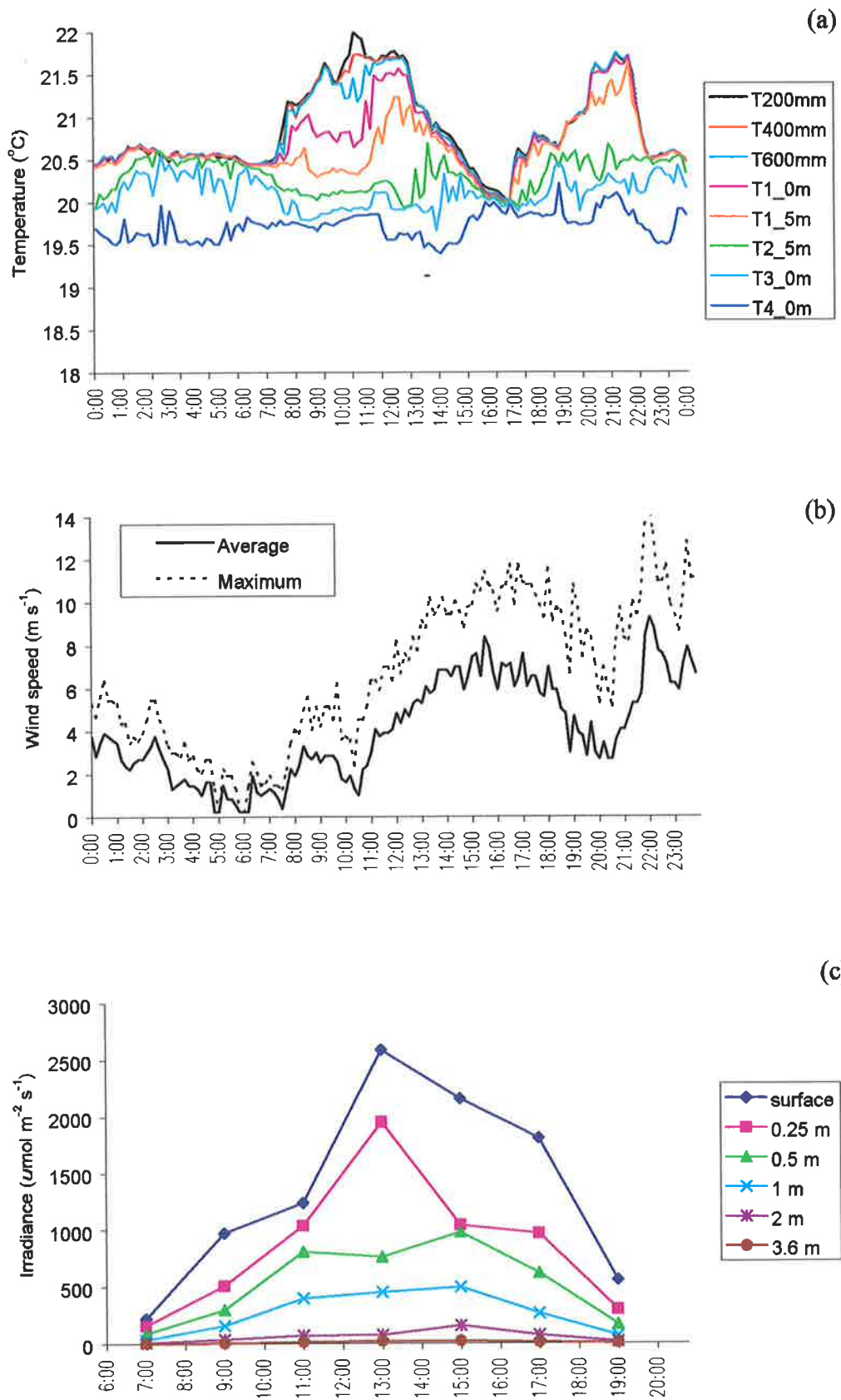


Figure 2.14 Variation in thermal structure (a), wind speed (b) and surface irradiance (c) at Myponga Reservoir on the 10 January 2000.

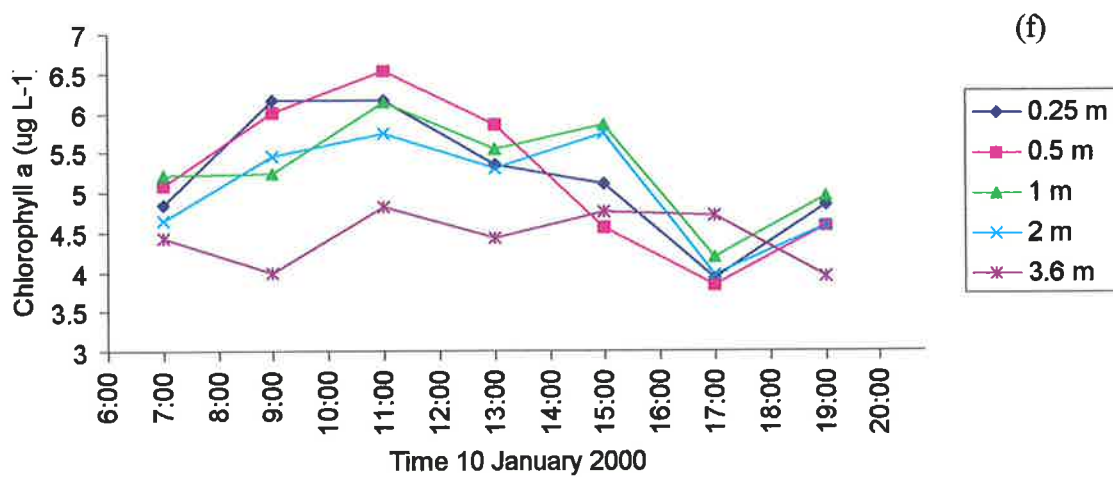
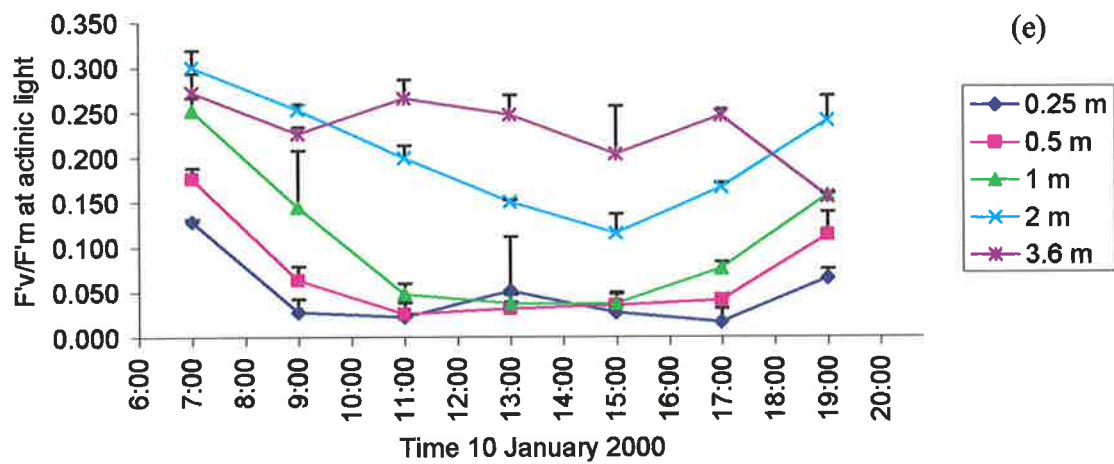
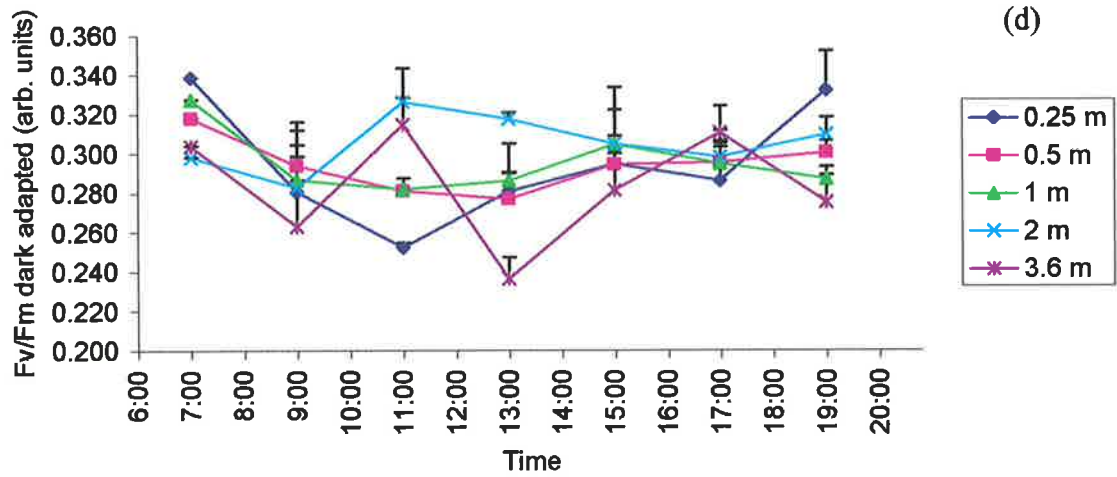


Figure 2.14 Variation in F_v/F_m of bottled natural phytoplankton placed at discrete depths (d), F'_v/F'_m at actinic light intensities of natural phytoplankton taken from each sampling depth (e) and chlorophyll *a* concentration at each sampling depth (f).

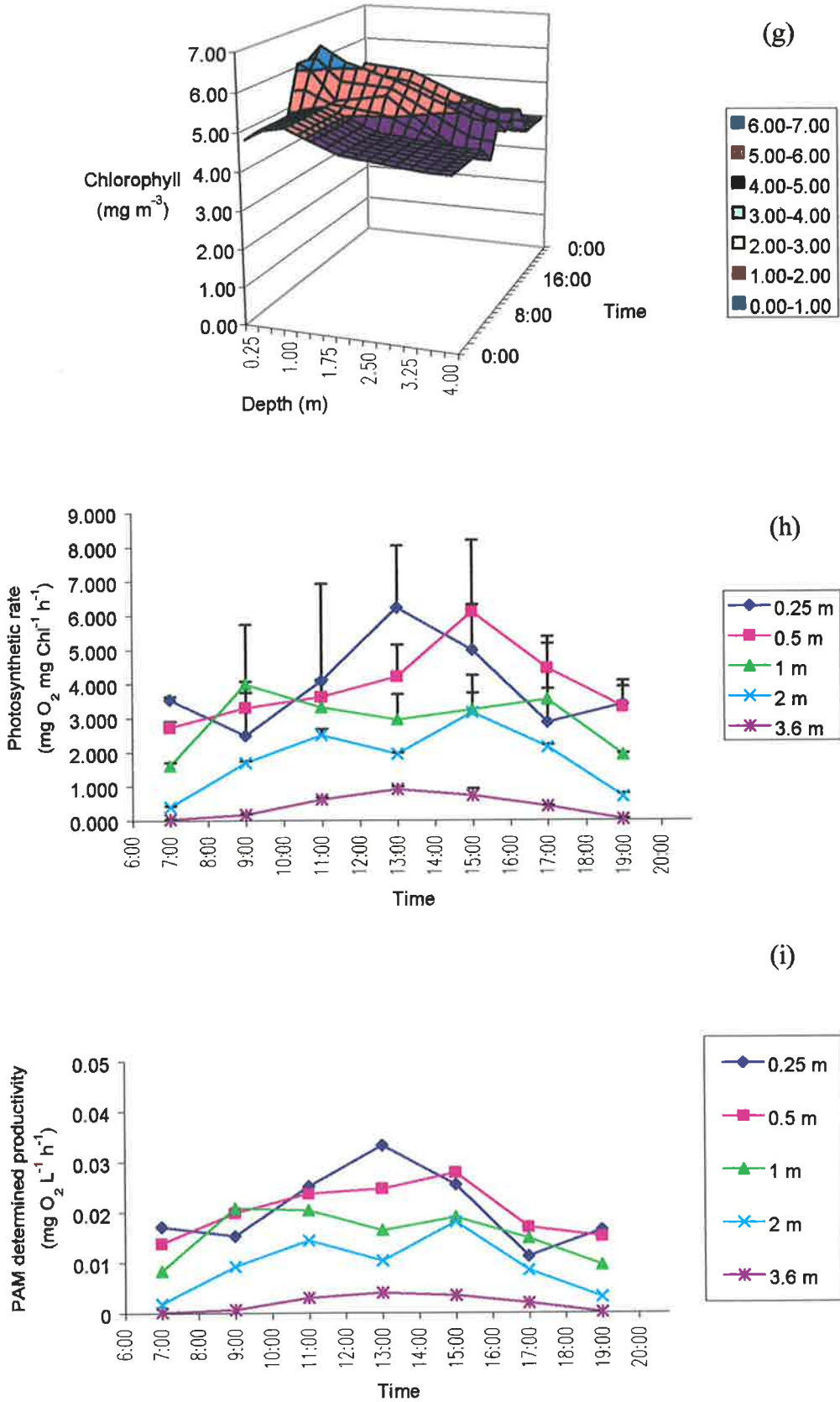


Figure 2.14 Variation in modeled chlorophyll *a* distribution over 4 m (g), fluorometry determined photosynthetic rates (h) and productivity (i) at each sampling depth.

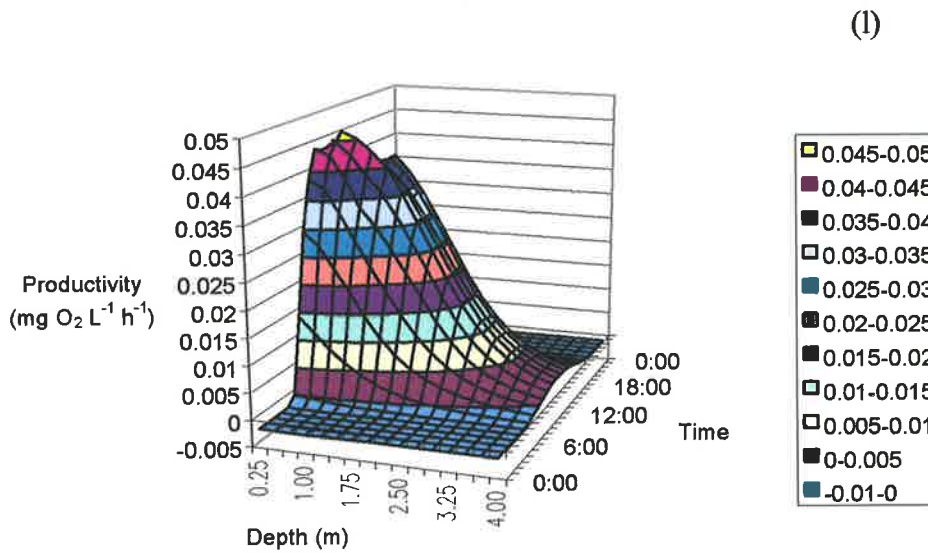
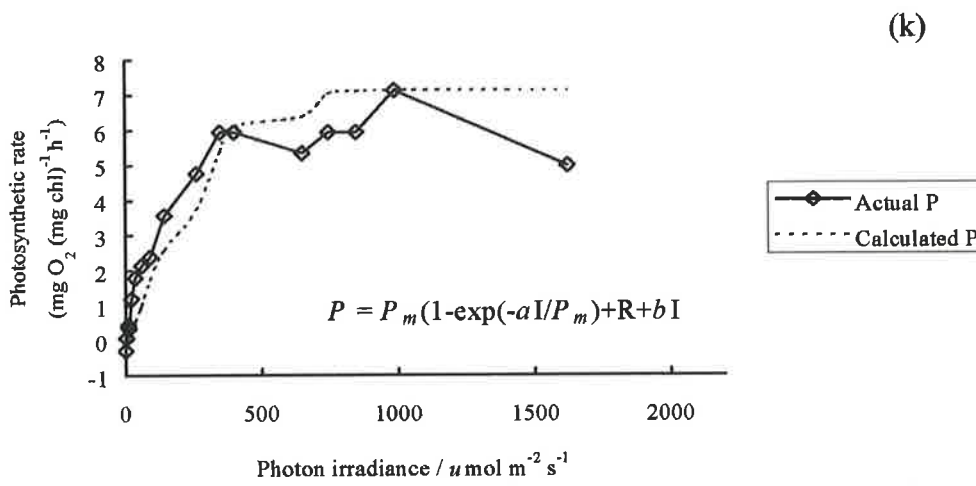
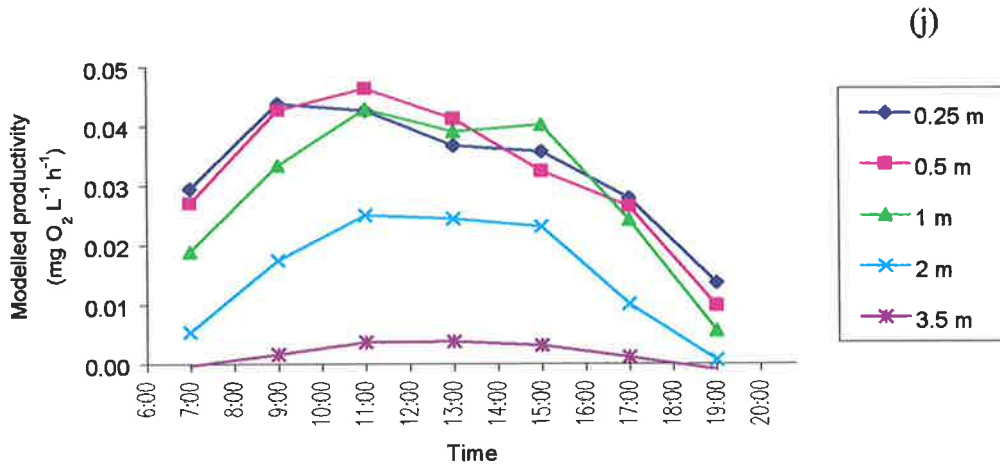


Figure 2.14 Variation in modeled productivity at each sampling depth (j), photosynthesis-irradiance curve for a surface sample from the reservoir (k) and depth-time modeled productivity (l) for natural phytoplankton in Myponga Reservoir on 10 January 2000.

Regel, R.H., Brookes, J.D., and Ganf, G.G., (2004) Vertical migration, entrainment and photosynthesis of the freshwater dinoflagellate *Peridinium cinctum* in a shallow urban lake.

Journal of Plankton Research, v. 26 (2), pp. 143-157.

NOTE:

This publication is included on pages 87-115 in the print copy of the thesis held in the University of Adelaide Library.

It is also available online to authorised users at:

<http://dx.doi.org/10.1093/plankt/fbh008>

Brookes, J.D., Regel, R.H., and Ganf, G.G., (2003) Changes in the photo-chemistry of *Microcystis aeruginosa* in response to light and mixing. *New Phytologist*, v. 158 (1), pp. 151-164.

NOTE:

This publication is included on pages 116-151 in the print copy of the thesis held in the University of Adelaide Library.

It is also available online to authorised users at:

<http://dx.doi.org/10.1046/j.1469-8137.2003.00718.x>

Chapter 5

The measurement of flow and small-scale turbulence around artificial mixing systems in a deep reservoir and shallow lake

5.1 Introduction

Water and habitat quality may become severely degraded in impounded water bodies as a consequence of thermal stratification and or eutrophication. Thermal stratification restricts vertical mixing and limits the transfer of water and dissolved substances, particularly oxygen between the epilimnion and the hypolimnion. Prolonged stratification may isolate the hypolimnion from the atmosphere creating an oxygen debt and a reducing environment within the hypolimnion. The symptoms of poor water quality include cyanobacterial blooms, high oxygen debts from high chemical and biological oxygen demand and the associated release of substances from reducing sediments such as phosphorus (P), iron (Fe), manganese (Mn), hydrogen sulfide and methane. The resolubilisation of Fe and Mn into the water column poses a problem for water supply reservoirs as treatment costs increase and their oxidation by chlorine or air in distribution systems causes 'dirty water' problems. In addition, a reduction in dissolved oxygen reduces the available habitat for zooplankton and higher trophic organisms.

The Torrens Lake is an example of a significantly degraded water body receiving pollutants from a highly developed urban-semi rural catchment. It displays symptoms of both cyanobacterial blooms, particularly excessive growth of *Microcystis* species and high oxygen debts. Despite its shallowness (2 m average depth) dissolved oxygen concentrations regularly approach 0 mg L^{-1} within the surface mixed layer and its management poses a significant challenge. In contrast, the Myponga Reservoir is located within a rural catchment and is prone to *Anabaena circinalis* growth during the spring-summer months of November to February, which is controlled by chemical means (CuSO_4). Prior to the installation of a bubble plume aerator, Myponga Reservoir experienced problems with Fe and Mn release from sediments reaching levels above water drinking water guidelines of 0.71 mg L^{-1} and 0.41 mg L^{-1} , respectively (Brookes *et al.*, 2000c).

Artificial mixing is a widely used technique to destratify and control oxygen deficiency and undesirable phytoplankton in lakes and reservoirs (Steinberg, 1983; Jungo *et al.*, 2001; Daldorph, 1998; Simmons, 1998). The type of system employed is dependent upon the specific water quality problem. Hypolimnetic oxygen injection is a technique, which permits oxygenation of the hypolimnion without disturbing natural stratification. Its objective is to improve sediment-water chemistry by increasing oxygen without permitting free vertical transport of oxygenated water. The theoretical advantage over complete mixing is that nutrients cannot be transported into the epilimnion, providing resources for phytoplankton within the euphotic zone. In contrast, phytoplankton control is based on reversing seasonal succession and the primary objective is to increase the degree of mixing and depth of the surface mixed layer. Increased mixing will lead to the entrainment and transport of phytoplankton vertically out of the euphotic zone leading to light limitation and suppression of problematic genera and promotion of turbulent-dependent phytoplankton (e.g. diatoms). Most bloom forming cyanobacteria (gas vacuolated) are well adapted to stratified water columns and consequently the disruption of thermal stratification may provide a less suitable habitat for many (e.g. *Microcystis*, *Anabaena*), although not all, cyanobacteria (e.g. *Planktothrix*).

The most frequently used mixing devices are bubble plume aerators (figure 5.1a). Bubble plume aerators are located near the bottom of the water body and operate by entraining water with fine air bubbles, which mixes and propagates an intrusion generating circulation and increasing the exchange of water between the shallow and deeper layers. The increased circulation reduces the differences in temperature, oxygen and nutrients between the epilimnion and hypolimnion. A recent approach, which is increasingly being applied in cyanobacterial control (Burch *et al.*, 2000; Kirke, 2000), includes the use of surface mounted impellers (figure 5.1b). The impellers operate by drawing warm surface water containing phytoplankton down a draft tube, where it exits and either it jets downwards or turns back on itself and eventually forms an intrusion. The depth of the intrusion is variable and dependent upon the thermal structure, which determines the buoyancy of the penetrating jet (Lewis, 2003). The system is appropriate in deep-water bodies where intrusions can develop below the euphotic zone.

Although, artificial mixing as a management technique has a long history, detailed effects on the physical, chemical and biological characteristics of the water column are limited (Hawkins and

Griffiths, 1993). A review of 50 artificial mixing projects in Australia found that only 75 % improved the oxygen status of the water body, but only 16 % influenced the concentration and composition of phytoplankton communities (McAuliffe and Rosich, 1990). A more recent review of hypolimnetic oxygenation reported that it is a successful management option with numerous water quality benefits (Beutel and Horne, 1999). Artificial mixing is usually applied in relatively deep-water bodies (> 10 m) where phytoplankton can be deeply mixed relative to the euphotic depth, reducing their access to light. Artificial mixing in shallow lakes is unlikely to reduce phytoplankton blooms by restricting light availability, however, it may indirectly limit blooms by oxygenating the sediments and reducing nutrient release and limiting the phosphorous available for growth.

The applications of hydrodynamic simulation models such as DYRESM (Imberger *et al.*, 1978) are assisting in designing artificial mixing systems in managing water quality (Cox *et al.*, 1998; Imteaz and Asaeda, 2000; Lewis *et al.*, 2002), but empirical data on mixer performance is scarce. In particular, field data of the zone of influence or turbulent intensity have rarely been quantified and or linked to biological processes. Mixing processes are complex and consist of eddies of various sizes and time scales that interact and exchange momentum energy and mass among each other. Critical flow velocities and shear velocities are increasingly being reported in relation to cyanobacterial growth (Mitrovic *et al.*, 2003). The influence of large scale turbulent mixing on the light climate of phytoplankton has been extensively studied (e.g. Visser *et al.*, 1996), but the role of turbulence at small-scales (i.e. mm to cm) is a relatively neglected factor in phytoplankton ecology. Recent studies have indicated that small-scale shear may be significant in the control of cyanobacterial blooms (Moisander *et al.*, 2002; O'Brien *et al.*, *in review*). Presently, there is no evidence as to whether entrainment and transport through a surface mechanical mixer and subsequent exposure to turbulence directly affects phytoplankton. Measurements of the turbulent kinetic energy dissipation rate, ϵ is a means by which large scale turbulent mixing can be related to the small-scale shear environment of the phytoplankton (Sanford, 1997).

Recently in South Australia, artificial mixing systems have been installed to improve water quality and reduce the growth of cyanobacteria. In 1999, two surface mounted mechanical mixers were installed in the Myponga Reservoir to arrest *Anabaena* growth as part of a Cooperative Research Centre for Water Quality and Treatment investigation (project 2.5.1 *Artificial mixing for destratification and control of cyanobacterial growth in reservoirs*). The effects of artificial

mixing and CuSO_4 dosing on phytoplankton succession have been simulated by Lewis *et al.* (*in press*). Previously, in 1994 a bubble plume aerator had been installed and is successfully decreasing Fe and Mn sediment release (Brookes *et al.*, 2000c). While in the 2000 summer, three bubble plume aerators were temporarily installed in the Torrens Lake in an attempt to control *Microcystis* growth. In 2002, these aerators were replaced with 11 submerged aspirators and 3 high volume surface aerators as a means to decreasing the incidence of anoxia during summer. These installations provided the opportunity to quantify the intensity of turbulence generated by various mixing devices and to compare this with the turbulence generated by wind forcing alone. A further aim was to assess using flow cytometry and fluorescent dyes whether entrainment through a mechanical mixer and draft tube and subsequent exposure to turbulence deleteriously affects Myponga Reservoir phytoplankton. The primary hypothesis of this study was that the artificial mixing devices would generate higher turbulent kinetic energy dissipation rates under thermally stratified conditions compared to wind forcing on the surface layer and potentially influence phytoplankton activity directly through the action of shear stress.

The primary objectives of this study were:

- To characterize the flow and turbulent intensities below a surface mechanical mixer in the Myponga Reservoir
- To determine whether or not entrainment and transport through the mechanical mixer and draft tube system affects the physiological and physical condition of Myponga Reservoir phytoplankton.
- To determine whether or not the physiological and physical condition of reservoir phytoplankton varies between sites immediately adjacent to the mixer compared to a site 70 m away over a depth of 20 m.
- To characterize and quantify the turbulent intensities around a bubble plume aerator, a submerged aspirator and a high volume aerator within the Torrens Lake.

5.2 Materials and methods

5.2.1 Field sites and artificial mixing systems

Myponga Reservoir (138° 25' E 35° 24' S) is a supply reservoir consisting of a basin (35 m deep) and a 2 km long side arm (17 m deep) located 70 km south of Adelaide in South Australia (figure 1.6). The surface mounted mechanical mixers (figure 5.2) consist of 8 impeller blades, with a radius of 2.5 m and pitch of 15°. The mixers are driven by 4 kw motors, which generate a flow of 3.5-4 m³ s⁻¹. The draft tube below the impellers is 13 m long and 2 m in diameter (figure 5.3). The mixers were located within the reservoir as shown in figure 5.4.

The Torrens Lake (138° 35' 14.2" E 34° 55' 4.0" S) is a shallow urban recreational lake adjacent to the central business district of Adelaide, South Australia (figure 1.6). In 2000, three bubble plume aerators each consisting of mobile diesel air compressors connected to 100 m long perforated pipes were installed approximately 0.2 m above the sediment at three locations (Albert Street Bridge, Morphett Street Bridge, city weir) within the Torrens Lake. In 2002, 11 submerged aspirators and 3 fountains were placed approximately 200 m apart in the lower Torrens Lake between Hackney Street Bridge and the city weir at a depth of 1.4 to 3.7 m. The operational characteristics of the mixers differ; the aerator draws in surface water (at a nominal rate of 0.2 m³ s⁻¹) and forces it out as airborne spray 1.4-1.5 m high with a radius of 3-3.4 m. The aspirators draw water from the deployment depth, jets it out and by venturi action incorporate air from the airline. The surface aerators achieve greater oxygenation of the water column than the submerged units, while providing surface disturbance and some evaporative cooling. The specified volume influenced by the submerged units ranged from 0.8 ML (3hp unit) to 3.9 ML (5 hp unit).

5.2.2 Myponga Reservoir experiments

5.2.2.1 Surface mixer flow characteristics

To measure flow under the draft tube of a surface mechanical mixer, an aluminum frame (see Lewis, 2003) was constructed and attached to the pontoon suspending the mixer located in the

main basin of the reservoir (figure 5.2). On 5 February 2002, water velocity was measured using a current probe (refer to 5.2.4) at four depths; 14.3, 16.3, 20.3 and 22.3 m and four radial distances from the center of the draft tube; 0.1, 0.5, 1.2 and 4.6 m.

The thermal structure near the mixer was measured using the temperature probe on the current probe and a Hydrolab CTD (DataSonde 4) suspended at the surface near the impeller. Meteorological and thermistor chain data were collected from a weather station 300 m east of the mixer. Temperature was recorded every 10 minutes over the depth of the water column using Betatherm temperature sensors with a resolution of ± 0.01 °C. Wind velocity and direction was measured with an anemometer 2 m above the water surface (Climatronics WM-111).

5.2.2.2 Phytoplankton transport through draft tube

To determine whether or not transport through a mechanical mixer and draft tube would directly affect phytoplankton in the short term, water samples were collected on 5 February 2002 from the surface prior to entrainment, and at the same locations as velocity profiles below the draft tube using a low velocity pump and hosepipe. Samples were also pumped from the surface through a hosepipe of the same length and analysed as a control for the sampling process. In combination with flow cytometry, phytoplankton metabolic activity and viability were analysed using the fluorescent probes, fluorescein diacetate and Sytox green, respectively (see phytoplankton and flow cytometry analysis 5.2.2.4). Analysis was undertaken within 30 minutes of collection and velocity profiling. Samples were preserved in Lugol's iodine to enable identification of species in the laboratory.

5.2.2.3 Phytoplankton adjacent to and 70 m from surface mechanical mixer

To evaluate whether or not turbulence in the vicinity of the surface mixer as generated by an intrusion or water existing the draft tube affected reservoir phytoplankton, water samples were collected for phytoplankton and flow cytometry analysis (5.2.2.4), 2 m adjacent to the mixer and at a distance of 70 m, over a depth of 20 m on the 25 January 2001. No turbulence measurements were conducted. Samples were collected at 1, 3, 5, 10, 15 and 20 m depth. Reservoir

phytoplankton metabolic activity and physical characteristics were compared and analysed using fluorescein diacetate and flow cytometry. Samples were preserved in Lugol's iodine to enable identification of species in the laboratory.

5.2.2.4 Phytoplankton and flow cytometry analysis

Phytoplankton in the Myponga Reservoir experiments (5.2.2.2 and 5.2.2.3) were analysed using fluorescent stains and flow cytometry. Fluorescein diacetate (FDA) and Sytox green were used to quantify phytoplankton esterase activity and cell viability, respectively (refer to chapter 2). Metabolically active cells are represented by high fluorescence and a decrease in activity is indicated by a decrease in fluorescence. Conversely, viable cells do not fluoresce while nonviable cells display high fluorescence, using the Sytox stain.

5.2.2.4.1 Metabolic activity and FDA staining technique

The esterase activity of reservoir phytoplankton was determined by using the FDA staining procedure outlined in chapter 2. For each natural field sample, 400 μL of algae was placed in a Falcon polystyrene tube with 300 μL of FDA working solution and the sample was incubated at room temperature for 7 minutes. The final FDA concentration was 40 μM , consistent with the recommendations of Geary *et al.* (1997). Esterase activity was interpreted as the mean rate of FDA conversion to fluorescein ($\text{FDAC cell}^{-1} \text{ min}^{-1}$), calculated by dividing the mean fluorescein arbitrary fluorescence by the incubation time (7 min.). In addition, because the flow cytometer provided fluorescence data for individual cells, frequency histograms of these data were used to define esterase activity states (Regel *et al.*, 2002). Three states were defined: a low activity state, $S1_{\text{fda}}$ corresponded to the activity of heat-treated cells (microwave for 2 min.), a normal state $S2_{\text{fda}}$, corresponded to the distribution of an untreated metabolically active population and a higher activity state, $S3_{\text{fda}}$ corresponded to an esterase activity above the normal range. The percentage of cells in $S1_{\text{fda}}$ relative to the control ($\%S1_{\text{fda}}$) was of primary importance as it indicated whether turbulence exerted a detrimental impact.

5.2.2.4.2 Cell viability and Sytox staining technique

The viability of reservoir phytoplankton was determined by using the Sytox staining procedure outlined in chapter 2. For each sample, 0.98 mL of algae was placed into a Falcon polystyrene tube with 0.02 mL of Sytox green working solution (1 μ M in DMSO) and the sample was incubated at room temperature for 8 minutes. Cell viability was interpreted by defining two viability states on frequency histograms; a living state, $S1_{\text{sytx}}$ and a dead state, $S2_{\text{sytx}}$. $S1_{\text{sytx}}$ and $S2_{\text{sytx}}$ were defined by the distributions of both living and dead (microwave for 2 min.) reservoir phytoplankton, respectively. The percentage of cells in ($\%S2_{\text{sytx}}$) was of primary importance as it indicated whether turbulence killed any phytoplankton cells.

5.2.2.4.3 Flow cytometry

A Becton Dickinson FACStrak flow cytometer (FCM) with a 488 nm argon excitation laser was used to measure cell fluorescence and morphological characteristics as described in chapter 2. The green fluorescence (emission wavelength 535 nm) of either fluorescein or Sytox was separated from red, chlorophyll fluorescence using short pass narrowband filters. Stain fluorescence and chlorophyll fluorescence were measured in channels CH1 and CH2, respectively. Cell size and granularity were measured as forward light (FSC) and side scatter (SSC), respectively.

5.2.2.4.4 Statistical analysis of phytoplankton measurements

A Welch one-way analysis of variance (ANOVA) test was used to compare treatments with controls for all phytoplankton measurements, as variance between treatments was not homogenous. Percentage data from either $\%S1_{\text{fda}}$ or $\%S2_{\text{sytx}}$ results were $\arcsin\sqrt{p}$ transformed prior to ANOVA analysis. A 5 % level of statistical significance was used and the term 'significant' is used exclusively. Means are presented +/- standard deviation (s.d.), where $n = 3$.

5.2.3 Torrens Lake experiments

5.2.3.1 Bubble plume aerator

To gain an appreciation of turbulence intensity and the zone of influence generated by a bubble plume aerator, water velocity profiles were taken at four locations around one Torrens Lake aerator (Albert Street Bridge) on the 22 February 2001 (figure 5.5). The orientation of the aerator line was parallel with the banks in this stretch of the lake and was pointing 320 °N. The water column was profiled from a securely anchored flat bottom boat at 0.1 m increments to the sediment (~ approximately 2 m depth) using a current probe (refer to 5.2.4) as illustrated in figure 5.7. Water velocities were corrected for a heading of 320° N. Positive values in the x and y Cartesian represents 320° N and 50° N, respectively. Positive values in the z direction indicate upward flow. The temperature probe on the current probe was used as a second index to determine circulation. Meteorological data were collected from a weather station 1-km downstream of the aerator at the City Weir. Temperature was recorded every 10 minutes by 20 thermistors over 5.5 m of the water column using Betatherm temperature sensors with a resolution of ± 0.01 °C. Wind velocity and direction was measured at 2 m above the water surface (Climatronics WM-111). Water samples were collected near the aerator for phytoplankton species identification.

5.2.3.2 Submerged aspirator and high volume surface aerators

Velocity and temperature measurements were recorded in the vicinity of one sub-triton aspirator, SA (#2) and one high volume aerator, HVA (#3, 5 hp unit) both located at the western end of the Torrens Lake (figure 5.6). The SA was at a depth of 3.0 m. Measurements were taken at transects bearing 270° and 190° N (SA) and 270° and 150° N (HVA). Velocity and temperature profiles were measured from a boat (figure 5.7) taken at 0.2 m depth intervals, at distances between 3 and 15 m from the central point of the mixing systems on the 23 March and 2 April 2002. Meteorological data were collected from a fixed weather station deployed near the City Weir about 100 m west of aspirator # 2 as described above.

5.2.3.3 Wind versus mixer generated circulation

The volume of water influenced by mixers is dependent upon the wind speed, the degree of thermal stratification (density differences), the air temperature and solar irradiance as well as the velocity of the water in both the horizontal and vertical planes. To trace the circulation created by the Torrens Lake mixers and to distinguish it from wind-induced circulation, measurements were carried out during periods of thermal stratification.

To distinguish between naturally and artificially generated velocities the assumption was made that mixer generated velocities would have to be greater than or equal to the shear velocity (u^*) generated by wind speeds normally encountered in the lake. Typical daily average wind speeds on the Torrens Lake during summer range from 1 to 3 m s^{-1} . Consequently, u^* can be approximated as the wind speed divided by 1000 (Reynolds, 1997) and has a range of 0.001 to 0.003 m s^{-1} . Therefore it was assumed that measured horizontal or vertical velocities of less than 0.001 m s^{-1} could not be distinguished from either artificial or wind induced circulation. The volume of water influenced by the mixers was assumed to be the volume of a cylinder of radius equivalent to the radial extent of unstable temperature profiles and where velocities fell below 0.001 m s^{-1} . The volume of water influenced by mixers is dependent upon the wind speed, the degree of thermal stratification (density differences), the air temperature and solar irradiance as well as the velocity of the water in both the horizontal and vertical planes.

5.2.4 Flow velocity and turbulence measurement and analysis

Flow velocities for all experiments were determined using a Sontek acoustic Doppler velocimeter current probe (ADV) at 50 Hz. The ADV records velocity in both the horizontal and vertical planes and corrects for compass heading, pitch and roll. Readings were integrated over 2 minutes at 50 Hz. WINADV 32 processing software (Wahl, 2001) was used to filter the time series velocity data and provided an average velocity value for each depth, time and location. The time series data were filtered for probe correlation and signal to noise ratios greater than 90 % and 20 %, respectively. The radial velocities were corrected for their corresponding transects headings. Positive radial velocities indicate flow away from the mixing device; negative values indicate

flow towards the mixing device. Positive vertical velocities represent flow towards the surface and negative values indicate flow towards the sediments.

The intensity of turbulence was calculated directly through velocity time series data and was represented as the *turbulent intensity*, the *shear velocity* and the *turbulent kinetic energy dissipation rate*. In turbulent flow, the instantaneous velocity can be statistically separated into mean and fluctuating (or turbulent) components. The Reynolds decomposition equation (1) demonstrates that when flow velocity (u) is measured over time at a fixed point in space, it can be decomposed into a mean component (U) and a fluctuating component of the velocity, (u').

$$u = U + u' \quad (1)$$

The intensity of turbulence can be estimated from the time-averaged fluctuations in horizontal (u_x , u_y) and vertical velocity (u_z) at any given point. Turbulent intensity, u^{*2} ($m^2 s^{-2}$) was determined from the sum of the root mean square of the velocity fluctuations in the x, y and z directions:

$$u^{*2} = [(u_x)^2 + (u_y)^2 + (u_z)^2]^{0.5} \quad (2)$$

Whereas the shear velocity, u^* ($m s^{-1}$) was calculated as:

$$u^* = ([(\pm u_x)^2]^{0.5} [(\pm u_z)^2]^{0.5})^{0.5} = (u^{*2})^{0.5} \quad (3)$$

where for example u^*_x was calculated from the WINADV software as the root mean square of the velocity fluctuations about the mean current velocity, $RMS [V_x'] = \sqrt{(V_x')^2} = \sqrt{(\sum V_x^2 - (\sum V_x)^2 / n) / (n-1)}$, which is equal to the standard deviation of the individual velocity measurements.

Unfortunately, unlike Nortek ADVs and software, the Sontek ADV does not have software enabling the direct calculation of the turbulent kinetic energy dissipation rate. Consequently, a Fortran program was developed (unpublished, appendix A) based upon the homogenous isotropic turbulence theory and Eulerian spectral analysis following Kit *et al.* (1995). Time series velocity data for each Cartesian component (u_x , u_y , u_z) including the sum of all three, $u_{mag} (= \sqrt{u_x^2 + u_y^2 + u_z^2})$

u_z^2) were considered in terms of a Eulerian frequency (ω) spectrum to aid Fast Fourier transformation. The behaviour of turbulence once generated can be described by the homogenous isotropic theory (Batchelor, 1967). It predicts that in the inertial subrange of the frequency spectrum where equilibrium is established between energy cascading from large-scale motion and energy lost to viscous dissipation (and there is no direct external input of energy), the turbulent kinetic energy can be described by the shape:

$$E(\omega) = \alpha \varepsilon^{2/3} u_{\text{rms}}^{2/3} \omega^{-5/3} \quad (4)$$

where $E(\omega)$ is the spectral density at angular frequency ω , α is a constant ~ 0.8 (Kit *et al.*, 1995) for $E(\omega)$ representing 1-dimensional variance spectrum for a single velocity component (u_x or u_y or u_z) and ~ 1.5 (Gross *et al.*, 1994) for $E(\omega)$ representing a 3-dimensional energy spectrum (u_{mag}). ε is the turbulent kinetic energy dissipation rate ($\text{m}^2 \text{s}^{-3}$) and $u_{\text{rms}} = \sqrt{(u')^2}$ is the root mean square of the turbulent velocity (u') for each Cartesian component (u_x , u_y , u_z) or u_{mag} . Equation 4 is only applicable to calculate ε if the slope of a $\log E(\omega)$ vs $\log \omega$ approximates $-5/3$ in the inertial subrange, being consistent with the theory of isotropic turbulence and the Kolmogorov $k^{-5/3}$ law first derived by Obukhov (1941). Plots of $\log E(\omega)$ vs $\log \omega$ were constructed for each velocity profile to verify the calculation of ε .

The smallest scale of turbulence and the small size limit of the equilibrium range are defined by the Kolmogorov scale, η (m). It provides an indication of the scale at which turbulent kinetic energy is dissipated into heat by the action of fluid viscosity, ν and is defined as:

$$\eta = (\nu^3 / \varepsilon)^{0.25} \quad (5)$$

where ν approximates $1 \times 10^{-6} \text{ m}^2 \text{ s}^{-1}$ at 20°C and ε is the turbulent kinetic energy dissipation rate ($\text{m}^2 \text{ s}^{-3}$).

5.2.5 Wind generated turbulent dissipation rates

To evaluate whether or not the artificial mixing systems generated less, more or an equivalent degree of energy dissipation compared to wind forcing, theoretical calculations were made for a

range of wind velocities. In a homogeneous fluid where the only forcing is surface wind stress, the dissipation rate can be estimated from the equation (MacKenzie and Leggett 1993):

$$\varepsilon = \mu^{*3} / \kappa z \quad (6)$$

where μ^* is the shear velocity or turbulent velocity, κ is von Karman's constant (0.4) and z is depth. The shear velocity, $\mu^* = (\tau_o / \rho_w)^{0.5}$ was estimated using a water density, ρ_w of 999 kg m^{-3} (30°C) and a quadratic law was used for the surface wind stress, $\tau_o = \rho_a c u_{10}^2$. An air density, ρ_a of 1.2 kg m^{-3} and dimensionless frictional drag coefficient, c of 1.3×10^{-3} (Reynolds, 1994a) was used. The wind velocity at 10 m above the surface, u_{10} was calculated using the following equation:

$$u_{10} = u_m (\ln(10) - \ln(z_o)) / (\ln(z_m) - \ln(z_o)) \quad (7)$$

where u_m is the wind velocity at measured height, z_m is the height of the anemometer above surface water and z_o is a constant equal to 1.15×10^{-4} .

5.3 Results

5.3.1 Turbulence analysis

The Eulerian spectrum for either one (u_x , u_y , u_z), two ($u_{x,y}$) or three dimensional (u_{mag}) spectral analyses generally approximated a power law relationship, verifying the use of equation 4 to calculate turbulent kinetic energy dissipation rates (ε). For example, three power spectra for velocity profiles measured below the mechanical mixer draft tube (a), bubble plume aerator (b) and the submerged aspirator (c) are shown in figure 5.8. The results are plotted in log-log coordinates to enable identification of regions where a power law behaviour applies. In the frequency range, ω of 0.1 to 90 rad s^{-1} , the spectra show a decay that follows approximately a $-5/3$ law (slope of line). The slopes approximated $-5/3$ for all field measurements.

* Conversion of units: $100 \text{ mm}^2 \text{ s}^{-3} = 1 \text{ cm}^2 \text{ s}^{-3} = 1 \text{ erg g}^{-1} \text{ s}^{-1} = 10^{-1} \text{ W m}^{-3} = 10^{-4} \text{ W kg}^{-1} = 10^{-4} \text{ m}^2 \text{ s}^{-3}$.

5.3.2 Myponga Reservoir experiments

5.3.2.1 Surface mixer flow characteristics

5.3.2.1.1 Meteorological conditions

On the day of flow velocity and phytoplankton sampling, the meteorological conditions were relatively calm for Myponga Reservoir (figure 5.9). Air temperature varied between 13 °C at 03:00 h and 19 °C at 13:40 h on the 5 February (figure 5.9a). Average wind speeds were generally below 5 m s⁻¹ during profiling (figure 5.9b). However, maximum wind speeds reached 9 m s⁻¹. Temperature profiles indicated that the water column was isothermal to 30 m until 08:00 h, when surface warming resulted in a temperature gradient in the epilimnion. Temperatures reached 21.5 °C at the surface, whereas below 5 m the water column was evenly mixed and the temperature ranged between 18.5 and 20 °C (figure 5.9c).

5.3.2.1.2 Flow velocities below the mixer

The radial (horizontal), vertical and sum of velocity profiles at 4 depths below the surface mixer draft tube are shown in figure 5.10. Radial velocity ($u_{x,y}$) tended to increase away from the draft tube at 14.3, 16.3 and 22.3 m, but generally decreased with depth (figure 5.10a). A gradient in radial velocities was evident with a maximum velocity of 0.1 m s⁻¹ at 14.3 m at a distance of 0.5 m. Typical for a jet, the vertical velocity (u_z) component of the flow was approximately 10 fold greater than horizontal components at 14.3 m and radial distance of 0.1 m (figure 5.10b); consequently the turbulent flow was not isotropic. Velocity decreased rapidly with depth from 1 m s⁻¹ at 14.3 m to 0.1 m s⁻¹ at 16.3 m. The sum of the horizontal and vertical velocity components, u_{mag} followed a similar pattern to the vertical component in magnitude (figure 5.10c). A qualitative summary of the flow below the draft tube is presented in table 5.1.

5.3.2.1.3 Turbulent intensity, shear velocities and turbulent kinetic energy dissipation rates

Turbulent intensity varied between 5×10^{-4} and 4.5×10^{-3} m² s⁻² below the Myponga Reservoir surface mixer draft tube (figure 5.11a). Turbulent intensity was generally higher directly below

the draft tube at 14.3 and 16.3 m compared to 20.3 and 22.3 m depth profiles. Shear velocities followed a similar pattern and ranged from $2.3 \times 10^{-2} \text{ m s}^{-1}$ at 22.3 m to $6.6 \times 10^{-2} \text{ m s}^{-1}$ at 16.3 m (figure 5.11b). Calculated turbulent kinetic energy dissipation rates were high at all depths and ranged from $5 \times 10^{-5} \text{ m}^2 \text{ s}^{-3}$ to $1 \times 10^{-1} \text{ m}^2 \text{ s}^{-3}$. In contrast to turbulent intensities, dissipation rates tended to increase with depth below the draft tube. At 14.3 m depth, ϵ ranged between $5 \times 10^{-7} \text{ m}^2 \text{ s}^{-3}$ and $1 \times 10^{-6} \text{ m}^2 \text{ s}^{-3}$, while at 16.3 m it ranged between $1 \times 10^{-6} \text{ m}^2 \text{ s}^{-3}$ to $7 \times 10^{-6} \text{ m}^2 \text{ s}^{-3}$. At these depths, the dissipation tended not to vary with radial distance below the draft tube.

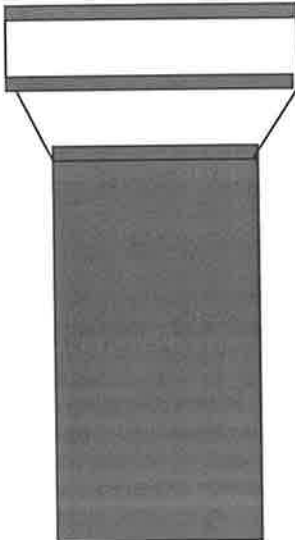
5.3.2.2 Phytoplankton transport through mixer and draft tube

Transport through the mixer and draft tube and consequent exposure to turbulent intensity between 5×10^{-4} and $4.5 \times 10^{-3} \text{ m}^2 \text{ s}^{-2}$ had no effect on reservoir phytoplankton (figure 5.12). There were no significant effects on phytoplankton metabolic activity, cell viability, chlorophyll fluorescence, cell size or cell granularity sampled at any of the 4 depths or radial distances from the draft tube ($p > 0.05$). Figure 5.12(a-e) shows minor variation in phytoplankton responses at a depth of 16.3 m. Phytoplankton composition at the time of sampling consisted predominantly of diatoms (*Cyclotella*, *Nitzschia* species) and greens (*Scenedesmus*, *Ankistrodesmus*, *Chlamydomonas*, *Actinastrum* species), which were small in size and dependent upon turbulent conditions for suspension.

5.3.2.3 Phytoplankton adjacent to and 70 m from surface mixer

Phytoplankton were analysed using flow cytometry near the mixer (~2 m from draft tube entrance) and 70 m away to a depth of 20 m (figure 5.13). Phytoplankton composition was diverse but in terms of biovolume, dominated by diatoms (approximately $3.5 \times 10^6 \mu\text{m}^3$) particularly *Cyclotella* and *Nitzschia* species. Green algae were second most dominant in terms of biovolume (approximately $6.6 \times 10^4 \mu\text{m}^3$), and genera included *Ankistrodesmus*, *Actinastrum*, *Scenedesmus* and *Oocystis* species. Other inferior genera present include *Anabaena*, *Chroomonas*, *Dictyosphaerium*, *Cryptomonas*, *Crucigena* and *Aphanocapsa* species. Relative chlorophyll fluorescence cell^{-1} decreased with depth from approximately 450 arbitrary units at the surface to 280 arbitrary units at 10 m for both sites (figure 5.13a). Although not significant at 10 m ($p = 0.238$), 15 m ($p = 0.192$) or 20 m ($p = 0.156$) the average esterase activity of the phytoplankton

Table 5.1 Horizontal and vertical direction of water movement below a surface mixer within Myponga Reservoir. Arrows refer to velocities $> 0.01 \text{ m s}^{-1}$. Angled arrows reflect both vertical and horizontal velocities.

Depth (m)	Radial distance (m)			
0.0				
13.0				
	0.1	0.5	1.2	4.6
14.3	↘	↘	↘	↘
16.3	↘	↘	↘	→
20.3	↘	↗	↗	→
22.3	→	↗	↗	↘

community expressed as FDA conversion rate ($\text{FDAC cell}^{-1} \text{ min}^{-1}$) was consistently higher at the mixer than at 70 m away (figure 5.13b). FDA conversion rates varied between 85 and 115 units $\text{cell}^{-1} \text{ min}^{-1}$. In contrast, at 70 m, FDA conversion rates varied between 50 and 100 units $\text{cell}^{-1} \text{ min}^{-1}$. Furthermore, there was a slight tendency for FDA conversion rates to decrease with depth at both the mixer and 70 m site. The distribution of esterase activity into 3 states showed that there was more variation in esterase activity for samples from the mixer (figure 5.13c) compared to the 70-m site (figure 5.13d). For the mixer samples, there were generally more cells in both $S1_{\text{fda}}$ and $S3_{\text{fda}}$ states. Cell viability using Sytox green was not investigated. Cell size as indicated by arbitrary forward scatter measurements significantly increased as the mixer site from 1 to 10 m depth compared to the 70 m site (figure 5.13e). There were no significant differences in cell granularity as indicated by side scatter between the mixer and 70 m site (figure 5.13f).

5.3.3 Torrens Lake experiments

5.3.3.1 Bubble plume aerator

5.3.3.1.1 Meteorological conditions

Meteorological conditions were relatively calm at the city weir, 1 km downstream of the bubble plume aerator on 22 February 2001 (figure 5.14). Air temperature varied between 15 °C at 03:30 h and 27 °C at 14:00 h (figure 5.14a). Average wind speed generally remained below 3 m s⁻¹, except for a brief period at 14:00 h when wind speed reached 4 m s⁻¹ (figure 5.14b). During velocity profiling in the afternoon, the water column was thermally stratified at the city weir (figure 5.14c). A persistent thermocline was evident below 3 m and a thermal gradient developed in the upper 2 m between 08:30 and 17:00 h. After 17:00 h, the surface mixed layer depth increased to 2 m, as air temperatures decreased and maximum wind speeds remained above 4 m s⁻¹.

5.3.3.1.2 Temperatures and flow velocities

Flow dynamics around the Torrens Lake aerator were assessed at 4 sites using both temperature and velocity measurements (figure 5.15). Temperature profiles varied between sites within the range of 24-27 °C (figure 5.15a). At site 1, which was directly above the aerator, temperature did not change with depth as would be expected under mixed conditions. Upward vertical velocities, u_z were high; reaching 0.12 m s⁻¹ at 0.8 m depth, but flow slowed as it reached the surface (figure 5.15b). Radial velocities were divided into an u_x (+ve 320 °N) and u_y (+ve 50 °N) Cartesian components. At depth, flow was towards the aerator with direction changing in the x-axis, however above 0.7 m, the flow started to spread away from the aerator towards the western bank as indicated by negative u_y velocities reaching 0.014 m s⁻¹ (figure 5.15b).

At site 2, which was 6 m away on the western side of the aerator, there was minimal variation in temperature with depth (figure 5.15a). Radial and vertical velocities varied in direction at 0.1 to 0.2 m depth increments throughout the water column, indicating the formation of small (0.1-0.2 m) eddies (figure 5.15c). The velocity of these eddies tended to increase with depth.

At site 3, 2 m east of the aerator, temperature varied slightly with depth, as a warm water intrusion was evident between 0.7 and 1.3 m (figure 5.15a). A peak in temperature of 26 °C between 0.7 and 1.3 m indicated a slight warm water intrusion. Flow predominantly moved away from the aerator with little vertical movement- +ve u_x , u_y values (figure 5.15d). Flow velocities did not exceed 0.02 and 0.005 m s⁻¹ radially and vertically, respectively.

At site 4, which was approximately 15 m longitudinally south of the aerator, there was a prominent increase in temperature from 26 to 27 °C between 0.8 and 1.3 m depth, suggesting a warm water intrusion (figure 5.15a). At this depth, flow was moving away from the aerator (figure 5.15e). Above 0.8 m, flow moved slowly (~0.005 m s⁻¹) towards the aerator. Similarly, below 1.3 m, flow tended to move towards the aerator in a northwesterly direction. Significant vertical flow was not recorded at any depth.

5.3.3.1.3 Turbulent intensity, shear velocity and turbulent kinetic energy dissipation rate

Turbulent intensity varied by 100 fold, ranging from 3.5×10^{-5} to 6.4×10^{-3} m² s⁻² around the bubble plume aerator (figure 5.16a). Turbulent intensity was highest at site 1, in the top 1 m above the aerator reaching 6.4×10^{-3} m² s⁻² at 0.8 m. Below 1.0 m, turbulent intensity approximated 1×10^{-4} m² s⁻². Similarly, at sites 2 and 3, east and west of the aerator turbulent intensity approximated 1×10^{-4} m² s⁻² over the entire water column. At site 4, turbulent intensity was slightly higher than at sites 2 and 3 approximating 2×10^{-4} m² s⁻². Shear velocity followed a similar pattern to turbulent intensity in its fluctuations with depth and site (figure 5.16b). Shear velocities ranged from 5.9×10^{-3} to 7.9×10^{-2} m s⁻¹ and were highest at site 1 in the top 1 m of the water column. Turbulent kinetic energy dissipation rates, ϵ were at all sampling sites and depths and ranged between 1.76×10^{-6} m² s⁻³ to 3.35×10^{-4} m² s⁻³ (figure 5.16c). There was a large degree of variation with depth for each site profiled. For example at site 3, ϵ varied by a factor of 100 from 9.04×10^{-6} m² s⁻³ to 3.35×10^{-4} m² s⁻³ with a change in depth from 0.475 to 0.675 m, respectively.

5.3.3.2 Submerged aspirator (SA)

5.3.3.2.1 Meteorological conditions

Meteorological conditions at the city weir were calm on the two days (23 March 2002, 2 April 2002) of velocity profiling around the submerged aspirator and high volume aerator (figures 5.17, 5.18). Air temperature varied between 15 °C at 05:00 h to 27 °C at 16:30 h on March 23 and between 18 °C at 03:00 h and 26 °C at 16:00 h on April 2 (figure 5.17a, 5.18a). Wind speed was similar on both days rising at dawn and diminishing at dusk. Average wind velocity varied between 1 and 2 m s⁻¹, although maximum wind speed did reach 4 m s⁻¹ (figures 5.17b, 5.18b).

Temperature profiles differed between the two days (figures 5.17c, 5.18c). On March 23 there was no evidence of a pre-dawn, persistent, deep thermocline, whereas, on April 2 a persistent, pre-dawn thermocline was evident below 3 m. However, during both days temperature stratification persisted until at least 23:00 h. On both days a thermal gradient built up in the upper 2 m between 07:30 h and 18:00 h (figures 5.17c, 5.18c). Between these times the depth of the surface mixed layer was less than 1 m but deepened as the air temperature fell below the lake temperature when convective and wind induced mixing became the dominant influences.

Data from the meteorological station was used to compare temperature profiles of the undisturbed water column with the profiles obtained in the vicinity of the mixers. Since the mixers were located at sites that were shallower than the weather station only the temperature profiles above 3 m were used in the comparisons.

5.3.3.2.2 Temperature and velocity profiles

The temperature profile at a distance of 3 m from the aspirator in the direction (190°) of the aspirator jet appeared unaffected, presumably because warmer, surface water had not been entrained (figure 5.19a). However, at all other distances along both transects the water temperatures were significant below those at 3 m (190°) and at the meteorological station. At 4 and 5 m (190°) the temperature gradient had eroded since surface and bottom temperatures were similar. At 10 m along the same bearing the surface water was cooler than the deeper water,

which suggests an unstable water column. At 3 m, in a 270° direction a temperature gradient was present but was being eroded. Similarly, at 6 and 15 m (270°) the water column was unstable since the surface temperatures were lower than the bottom temperatures (figure 5.19a).

The overall pattern of radial velocities shows that radial flow is not symmetrically distributed around the aspirator, the zone of influence is less than 10 m along the 190° transect and equal to or less than 6 m along the 270° transect. However, there is notable disruption of the temperature profiles associated with the positive radial velocities measured at depths of between 0.7 and 3 m, which entrain warmer surface water and provide an overall cooling effect.

190° N transect

Radial velocities measured at 3 m along the 190° N transect line showed that water was moving towards the aspirator throughout the water column (figure 5.20, Table 5.2). At 4 m along the same transect line no radial velocity was encountered in the top 0.9 m but below this depth, flow was away from the aspirator. At 5 m flow was away from the aspirator but towards it at the surface and 0.7 m depth. At 10 m, radial flow was intermittent with only 50 % of the depths recording a significant velocity (i.e. $> 0.01 \text{ m s}^{-1}$) and of these; three measurements indicated flow was away and four indicated that flow was towards the aspirator.

Vertical flow at 3 m in the top 0.9 m was towards the sediment; however below this there was only one depth at which a measurable upward velocity was recorded (2.9 m) at all other depths the only significant velocities were radial (figure 5.21, table 5.2). At 4 m, no detectable flow occurred at the surface, but from 0.7 to 1.9 m downward flow was measured. From 2.3 to 2.9 m the direction of flow was upwards. At 5 m surface flow was upwards but from 1.3 to 2.1 m the vertical component was below the threshold. Below this depth, the flow was predominantly towards the surface, but at 10 m velocities were towards the sediment (figure 5.21, table 5.2).

270° N transect

Radial velocities measured at 3 m along the 270° N transect line showed that surface water movement was away from the aspirator; between 0.7 and 1.5 m there was no measurable radial flow (figure 5.20, table 5.2). Radial flow was away from the aspirator at 1.7 and 1.9 m but was

towards the aspirator between 2.1 and 3.1 m depths. At 6 m radial flow was away from the aspirator and was restricted to a single depth (0.9 m). At 2.1 m and below, radial flow was all towards the aspirator. At 15 m radial flow was slightly above the critical level (i.e. $> 0.01 \text{ m s}^{-1}$) with only 5 of the 14 depths recording a measurable velocity, and generally these indicated a flow direction away from the aspirator.

Close to the aspirator at the surface (0-0.7 m) the vertical velocity was downwards at 0.08 m s^{-1} in contrast, flow between 0.7 and 1.5 m was upwards. There was no measurable vertical flow between 1.7 and 1.9 m; however, below this depth flow was undetectable (2.3 and 2.9 m) or upward (figure 5.21), table 5.2). At 6 m from the aspirator, the flow direction was towards the sediment over the entire water column. At 15 m, significant vertical flow was only recorded at 5 of the 14 sampling depths and the general movement of water was downwards (figure 5.21, table 5.2).

5.3.3.2.3 Turbulent intensity, shear velocity and turbulent kinetic energy dissipation rate

Turbulent intensities along the 190° transect of the submerged aspirator ranged between $1 \times 10^{-4} \text{ m}^2 \text{ s}^{-2}$ to $6 \times 10^{-3} \text{ m}^2 \text{ s}^{-2}$ over the radial profiles (figure 5.22a). Turbulent intensity followed a similar pattern over depth approximating $5 \times 10^{-4} \text{ m}^2 \text{ s}^{-2}$ at radial distances of 3 and 10 m, but increased with depth at radial distances of 4 m and 5 m, consistent with large radial flow velocities away from the aspirator (figure 5.20). Shear velocity followed a similar pattern to turbulent intensity and ranged from $1.03 \times 10^{-2} \text{ m s}^{-1}$ at 3 m to $7.8 \times 10^{-2} \text{ m s}^{-1}$, 1 m away at a radial distance of 4 m (figure 5.22b). Turbulent kinetic energy dissipation rates varied by a factor of 100, ranging from $5.9 \times 10^{-7} \text{ m}^2 \text{ s}^{-3}$ to $5.4 \times 10^{-5} \text{ m}^2 \text{ s}^{-3}$ close to the aspirator (figure 5.22c). However, there was no clear pattern in dissipation with distance from the aspirator or with the depth of the profiles with most calculations approximating $5 \times 10^{-6} \text{ m}^2 \text{ s}^{-3}$.

Turbulent intensities along the 270° transect line of the submerged aspirator ranged between $8.5 \times 10^{-5} \text{ m}^2 \text{ s}^{-2}$ and $9.6 \times 10^{-4} \text{ m}^2 \text{ s}^{-2}$ (figure 5.23a). Turbulent intensity was more variable with radial distance and depth of each profile. For example at 6 m, turbulent intensity increased from $8.5 \times 10^{-5} \text{ m}^2 \text{ s}^{-2}$ to $8 \times 10^{-4} \text{ m}^2 \text{ s}^{-2}$ with an increase in water depth of 0.75 m. Shear velocity ranged between 9.2×10^{-3} and $3.1 \times 10^{-2} \text{ m s}^{-1}$ (figure 5.23b). Similarly, it showed a high degree of

variation with depth and radial distance. The calculations of turbulent kinetic energy dissipation along the 270° transect line showed greater variability than profiles along the 190° transect line (figure 5.23c). Turbulent kinetic dissipation rate varied between $8.4 \times 10^{-7} \text{ m}^2 \text{ s}^{-3}$ to $2.1 \times 10^{-4} \text{ m}^2 \text{ s}^{-3}$ and the greatest variability was evident at a radial distance of 15 m over depth.

Table 5.2 Horizontal and vertical direction of water movement along transects 190° N and 270° N between 3 and 15 m distance from the submerged aspirator. Arrows refer to velocities > 0.01 m s⁻¹. Angled arrows at 0°, 90°, 180° and 270° reflect where only one of the velocities was significant. Blanks = velocities below the critical level.

Distance (m) from aspirator at 270° N			Depth (m)	Distance (m) from aspirator at 190° N			
15	6	3		3	4	5	10
	↓	↙	0	↙		↖	↖
	↓	↑	0.7	↙	↓	↖	→
↗	↙	↑	0.9	↙	↓	→	
←	↓	↑	1.1	←	↘	↘	↓
←	↓	↑	1.3	←	↘	→	→
↙	↓	↑	1.5	←	↓	→	→
↓	↓	←	1.7	←	↘	→	↙
←	↓	←	1.9	←	↘	→	
↓	↘	↙	2.1	←	→	→	↙
↓	↘	→	2.3	←	↗	↗	↓
	↘	↗	2.5	←	→	↗	↓
	↘	↑	2.7	←	↗	↗	↓
	↘	→	2.9	↖	↗	→	↙
	↘		3.1	←		↗	↓

5.3.3.3 High volume surface aerator (HVA)

5.3.3.3.1 Meteorological conditions

Refer to 5.3.3.2.1 for a description of the meteorological conditions at the time of velocity profiling around the aerator.

5.3.3.3.2 Temperature and velocities

Surface and bottom temperatures along the 150° transect increase as the distance from the aerator lengthened (figure 5.24). Profiles closer to the aerator have bottom temperatures that are significantly higher than at the surface, which suggests unstable water columns due to the action of the aerator. At 6 m along the 270° transect the bottom temperature is higher than the surface but at 12 m and 15 m the water column is isothermal. The profile at 10 m, sandwiched between unstable profiles at 6 m and 12 m, shows a typical thermal gradient uninfluenced by the action of the aerator. The general influence of the aerator is to reduce the average water column temperature compared with the temperatures measured at the meteorological station and to create unstable or isothermal temperature profiles.

150° N transect

At 4 m from the aerator along the 150° N, radial flow was away from the aerator. At 6 m the flow was confused in the top 1.1 m but below this depth movement was away from the aerator although no detectable flow was measured below 1.9 m (figure 5.25, table 5.3). At 11 m from the aerator, 40 % of the radial velocities were below the threshold, whilst at 13 m radial flow was away from the aerator in the top 0.9 m, but were absent below 0.9 m (figure 5.25, table 5.3).

At 4 m, all significant vertical velocities, except at the surface, were downwards (figure 5.26). At 6 m, surface flow was downwards but below 0.7 m the flow direction was upward and no flow was observed at 1.1, 2.1 and 2.3 m. The vertical direction of flow at 11 m was confused with both upward and downward flow measured. At 13 m, the only significant vertical flow was below 1.3 m and this was towards the sediment (figure 5.26, table 5.3).

270° N transect

The predominant radial velocities at depths greater than 1.5 m and radial distances of 6 to 12 m are towards the aerator (figure 5.25). However at 10 m, the flow is away from the aerator at the surface but towards the aerator deeper in the water column. At a radial distance of 15 m, radial velocities were below the critical velocity over the entire water column.

Vertical flow was upwards at a radial distance of 6 m and measurements taken at the surface and from 1.9 to 2.3 m, although at intermediate depths the flow pattern was random (figure 5.26). At 10 m, 50 % of the vertical velocities were towards the surface whereas at 12 m and 15 m, the flow was generally towards the surface.

Table 5.3 Horizontal and vertical direction of water movement along transects 150° N and 270° N between 4 and 15 m distance from the high volume aerator. Arrows refer to velocities > 0.01 m s⁻¹. Angled arrows at 0°, 90°, 180° and 270° reflect where only one of the velocities was significant. Blanks = velocities below the critical level.

Distance (m) from aerator at 270° N				Depth m	Distance (m) from aerator at 150° N			
15	12	10	6		4	6	11	13
↖	↑	←	↖	0	↗	↓	↙	→
↑	↖	↖	→	0.7	→	↓	↓	→
↑	↖	↖	→	0.9	→	↖	↑	→
↑		↗	→	1.1	↓		←	
↑	↑	→	↓	1.3	→	↗	↑	↓
↑	↑		↖	1.5	→	↗	↗	↓
↑	→	↗	→	1.7	→	↗	↓	↓
↑	→	→	↗	1.9	↓	↗	↓	↓
↑	↑	↓	↗	2.1	↓		↗	↓
		↗	↗	2.3	→			

5.3.3.3.3 Turbulent intensity, shear velocity and turbulent kinetic energy dissipation rate

Turbulent intensity along the 150° transect line around the high volume aerator ranged from $8.9 \times 10^{-5} \text{ m}^2 \text{ s}^{-2}$ to $1.1 \times 10^{-3} \text{ m}^2 \text{ s}^{-2}$ (figure 5.27a). Turbulent intensity tended to decrease with radial distance away from the aerator. Shear velocity ranged between 9.5×10^{-3} to $3.3 \times 10^{-2} \text{ m s}^{-1}$ (figure 5.27b), while turbulent kinetic energy dissipation rates generally decreased with depth and ranged from $8 \times 10^{-7} \text{ m}^2 \text{ s}^{-3}$ to $3.6 \times 10^{-3} \text{ m}^2 \text{ s}^{-3}$ (figure 5.27c).

Along the 270° transect line, turbulent intensity showed reduced variability with radial distance ranging from $1 \times 10^{-4} \text{ m}^2 \text{ s}^{-2}$ to $1.3 \times 10^{-3} \text{ m}^2 \text{ s}^{-2}$ (figure 5.28a). Similarly, shear velocity displayed reduced variability with radial distance and depths compared to the 150° transect line (figure

5.28b). Values at each radial distance tended to decrease with depth. In contrast, turbulent kinetic energy dissipation rates tended to increase with depth and ranged from $8.4 \times 10^{-7} \text{ m}^2 \text{ s}^{-3}$ to $1.3 \times 10^{-4} \text{ m}^2 \text{ s}^{-3}$ over all radial distances and depths (figure 5.28c). However, generally dissipation rates approximated $5 \times 10^{-6} \text{ m}^2 \text{ s}^{-3}$.

5.3.4 Wind-generated turbulence

Turbulent intensity and energy dissipation in natural systems is often primarily dependent upon the strength of wind forcing and the viscosity of the water body. In the simplest case, with constant wind acting upon the surface of a water body of uniform temperature and unconstrained sides or bottom, the energy of large eddies at the surface is progressively transferred to smaller and smaller eddies into deeper and deeper water until it is overcome by viscosity. Consequently, the magnitude of turbulent intensity and turbulent kinetic energy dissipation rates increase with wind velocity and decrease with depth (figure 5.29). For example, a wind speed of 5 m s^{-1} generates a turbulent intensity and shear velocity of $3.9 \times 10^{-5} \text{ m}^2 \text{ s}^{-2}$ and $6.2 \times 10^{-3} \text{ m s}^{-1}$, respectively (figure 5.29a). A 2-fold increase in wind speed to 10 m s^{-1} , which is regularly recorded at Myponga Reservoir and the Torrens Lake, generates a turbulent intensity and shear velocity of $1.6 \times 10^{-4} \text{ m}^2 \text{ s}^{-2}$ and $1.2 \times 10^{-2} \text{ m s}^{-1}$, respectively. A wind speed of 5 m s^{-1} generates a dissipation rate of 1×10^{-5} and $5 \times 10^{-7} \text{ m}^2 \text{ s}^{-3}$ at 0.01 m and 2 m depth, respectively (figure 5.29b). A greater velocity of 10 m s^{-1} generates a dissipation rate of approximately 1×10^{-4} and $5 \times 10^{-6} \text{ m}^2 \text{ s}^{-3}$ at 0.01 m and 2 m depth, respectively.

5.4 Discussion

Measurement of hydrodynamic parameters such as current velocity and shear velocity can provide useful information on the efficiency of artificial mixing systems, their zones of influence and their behavior under contrasting environmental conditions (e.g. isothermal versus thermally stratified). Furthermore, the characterisation of physical processes including turbulence is fundamental to explain phytoplankton distribution, photosynthesis and community composition. As demonstrated in chapters 3 and 4, quantification of shear velocity is important to characterize phytoplankton cell entrainment and subsequent distribution and resultant effects on

photosynthesis. Additionally, knowledge of the zone of influence can provide information on the likely distribution of dissolved oxygen, which may be useful in water supply and or habitat remediation (expansion) in anoxic water bodies.

5.4.1 Measurement of turbulence

There is no precise means or parameter which totally describes turbulence, although the turbulent kinetic energy dissipation rate is often considered the best measure of intensity in small-scale turbulence (Peters and Marrase, 2000). However, its measurement assumes isotropy and that the energy spectra decays at a rate of $-5/3$, consistent with the Kolmogorov homogenous isotropic theory. Turbulence in the upper mixed layer of the ocean and or lakes has been referred to as quasi 2 dimensional because of the disparity between the largest scales of horizontal and vertical motion and therefore the Kolmogorov energy cascade technique using velocity time series data may not always be applicable (Frisch, 1996).

The developed Fortran program (appendix A) incorporating Eulerian spectral analysis was similar to the linear regression method of Stiansen (2001). Stiansen used velocity-time series data to quantify turbulent intensity within a tank with an oscillating grid and found good agreement with five other methods for calculating the turbulent kinetic energy dissipation rate. The three major advantages of the method over other techniques such as, not requiring characteristic length scales, applicability of the method under zero mean circulation conditions and the use of single velocity time series data (which can be provided by relatively inexpensive current meters), as outlined by Stiansen (2001), are equally applicable to the method used in this study. Stiansen later used the technique to investigate shear-generated turbulence in Norwegian fjords (Stiansen, 2001). Furthermore, Veron and Melville (1999) measured the turbulent kinetic energy dissipation rate in the upper mixed layer and found that acoustic Doppler velocimeter measurements were satisfactory such that wave number spectra exhibited a $-5/3$ slope.

In this study, we report the intensity of turbulence as both the turbulent intensity (u'^2) and the turbulent kinetic energy dissipation rate (ϵ) as determined directly from velocity time series data as opposed to indirectly through variations in temperature or scalars coupled to turbulence (i.e. microstructure profilers). Spectral analysis of the radial velocity data revealed that the decay of

energy followed a $-5/3$ slope (figure 5.8) and we were therefore confident that the turbulent kinetic energy dissipation rates were valid. Furthermore, we were predominantly concerned with small-scale turbulence. Reviews of advantages and limitations of other methods to measure and calculate turbulence can be found in Peters and Redondo (1997) and Sanford (1997).

5.4.2 Myponga mixer flow and turbulence analysis

The measured flow below the surface mixer in Myponga Reservoir was typical of a jet with vertical velocities exceeding horizontal velocities. Vertical velocities decreased rapidly below the draft tube falling from 1 to 0.1 m s^{-1} over 2 m, as a result of the hypolimnion density barrier. Intensive investigations of the surface mixer hydrodynamics by co-workers have shown that the depth of jet penetration is highly dependent upon the thermal structure of the reservoir (Lewis *et al.*, *in prep.*). Under isothermal and weakly stratified ($\leq 0.3 \text{ }^\circ\text{C}$) conditions, the jet penetrated to the depth of the reservoir ($\sim 35 \text{ m}$), whereas during stratified conditions on the day of sampling, the buoyancy of the jet caused it to penetrate only to 20.3 m and turn back on itself as demonstrated by horizontal flow in figure 5.1 and illustrated in table 5.1.

This has important implications for the environment of a phytoplankton cell. Not only does the time cells spend in darkness change, but also the intensity of turbulence, which they experience. A stable hypolimnion contains the jet and consequently limits the space over which the turbulent energy can dissipate. The less space available for energy dissipation the greater will be its intensity and the rate of energy dissipation and the finer will be the smallest eddies before inertial energy is overcome by viscosity.

Turbulence flow analysis demonstrated that energy dissipation rates tended to increase with depth below the draft tube, but decrease radially as the energy was not constrained. Turbulent kinetic energy dissipation rates varied by several orders of magnitude, but generally decreased further away from the draft tube. Turbulent kinetic energy dissipation rates ranged between $5 \times 10^{-7} \text{ m}^2 \text{ s}^{-3}$ and $1 \times 10^{-4} \text{ m}^2 \text{ s}^{-3}$, which are generally considered high (Peters and Marrase, 2000).

The extent to which phytoplankton are entrained is dependent upon the magnitude of shear velocity, u^* and the intrinsic swimming velocity of the phytoplankton cell (chapter 3). Shear

velocities, u^* were high and ranged from 2.3×10^{-2} to $6.6 \times 10^{-2} \text{ m s}^{-1}$ and therefore at these locations all phytoplankton including motile species would be entrained or imbedded in the flow as it exited the draft tube. Furthermore, earlier investigations, which measured flow velocity at radial increments of 2 m up to 70 m from the mixer and over depth to 19.5 m at 0.5 m increments, showed that motile and non-motile phytoplankton would be entrained into the mixer (Lewis, 1999). The results also clearly demonstrated that the lateral extent of entrainment decreases away from the mixer due to viscous dissipation. Attempts were previously made to track the movement of drogues towards the surface mixers, but often wind forcing dominated drogue movement and an accurate zone of influence could not be determined. Moreover, chlorophyll fluorescent profiling was undertaken to determine whether or not a peak in a signal would be detected within the intrusion, but due to copper sulphate dosing chlorophyll concentrations were often too low.

Based upon flow velocities, the theoretical exposure time of cells to high turbulent flow below the draft tube would be short. After entrainment by the impellers a cell would take 14 seconds to reach the bottom of the draft tube ($u_z \sim 1 \text{ m s}^{-1}$). From 14 to 22 m, the flow decreased to 0.1 m s^{-1} , which increased the time the cell was exposed to turbulence to 60 seconds. If the cell then moved in a radial direction at 0.1 m s^{-1} , it would take 50 seconds to reach 5 m. If a cell took 30 seconds to be entrained at the surface by the impellers then the total exposure time to highly turbulent conditions would be approximately 194 seconds, excluding far field flow dynamics. To some extent the response of a cell will be dependent upon the turbulent intensity of the intrusion developing away from the draft tube (Lewis *et al.*, *in prep.*). However, over a longer time period this would be difficult to distinguish from light dose affects.

The response of the phytoplankton community to turbulence generated by the mixer will likely depend upon the exposure time to turbulence and the species present within the reservoir. The shorter the exposure time, the less probable turbulence will exert any direct affects on phytoplankton cells. On the day of profiling, the phytoplankton community consisted predominantly of diatoms. Measurements of cell metabolic activity and viability indicated that flow through the mixer draft tube had no discernible impact on phytoplankton at small-scales in the short term. Similarly, there were no discernible differences in metabolic activity of phytoplankton from samples taken near (2 m) and far (70 m) from the mixer over 20 m depth. On the day of sampling the phytoplankton community also consisted of turbulent dependent genera

such as *Cyclotella* and *Nitzschia* species. These findings would be expected as the phytoplankton community is generally dominated by low light preferring species, which are adapted to turbulent conditions, and prevail even without artificial mixing within Myponga Reservoir. A recent model incorporating the surface mixers into PROTECH (Elliot *et al.*, 2001 references therein) demonstrated that artificial mixing had little discernible affect on the phytoplankton community (Lewis *et al.*, *in press*).

5.4.3 Torrens Lake bubble plume aerator flow and turbulence analysis

Flow velocity measurements described a basic pattern of a bubble plume aerator with water moving upwards above the perforated pipe and spreading radially outwards at the surface. The plunging of surface flow and the development of an intrusion was not detectable as a result of the narrowness and shallowness of the field location. Sites 1, 2 and 3 were within the reach of the lake occupied by the aerator and site 4 was downstream of the aerator. It is likely that there was lateral water movement above the aerator upstream, which was not detectable in this study. However, flow was measured at site 4, moving towards the aerator at depth. Interestingly, at site 2, small eddies were discernible with a diameter ranging between 0.1 and 0.2 m.

Turbulent intensity, shear velocity and turbulent kinetic energy dissipation rates varied between the four sites. Turbulent intensity, u'^2 and shear velocity, u^* ranged between 3.5×10^{-5} and $6.4 \times 10^{-3} \text{ m}^2 \text{ s}^{-2}$ and 5.9×10^{-3} and $7.9 \times 10^{-2} \text{ m s}^{-1}$, respectively. The likelihood of disentrainment of phytoplankton cells would increase radially away from the aerator. At most sites, the magnitude of measured shear velocities suggests that cells would be entrained within the flows generated by the bubble plume aerator. However, if cells were transported horizontally within any intrusions their own intrinsic swimming, floating or sinking velocity may become more dominant as shear velocity weakened within the intrusion. This would be particularly evident on the 'edges' of the intrusion where shear velocity would be reduced due to viscosity.

The calculated turbulent kinetic energy dissipation rate ranged between 1.76×10^{-6} and $3.35 \times 10^{-4} \text{ m}^2 \text{ s}^{-3}$ and values were in a similar range to those measured under the surface mixer in Myponga Reservoir. The turbulent kinetic energy dissipation increased at sites 2 and 3 compared to site 1,

probably due to the lakeshore confining the space over which the turbulent energy could be dissipated. It is likely that outside of the longitudinal length of the aeration system, the dissipation rates would decrease quickly and become more heterogeneous and approach intensities commonly generated by wind forcing.

At the time of sampling, the dominant phytoplankton consisted of *Cyclotella* (4850 cells mL⁻¹) and *Microcystis* (168 cells mL⁻¹) in the vicinity of the bubble plume aerator. *Cyclotella* is adapted to mixing for suspension and access to light, whereas *Microcystis* can tolerate periods of mixing (Ganf, 1974; Reynolds, 1989).

5.4.4 Torrens Lake aspirator and aerator flow and turbulence analysis

Both the submerged aspirator and the surface aerator had a significant influence on the thermal structure of the water column. Based upon the velocity data, the zone of influence of the submerged aspirator does not extend beyond a radial distance of 15 m. The distance to which radial velocities were detected can be used to calculate the nominal volume of water influenced by the aspirator. The velocities generated below 0.01 m s⁻¹ could not be attributed solely to either the aspirator or the aerator since at the average wind speed characteristic of the Torrens Lake wind driven velocities were of this magnitude. If velocities are assumed to be symmetrically distributed around the aspirator, the maximum nominal volume influenced by the 5 hp aspirator (with a 70 m air cable) at a depth of 3 m would be equivalent to the volume of a cylinder of radius 15 m and height 3 m. Thus the nominal volume would be 2.11 ML, which is less than that of 3.9 ML suggested by the manufactures for aspirator performance when the airline is closed. Realistically, this nominal volume is an overestimate since the evidence from the velocity measurements does not suggest a symmetrical distribution of velocities around the aspirator. The temperature data suggest a more extended zone of influence since even at 10 and 15 m distance from the aspirator the temperature profiles indicated a significantly cooler water column and erosion of the temperature gradient compared with that measured at the meteorological station. The temperature gradients during current velocity profiling were significant but not as pronounced as would be found during the summer months of December to February. A stronger summer temperature gradient would further restrict the zone of influence below that estimated

from the velocity data. The performance of the aspirator could be improved by the installation of a snorkel air inlet close to the aspirator to overcome the resistance offered by a 70 m air cable.

The calculated turbulent intensities for the aspirator and aerator were similar and ranged from 8.5×10^{-5} to $6 \times 10^{-3} \text{ m}^2 \text{ s}^{-2}$ and 8.9×10^{-5} to $1.3 \times 10^{-3} \text{ m}^2 \text{ s}^{-2}$, respectively. Subsequent, shear velocities ranged from 9.2×10^{-3} to $7.8 \times 10^{-2} \text{ m s}^{-1}$ and 9.5×10^{-3} to $3.3 \times 10^{-2} \text{ m s}^{-1}$ for the aspirator and aerator, respectively. If we assume the minimum shear velocity to equal $9.2 \times 10^{-3} \text{ m s}^{-1}$, then the intrinsic velocity (floating, swimming or sinking) of a phytoplankton cell would need to be $6.13 \times 10^{-4} \text{ m s}^{-1}$ (2.21 m h^{-1}). Consequently, at these shear velocities it is likely that phytoplankton cells would remain entrained within the flows in the immediate vicinity of the respective mixing devices and experience a fluctuating light climate. If we assume a euphotic depth of 2 m and a mixed depth of 3 m generated by the mixers, the resulting $Z_{\text{eu}}/Z_{\text{mix}}$ ratio is 0.67. Based on the calculations by Brookes *et al.* (*in prep.*) this is not likely to have an affect on the photosynthesis or growth of the problematic cyanobacterium *Microcystis*, that is often recorded in the lake. Consequently, control of species such as *Microcystis* using artificial mixing is inappropriate for the Torrens Lake (Brookes *et al.*, *in prep.*).

The turbulent kinetic energy dissipation rates generated by the aspirator and aerator ranged between 5.9×10^{-7} to $2.1 \times 10^{-4} \text{ m}^2 \text{ s}^{-3}$ and 8×10^{-7} and $3.6 \times 10^{-3} \text{ m}^2 \text{ s}^{-3}$, respectively. These values cover a broad range and were similar to those measured around the bubble plume aerator and below the surface mixer within the Myponga Reservoir.

5.4.5 Comparisons between artificial and naturally generated turbulence

The turbulent intensities, shear velocities, and turbulent kinetic energy dissipation rates measured below the surface mixer and around the bubble plume aerator, aspirator and surface aerator are higher than those typically generated by average wind speeds at the Myponga Reservoir or Torrens Lake. The shear velocities are comparable to those typically found in wind mixed layers (wind speeds of $10\text{-}100 \text{ m s}^{-1}$) and river channels and streams as illustrated in figure 5.30, after Reynolds (1997).

Using the model developed by MacKenzie and Leggett (1993) showed that a 5 m s^{-1} wind speed would generate an average turbulent kinetic energy dissipation rate of $1.7 \times 10^{-7} \text{ m}^2 \text{ s}^{-3}$ over 2 m. A 10 m s^{-1} wind speed would generate an average turbulent kinetic energy dissipation rate of $1.4 \times 10^{-5} \text{ m}^2 \text{ s}^{-3}$, which is more comparable to measured intensities around the mixing devices. Consequently, the hypothesis that artificial mixing systems will generate higher turbulent intensities compared to wind forcing is correct at low wind velocities ($< 5 \text{ m s}^{-1}$). Table 5.4 summarises the range of turbulent intensities, shear velocities and turbulent kinetic energy dissipation rates measured around the mixers and values recorded in lakes and oceans. The table also includes calculations of the smallest Kolmogorov eddy size (η).

Turbulence kinetic energy dissipation rates have been measured in many diverse hydrographic settings ranging from lakes (MacIntyre, 1993, 1998), estuaries (Reynolds and West, 1988), benthic boundary layers (Heathershaw, 1976) to surf zones (George *et al.*, 1994) and several are summarized in table 5.4. Values reported for the ocean range from 2.8×10^{-11} to $4.7 \times 10^{-3} \text{ m}^2 \text{ s}^{-3}$ (Osborn, 1980; Gargett *et al.*, 1979; MacKenzie and Leggett, 1993; Marmorino and Caldwell, 1978 Simpson *et al.*, 1996; Terray *et al.*, 1996), whereas, Yamazaki and Osborn (1988) gave the interval of 10^{-10} to $10^{-2} \text{ m}^2 \text{ s}^{-3}$ for the entire ocean with the latter representing an extreme situation with a strong tidal current. Stiansen (2001) reported a range of $4 \times 10^{-10} \text{ m}^2 \text{ s}^{-3}$ to $2 \times 10^{-5} \text{ m}^2 \text{ s}^{-3}$ in Norwegian fjords. Dissipation rates of $5 \times 10^{-8} \text{ m}^2 \text{ s}^{-3}$ to $4 \times 10^{-7} \text{ m}^2 \text{ s}^{-3}$ have been measured within Langmuir circulations generated by $6 - 8 \text{ m s}^{-1}$ wind speeds (Plueddemann *et al.*, 1996) and values of $1 \times 10^{-6} \text{ m}^2 \text{ s}^{-3}$ have been reported for rivers (Dallimore *et al.*, 2001).

Presently, there is uncertainty regarding the level of turbulence, particularly in the upper mixed layer of the ocean, the levels encountered by plankton in natural systems and concerns regarding the level of turbulence simulated in biological experiments with zooplankton and phytoplankton (Peters and Redondo, 1997; Peters and Marrasé, 2000). A recent review of biological-turbulence experiments by Peters and Marrasé (2000) revealed that most laboratory experiments on the effects of plankton have been carried out in regimes with much higher turbulent energy than

Table 5.4 Summary of selected shear velocities, turbulent kinetic energy dissipation rates and Kolmogorov (η) eddy sizes, measured in various hydrographic settings. Adapted from Reynolds (1994a).

Location/ conditions	Shear velocity (m s^{-1})	Turbulent kinetic energy dissipation rate ($\text{m}^2 \text{s}^{-3}$)	η (mm)	Reference
Surface mixer	2.3×10^{-2} -	5×10^{-7} - 1×10^{-4}		This study
Myponga Reservoir	6.6×10^{-2}			
Bubble plume	5.9×10^{-3} -	1.8×10^{-6} - 3.4×10^{-4}		This study
aerator, Torrens Lake	7.9×10^{-2}			
Aspirator, Torrens Lake	1×10^{-2} -	5.9×10^{-7} - 2.1×10^{-4}		This study
Surface aerator, Torrens Lake	7.8×10^{-2}			
Bodensee, winter winds ($5\text{-}20 \text{ m s}^{-1}$)	9.5×10^{-3} -	8×10^{-7} - 3.6×10^{-3}		This study
Bodensee summer winds ($<8 \text{ m s}^{-1}$)	3.3×10^{-2}			
Lough Neagh, winds ($10\text{-}20 \text{ m s}^{-1}$)	6.2×10^{-3} -	1.4×10^{-8} - 2.2×10^{-7}	2.9-1.5	Reynolds (1989)
Ashes Hollow (hill stream)	2.5×10^{-2}			
River Thames (Reading)	$<1 \times 10^{-2}$	$<1.3 \times 10^{-7}$	>1.7	Reynolds (1989)
Open ocean	1.3×10^{-2} -	5.4×10^{-7} - 4.3×10^{-6}	1.2-1.7	Calculated-Reynolds (1994a)
Shelf (Irish Sea)	2.5×10^{-2}			
Tidal estuary (Severn)	3.1×10^{-3}	1.5×10^{-6}	0.9	Reynolds (1988b)
Lakes	9.4×10^{-3}	5.1×10^{-6}	1.2	Reynolds (1988b)
Surf zones	$<3.3 \times 10^{-2}$	3.8×10^{-7}	>1.27	Nixon (1988)
Surface/wave zone	$<1.2 \times 10^{-1}$	4×10^{-5}	>0.4	Nixon (1988)
Stratified lake interior	1.3×10^{-1} -	5.5×10^{-4} - 5×10^{-6}	0.2-	Reynolds and West (1988)
Benthic boundary layer	4.3×10^{-2}	1.4×10^{-8} - 4×10^{-2}	0.67	Reynolds (1994a)
		1×10^{-2}	0.7-2.9	George <i>et al.</i> (1994)
		1×10^{-3} - 9×10^{-7}	0.17-30	Veron and Melville (1999)
		10^{-10} - 10^{-7}		Gargett (1989)
		10^{-2} - 10^{-1}		MacIntyre (1993)
				Heathershaw (1976)

normally found in nature. Peters and Marrasé (2000) found that turbulence intensities in 26 studies ranged from 7.4×10^{-8} to $1.5 \text{ m}^2 \text{ s}^{-3}$, with a geometric mean of $9.8 \times 10^{-5} \text{ m}^2 \text{ s}^{-3}$. Despite these values being higher than those measured in the euphotic zone of oceanic environments, they are comparable to those measured in the Myponga Reservoir and Torrens Lake. Consequently, laboratory data from experiments, which simulated high levels of turbulence, may provide useful insights into the effects of artificial mixing on freshwater plankton, particularly phytoplankton. Based on existing data, Peters and Marrasé (2000) report that a threshold value of $1 \times 10^{-5} \text{ m}^2 \text{ s}^{-3}$ ($0.1 \text{ cm}^2 \text{ s}^{-3}$) determines whether turbulence will exert a detrimental effect on phytoplankton. Values higher than $1 \times 10^{-5} \text{ m}^2 \text{ s}^{-3}$ have caused growth inhibition in several species predominantly dominated by dinoflagellates (Peters and Marrasé, 2000).

5.4.6 Conclusions

The measurement of flow and turbulence will provide further insights into the effects of artificial mixing strategies on aquatic ecosystems, ranging from sediment resuspension to phytoplankton dynamics. A recent study by Mitrovic *et al.* (2003) highlights the usefulness of reporting results in hydrodynamic terms in relation to phytoplankton dynamics to enable comparisons between different systems. Mitrovic *et al.* (2003) reported that a critical velocity of 0.05 m s^{-1} was sufficient for the suppression of persistent thermal stratification and concurrent *Anabaena* growth in the Barwon Darling River. They also found that the shear velocity (u^*) under weak wind mixing at the study locations varied between 2.66×10^{-3} and $2.91 \times 10^{-3} \text{ m s}^{-1}$ at critical flow velocities.

This study has provided an insight into the turbulent intensities generated by artificial mixing systems in fresh water bodies. In conclusion, artificial mixing systems generate high turbulent intensities, shear velocities and turbulent kinetic energy dissipation rates within their vicinity. No discernible effect of turbulence on phytoplankton was detected with transport through a surface mixer and it is hypothesized that any effects will be species-specific and depend highly on the exposure time to turbulence. In chapter 6, the influence of small-scale shear at levels measured in the Myponga Reservoir and Torrens Lake on *Microcystis aeruginosa* is investigated under controlled laboratory conditions.

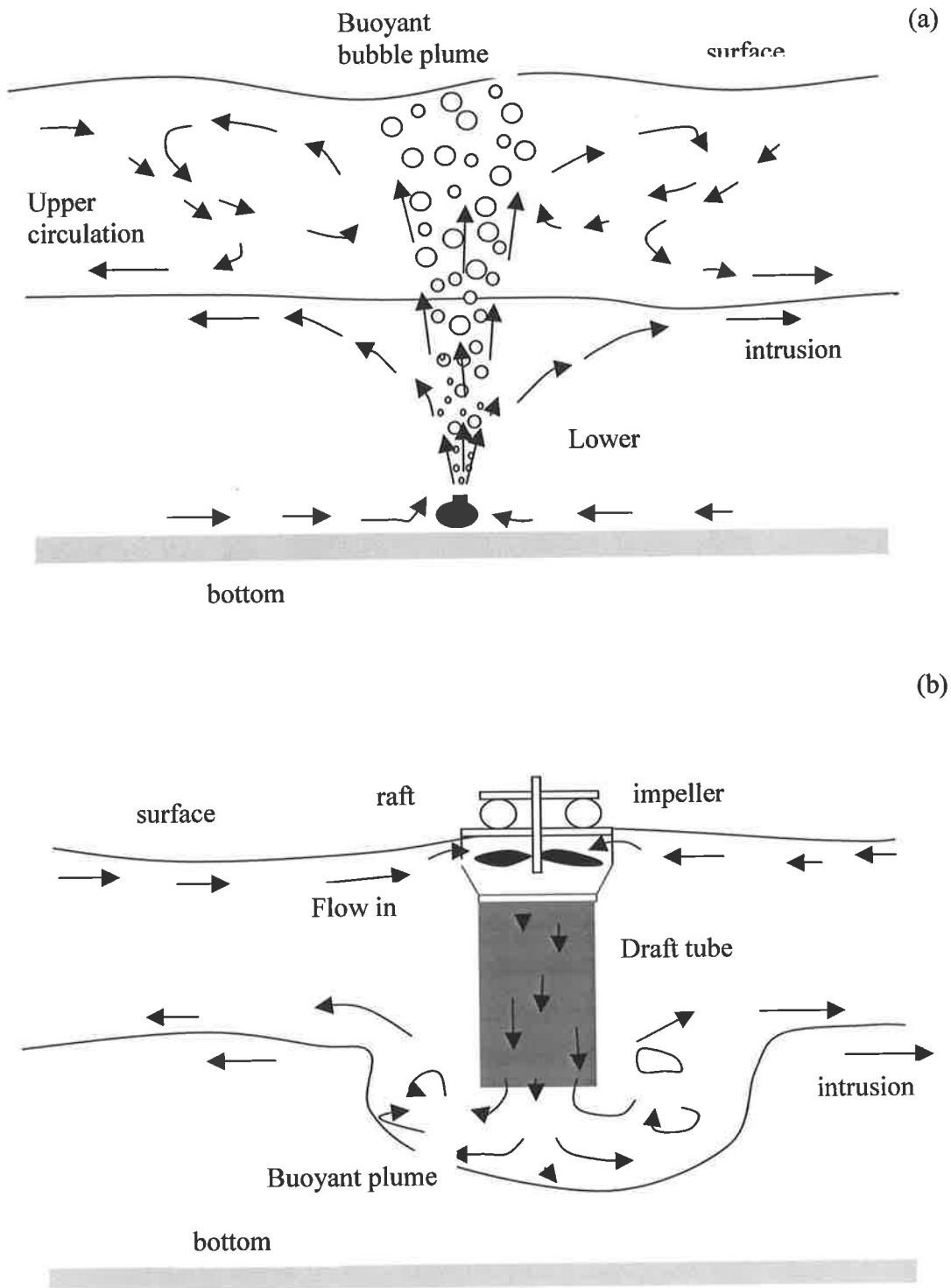


Figure 5.1 Schematic diagram of flow by bubble plume aeration (a) and surface mounted mechanical mixing (b).

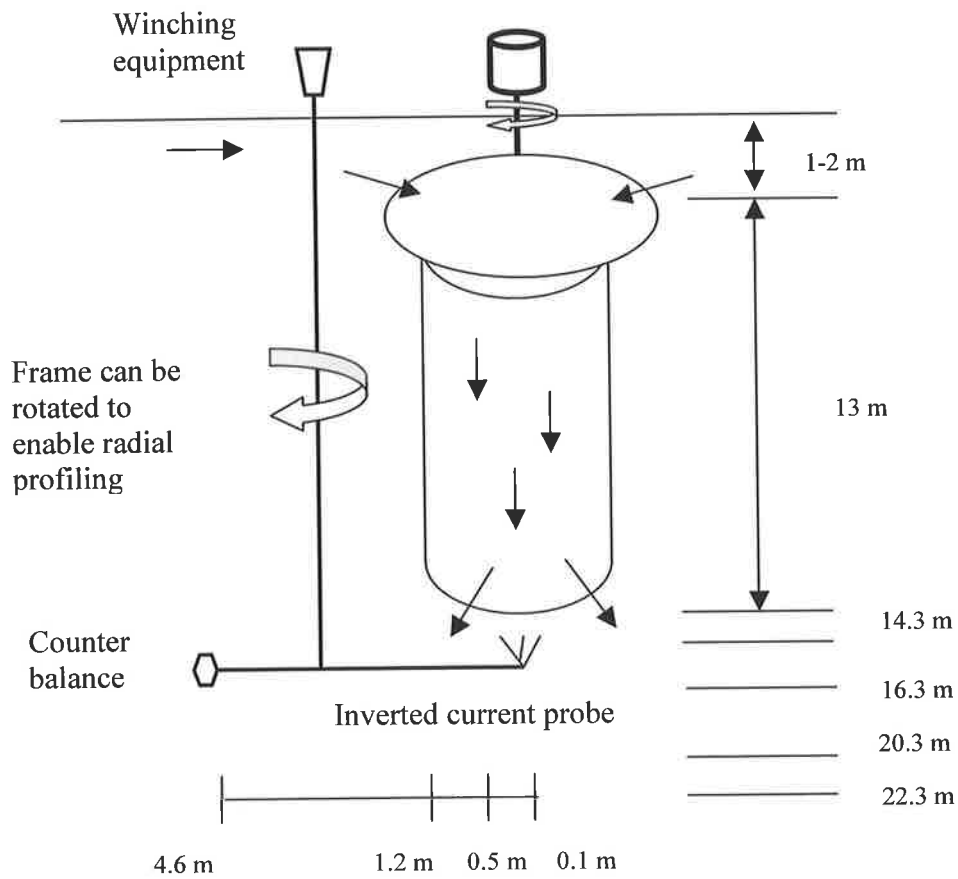


Figure 5.2 Schematic diagram of the surface mounted mechanical mixer in Myponga Reservoir. Water is entrained by impellers from the surface, down a draft tube where it exits. The entrained flow resembles a swirling jet (Lewsi *et al.*, *in prep.*). A current probe was attached to an aluminum bracket to enable current velocity measurements below the draft tube at different depths and radial distances.



Figure 5.3 Photographs of the surface mounted mechanical mixer in the Myponga Reservoir, South Australia.

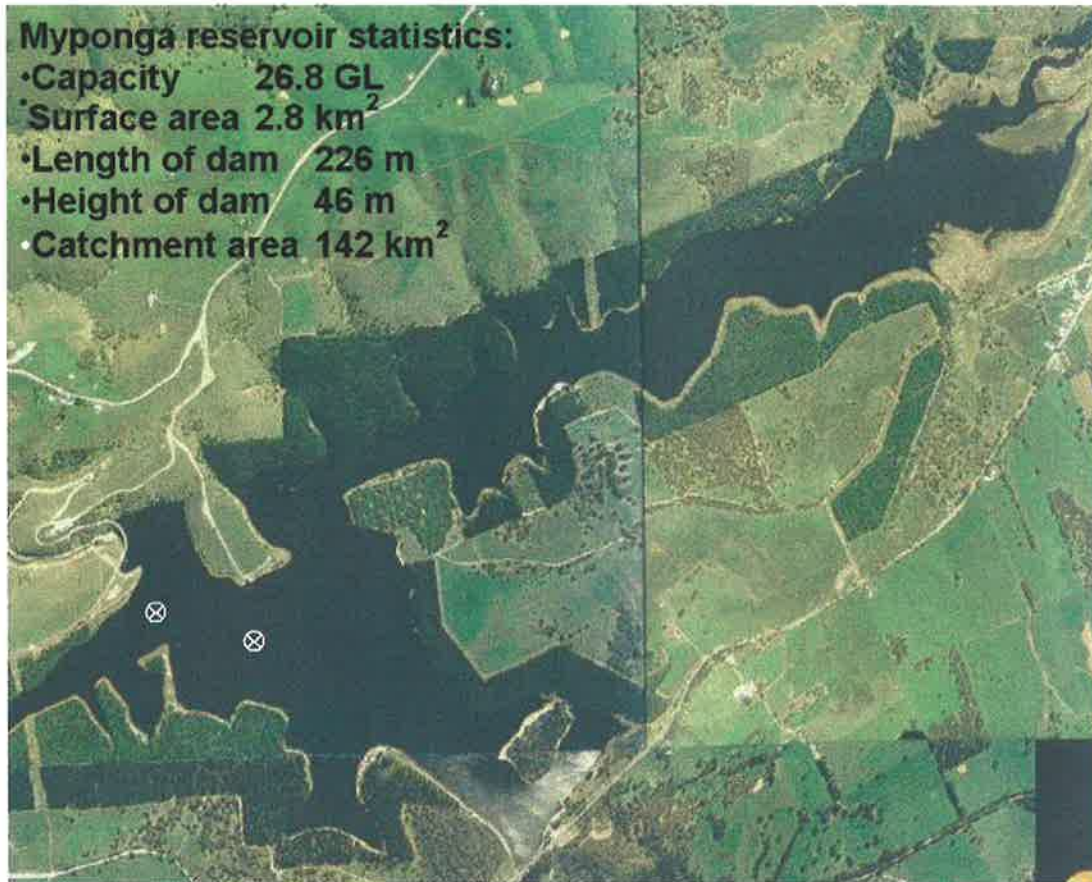


Figure 5.4 Map of Myponga Reservoir showing the location of two surface mounted mechanical mixers (white encircled crosses).

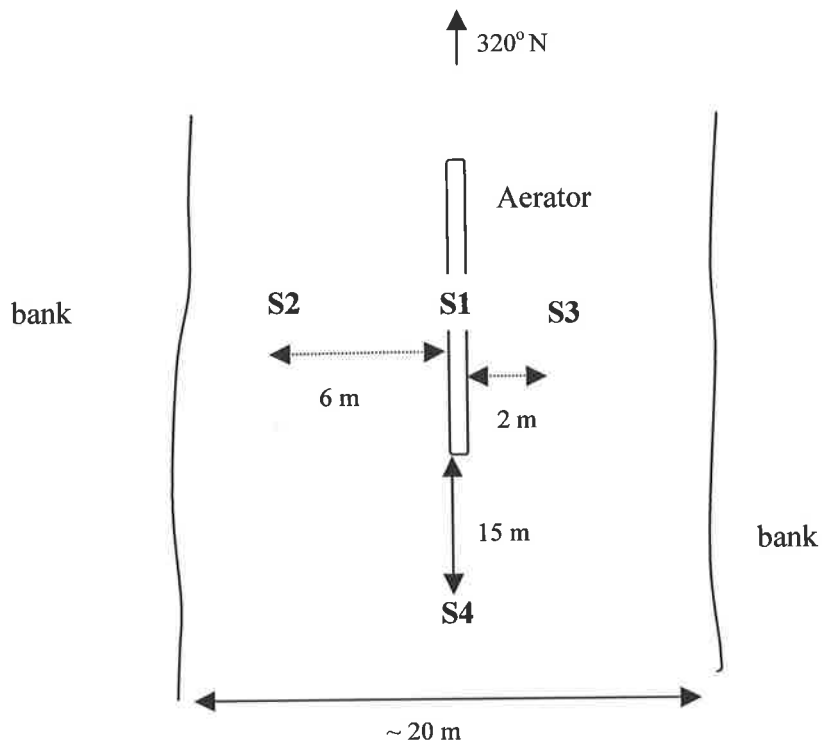


Figure 5.5 Location of water velocity profiling sites around the Albert Street Bridge bubble plume aerator within the Torrens Lake (longitudinal view from above). The four sites were chosen to gain an appreciation of the zone of influence and intensity of turbulence. At each of the four sites, current velocity profiles were taken every 0.1 m from the surface to the sediment using a current velocity ADV probe.

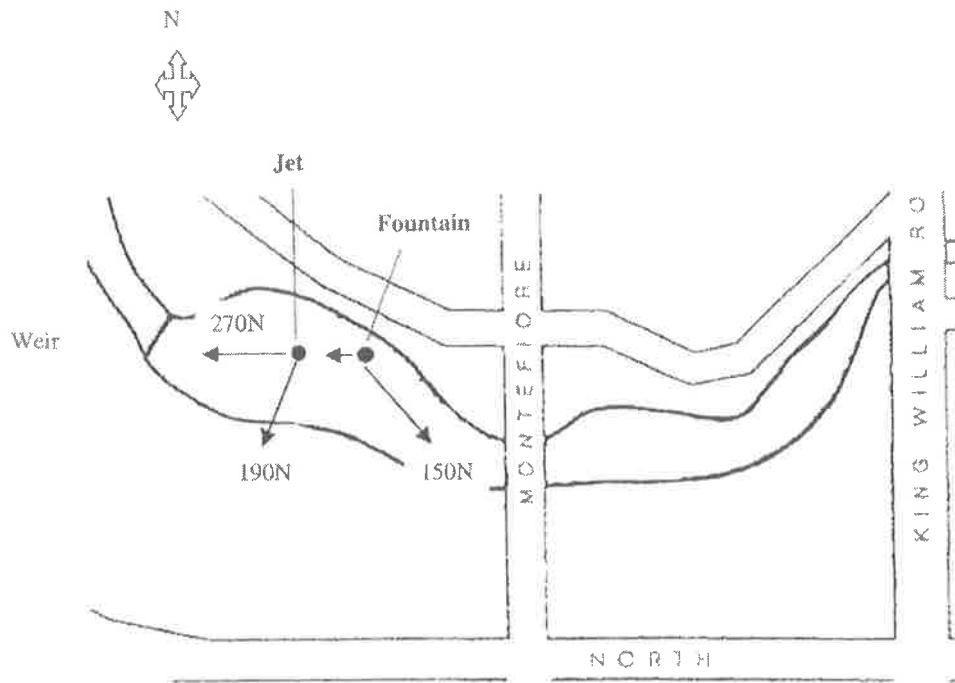


Figure 5.6 Location of submerged aspirator (jet) and high volume surface aerator (fountain) and direction of transect lines within the Torrens Lake, South Australia. Measurements were taken from a flat bottom boat as shown in figure 5.7.

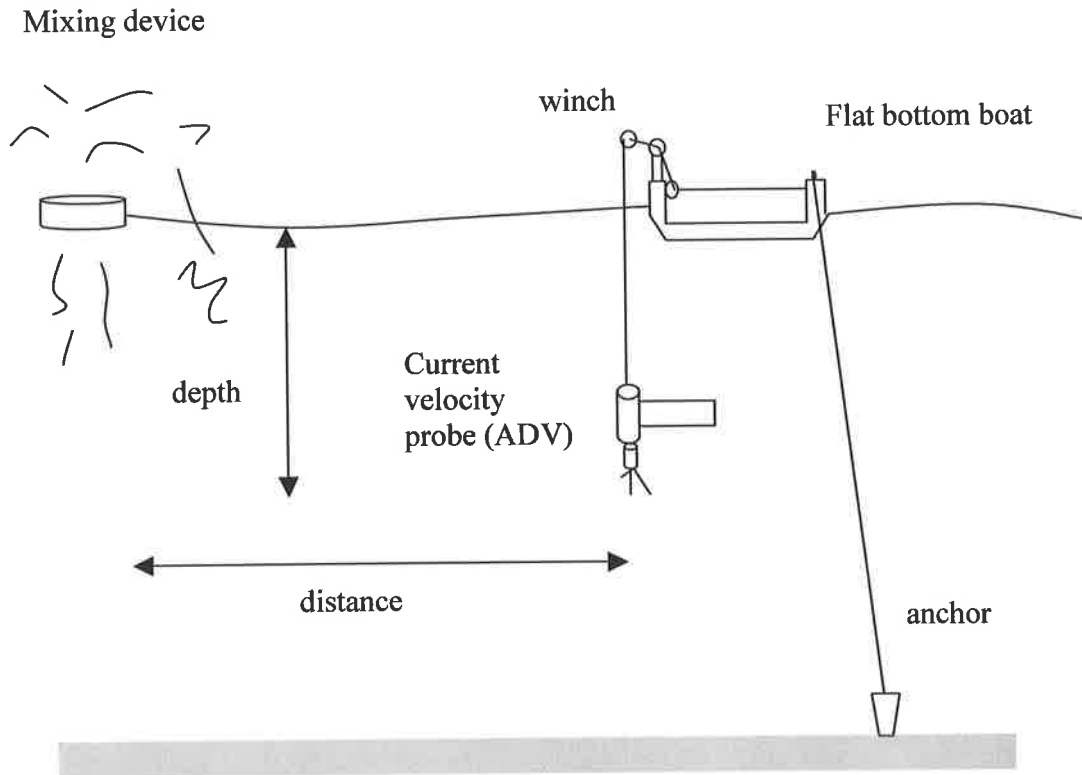


Figure 5.7 Current velocity profiling and boat set up. A Sontek acoustic Doppler velocimeter probe (ADV) at 50 Hz was used for all measurements. WINADV 32 processing software (Wahl, 2001) was used to filter the time series velocity data and provided average values for each depth and time.

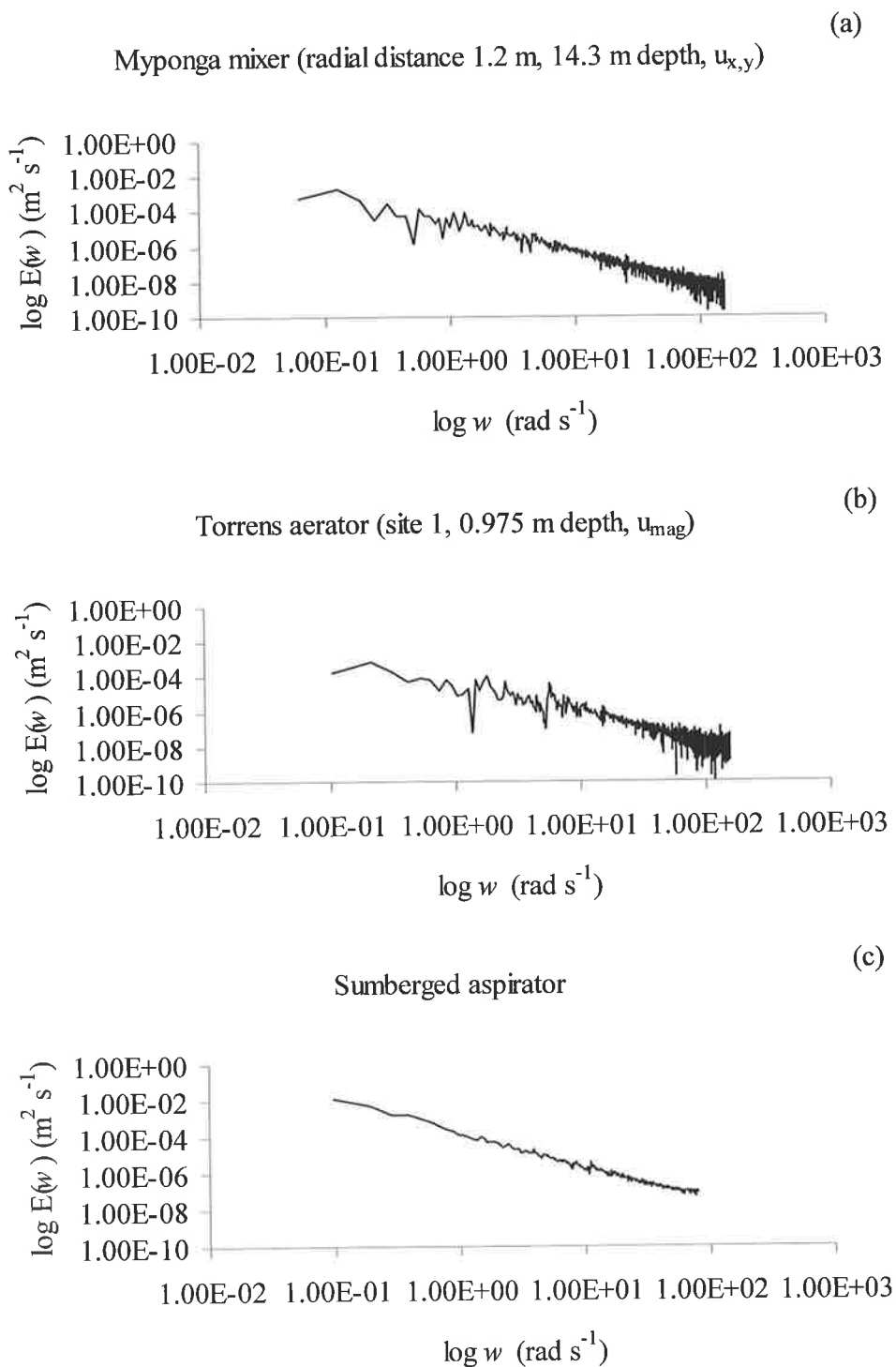


Figure 5.8 Energy spectra estimated from acoustic Doppler velocimetry (ADV) below a Myponga Reservoir surface mixer (a), around a Torrens Lake Bubble plume aerator (b) and submerged aspirator (c).

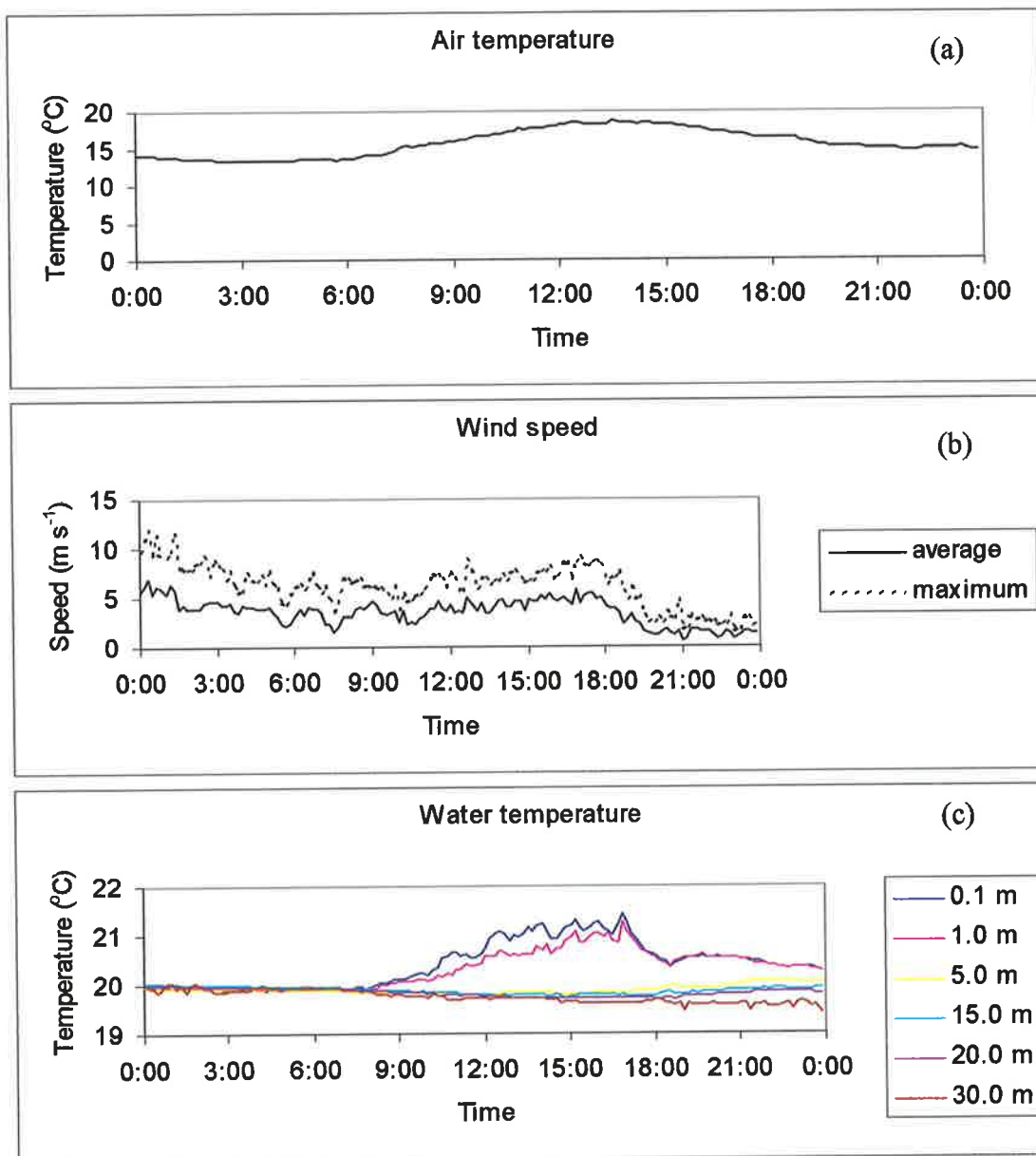


Figure 5.9 Meteorological conditions at the Myponga Reservoir on the 5 February 2002, measured at meteorological station 1 300 m east of the surface mixer – air temperature (a), wind speed (b) and temperature structure (c) throughout the day.

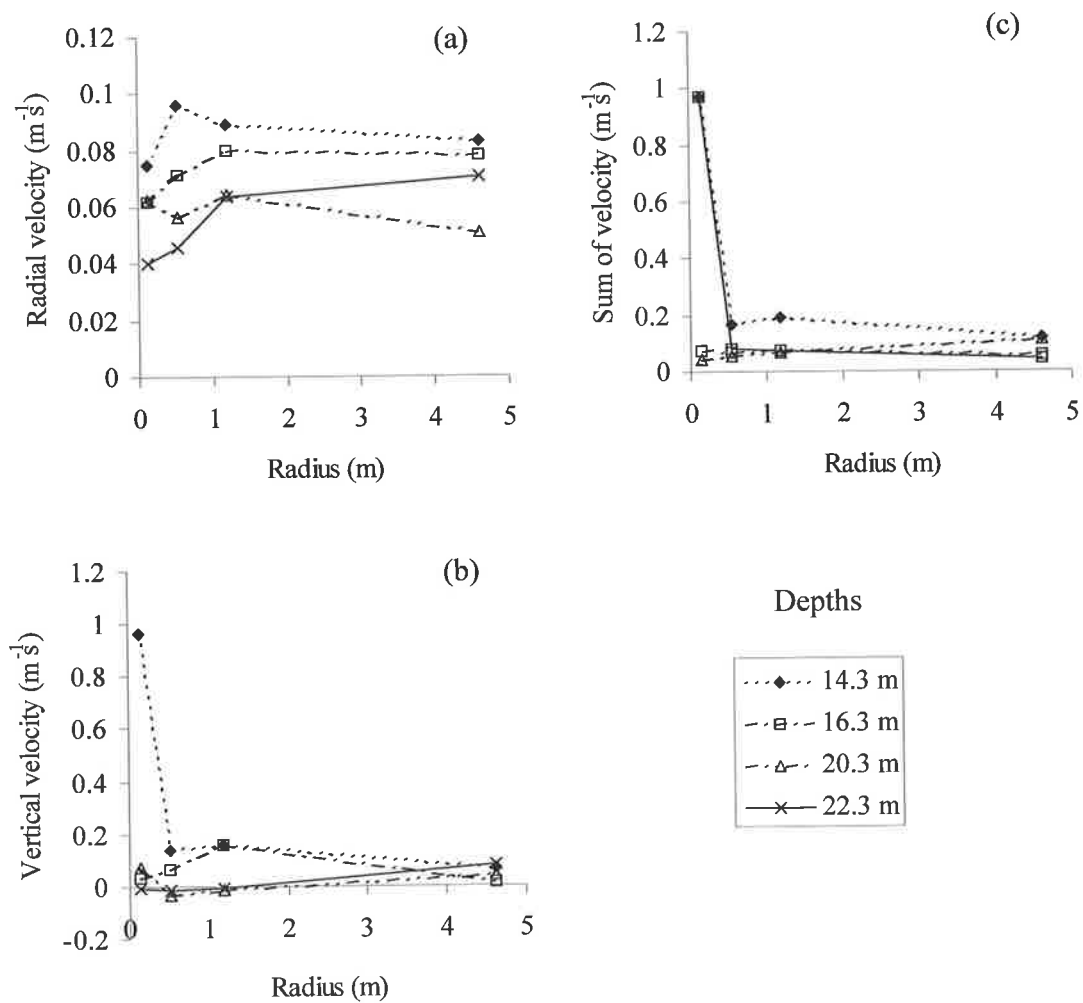


Figure 5.10 Radial (a), vertical (b) and sum of velocity components (c) at 4 depths below the Myponga surface mixer draft tube. All velocities are in $m s^{-1}$ and the radius is measured from the center-line of the mixer.

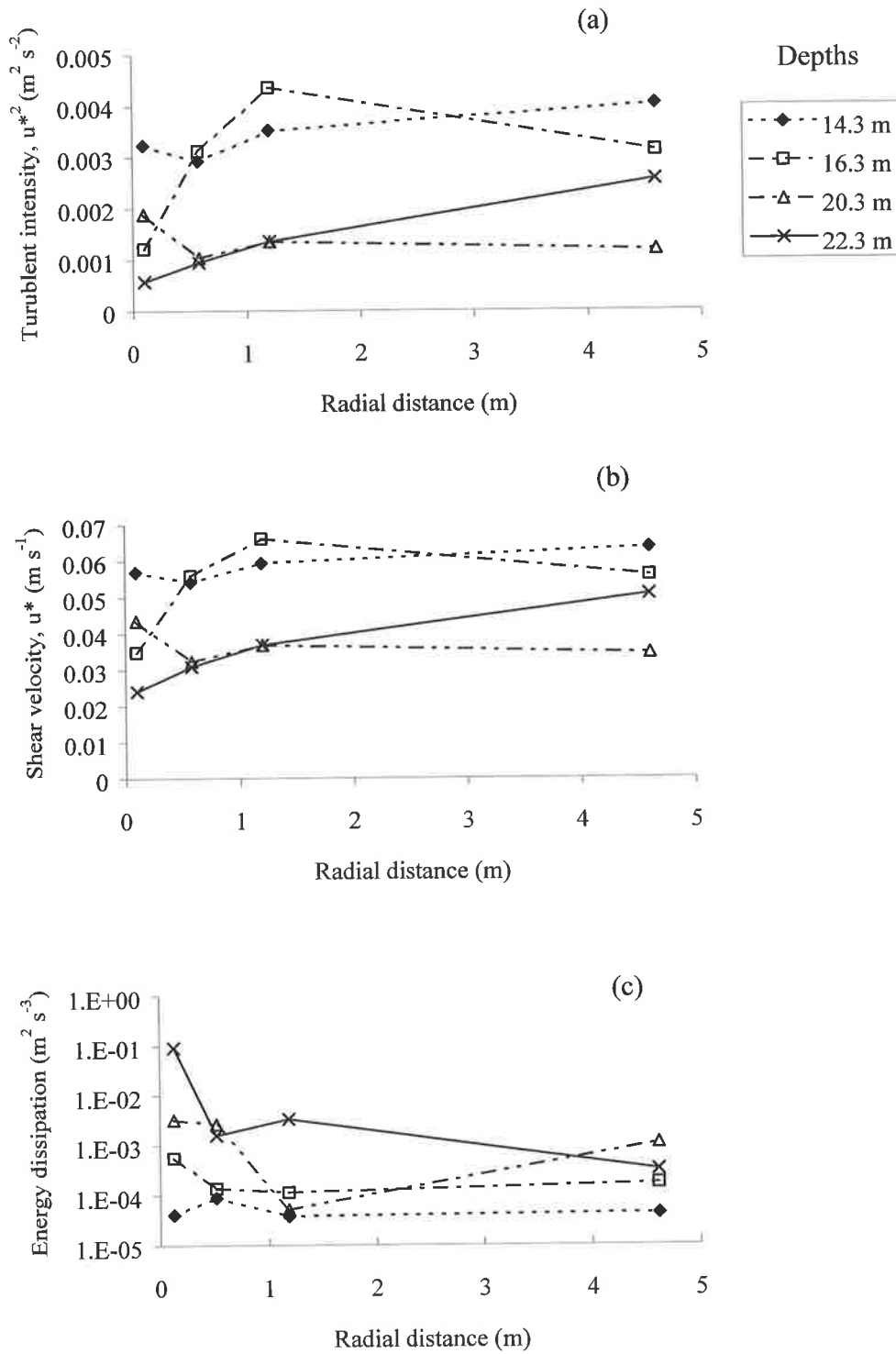


Figure 5.11 Calculated turbulent intensities, u^{*2} (a), shear velocities, u^* (b) and turbulent kinetic energy dissipation rates, ϵ (c) below the Myponga Reservoir surface mixer draft tube. Turbulent intensities ($m^2 s^{-2}$) and turbulent kinetic energy dissipation rates ($m^2 s^{-3}$), based on u_{radial} were calculated from equations 2 and 4, respectively.

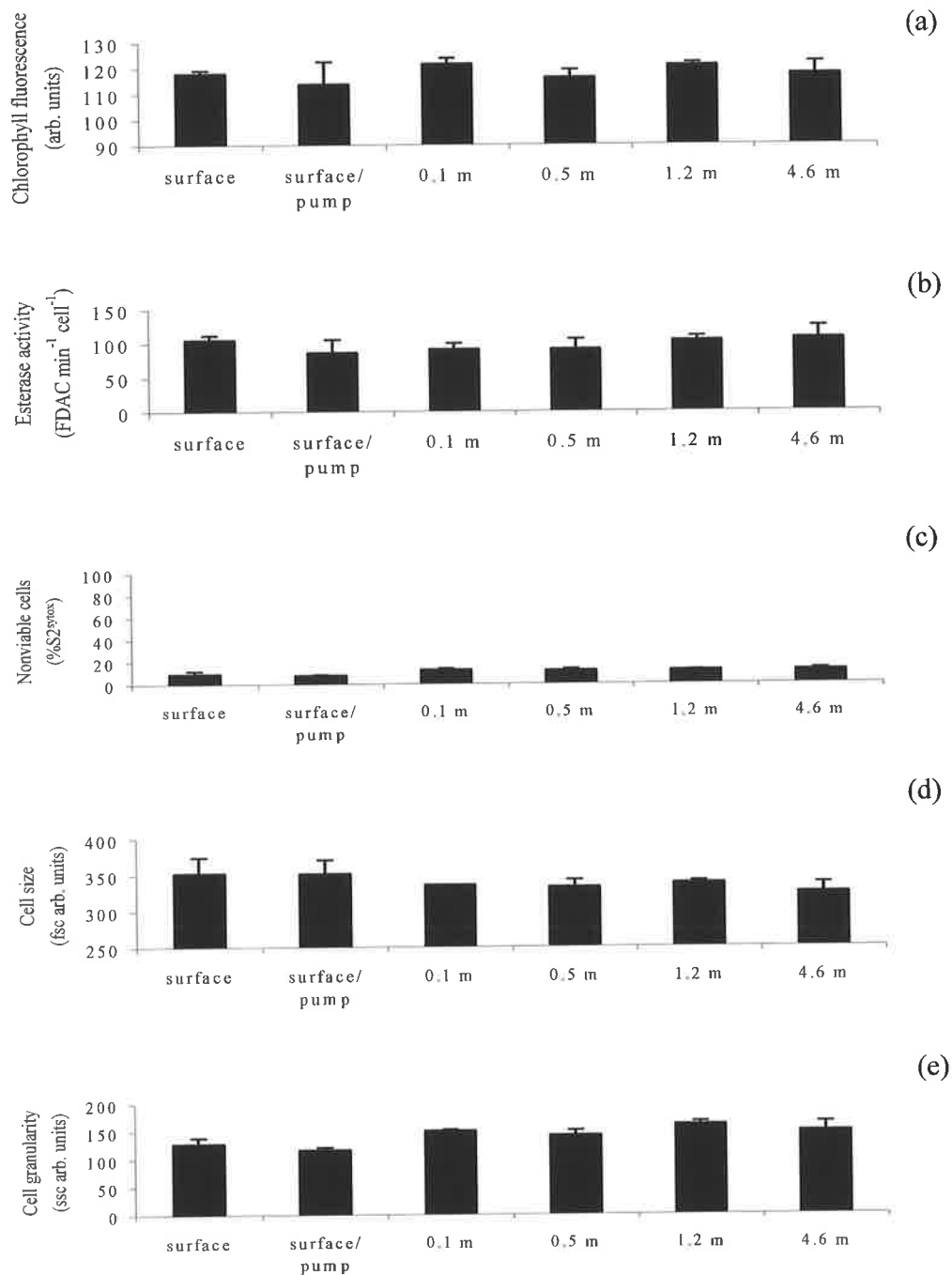


Figure 5.12 Effect of transport through the Myponga Reservoir surface mixer draft tube on phytoplankton chlorophyll fluorescence (a), esterase activity-mean FDA conversion rate (b), % of non viable cells in the population-S_{2syt} (c), cell size (d) and cell granularity (e). Results presented are taken from samples taken from 16.3 m and at 4 radial distances (0.1, 0.5, 1.2 and 4.5 m). There were no significant differences ($p > 0.05$) amongst the biological parameters when comparing sampling positions to surface samples taken from above the impeller for all depths and radial distances. The surface pump sample acted as a control to ensure that pumping did not affect phytoplankton characteristics.

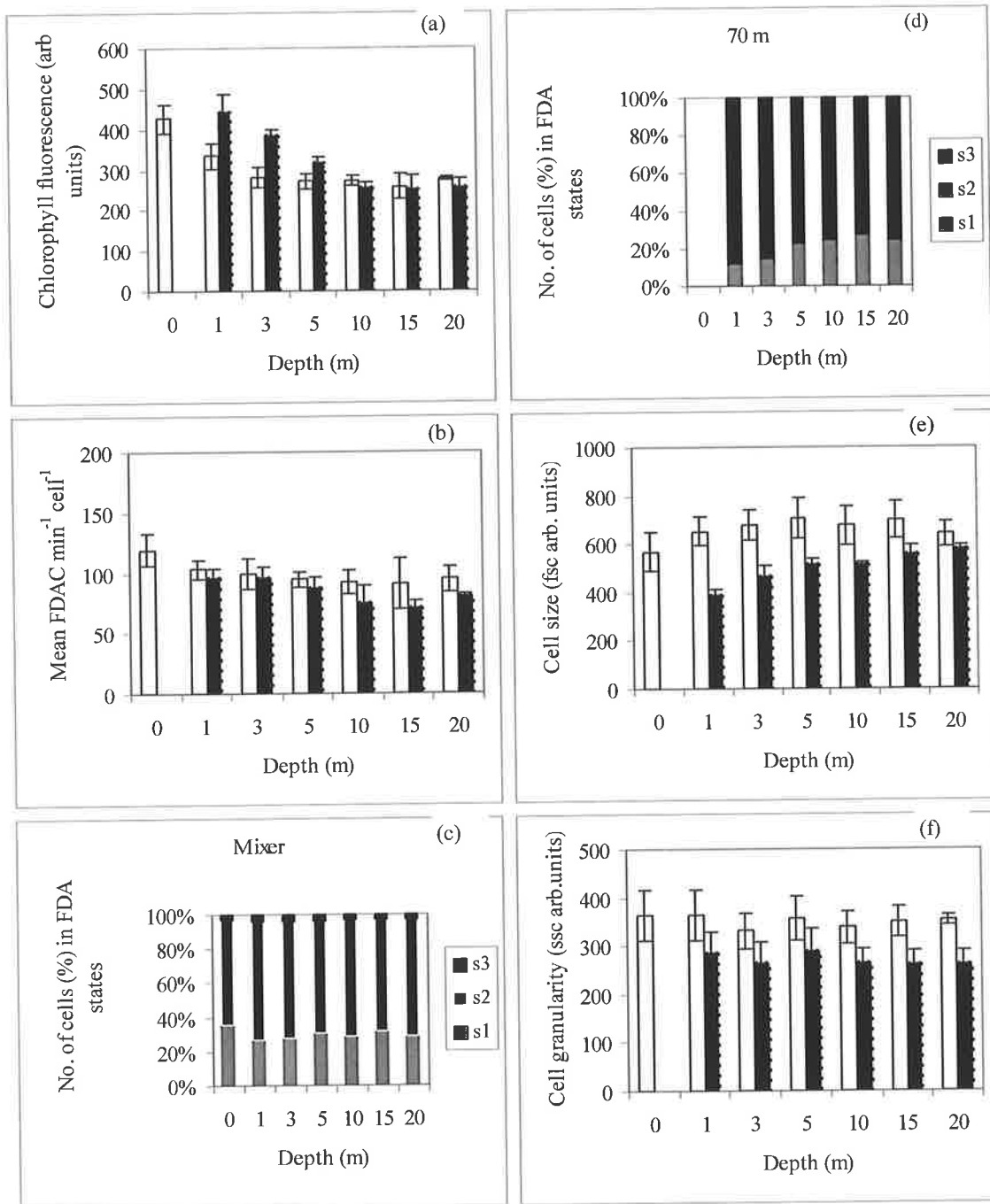


Figure 5.13 Comparison of Myponga Reservoir phytoplankton (2 January 2001) activity and physical characteristics between the surface mixer site (open) and a site 70 m away (bold). Comparisons were made with depth between chlorophyll fluorescence cell⁻¹ (a), esterase activity-FDA conversion rate (b), % of cells in each esterase activity state for the mixer (c) and 70 m (d), cell size (e), and cell granularity (f).

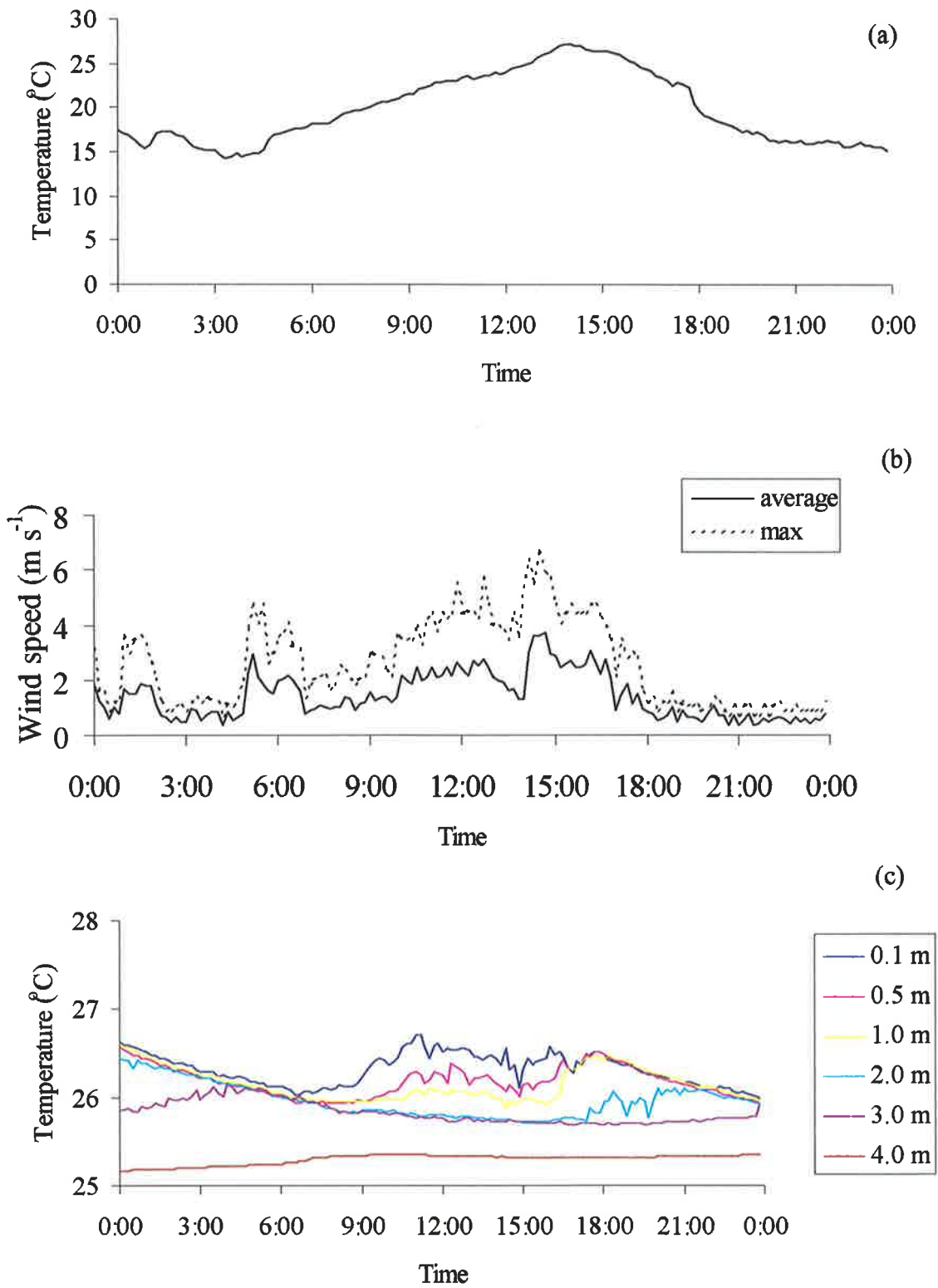


Figure 5.14 Meteorological conditions at the Torrens Lake city weir (1 km down stream of the profiled aerator) on the 22 February 2001- air temperature (a), wind speed (b) and water temperature profiles (c).

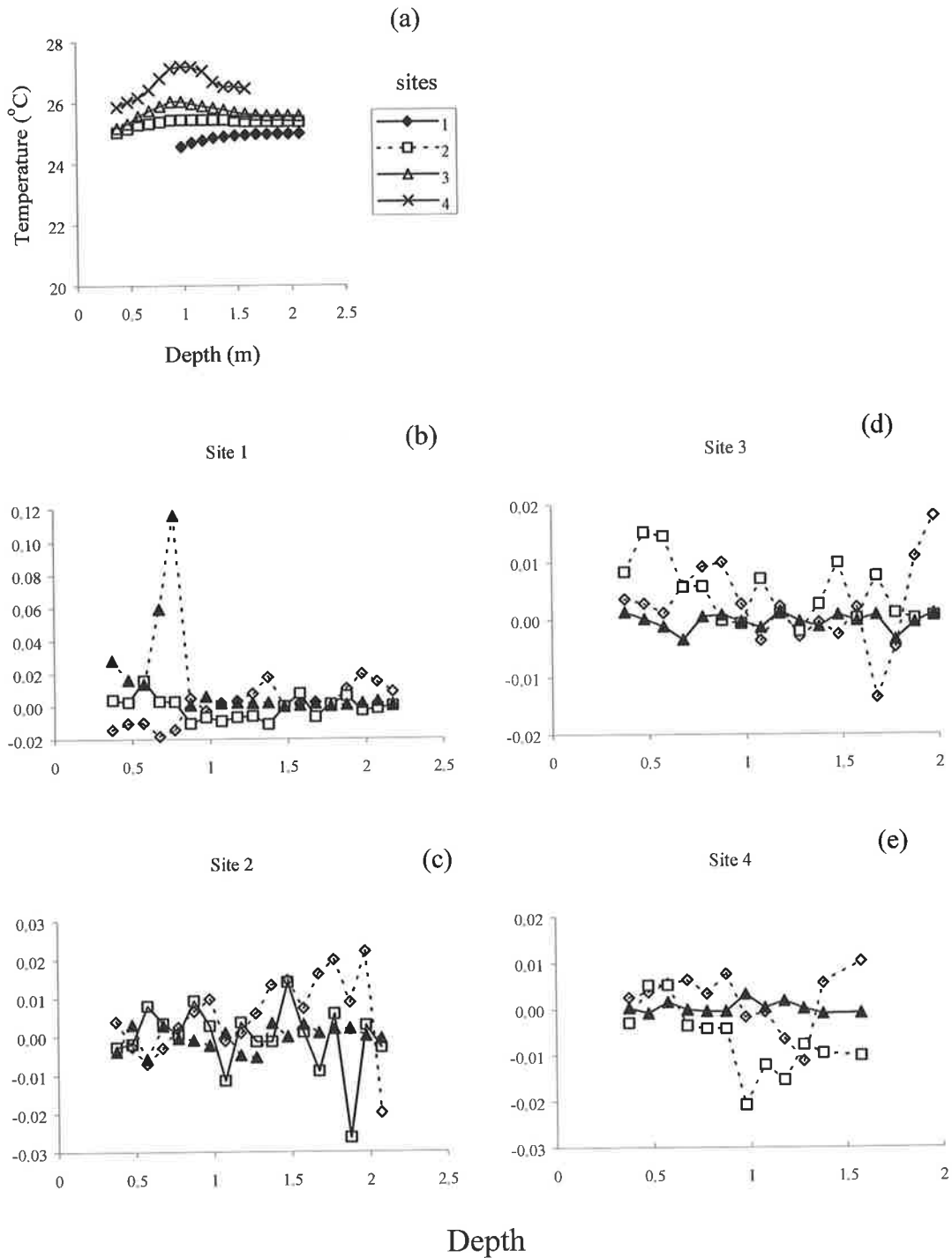


Figure 5.15 Temperature (a) and velocity profiles, u (m s^{-1}) at sites 1 (b) – 4 (e) around a bubble plume aerator within the Torrens Lake. Cartesian components; open diamonds = x , open squares = y , bold triangles = z . Positive values indicate flow away from the aerator and positive z values indicate upward flow.

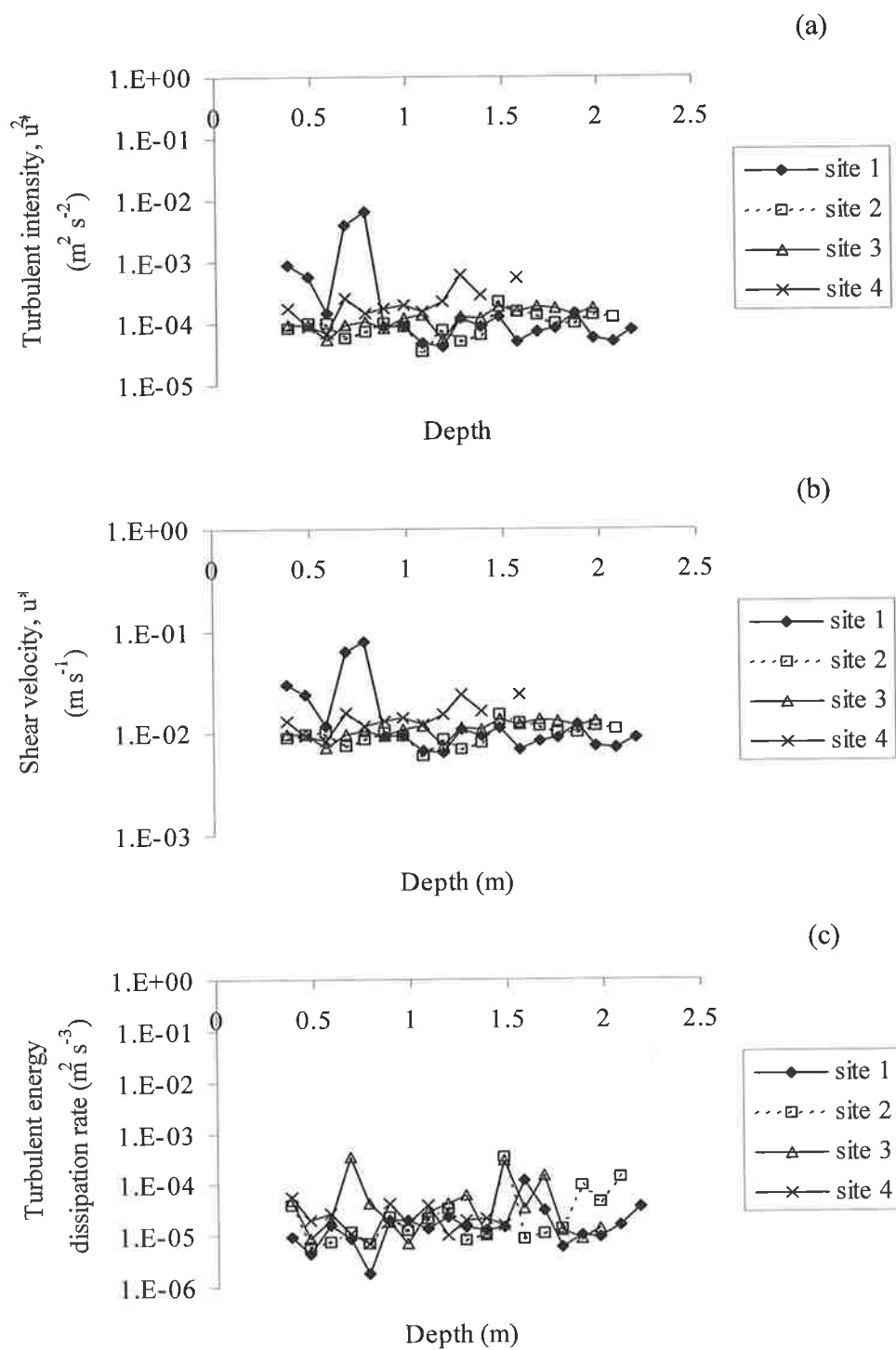


Figure 5.16 Calculated turbulent intensities (a), shear velocities (b) and turbulent kinetic energy dissipation rates (c) at 4 sites (1-4) around the bubble plume aerator in the Torrens Lake. Turbulent intensities were calculated as the product of the root mean square of the u_x and u_z velocities (equation 3) and dissipation rates were calculated using spectral analysis of radial velocities (equation 4).

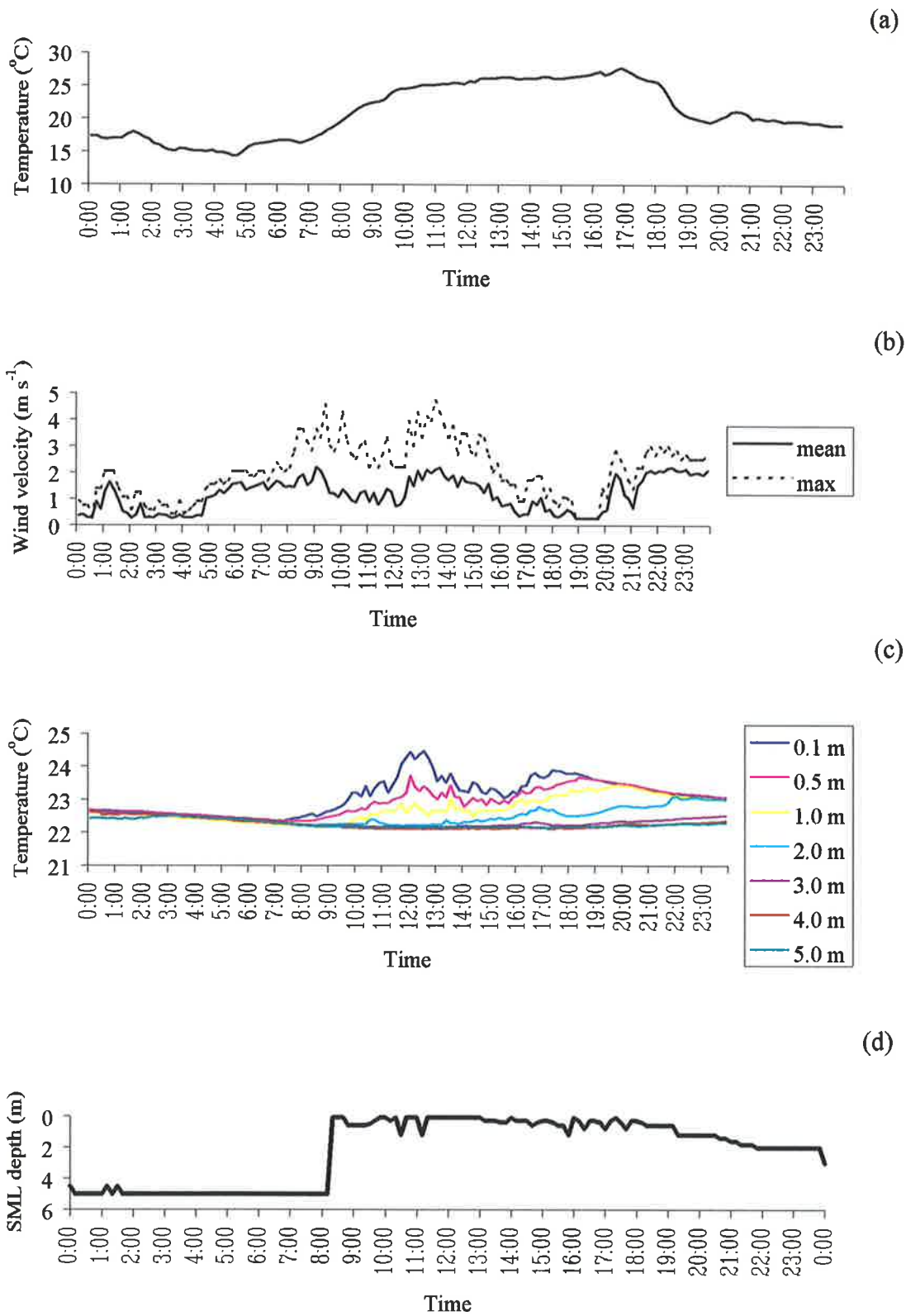


Figure 5.17 Meteorological conditions at the city weir on the Torrens Lake- air temperature (a), wind speed (b), water temperature (c) and surface mixed layer calculations (d) on the 23 March 2002.

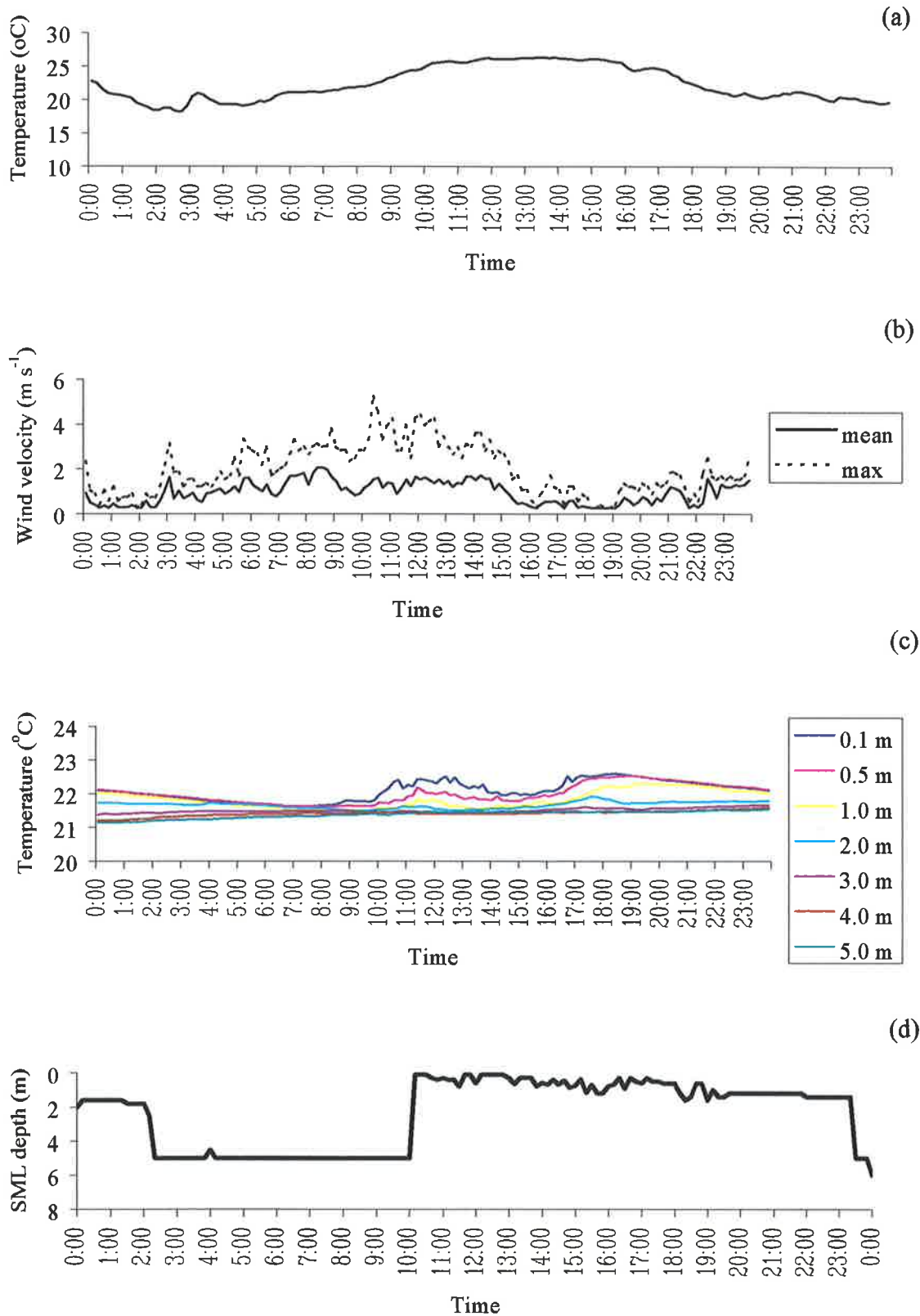


Figure 5.18 Meteorological conditions at the city weir on the Torrens Lake- air temperature (a), wind speed (b), water temperature (c) and surface mixed layer calculations (d) on the 2 April 2002.

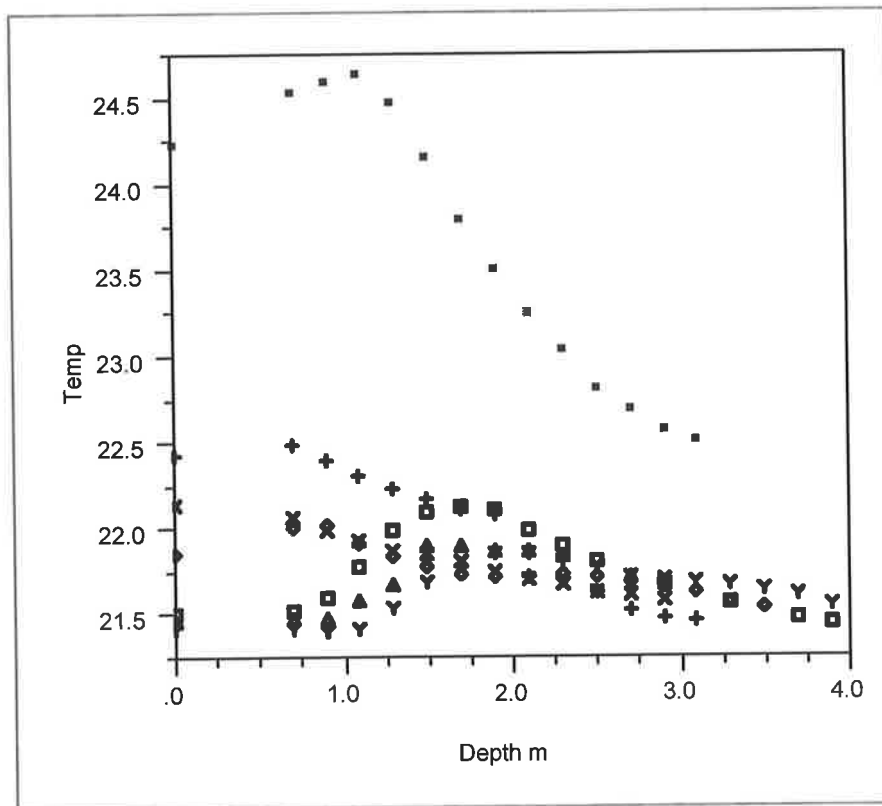


Figure 5.19 Temperature profiles recorded along two transects (190° and 270° North) at distances between 3 and 15 m from the submerged aspirator. Radial distances and symbols in figure; 190° transect: dot = 3 m, x = 4 m, diamond = 5 m, y = 10 m and 270° transect: cross = 3 m, square = 6 m and the triangle represents 15 m.

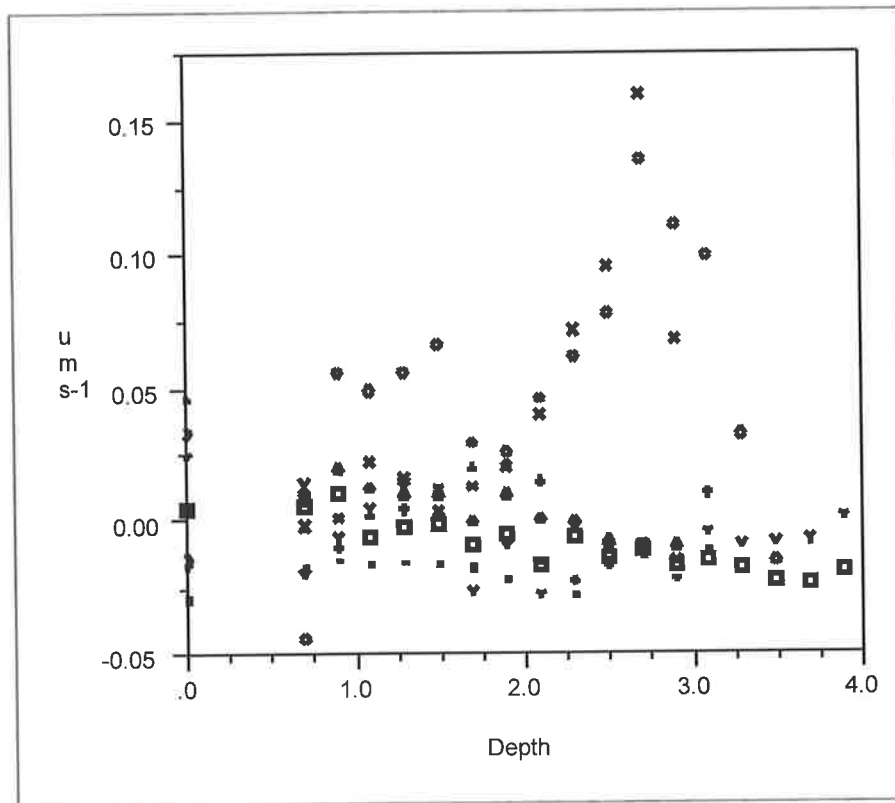


Figure 5.20 Radial velocities (u) measured along two transects (190° and 270° North) at distances between 3 and 15 m from the aspirator. Positive values indicate flow away from the aerator and negative values indicate flow towards the aerator. Velocities in the range $+0.01$ and -0.01 m s^{-1} are below the critical velocity as determined by u^* (wind generated turbulent intensity). Note all velocities are in m s^{-1} . Radial distances and symbols in figure; 190° transect: dot = 3 m, x = 4 m, diamond = 5 m, y = 10 m and 270° transect: cross = 3 m, square = 6 m and the triangle represents 15 m.

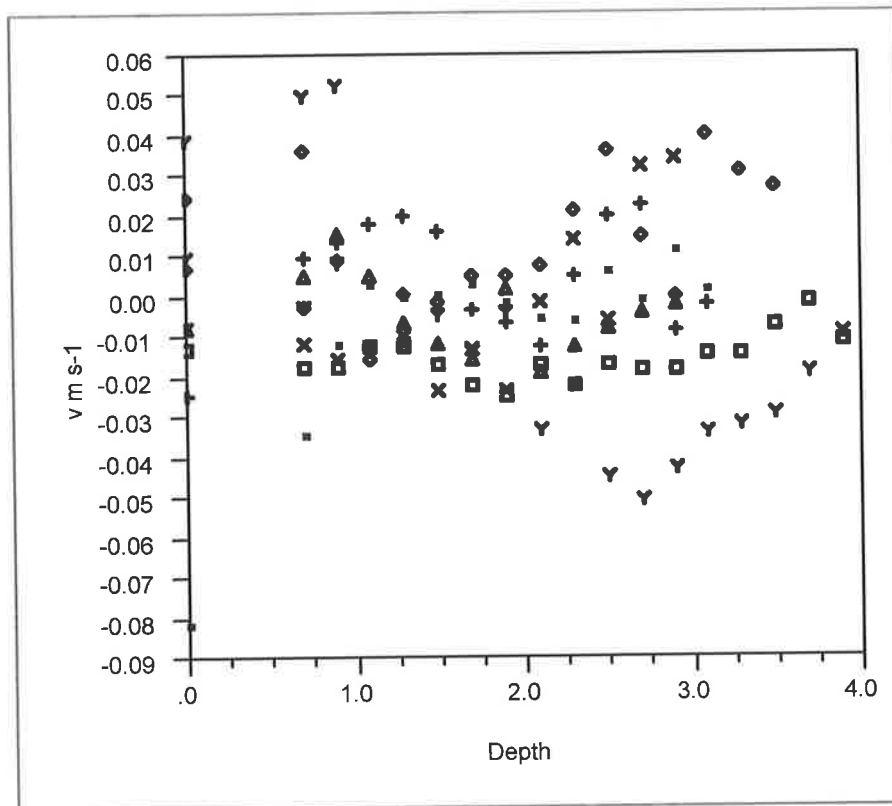


Figure 5.21 Vertical velocities (v) measured along two transects (190° and 270° North) at distances between 3 and 15 m from the aspirator. Positive values indicate flow away from the aerator and negative values indicate flow towards the aerator. Velocities in the range $+0.01$ and -0.01 m s^{-1} are below the critical velocity as determined by u^* (wind generated turbulent intensity). Note all velocities are in m s^{-1} . Radial distances and symbols in figure; 190° transect: dot = 3 m, x = 4 m, diamond = 5 m, y = 10 m and 270° transect: cross = 3 m, square = 6 m and the triangle represents 15 m.

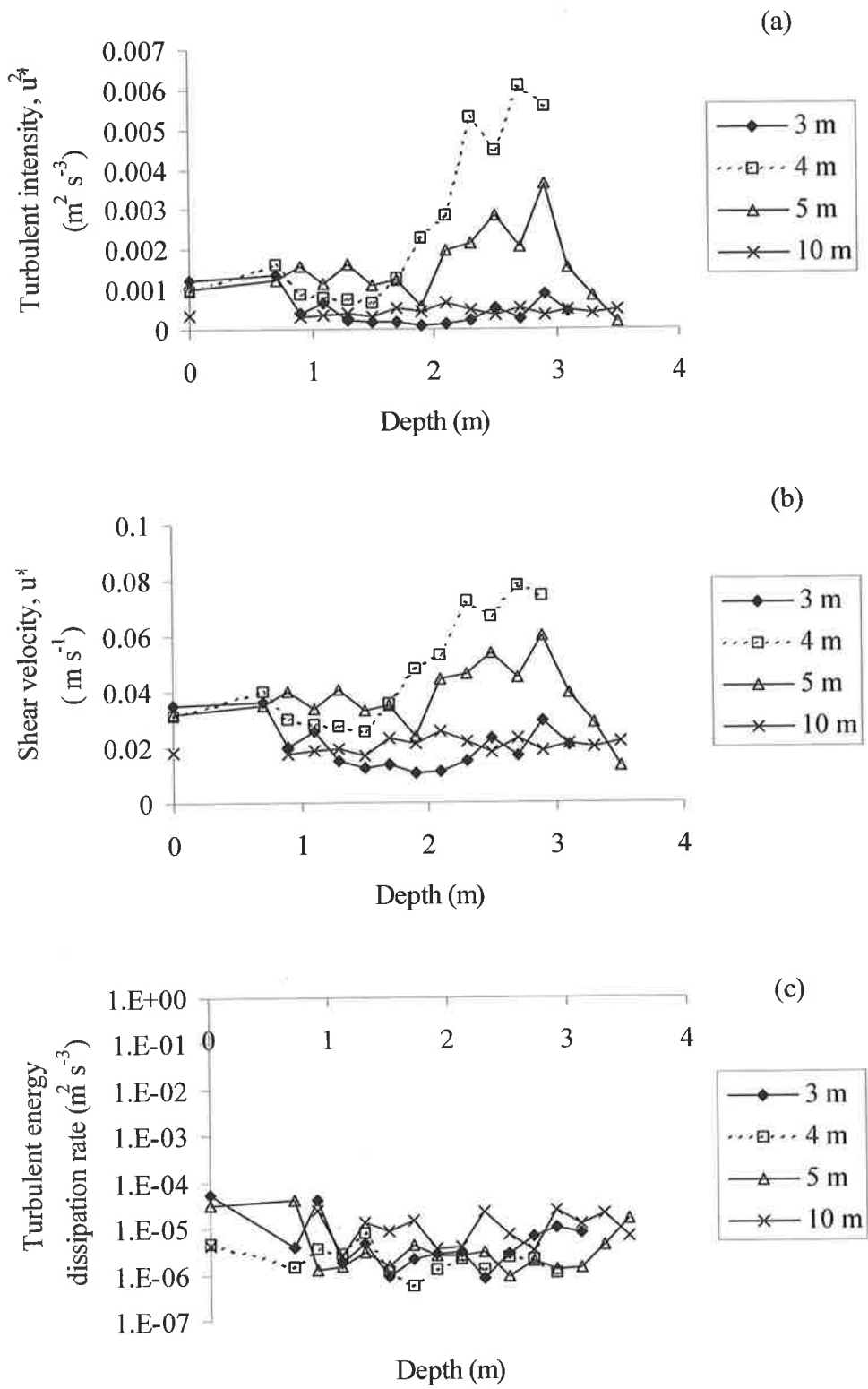


Figure 5.22 Calculations of turbulent intensity (a), shear velocity (b) and turbulent kinetic energy dissipation rates (c) along the 190° N transect of the submerged aspirator (SA) within the Torrens Lake.

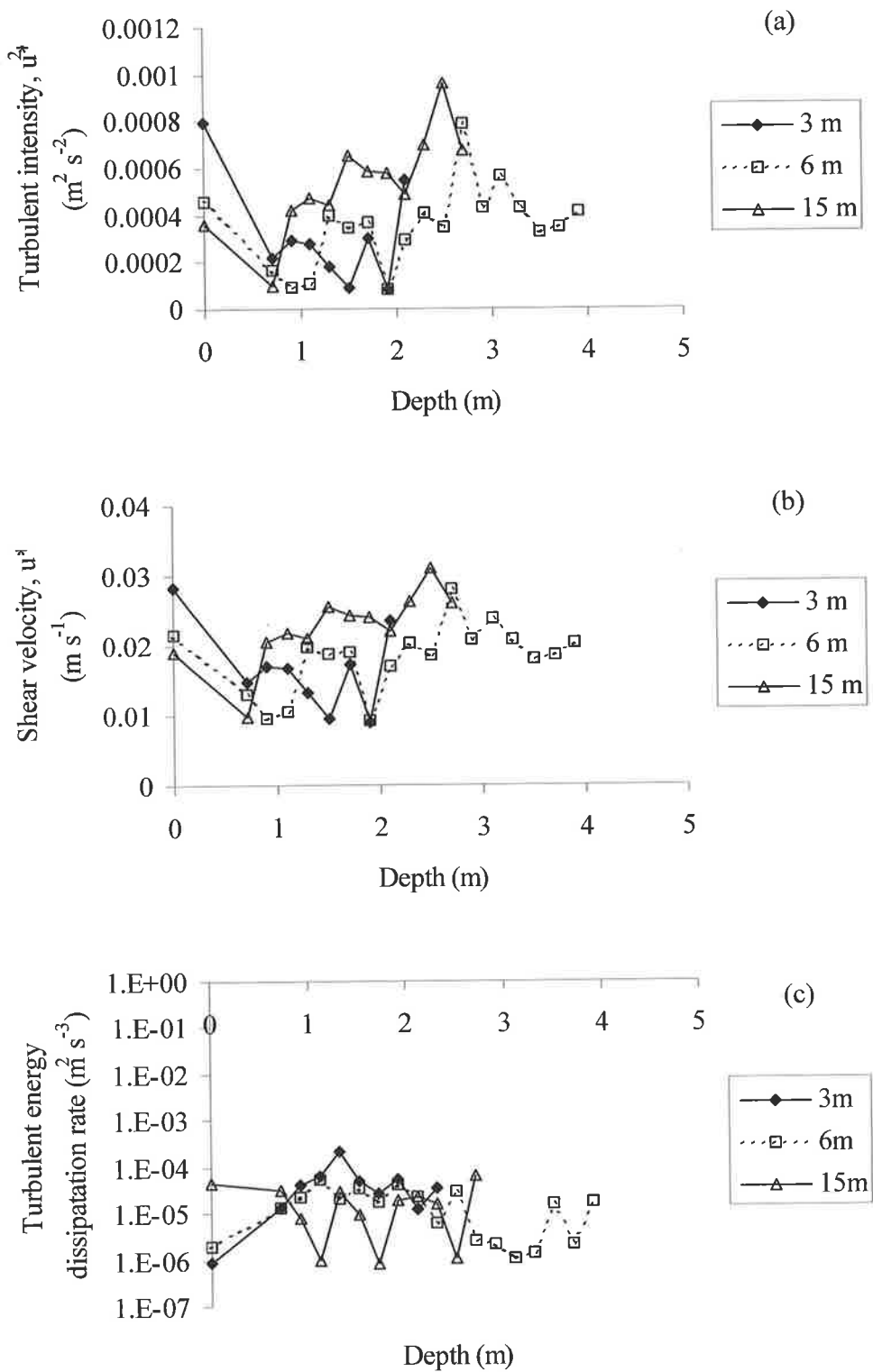


Figure 5.23 Calculations of turbulent intensity (a), shear velocity (b) and turbulent kinetic energy dissipation rates (c) along the 270° N transect of the submerged aspirator (SA) within the Torrens Lake.

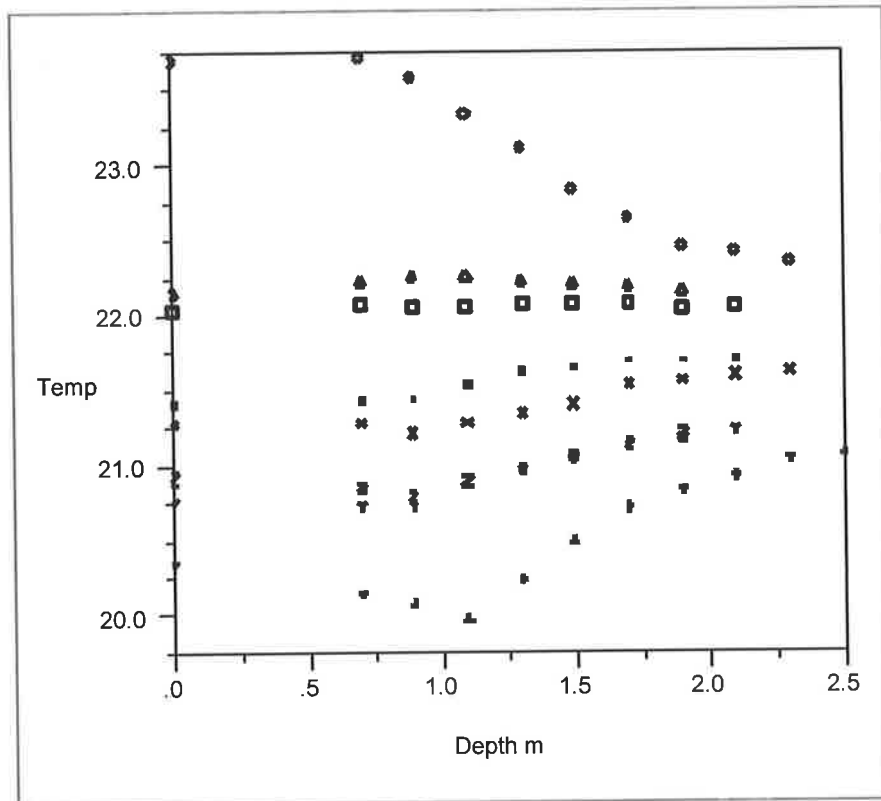


Figure 5.24 Temperature profiles recorded along two transects (150° and 270° North) at distances between 3 and 15 m from the aspirator. Radial distances and symbols in figure; 150° transect: cross = 4 m, z = 6 m, y = 5 m, y = 11, dot = 13 m and 270° transect: x = 6 m, diamond = 10 m, square = 12 m and the triangle represents 15 m.

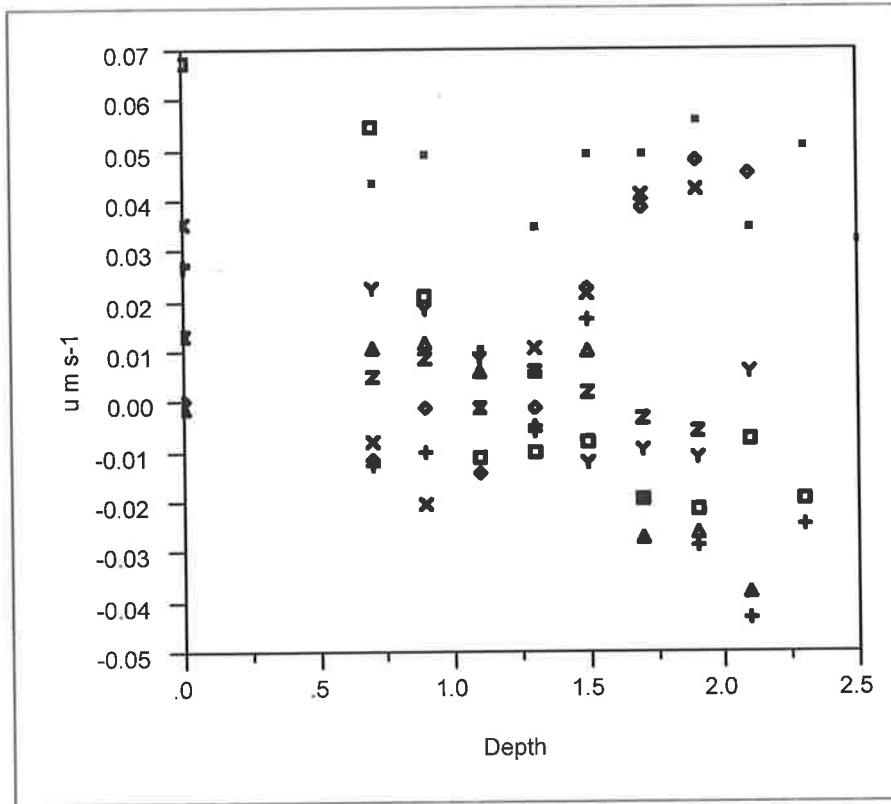


Figure 5.25 Radial velocity (u) profiles measured along two transects (150° and 270° North) at distances between 3 and 15 m from the high volume aerator. Velocities in the range $+0.01$ and -0.01 m s^{-1} are below the critical velocity as determined by u^* (wind generated turbulent intensity). Note all velocities are in m s^{-1} . Radial distances and symbols in figure; 150° transect: dot = 4 m, x = 6 m, diamond = 11 m, y = 13 m and 270° transect: cross = 6 m, square = 10 m, triangle = 12 m and z represents 15 m.

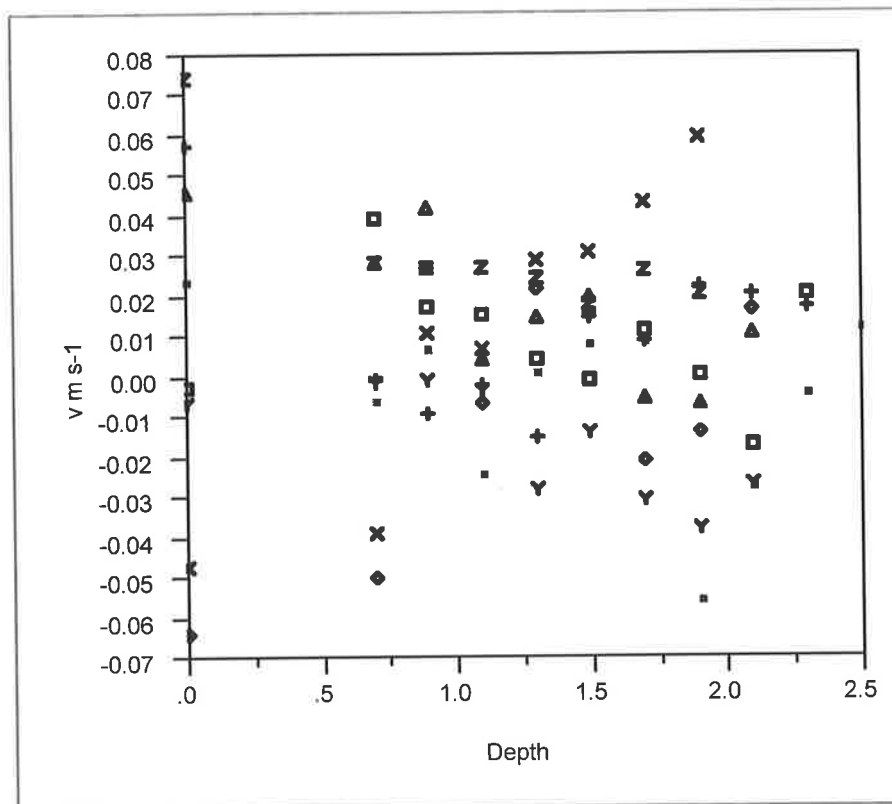


Figure 5.26 Vertical velocity (v) profiles measured along two transects (150° and 270° North) at distances between 3 and 15 m from the submerged aerator. Velocities in the range $+0.01$ and -0.01 m s^{-1} are below the critical velocity as determined by u^* (wind generated turbulent intensity). Note all velocities are in m s^{-1} . Radial distances and symbols in figure; 150° transect: dot = 4 m, x = 6 m, diamond = 11 m, y = 13 m and 270° transect: cross = 6 m, square = 10 m, triangle = 12 m and z represents 15 m.

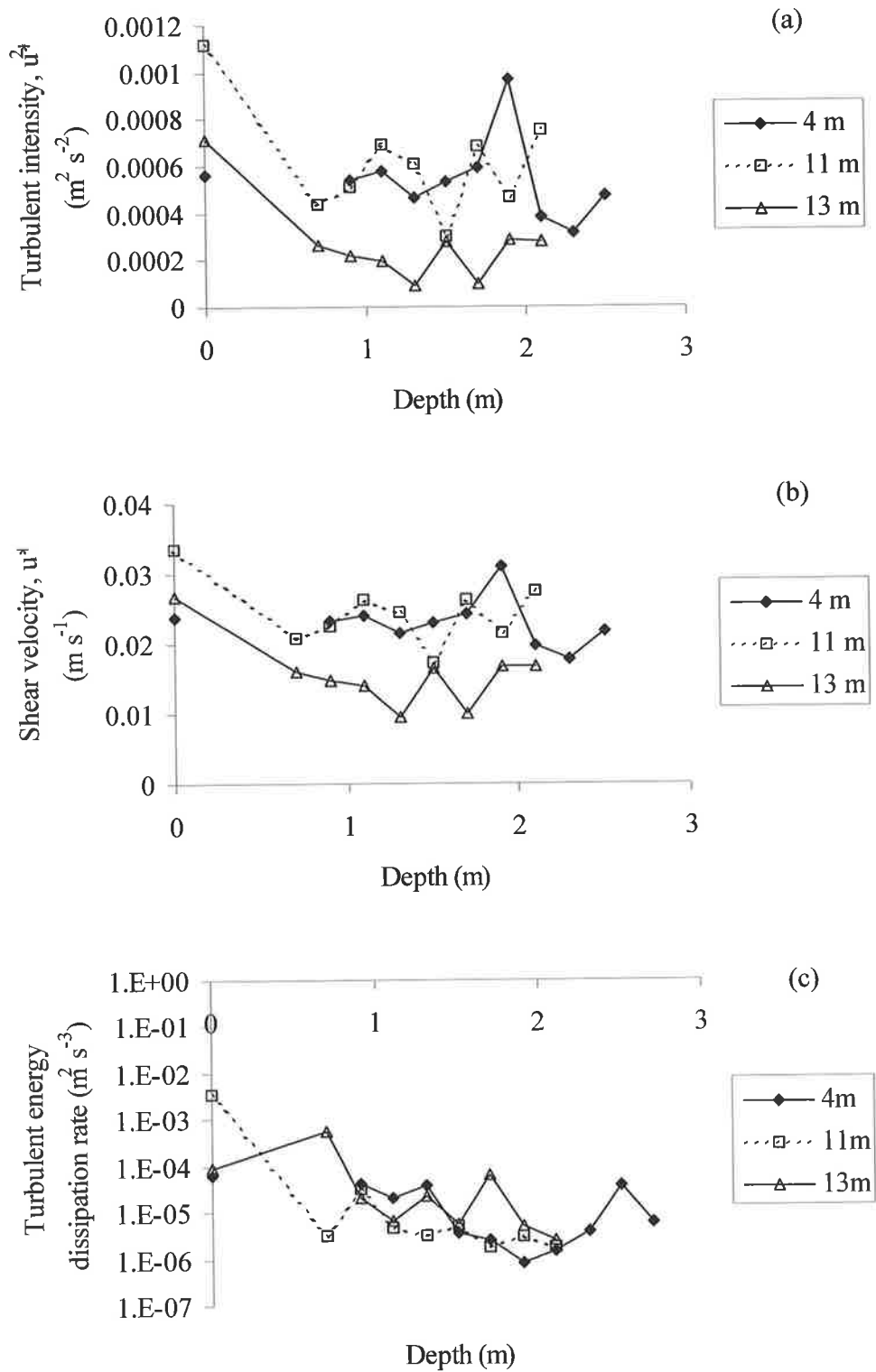


Figure 5.27 Calculations of turbulent intensity (a), shear velocity (b) and turbulent kinetic energy dissipation rates (c) along the 150° N transect of the high volume aerator (HVA) within the Torrens Lake.

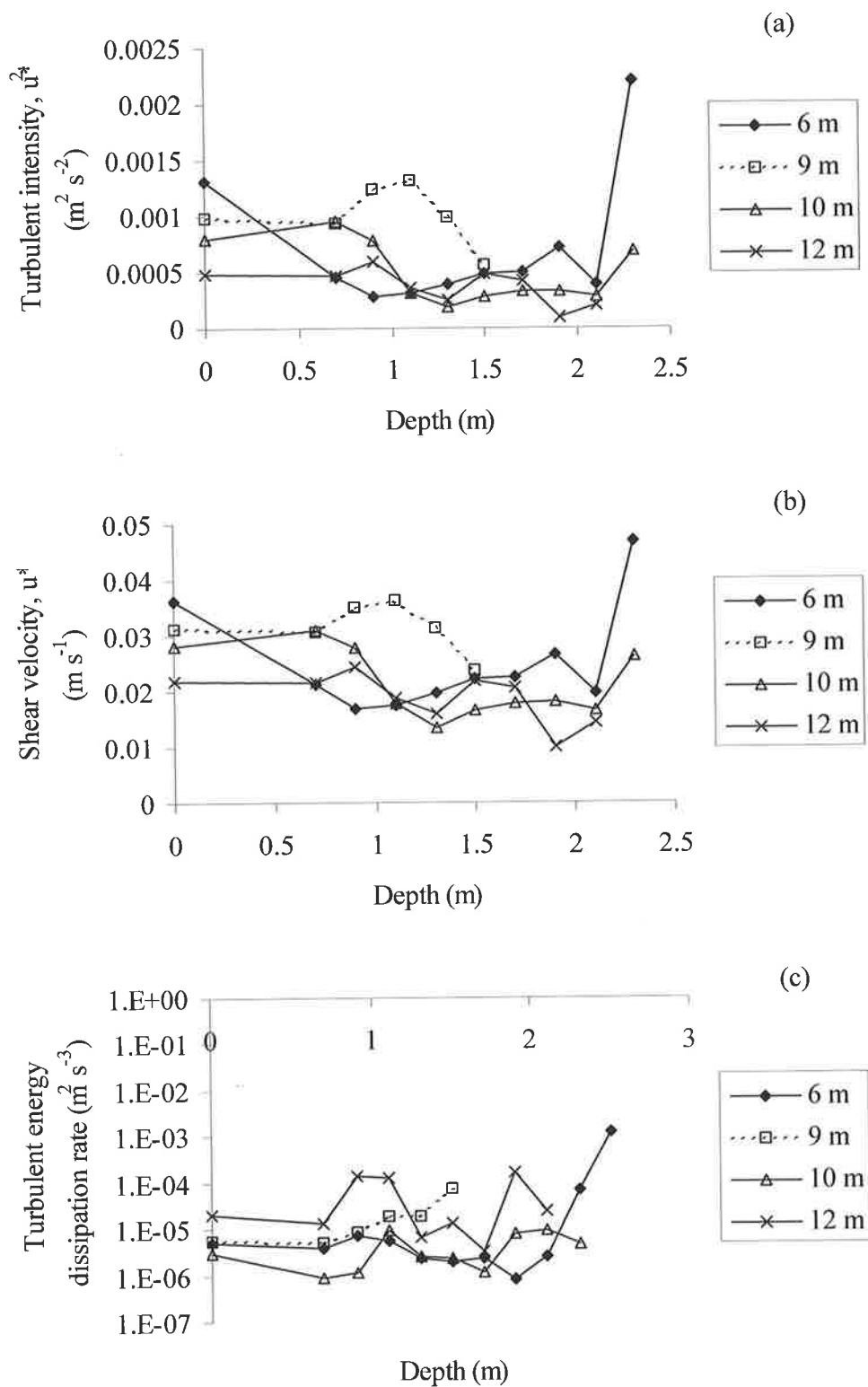


Figure 5.28 Calculations of turbulent intensity (a), shear velocity (b) and turbulent kinetic energy dissipation rates (c) along the 270° N transect of the high volume aerator (HVA) within the Torrens Lake.

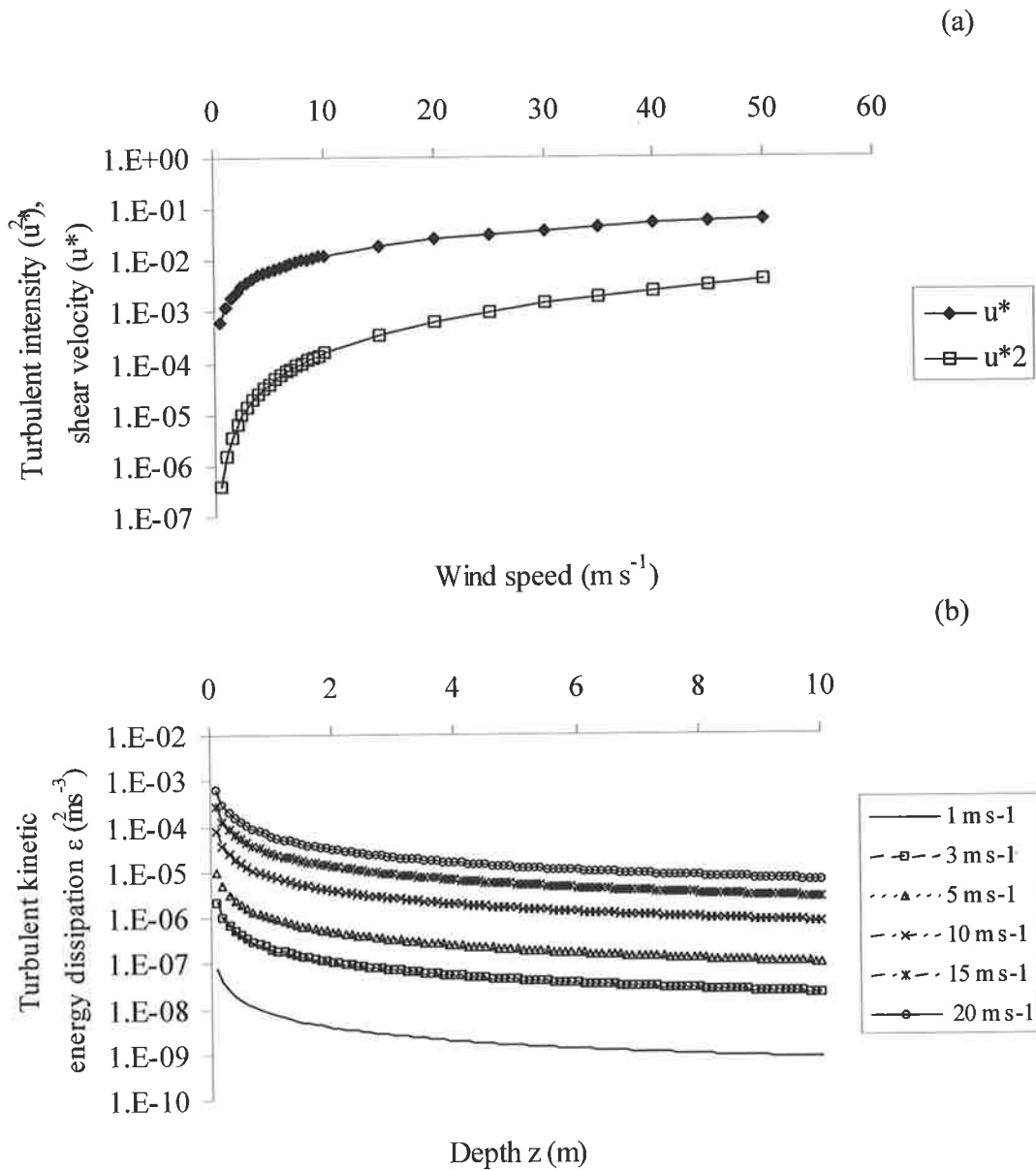


Figure 5.29 Influence of wind speed ($m s^{-1}$) on turbulent intensity, u^{*2} and shear velocity, u^* (a) and wind speed and depth, z (m) on turbulent kinetic energy dissipation rates, ϵ (b). Turbulent intensities and shear velocities were calculated using equation 6 and are in units $m^2 s^{-2}$ and $m s^{-1}$, respectively. Dissipation rates were calculated using equation 4 and expressed as $m^2 s^{-3}$.

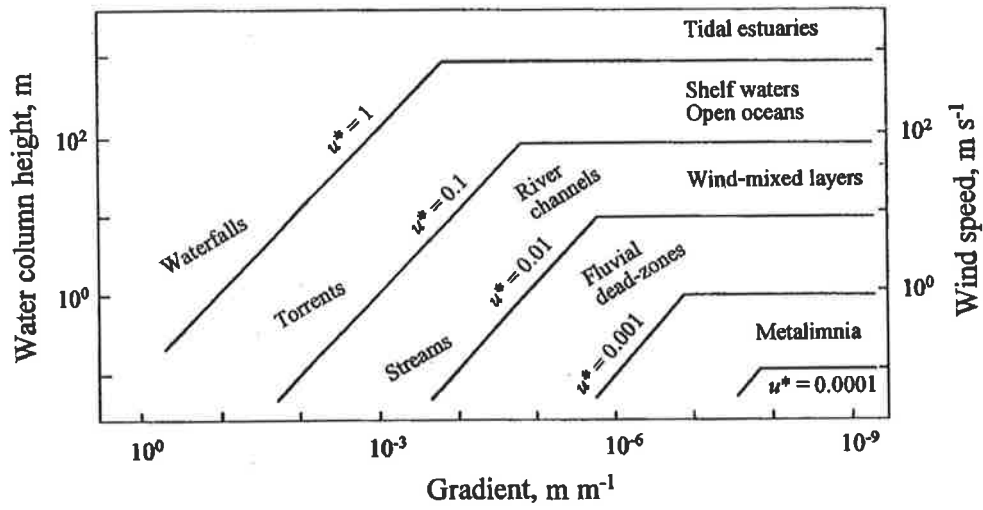


Figure 5.30 Distribution map of approximate shear velocity, u^* values with respect to bed gradient, water column height and wind speed on the water surface. After Reynolds, 1994a, figure 6.2b, page 153).

Regel, R.H., Brookes, J.D., Ganf, G.G., and Griffiths, R.W., (2004) The influence of experimentally generated turbulence on the Mash01 unicellular *Microcystis aeruginosa* strain.
Hydrobiologia, v. 517 (1), pp. 107-120.

NOTE:

This publication is included on pages 216-238 in the print copy of the thesis held in the University of Adelaide Library.

It is also available online to authorised users at:

<http://dx.doi.org/10.1023/B:HYDR.0000027341.08433.32>

Chapter 7

Spatial and temporal heterogeneity of phytoplankton in a shallow urban lake

7.1 Introduction

The unpredictability and diversity of phytoplankton community composition in lakes continues to intrigue plankton ecologists and water resource managers who attempt to describe and explain observed patterns. Phytoplankton communities are often characterized by numerous species whose abundances can change on time scales ranging from hours to weeks. The short time scale of cell generation, exposes phytoplankton to great environmental variability whereby physiological limits and pre-adaptations will determine which species will persist, which will prosper and which will decline (Reynolds 1997).

Changes in community composition are a function of autogenic (internal) and allogenic (external) selection processes (Reynolds, 1988c) whereby the primary driving factors are the attributes of individual species that enable them to gather light and nutrients, in a competitive habitat where the physical environment permits access to resources. The selectivity of phytoplankton is based upon their relative adaptations to either develop populations quickly in a 'bare' environment (*r* species traits) or to be specialized and develop populations more slowly under conditions with segregated resources (*K* species traits). Reynolds (1997) revised an earlier work (Reynolds 1988a) to classify phytoplankton on the basis of the classification developed for terrestrial plants (Grime, 1979) as invasive (C-species), acquisitive (S-species) or acclimating (R-species) strategists (figure 7.1). The classification defines phytoplankton as being primarily adapted to exploit undisturbed, resource replete habitats (C-species) or to survive resource depleted habitats (S-species) or to function in well mixed water bodies (R-species) with high frequency light fluctuations (Reynolds, 1997).

Phytoplankton succession considers that autogenic factors (e.g. relative uptake rates of nutrients, light harvesting capability) lead the community to equilibrium, whereby the water body is

initially colonized by small invasive r -C species whose rapid growth gradually diminishes resources and the population may become limited by light, nutrients or zooplankton grazing. The internal phytoplankton processes that modified the water body increase interspecific competition and select for specialized K -S, R species, which may dominate the community leading to the exclusion of earlier succession species (Reynolds, 1984; Reynolds 1993) and a decrease in diversity. The sequence is one of decreasing growth rates and increasing investment in resource gathering and metabolic conservation (Reynolds, 1997). However, in numerous water bodies' equilibrium is never reached due to external allogenic factors (the cardinal points of Round, 1971) disrupting and overriding the successional stage.

External disturbances such as episodes of wind mixing, floods, storms or processes associated with nutrient replenishment may delay, arrest or dismantle successional development (Reynolds, 1997). The altered conditions may provide opportunities for early successional species to grow again. For example, the alternation between turbulent mixing and stratification has been widely demonstrated to terminate and initiate autogenic phases in phytoplankton succession (Lewis 1978; Reynolds, 1980; Reynolds and Reynolds, 1985). Moreover, if the disturbance is of insufficient intensity and frequency to completely eliminate the existing community, species richness and diversity may increase, compromising species found in both early and late successional stages.

The intermediate disturbance hypothesis (IDH) was originally introduced by Connell (1978) to explain the high diversity in tropical rainforests and coral reefs and has also been accepted to reconcile equilibrium and non-equilibrium arguments to explain phytoplankton community patterns and diversity (Reynolds *et al.*, 1993). It states "disturbance events, when intermediate in intensity and frequency relative to community recovery rates, can increase species richness in mature communities by creating opportunities for colonization by early successional species that would otherwise be eliminated by competition". With little disturbance, competitive exclusion will reduce diversity (autogenic selection), whereas under high disturbance only a few specialized colonizer species will be able to survive the rapidly changing environment (allogenic selection). At intermediate disturbance a mixture of functional C-S-R species are present and diversity is maximal. An increase in phytoplankton species richness or diversity as a consequence of disturbance has been demonstrated in a number of field (Chorus and Schlag, 1993; Holzmann,

1993; Jacobsen and Simonsen, 1993; Sommer, 1993), laboratory (Grover, 1988; Sommer, 1995) and modeling studies (Elliot *et al.*, 2001).

In contrast to temperate stratified lakes (e.g. Reynolds, 1982) phytoplankton composition in small, shallow, urban lakes is highly unpredictable due to the vulnerability of the lake to disturbances associated with their surrounding catchment, hydraulic exchange and often their irregular shapes. As stated by Reynolds (1997) there is “very little about them which can be generalized”. Rainfall events during summer may constitute a major disturbance and via storm water runoff affect the phytoplankton community by flushing and diluting the population, re-introducing nutrients, re-suspending nutrients from sediments, or by increasing turbulence levels and depth of the mixed layer. In addition, light limitation even during large wind mixing events is less likely in shallow lakes due to the depth of light penetration resulting in large euphotic to mixed depth ratios. Furthermore, in Mediterranean climates major meteorological changes may occur irregularly but frequently over time spans of hours to days. These events often change the thermal structure of a water body from stratified to isothermal and *visa versa*. If meteorological changes coincide with a major rainfall, the effect may be so dramatic as to change the lake into a river within hours. Conversely, the resumption of calm weather will cause the river to switch back to a lake with no discharge.

The vulnerability to disturbance at a local scale suggests that allogenic factors are more influential compared to autogenic factors in governing species composition in small shallow lakes. At an intermediate frequency and intensity, the input of nutrients from storm water runoff can relax nutrient competition between species and increase the biomass of earlier successional or rare species leading to higher diversity (Barbiero *et al.*, 1999). In addition, the relative depth of the surface mixed layer to overall depth may contribute to increased diversity in shallow lakes. Since the highest sinking velocities of diatoms or C strategists are much lower than the turbulent shear velocities generated by a wind of 1 m s^{-1} , even the slightest wind will allow entrainment and circulation in the mixed layer (Reynolds, 1989). Consequently, motile S strategists and non-motile turbulent dependent C strategists may coexist in shallow lakes.

The Torrens Lake is a small, shallow, urban lake that meanders through a 3 km section of Adelaide and experiences a mediterranean climate. During summer it typically becomes thermally stratified although, due to its small size and large urban/semi rural catchment it quickly

receives storm water runoff turning into a flowing river. Physical and chemical conditions can rapidly change as a result of southerly cold fronts bringing rain and high wind speeds in summer, which occur on average 4 times each January (Australian Bureau Meteorology). Water quality is often compromised by brief summer rainfall events, which contribute nutrients and carbon via storm water and lead immediately to anoxia in the hypolimnion.

The lake provides an ideal study site to examine temporal and spatial phytoplankton community dynamics in relation to allogenic disturbances such as rainfall and associated nutrient inputs and wind mixing events and autogenic succession. The irregular longitudinal shape of the Torrens Lake adds an extra dimension to phytoplankton dynamics as it may create a number of smaller habitats within its reaches. The upstream section will generally receive storm water and nutrients first compared to down stream sites. However, downstream sites are generally deeper and more exposed to wind-induced mixing. With a rainfall and flushing event they may also receive populations of species, which have been washed down from upstream sites.

The first hypothesis of this study was that the greater the rate of hydraulic exchange, the more likely that the community will be dominated by invasive C-strategist species. Secondly, that allogenic processes will govern the phytoplankton community and autogenic succession will not proceed to equilibrium. Secondly, Lastly, upstream sites in close proximity to storm water drains will be dominated by invasive C-strategist species, while downstream sites will contain more specialized species such as S or R strategists. The objectives of this study were to: (1) assess the spatial variation in phytoplankton composition and lake conditions, (2) assess the temporal variations in phytoplankton composition during summer, (3) determine which allogenic factors (cardinal points) influence or act as a disturbance to the phytoplankton community, (4) determine whether or not the respective disturbances are consistent with the intermediate disturbance hypothesis.

7.2 Materials and methods

7.2.1 The Torrens Lake and study sites

The Torrens Lake (138° 35' 14.2" E 34° 55' 4.0" S) was created by the construction of a weir across the River Torrens. The lake is fed by the River Torrens, which drains the western Mount

Lofty Ranges via six creeks, and by storm water draining from the local urban catchment. During winter the lake resembles a river, however, water-harvesting strategies by South Australian Water means that the Kangaroo Creek Dam impounds the river 20 km upstream, and consequently in the absence of rain, summer flows are negligible. Below the weir, the Torrens River flows approximately 10 km to reach the Gulf of St Vincent. A flow monitoring station is located approximately 3 km downstream of the weir, at Holbrookes Road. A summary of the morphometry data is provided in table 7.1. During summer the Lake occupies and meanders through a 3 km section of Adelaide (figure 7.2). The upper section is typically narrow, shallow (<1 m) and sheltered by surrounding trees and high banks (figure 7.3a, b). The river broadens in the middle section (figure 7.3c) of the lake and is often in the lee of trees and buildings. In the lower section near the weir (figure 7.3d, e), the lake further broadens and deepens to 5.5 m and consequently is more exposed to wind mixing compared to the upper reaches.

Table 7.1 Morphometric data for the Torrens Lake

Surface area	0.15 km ²
Volume	478 ML
Mean depth	2.6 m
Maximum depth	5.5 m
Hydraulic retention	6 hours – 60 days
Lower Rural and urban catchment area	158.3 km ²
Upper rural/watershed to Kangaroo Creek Reservoir	336.5 km ²
Discharge to St Vincent Gulf	40,000 ML annum ⁻¹

Fourteen sites were chosen along the lake from the Hackney Street Bridge (site A₁) to the weir (site L) for the phytoplankton-monitoring program (figure 7.2). The sites were approximately 100-200 m apart and were chosen based upon their contrasting orientation and morphometry, proximity to storm water drains and aerators. In the year 2000, three bubble plume aerators consisting of approximately 100 m long perforated pipe connected to mobile diesel air-compressors were located in close proximity to sites E, I and L. As reported in chapter 5, flow velocity profiling was conducted around the site E bubble plume aerator and although the water column was relatively well mixed in the aerator's immediate vicinity, the zone of influence was considered small and limited (<15 m).

7.2.2 Monitoring Program

Monitoring of phytoplankton composition, water clarity, chlorophyll *a* concentration, nutrient concentrations and dissolved oxygen profiles of the water column were undertaken between the 12th of January and the 9th of May 2001. Initially sampling was undertaken at all 14 sites. However, later in the program between 5 and 14 sites were sampled due to time and cost constraints. The five sites sampled consistently were A₂, D, E, H and L.

Integrated samples of phytoplankton, chlorophyll and nutrient concentrations were collected over the entire water column using a plastic conduit pipe. Chlorophyll *a* concentration was initially expressed as $\mu\text{g L}^{-1}$, but interpolated to mg m^{-2} to enable site comparisons. Phytoplankton identification and cell counts were determined using a Sedgwick-Rafter chamber and a Zeiss microscope following preservation in Lugol's iodine.

Phytoplankton richness was determined from the number of taxa (*s*) while diversity (H'') was calculated using the Shannon-Weaver function incorporating phytoplankton biovolumes (Pielou, 1975):

$$H'' = -\sum b_i/B \log_2 (b_i/B) \quad (1)$$

where *B* is the total biovolume, b_i is the biomass of the *i*th of *s* taxa present. The more genera that are present, the greater the diversity until:

$$H''_{\max} = \log_2 s \quad (2)$$

Phytoplankton community change was determined using the summed difference index (SD) proposed by Lewis (1978):

$$SD = \sum_i \{ |[b_i(t_1)/B(t_1)] - [b_i(t_2)/B(t_2)]| \} / (t_2 - t_1) \quad (3)$$

where $b_i(t_1)$ is the abundance of the *i*th taxa, and *B*(*t*) the community size at time *t*. Abundance was expressed as the number of cells mL^{-1} .

Chlorophyll *a* was determined following 24 h extraction in ethanol. Nutrient (TKN, NH₄, NO_x, TP, FRP) analyses were performed by the Australian Water Quality Centre according to NATA approved standards. During sampling for the above, profiles of water temperature/ dissolved oxygen and water clarity (light attenuation) were taken using a Hydrolab CTD and a LICOR underwater quantum sensor (LI 192SA), respectively. All light attenuation coefficient regressions were based upon \ln .

Monitoring of physical variables was undertaken at a meteorological station deployed near the weir (site L). Wind velocity and direction (Climatronics WM-111) measured 2 m above the surface, down welling short wave radiation (300 - 3000 nm, Middleton EP08) and upwelling and down welling long wave radiation (3 - 60 μm , Middleton CN1 - R) were measured and logged every 10 minutes. Temperature was recorded every 2 minutes by 20 thermistors spanning the 5.5-m water column (Betatherm, resolution ± 0.01 °C).

Temperature was also recorded upstream near sites B and C (figure 7.2) at 5 depths (0.1, 0.3, 0.5, 1 and 1.8 m) using suspended Optic Stowaway thermistors (resolution ± 0.1 °C). Temperature profiles were used to derive an index of the degree of mixing, the surface mixed layer depth (SML). The SML was defined as the shallowest depth (m) at which the difference between two adjacent thermistors was ≥ 0.1 °C.

7.2.3 Statistical analysis

NMS ordination (Sorensen, Bray-Curtis) was used to evaluate relationships between allogenic factors and phytoplankton composition. User supplied seed = 123 and r^2 value was set to 0.3 and the stress factor < 20 . In the ordination, physical and chemical data were categorized as follows:

- a) FRP limitation? Yes (allocated 0 if concentration < 0.01 mg L⁻¹), No (allocated 1 if concentration ≥ 0.01 mg L⁻¹)
- b) NO_x limitation? Yes (allocated 0 if concentration < 0.1 mg L⁻¹), No (allocated 1 if concentration ≥ 0.1 mg L⁻¹).
- c) Water column stability? Allocated 0 if lake was isothermal, allocated 1 if lake was diurnally stratified, allocated 2 if lake was persistently stratified. The

- ordination included the dominant lake status for the single date (stability1), for the past 5 days (stability5) and for the past 7 days (stability7).
- d) Persistent parent thermocline? Yes (allocated 1), No (allocated 0).
 - e) Average surface mixed layer water temperature after midday? For single day (SML1), approximate average over past 5 days (SML5), approximate average over past 7 days (SML7).
 - f) Euphotic/ mixed depth ratio (Z_{eu}/Z_{mix})? If <1 (allocated 0), if ≥ 1 (allocated 1).
 - g) Light attenuation coefficient, K_d

Due to the constraints associated with instrumentation and measurement of physical parameters (i.e. temperature) a number of assumptions were made. Temperature data from site B was extrapolated to sites A₂, D and E, while data from site L was extrapolated to site H.

7.3 Results

7.3.1 Torrens Lake limnological characteristics

7.3.1.1 Hydrological and meteorological conditions

There were several large rainfall events during the sampling program, which resulted in discharge of water from the lake (figure 7.4). A rain event of approximately 15 mm is enough to replace 2/3 of the volume of the lake. Large rain events occurred on the 26 January (19.6 mm), 12 February (8.6 mm), 16 March (13.8 mm), 20 March (15.6 mm), 7 April (11.2 mm) and 22 April (5 mm). Rainfall events that resulted in the highest daily discharge at Holbrookes Road occurred on 16 March, 20 March and 7 April. The elevated discharge in May is due to the drawing down of water levels in the Kangaroo Reservoir in the upper Torrens catchment.

Within the Torrens Lake, summer rainfall events are associated with the replenishment of nutrients, decreases in dissolved oxygen as a result of bacterial respiration of organic carbon, decreased water temperatures leading to isothermal conditions and the dilution and or washout of phytoplankton populations. The impact of rainfall is initially more significant at the upper sites of the lake (A₁ to F) where First Creek and several drains enter.

A summary of meteorological data measured at the weir is shown in figures 7.5a, b and c. Daily average air temperature was generally above 20 °C for January and February but tended to decrease in Autumn (March-May) (figure 7.5a). Daily average wind velocity was generally between 1 and 4 m s⁻¹ while maximum velocities reached up to 7 m s⁻¹ on several occasions (figure 7.5b). There were prolonged periods when wind velocity was <2 m s⁻¹ including the 17-29 January, 6-13 February, 23 February–3 March, 13-21 March, 4-19 April, 23-28 April and in early May. Daily average and maximum instantaneous surface irradiance (short wave radiation) was high but punctuated by several decreases associated with summer rain events and cloud cover (figure 7.5c). It is also evident that as Summer transgressed into Autumn the day length shortened and surface irradiance tended to decrease.

7.3.1.2 Water column stability

During the monitoring program, water column stability changed significantly from persistent stratification to isothermal conditions, and was a function of cool weather changes, air temperature, wind velocity and rainfall. Water temperature profiles for sites L (weir) and B are shown in figures 7.6 and 7.7, respectively. Daily average surface mixed layers (SML) for site L is shown in figure 7.8. For the majority of January, the lake was persistently thermally stratified, except for a brief period (14 January) when wind velocities reached 10 m s⁻¹ and decreased the SML to 3.0 m. The storm event on January 26 generated fully mixed conditions into February. In February, high temperatures and low wind velocities resulted in another period of persistent stratification until a cool change and rainfall on 12 February. Rainfall temporally resulted in isothermal conditions at sites B and L (figures 7.6 and 7.7). For the remainder of February, the lake underwent diel stratification as a result of wind induced mixing in the afternoons and cooler air temperatures. A persistent parent thermocline was evident at site B from mid February to early March (figure 7.). Water temperatures fell in March as a result of rainfall and lower air temperatures. Despite low water temperatures, the SML varied between 0.5 and 3 m. In April, stratification was predominantly diurnal at sites B (figure 7.7) and L (figure 7.6) and the SML depth was generally below 1 m at the weir (figure 7.8). Late April and early May were characterized by calm weather with low average wind velocities, although the low water temperatures (~ 17 °C) resulted in a deep SML of 2.5 m at site L.

7.3.1.3 Nutrients

Nutrient concentration within the Torrens Lake was a function of phytoplankton growth and storm water runoff. However, it should be noted that internal nutrient recycling may also have contributed to pelagic concentrations but was not explored in this study. Filterable reactive phosphate and inorganic nitrogen are considered to be available to phytoplankton and are assumed to be limiting when concentrations fall below 0.01 mg L^{-1} and 0.1 mg L^{-1} , respectively for either, on average for the entire growing season or absolutely for half the growing season (Sas, 1989; Oliver and Ganf, 2000). Figure 7.9a and b show respective integrated total phosphorus (TP) and filterable reactive phosphate (FRP) concentrations, for sites A₂, E, H and L during the monitoring period. At site A₂, phosphorus is limiting until rainfall in mid March when concentrations reach 0.035 mg L^{-1} and remain just above limiting concentrations for the remainder of the study period. In contrast at sites E-L, FRP concentrations increased above limiting levels in early February as a result of rainfall on January 26 and consequent storm water runoff. However, in late February and in early March there was phosphorus limitation throughout the lake. Rainfall in mid March increased concentrations at site E, but not sites H and L. Towards the end of the monitoring period concentrations tended towards limitation levels.

Total Kjeldahl nitrogen (TKN (organic nitrogen and ammonia) and inorganic nitrogen (NO_x) (nitrate and nitrite) concentrations are shown in figures 7.10a and b, respectively. In contrast to FRP, NO_x is not limiting at site A₂ over the study period (figure 7.10b). However, there were two sharp decreases in concentration in early and mid February as a result of phytoplankton growth. Conversely, there were two large increases one after rainfall on the 12 February and the second late in the sampling period. At sites E, H and L, nitrogen was limiting in January and early February. Rainfall on the 12th of February temporally replenished nitrogen above limiting concentrations. However, between late February and early March nitrogen decreased to limiting levels. Rainfall in mid March increased concentrations to levels measured at site A₂ (approximately 0.6 mg L^{-1}). There was no nitrogen limitation within the lake for the remainder of the sampling period.

7.3.1.4 Dissolved oxygen

Dissolved oxygen (DO) concentration was continuously logged at site L (figure 7.11). DO concentrations at 0.5 and 4.5 m depth varied extensively as a result of rainfall events, bacterial respiration, stratification, mixing and phytoplankton growth. Inflows from rainfall resulted in a decrease in DO on most occasions. Anoxic conditions occurred post rain events on the 27 January, 17 March, 8 April, 23 April and 2 May. DO varied spatially within the lake, the lowest concentrations were generally measured at downstream sites, while supersaturating (11-13 mg L⁻¹) concentrations were recorded at upstream sites due to phytoplankton photosynthesis.

7.3.1.5 Water clarity

Water clarity as represented by light attenuation coefficient (K_d) varied temporally and spatially and was dependent upon chlorophyll concentrations and rainfall events (figure 7.12a). Values ranged from 0.84 m⁻¹ to approximately 6 m⁻¹ at sites A₂ and B, respectively. Light attenuation was generally high with high chlorophyll concentrations and consequently tended to increase at upstream sites. On 12 January above site C, K_d approximated 6 m⁻¹ and decreased to 1.9 m⁻¹ at site L. However, after rainfall on the 26 January and subsequent washout, K_d measurements on the 2 and 8 February ranged between 1-2 m⁻¹ across all sites. This pattern of increase with chlorophyll and decrease with rainfall was repeated during the sampling period (figure 7.12a).

The euphotic depth (Z_{eu}), which is defined as the depth to which 1% of sub-surface irradiance penetrates (Talling, 1971) is shown in figure 7.12b. The euphotic depth ranged from 0.77 m at sites A₂ and B to 5.45 m at site L.

7.3.1.6 Ratio of euphotic to mixed depth

The ratio of the euphotic depth to mixed depth (Z_{eu}/Z_{mix}) is an indicator of the proportion of time a phytoplankter suspended within the Z_{mix} would spend in light and the ratio varied extensively from 0.49 to 8 (figure 7.12c). Based upon the depth of the lake, light penetration and the minimum Z_{eu}/Z_{mix} ratio of 0.49 it is unlikely that phytoplankton would be light limited at any site.

7.3.2 General description of phytoplankton

7.3.2.1 Chlorophyll *a* concentration

Chlorophyll *a* concentration varied spatially and temporally within the Torrens Lake and ranged from 28 to 917 mg m⁻² (figure 7.13a). In early January, phytoplankton chlorophyll *a* was high at sites B, D and E, compared to sites A₂, H and L. Rainfall events such as on the 26 January, 12 February and 16 March generally decreased chlorophyll *a* by diluting and flushing phytoplankton downstream. For example, the 26 January rain event (19.6 mm) caused 130 ML or about 30 % of the lake to be discharged and if phytoplankton concentration is considered to be higher in the surface layer, this accounts for the large decrease from 700 to 100 mg of Chl *a* m⁻² (sites, A₂, D, E, H, L). However, chlorophyll *a* sharply increased at all sites after the 26 January rain event. Small increases in chlorophyll were also evident after the 12 of February rain event at all sites except L. After mid February phytoplankton chlorophyll *a* decreased. The lowest chlorophyll *a* concentrations were measured post the 16 March rain event.

7.3.2.2 Cell volume

Total cell volume concentrations (figure 7.13b) of phytoplankton at selected sites within the Torrens Lake ranged from 1.43 x 10⁴ to 1.83 x 10⁸ μm³ mL⁻¹. A comparison of figures 7.13a and b indicates that chlorophyll *a* and cell volume followed a similar pattern throughout the study period. Rainfall events on the 26 January, 12 February and 16 March decreased volumes by a factor of 100, 10 and 100, respectively, for most sites.

7.3.2.3 Phytoplankton species composition

Phytoplankton composition consisted of 31 genera from six divisions, which varied both spatially and temporally within the Torrens Lake. Table 7.2 summarises the recorded genera, conditions and sites in which they prevailed and their C-S-R functional classification according to Reynolds (1997). Cluster analysis was used to determine which sites within the Torrens Lake could be grouped together on the basis of phytoplankton composition and any indicator species (Table 7.3). Numbers in parentheses are the p values for the indicator species. Generally upstream sites were grouped together with *Chlamydomonas* often calculated as an indicator species, while sites

in the middle section of the lake varied in their grouping and indicator species. *Microcystis* was often a significant indicator of site groupings downstream towards site L. Sites, A₂, B, D, E, H and L were considered representative of the Torrens Lake.

Cyanobacteria were recorded at all sites and three contrasting genera (*Microcystis*, *Anabaena*, *Planktothrix*) reached high concentrations. Minor genera included *Chroococcus* and *Aphanizomenon*. At site A₂ there were few significant recordings of cyanobacteria, except for a peak of *Microcystis*, *Anabaena* and *Planktothrix* coexisting in early March before rainfall (figure 7.14). This peak doubled in magnitude and was extended for a further 2 weeks at site B, regardless of rainfall (figure 7.15a). At downstream sites, three phases of cyanobacteria domination were evident (figures 7.16a – 7.19a). After the January 26 rain event, *Microcystis* biomass was high for 2 weeks, which was then overshadowed by the R-strategist, *Planktothrix* in mid February and *Anabaena* in late February-early March. Cell concentrations decreased after rainfall on 16 March.

Cyclotella was the dominant diatom across all sites, while other genera included *Gyrosigma*, *Amphora* and *Aulocoseira*. At site A₂, *Cyclotella* was present over the entire study period and was a significant indicator species on 2 and 8 of February (figure 7.14b). Interestingly, *Cyclotella* coexisted with the dinoflagellates, *Peridinium* and *Glenodinium* in January during a period of strong stratification. *Cyclotella* concentrations decreased on two occasions, temporally in early February and for approximately 1 week in mid March as a result of washout. *Amphora* and *Gyrosigma* increased above detectable levels after the 26 January and 16 March rain events, respectively. Unlike at other sites, *Aulocoseira* was not recorded at site A₂. At sites B, D and E, *Cyclotella* approximated 1000 cells mL⁻¹, except temporally after the January 26 and March 16 rain events (figure 7.15b, 7.16b, 7.17b). Diatom diversity was highest at site E with 5 genera (*Gyrosigma*, *Navicula*, *Asterionella*, *Cyclotella* and *Aulocoseira*), probably because of bubble plume aeration. At sites H and L, *Cyclotella* was not affected by washout and dilution as a result of rainfall (figure 7.18b, 7.19b). However, *Aulocoseira* was recorded at higher concentrations compared to upstream sites.

Peridinium was the dominant dinoflagellate recorded and tended to dominate in January and early February, consistent with periods of stratification (figures 7.14c – 7.19c). *Glenodinium* and *Ceratium* were recorded on several occasions but only reached detectable levels. *Euglena* and

Trachelomonas were the only Euglenoids recorded. *Trachelomonas* was a rare genus whereas *Euglena* reached relatively high numbers (100-1000 cells mL⁻¹) on several occasions at different sites (figures 7.14c – 7.19c). At site B, it increased immediately after rainfall (12 February) but at other sites such as H, it decreased in biomass after rainfall (12 February). *Cryptomonas* was a common genus reaching relatively high concentrations after rainfall (figures 7.14c – 7.19c). At site A₂, it was recorded in mid February and early April whereas sites B-L it was recorded only in early April (figures 7.14c, 7.15c).

Genera from Chlorophyceae comprised a small total biovolume and concentration compared to other division. However, it was the most diverse division with 13 different genera recorded. *Chlamydomonas* was the dominant genus at upstream sites (figure 7.14e, 7.15e), and there were several subdominant genera, which occurred temporally at other sites. At site A₂, the *Chlamydomonas* bloom reached 10,000 cells mL⁻¹ and persisted through early rain events until decreasing in mid March (figure 7.14e). At site B, the bloom was smaller and was diluted by the 26 January and 12 February rain events (figure 7.15e). At sites D and E, the bloom was restricted to a 2-week period in mid-February (figures 7.16e, 7.17e). In contrast to upstream sites, *Chlamydomonas* did not exceed 100 cells mL⁻¹ at sites H and L (figures 7.18e, 7.19e).

The subdominant chlorophytes varied spatially and temporally. *Scenedesmus* biomass exceeded 100 cells mL⁻¹ at site A₂ in early April, at sites B and in D in mid-January and late March and at sites E and H in early-mid March. In contrast at site L, rainfall in mid-March did not terminate the *Scenedesmus* bloom (figure 7.19d). At sites B and L, *Coelastrum* reached 1000 cells mL⁻¹ in early February, but remained at detectable levels at all other sites. *Chlorella* reached 1000 cells mL⁻¹ at sites D and E in January, and after rainfall in mid-March at site E. The only other genera which exceeded detectable level was *Eudorina* at site L in early March (figure 7.19e). Rare genera recorded at most sites included: *Actinastrum*, *Ankistrodesmus*, *Oocystis*, *Crucigena*, *Gonium*, *Pediastrum*, *Botryococcus*, *Dictyosphaerium* and *Sphaerocystis* (figures 7.14d, e – 7.19d, e).

Table 7.2 Summary of all recorded genera within the Torrens Lake during sampling 12 Jan–9 May 2001. Genera were assigned a C-S-R classification after Reynolds (1997)-figure 39, page 170.

Genera	Lake conditions	Volume (μm^3)	C-S-R
Cyanophyceae			
<i>Anabaena circinalis/crassa</i>	Dominant, post rain, strong stratification, persisted longer downstream.	160.9	C-S
<i>Chroococcus</i> sp.	Rare but appeared as above, absent at A ₂	1000	
<i>Microcystis aeruginosa/flos aquae</i>	Dominant after 26 January rainfall but before <i>Anabaena</i>	113.1	S
<i>Planktothrix mougeotti</i>	Dominant between <i>Microcystis</i> & <i>Anabaena</i> blooms with intermittent stratification & increased wind mixing	49.1	R
<i>Aphanizomenon</i> sp.	Rare, recorded only at site B	32.1	C-S
Bacillariophyceae			
<i>Cyclotella</i> sp.	Dominant at all sites, highest cell numbers during increased wind mixing/ diurnal stratification	392.7	C-R
<i>Aulocoseira</i> sp.	Rare, recorded at sites B-L, bloomed briefly in mid January during wind mixing	392	R
<i>Asterionella</i> sp.	Rare, only recorded site E	2006.7	
<i>Gyrosigma</i> sp.	Rare, only recorded post rain events at D-L		
<i>Navicula</i> sp.	Rare, only recorded E & L	200	
<i>Amphora</i> sp.	Rare, recorded at all sites post rain events		
Dinophyceae			
<i>Peridinium cinctum</i>	Common at all sites during stratification, high concentration at site A ₂ compared to downstream		S
<i>Glenodinium</i> sp.	Rare, recorded at most sites, small bloom in mid-Jan during stratification at A ₂		S
<i>Ceratium</i> sp.	Rare, recorded only at deeper sites H & L		S
Euglenophyceae			
<i>Euglena</i> sp.	Common, recorded at all sites, increased post-rain	5890.5	
<i>Trachelomonas</i> spp.	Rare, recorded at all sites except L for a brief period in late February with intermittent deep mixing		
Cryptophyceae			
<i>Cryptomonas</i> sp.		1039.5	C-S-R
Chlorophyceae			
<i>Chlorella</i> sp.	Common at all sites, high concentration at site E with strong stratification	14.1	C
<i>Oocystis</i> sp.	Rare but recorded at all sites	268.1	C
<i>Scenedesmus</i> sp.	Recorded at all sites, high concentration in mid-late March with strong stratification	21.3	C-R
<i>Crucigena</i> sp.	Rare, recorded at all sites	113.1	
<i>Coelastrum</i> sp.	Rare, recorded post rain events	21205.8	C
<i>Actinastrum</i> sp.	Rare, recorded post rain events	39.3	C
<i>Ankistrodesmus</i> sp.	Rare, recorded pre/post rain events & +/- stratification	12.1	R
<i>Botryococcus</i> sp.	Rare, recorded at all sites	250	C
<i>Dictyosphaerium</i> sp.	Rare, recorded only at B	38.8	
<i>Chlamydomonas</i> sp.	Dominant, recorded at all sites, high concentration upstream Jan-Mar, concentration was site dependent	100.5	C
<i>Sphaerocystis</i> sp.	Rare, recorded only at L	268.1	
<i>Gonium</i> sp.	Rare, recorded at all sites	523.6	S
<i>Eudorina</i> sp.	Rare, recorded at all sites, high concentration at site L in early March post-rain + intermittent stratification		S
<i>Pediastrum</i> sp.	Rare, recorded between B-L	628.3	

Table 7.3 Torrens Lake site groupings (Gr) based on phytoplankton composition for each sampling date, using cluster analysis. Species represent 'indicator' species when $p < 0.05$.

Date	Gr	mrpp value	Gr 1 (p value)	Gr 2	Gr 3	Gr 4	Gr 5	Gr 6
12-Jan	3	6.095×10^{-5}	A ₁ , A ₂ <i>Chl</i> (0.014) <i>Eugl</i> (0.004)	B, C, D, E, F, H, I <i>Eud</i> (0.023)	I, J, K, L <i>Cycl</i> (0.006) <i>Mel</i> (0.003) <i>Cer</i> (0.005)			
2-Feb	6	4.314×10^{-5}	A ₁ , A ₂ , C <i>Cyc</i> (0.009) <i>Per</i> (0.007)	I, J, L <i>Mic</i> (0.005) <i>Cru</i> (0.014)	A ₃ , B	D, E, H	G	K
6-Feb	4	2.238×10^{-3}	A ₁ , A ₂ <i>Chl</i> (0.034)	A ₃ , F, L <i>Mic</i> (0.005) <i>Mel</i> (0.034) <i>Atk</i> (0.034)	E, G, I	B		
8-Feb	5	1.412×10^{-5}	A ₁ , A ₂ <i>Chl</i> (0.031) <i>Cyc</i> (0.012)	H, I, J, K, L <i>Mic</i> (0.001) <i>Atk</i> (0.007)	A ₃ , C <i>Ooc</i> (0.008)	E, F, G	B	
12-Feb	2	7.167×10^{-3}	B, D, E, F	H, I, J, L <i>Mic</i> (0.03)				
14-Feb	3	2.5×10^{-2}	D, E <i>Chl</i> (0.04)	F, H, I, J, L <i>Mic</i> (0.04)	C			
16-Feb	4	8.109×10^{-5}	A ₂ , C, D, E <i>Chl</i> (0.004)	F, G, H, I, J, K, L <i>Mic</i> (0.002) <i>Ped</i> ($p=0.02$)	A ₃ , B	A ₁		
19-Feb	2		C, D, E, F, H, I	L				
23-Feb	3	1.81×10^{-3}	A ₁ , A ₂ , B <i>Chl</i> (0.005) <i>Glen</i> (0.042) <i>Act</i> (0.013)	G, H, I, J, L <i>Mic</i> (0.001) <i>Mel</i> (0.015) <i>Pla</i> (0.001) <i>Ooc</i> (0.002)	A ₃ , C, D, E, F <i>Cyc</i> (0.02)			
27-Feb	3		C, D, F, H, I, K, L	E	J			
2-Mar	2	1.236×10^{-3}	A ₁ , A ₂ <i>Chl</i> (0.009)	A ₃ , B, C, D, E, F, G, H, I, J, K, L <i>Pla</i> (0.009)				
9-Mar	4	5.22×10^{-4}	A ₁ <i>Chl</i> (0.009)	A ₂ , A ₃ , C, D, E, F, J <i>Pla</i> (0.048) <i>Cyc</i> (0.025)	G, H, K, L <i>Sc</i> (0.05)	I		
15-Mar	3	5.81×10^{-3}	A ₁ , A ₂ <i>Gyr</i> (0.034)	B, E, F, H, I, J, L <i>Ana</i> (0.034) <i>Sc</i> (0.034) <i>Cry</i> (0.034) <i>Pla</i> (0.034)	D			
17-Mar	4	7.75×10^{-3}	A ₁ , A ₂ , D	E, H <i>Amp</i> (0.043)	K, L			
20-Mar	3	1.46×10^{-2}	B, E, F, H <i>Amp</i> (0.043)	I, J, L <i>Ana</i> (0.046) <i>Sc</i> (0.046)	D			
22-Mar	3		A ₂	D, E, H	L			
3-Apr	3		A ₂	E, H, L	B			
2-May	3		A ₂	E, H, L	D			
9-May	3		A ₂ , D	E, H	L			

Note: *Chl* = *Chlamydomonas*, *Eud* = *Eudorina*, *Cyc* = *Cyclotella*, *Mel* = *Aulocoseira*, *Cer* = *Ceratium*, *Per* = *Peridinium*, *Mic* = *Microcystis*, *Cru* = *Crucigena*, *Act* = *Actinastrum*, *Ooc* = *Oocystis*, *Ped* = *Pediastrum*, *Pla* = *Planktothrix*, *Gle* = *Glenodinium*, *Sc* = *Scenedesmus*, *Gyr* = *Gyrosigma*, *Ana* = *Anabaena*, *Amp* = *Amphora*.

7.3.3 Phytoplankton richness and diversity

Phytoplankton richness (number of genera) varied between 2 and 17 genera and was dependent on site and the extent of flushing due to rainfall (figure 7.20). In contrast to chlorophyll *a* measurements (figure 7.13a), richness often increased going downstream. Pre-rainfall (26 January), richness varied between 6 and 9 genera on the 12 and 19 of January. However, post rainfall (26 January), species richness was more variable ranging between 4 and 12 genera, suggesting both the loss and promotion of species. At sites A₂, B, D, E, H and L there were 8, 4, 12, 7, 7 and 10 genera, respectively (February 2). Species richness generally continued to increase on the 6 February. However, on the 12 of February (post rainfall) the number of genera counted decreased at all sites. Although, two days later richness again increased which continued to increase or remain high (> 6) until rainfall on the 16 of March. The number of genera dramatically decreased at site A₂, but interestingly not at site B. At site L, the number of genera decreased from 14 to 8. Although, another rain event on March 20, suppressed species richness at all sites except for site L, where it is likely that upstream flushing caused an increase in richness downstream. Richness on the 3 April ranged between 6 and 13 and was highest at site B. Sampling in May revealed variation in the number of genera between sites with a richness range of 4 to 12 genera.

Phytoplankton diversity as determined by the Shannon Weaver index varied between 0.15 and 3 for all sampling sites (figure 7.20b). At upstream A₂ and B sites, the index generally remained below 1.5 except for maximums in early March where it climbed to 2.1 units and 3 units for sites A₂ and B, respectively. Diversity generally remained higher at site D, ranging between 0.3 and 2.2 units, but was dependent upon rainfall. For the 26 January and 12 February rain events, diversity tended to increase prior to rainfall, decrease immediately after it and later recover to maximum levels (~7-14 days). However, after the 16 March rain event, diversity remained between 0.5 and 1.0 units. Diversity tended to increase downstream at sites E, H and L where values generally remained above 0.5 units for all sampling dates. Furthermore, a similar pattern to site D, of increase, decrease and recovery in diversity was evident with rainfall events.

7.3.4 Phytoplankton community change

It is clear that the composition of the phytoplankton community changed during the study period. The changes were not always consistent nor of the same magnitude across all sites. The summed difference index (SD) was used to measure the rate of community change across sites (figure 7.21). Rates of change less than 0.1 d^{-1} defined stable periods in the phytoplankton community while rates exceeding 0.1 d^{-1} indicate periods of significant change (Reynolds, 1980). Values of SD ranged from 0.01 to 0.89 d^{-1} and varied between sites. At site A₂, the phytoplankton community underwent intermittent periods of stability and change (figure 7.21a). The community was stable in early January, most of February and from late March to the end of the study period. While significant change occurred firstly in early February (1 week after rainfall) with the growth of *Peridinium*, *Cryptomonas*, *Euglena* (figure 7.14c) and chlorophytes (figure 7.14d, e) and secondly in early to mid-March with the growth of cyanobacteria (figure 17a) and *Trachelomonas* (figure 7.14c). In contrast, at sites B (figure 7.21b) and D (figure 7.21c) the phytoplankton communities underwent continuous significant change ($\text{SD} > 0.1 \text{ d}^{-1}$), as a result of numerous genera increasing and decreasing (figures 7.15, 7.16). However, it should be noted that at site D, SD did fall below 0.1 d^{-1} in early May, probably as a result of a long interval between sampling.

At site E, the phytoplankton community underwent continual change (figure 7.21d) except briefly in late February before *Anabaena* growth (figure 7.17a), on 4 March before *Scenedesmus* growth (figure 7.17d) and after April when there were no major changes in phytoplankton growth. At downstream sites (figure 7.21e, f), intermittent stability/ change was evident. At site H in early February, the community was stable ($\text{SD} < 0.1 \text{ d}^{-1}$) until *Microcystis* (figure 7.18a), *Euglena* (figure 7.18c) and *Cryptomonas* (figure 7.18c) concentrations decreased shortly after rainfall. However, for the remainder of February the community significantly changed as a result of increases in *Microcystis*, *Planktothrix* and *Anabaena* (figure 7.18a). Temporarily (2 March), the community remained stable until excessive *Scenedesmus* growth was recorded (figure 7.18d). For the remainder of March and April, the community underwent continual significant change as a result of decreases in cyanobacteria and sporadic increases in *Cryptomonas*, *Trachelomonas* and chlorophytes after rainfall (March 16).

At site L, the phytoplankton community went through the most periods of intermittent change and stability (figure 7.21f). There were 5 periods of dramatic change and stability. Until early February, numerous genera such as *Microcystis*, *Aulocoseira*, *Scenedesmus* and other chlorophytes were increasing in biomass, regardless of rainfall (26 January) and consequently $SD < 0.1 \text{ d}^{-1}$. The populations then reached maximum concentrations and the community remained relatively stable for approximately 10 days until 23 February, despite small decreases in chlorophyte concentrations. Excessive *Planktothrix* growth around 23 February and is likely to have caused SD to exceed 0.1 d^{-1} and when growth reached a plateau, SD temporarily fell below 0.1 d^{-1} (27 February). In early March, the community again underwent significant change as a result of large increases in *Anabaena*, *Scenedesmus* and *Eudorina* (figure 7.19a, d) and a decrease in *Cyclotella* concentrations (figure 7.19b). As these populations stabilized, SD fell below 0.1 d^{-1} . It is likely that rainfall on the 16 March led to a decrease in *Anabaena* and *Eudorina*, while *Cyclotella* increased, causing the community to change significantly. The community remained stable for a few days before *Cryptomonas* bloomed in early April and SD exceeded 0.1 d^{-1} .

7.3.5 Sample date groupings – identification of major change in phytoplankton

Cluster analysis was used to identify periods of major change in phytoplankton composition for 6 sites (figure 7.22). At site A₂, 5 different groups of sampling days were identified (figure 7.22a). The first group consisted of sampling days in January and February and 2 March, irrespective of rainfall and associated conditions on 26 January and 12 February. The indicator species for this group were the C-strategists, *Cyclotella* ($p = 0.016$) and *Chlamydomonas* ($p = 0.005$). However, sampling on 9 March was classified as a different group, as a result of decreases in *Cyclotella* and increases in cyanobacteria. 15 and 22 March were grouped together irrespective of rainfall on 16 March, suggesting that this rainfall event had little impact on phytoplankton composition. The phytoplankton community on 3 April was classified as another group as a result of increases in *Cyclotella*, *Scenedesmus* and *Cryptomonas*. The 2 and 9 May were the final grouping probably as a result of decreases in phytoplankton biomass in all genera except, *Planktothrix*.

Unlike at site A₂, disturbance affected the composition of phytoplankton at site B. Six groups were identified amongst sampling days (figure 7.22b). Interestingly, January 12 and 19 did not group together. Instead, 19 January was grouped with 12 February, 20 March and 3 April and

Cyclotella was the indicator species of this group ($p = 0.001$). The common factor among this grouping was that these days were prior to a disturbance such as rainfall. February 2 and 6 grouped together and the indicator genus was *Coelastrum* ($p = 0.033$). This suggests that rainfall triggered the growth of the usually rare genus *Coelastrum*. Conversely, February 8 and 16 grouped together irrespective of rainfall on the 12 of February. The indicator genus for this grouping was *Euglena* ($p = 0.015$). However, the 23 February was grouped separately, probably due to a reduction in *Euglena* concentration. The 2, 9 and 15 of March were grouped separately due to significant increases in *Anabaena* ($p = 0.011$) and *Planktothrix* ($p = 0.006$) compared to other sampling days. Interestingly, these genera coexisted approximately 14 days after rainfall and when physical conditions changed from moderate mixing to stratification.

At site D, the sampling days were divided into 6 groups (figure 7.22c). The 12 January and 2 of February were grouped independently as a result of low concentrations of either common or rare genera. The third group consisted of 19 January, 8, 12, 19 and 23 February and 20 March. *Cyclotella* was consistently high on these days (figure 7.16b) and was therefore an indicator genus ($p = 0.022$). However, sampling days 14 and 16 of February were grouped separately due to excessive growth of *Chlamydomonas* ($p = 0.021$). Similarly to site B, *Anabaena* ($p = 0.018$) and *Planktothrix* ($p = 0.001$) were indicator genera on sampling days 27 February, 2, 9 and 15 March. The final group (17, 22 March, 2, 9 May) was differentiated by the growth of the rare genera, *Amphora* (figure 7.16b).

At site E, the grouping of sampling days was highlighted by numerous indicator genera and six groups were identified (figure 7.22d). Similarly to site D, sampling days 12 January and 2 February were independent groups and were distinct due to low phytoplankton concentrations and no significant indicator genera. In contrast, sampling days during the month of February were grouped together in combination with 19 January. This period was highlighted by significant *Cyclotella* growth ($p = 0.04$) and high *Microcystis* growth ($p = 0.059$). This suggests that rainfall on 26 January and 12 February had no impact on *Cyclotella* growth, but nutrient input probably contributed to *Microcystis* growth. Additional nutrient input in combination with periods of mixing and stratification may have been responsible for increases in the abundance and concentrations of rare species and concentrations of cyanobacteria. Consequently, the 2, 9 and 15 March sampling days were grouped together and were represented by numerous indicator genera; *Anabaena* ($p = 0.016$), *Planktothrix* ($p = 0.002$), *Chlorella* ($p = 0.002$), *Crucigena* ($p = 0.002$),

Botryococcus ($p = 0.004$) and *Ankistrodesmus* ($p = 0.005$). These genera represent C-S-R strategists and imply that this phase was highlighted by coexistence and high diversity as would be generated by disturbances or a combination of disturbances (nutrient input, mixing, stratification) at an intermediate frequency. The latter half of March (17 and 22) grouped separately probably as mixing increased and selected for turbulent dependent species, resulting in significant increases in *Aulocoseira* ($p = 0.037$), *Gyrosigma* ($p = 0.025$) and *Amphora* ($p = 0.043$) compared to other sampling days. The final grouping included 20 March, 2 and 9 May and reflected days of lower phytoplankton concentrations.

At site H, 6 groups were identified during the sampling program based on phytoplankton composition (figure 7.22e). Similarly to sites D and E, sampling on 12 January and 2 February were grouped independently as a result of low phytoplankton concentrations and no dominant genera. However, the third group consisted of sampling days from throughout the period (19 January, 23, 27 February, 2, 20 March, 3 April, 2, 9 May). The fourth group consisted 8, 12, 14, 16 February and *Cyclotella* ($p = 0.019$) and *Microcystis* ($p = 0.01$) were significant indicator genera. This indicates that the 12 February rain event did not affect phytoplankton composition at this site; however, the increased growth of both these genera is probably related to increased in nutrient concentrations. In contrast, the phytoplankton composition changed in March as a direct result of rainfall on March 16. Prior to rainfall, the sampling days 9 and 15 of March were grouped together and the indicator genus was *Anabaena* ($p = 0.022$). Unlike at other sites, *Planktothrix* was not a significant indicator genus ($p = 0.057$). The phytoplankton composition post rain (17, 22 March) was represented by significant but temporary increases in *Aulocoseira* ($p = 0.05$), *Gyrosigma* ($p = 0.02$) and *Amphora* ($p = 0.02$).

Five groups were identified in the sampling program at site L (figure 7.22f). Unlike at upstream sites, the 12 and 19 of January were grouped together and were highlighted by temporary increases in *Aulocoseira* ($p = 0.004$) and *Euglena* ($p = 0.024$). Post rainfall, the phytoplankton community from early to mid February changed and *Microcystis* became dominant ($p = 0.001$), irrespective of rainfall on 12 February. However, in the latter half of February until early March, *Planktothrix* was dominant in the phytoplankton community ($p = 0.007$). Interestingly, this group also contained the sampling days 3 April and 2 May. The fourth group (9, 15, 20, 22 March, 9 May) highlighted the transition in cyanobacterial dominance to *Anabaena* ($p = 0.001$). *Scenedesmus* was also a significant indicator ($p = 0.032$).

7.3.6 Relationship between phytoplankton composition, sampling dates and major environmental changes

NMS ordination was used to evaluate relationships between allogenic factors and phytoplankton composition. At site A₂, ordination showed that phytoplankton were aligned to high water temperatures over the previous 1, 5 and 7 days, the presence of a persistent parent thermocline and a stable water column for the previous 1, 5 and 7 days (figure 7.23). Conversely, the phytoplankters were not correlated with FRP above the critical threshold concentration. Interpretation of phytoplankton dynamics and environmental factors affecting composition were limited at site B due to initial failure of thermistors and lack of nutrient data (sampling only carried out on the 12 January, 2 and 8 February). Although, ordination showed that cyanobacteria were more closely aligned with an increase in Z_{eu}/Z_{mix} , whereas *Euglena*, *Chlorella*, *Oocystis*, *Eudorina*, *Gonium*, *Glenodinium* and *Peridinium* were more aligned to the presence of a persistent parent thermocline and higher surface mixed layer water temperatures on the day of sampling (figure 7.23).

At site D, ordination showed that surface mixed layer temperature, water column stability, the presence of a persistent parent thermocline and NO_x status were important in determining phytoplankton composition (figure 7.23). Numerous species (*Chlamydomonas*, *Euglena*, *Cryptomonas*, *Microcystis*, *Chlorella*) aligned with conditions associated with thermal stratification (high water temperatures, stability, parent thermocline). Whereas rare species, such as, *Coelastrum*, *Trachelomonas* and *Amphora* aligned with conditions of sufficient NO_x. At site E, phytoplankton dynamics followed a similar pattern of phytoplankton at site D. Ordination showed that important allogenic factors were NO_x status, water column stability, surface mixed layer temperature and the presence of a persistent parent thermocline (figure 7.23). The species most strongly aligned to conditions associated with thermal stratification were *Euglena*, *Oocystis*, *Navicula* and *Microcystis*, while *Trachelomonas* aligned with conditions of sufficient NO_x.

At site H, ordination showed that surface mixed layer temperature at the time of sampling and over the past 7 days, light attenuation and FRP status were important factors determining phytoplankton composition (figure 7.23). The species, which aligned with conditions of sufficient FRP and high water temperatures and relative light attenuation, were *Euglena*, *Oocystis*, and *Actinastrum*. At site L, ordination revealed that surface layer temperature, FRP status and the

Z_{eu}/Z_{mix} ratio were important factors determining phytoplankton composition (figure 7.23). Species, which aligned with high water temperatures, sufficient FRP and high Z_{eu}/Z_{mix} ratios, were *Cryptomonas*, *Chroococcus*, *Coelastrum*, *Navicula* and *Microcystis*.

7.4 Discussion

Phytoplankton composition within the Torrens Lake was highly variable both temporally and spatially. The summed difference index and cluster analysis of sampling dates enabled the identification of periods of major change in phytoplankton composition and provided a starting point to evaluate the major allogenic influences. Temporally, the variability was a function of changes in meteorological conditions, predominantly rainfall that impacted upon storm water runoff into the lake. Spatially, the variability can be attributed to the contrasting morphometry of the sampling sites (e.g. depth, exposure) and passive horizontal transport associated with storm water runoff. In contrast to autogenic succession, it was clear that physio-chemical data and sample date groupings alluded to allogenic factors disturbing and governing community composition. Although there is a plethora of factors that influence and interact to define community structure, storm water runoff played a major role by diluting populations, replenishing nutrient supplies or decreasing water temperature and physical stability. However, due to the irregular shape of the lake (consistent with a river), the impact of the storm water runoff was not consistent at all sites, creating spatial heterogeneity within the community.

7.4.1 Allogenic factors

At the beginning of the sampling program, phosphorus and/ or nitrogen were at limiting concentrations within the Torrens Lake. However on several occasions, cold southerly fronts generated increased wind mixing in the lake and rainfall within its catchment. These events were discrete and short-lived but significant as indicated by perturbations in physio-chemical data. The large rainfall events produced storm water runoff, which quickly entered the lake and generally replenished nutrients. A comparison of chlorophyll data with discharge data reveals that storm water diluted and flushed phytoplankton downstream of the lake. Interestingly, nutrient replenishment was not homogenous throughout all of the sampling sites due to the locations of drains and catchment characteristics. For example the 26 January rain event did not increase

nutrients at site A₂, but did at site B (150 m downstream). Moreover, the composition of storm water, in terms of nitrogen and phosphorus, varied with rainfall events. For example, the 12 February rain event did not increase FRP, but increased NO_x at site A₂. In contrast, the 16 March rain event increased FRP, but not NO_x. This suggests that not all storm events will replenish the necessary plant nutrients, which in turn will depend upon where rainfall has fallen in the catchment (and land use) and the frequency of rainfall events. The influence of storm water runoff on sediment re-suspension and internal nutrient recycling was not evident. However, it is likely that internal nutrient recycling particularly under anoxic conditions contributed to pelagic concentrations (e.g. site L).

White and Pickett (1985) defined a disturbance event as 'any discrete event in time that disrupts ecosystem, community or population structure and changes resources, substrate availability or the physical environment'. Consequently, both the flushing and diluting of phytoplankton and the replenishment of nutrients acted as disturbances within the Torrens Lake. An additional effect of storm water runoff was the cooling of water temperatures and increasing the opportunity for wind mixing to break down thermal stability as was observed in the vertical thermal structure at site L. In a hierarchical context, Chorus and Schlag (1993) reported that physical stability followed by nutrients was the most important disturbance governing phytoplankton dynamics in two Berlin lakes. In contrast, the Torrens Lake is both shallow and nutrient limited in summer, which infers that nutrient replenishment is more important to phytoplankton dynamics than wind-induced mixing or artificial mixing. It is likely that if the Torrens Lake were eutrophic, the main effect of summer rain events would be to dilute phytoplankton populations.

It should be noted that the potential influence of artificial mixing by the three bubble plume aerators on phytoplankton composition was investigated using cluster analysis (Sorensen- Bray Curtis). For each sampling date, comparisons were made between the phytoplankton composition of sites in the immediate vicinity of the aerators (i.e. E, I, L) and those, which were further away, classified as 'non-aerated' (A₁, A₂, B, C, D, F, H, J). Aeration was found to have no significant affect on phytoplankton composition for all sampling dates ($p > 0.05$).

7.4.2 Phytoplankton composition and diversity

Seasonal phytoplankton dynamics in rivers is relatively poorly studied (Kohler, 1993), although according to Reynolds (1994b) some genera are relatively consistent among rivers such as *Cyclotella*, *Navicula*, *Ankistrodesmus*, *Chlorella*, *Crucigena*, *Scenedesmus*, *Pediastrum*, Cryptomonads, *Oscillatoria*, *Aphanizomenon* and *Microcystis* (Sabater and Munoz, 1990; Kohler, 1993). These taxa were also recorded within the Torrens Lake covering species with C-S-R strategies and generally their occurrence was consistent with their adaptive strategies, although periods of coexistence indicated the rapid change in conditions. According to Reynolds (1994b), the majority of species recorded in this study are consistent for numerous rivers whereby few species maintain dominance. The dominant C-strategists were *Chlamydomonas* and *Cyclotella*. *Chlamydomonas* is typically invasive (Reynolds, 1997), and its presence indicates that nutrient resources are sufficient for rapid population growth, and that there has been a recent disturbance. Large increases in concentrations were observed at upstream sites (A₂, B, D) after rainfall events (12 February), but their duration and intensity tended to decrease going downstream. The excessive growth of *Chlamydomonas* at upstream sites confirms the first hypothesis that this site is more suitable to C-strategists. At downstream sites, *Chlamydomonas* co-existed with other species such as *Cyclotella*, *Peridinium*, *Euglena* and *Cryptomonas*. *Cyclotella* was the most common genus and was evident across all sites and during the entire sampling program. Its abundance was probably related to the shallowness of the lake, which may have reduced sedimentation losses usually associated with stratification. Conversely, at site L, which was located at the deepest section of the lake, *Cyclotella* was far less prevalent which may be attributable to sedimentation during periods of strong stratification. Similarly, *Aulocoseira* was rare and only appeared at site L with a period of brief wind mixing in mid January. Other C-strategists observed included *Scenedesmus* and *Chlorella* but rarely did these genera exceed detectable limits probably due to competition with *Chlamydomonas* and *Cyclotella*. However, *Scenedesmus* and *Chlorella* did reach higher numbers briefly at site H in early March, and site B in early February for each species, respectively.

A number of S-strategists were observed during the study including *Peridinium*, *Ceratium*, *Anabaena*, *Microcystis*, and *Eudorina*. *Peridinium* was the dominant dinoflagellate and tended to occur during periods of stratification and lower nutrient concentrations. However, the genus was

often abruptly eradicated with the onset of wind mixing and or flushing associated with rainfall. As discussed in chapters 3 and 6, this genus is shear sensitive and turbulent sensitive species often decrease quickly from the phytoplankton community (Chorus and Schlag, 1993).

Microcystis was prevalent at all sites and its growth tended to be triggered by the replenishment of nutrients associated with storm water runoff and periods of diel stratification with afternoon wind mixing. *Microcystis* is well adapted to shallow lakes undergoing diel stratification such as Lake George (Ganf, 1974) due to its low energy requirements, and its ability to regulate its position after mixing has ended (Reynolds, 1989). The duration of its dominance tended to increase in the middle section of the lake (sites, D, E, H) compared to upstream sites, where it was competing with *Chlamydomonas*. However, although it coexisted with other cyanophytes, the onset of NO_x limitation led to a succession moving from *Microcystis* towards the heterocystous cyanobacteria, *Planktothrix* and *Anabaena*. *Planktothrix* dominance, as expected as a R-strategist, coincided with periods of intense wind mixing. The succession in eutrophic lakes has been reported to move from *Anabaena* to *Aphanizomenon* to *Microcystis* (Reynolds, 1971), which is in contrast to the Torrens Lake whereby *Microcystis* occurred before *Anabaena*, and *Aphanizomenon* was rare. Interestingly at site L in February, *Anabaena* a late successional species coexisted with *Scenedesmus*, an early successional species.

Cryptomonas and *Euglena* both responded to increased nutrient concentrations but high concentrations were often short lived due to either competition with other species or changes in physical conditions including flushing.

Phytoplankton richness and diversity was highly variable both temporally and spatially. On numerous occasions C-S-R strategists coexisted, suggesting that the community was governed by both allogenic succession with intermittent periods of autogenic succession. For instance, the change in cyanobacterial dominance from *Microcystis* to *Planktothrix* to *Anabaena* with increasing N-limitation represented succession. Richness and diversity tended to increase going downstream where the sampling sites were more variable and accommodating to more species.

7.4.3 Effect of disturbances on phytoplankton

The interaction of disturbance and phytoplankton composition is complex and depends on numerous factors such as the intensity and frequency of events, trophic status of the water body (Edson and Jones, 1988; Holzmann, 1993; Jacobsen and Simonsen, 1993; Reynolds, 1993; Padisak, 1993) and the stage of phytoplankton succession (early or late). As demonstrated by ordination, changes in phytoplankton composition cannot be attributed to a single factor but rather a combination of factors, each interacting such as storm water runoff leading to increased nutrients and cooler water temperatures.

The summer storm disturbances affected the phytoplankton community in a number of ways. Chlorophyll *a* and biovolume measurements demonstrated the immediate impact of storm water runoff was to cause dilution and displacement of the general phytoplankton community. Numerous species decreased in cell number such as: *Chlamydomonas* and *Anabaena* at site A₂ (after 16 March rainfall), *Chlorella*, *Peridinium* and *Euglena* at site B (after 26 January rainfall), *Cyclotella* at site D (after 26 January rainfall) and *Coelastrum* at site E (after 16 March rainfall). Although site dependent, on several occasions species such as *Cyclotella* (e.g. sites B, E) and *Microcystis* (e.g. sites D, E, H, L) persisted through the disturbance and increased their population size. It has been discussed that late successional species and in particular, *Microcystis* once established are difficult to disturb (Reynolds, 1993) but can be stimulated by storm events (Edson and Jones, 1988). Jacobsen and Simonsen (1993) found that although rainfall and storms increased the loss of an *Aphanizomenon* population in Lake Godstrup, they failed to break its dominance. Similarly, Edson and Jones (1988) found that cyanophytes composing of *Aphanocapsa* and *Gomphosphaeria* increased from 34 to 59 % of the total population two days after a storm. Other species such as *Euglena* (site B) and *Peridinium* (site D) decreased with rainfall and recovered to cell numbers similar to those at pre-rainfall within 7 days.

Another affect was to stimulate growth of earlier successional species, which were on the 'wane' such as *Chlamydomonas* (e.g. sites B, D, E), which increased population size within 7 days after the 12 February rainfall event at site B. In this case, the disturbance enabled re-colonisation by a C-strategist confirming hypothesis 1. Similarly, Barbiero *et al.* (1999) reported an increase in *Chlamydomonas* after a storm. Moreover, the replenishment of nutrients relaxed competition

between species, which enabled the growth of rare species above detectable limits. For example, *Cryptomonas* and *Scenedesmus* increased approximately 7-14 days after rainfall at site H.

As a result of a combination of factors such as increases in rare species, persistence of tolerant species, re-growth of earlier species and species displacement, both species richness and the Shannon-weaver index generally increased 7 days after a disturbance. An exception was at site A₂ that is probably due to the proximity of drains. Diversity was generally higher at site L due to the flushing of phytoplankton downstream. The 4 major rain events - 26 January, 12 February, 16 March and 7 April were between 17-28 days apart. Based on cell generation time relative to disturbance, Reynolds (1988d) calculated the disturbance scale to range from less than 3 days to represent a high frequency of disturbance to 30-35 days to represent the threshold for infrequent disturbances, which has been verified with field observations (Padisak, 1993). Consequently, the frequency of disturbances fell in the intermediate range, which verifies the intermediate disturbance hypothesis regarding diversity.

An assumption of the intermediate disturbance hypothesis is that not enough time is available for the exclusion of species due to autogenic processes. Conversely, the degree of organization and community development at any point in time is a measure of the effectiveness of the autogenic processes since the last disturbance (Reynolds and Reynolds, 1985). It was difficult to differentiate autogenic selection processes within the Torrens Lake due to phytoplankton heterogeneity across sites and the lack of zooplankton data. However, it is clear that C-S-R species co-existed throughout the study and there was no competitive exclusion of *r* species towards *K* species, which confirms hypothesis 2.

7.4.4 Implications for phytoplankton control and monitoring

The growth of cyanobacteria within the Torrens Lake poses a major water quality hazard for recreational users of the lake, and highlights the difficulty of cyanobacterial control in small shallow water bodies. An appreciation of the adaptive strategies and ecology of cyanobacteria underpins the options for their control. For instance, *Microcystis* and *Planktothrix* can persist through periods of wind mixing and consequently, artificial mixing is inappropriate in shallow water bodies. Furthermore, both *Planktothrix* and *Anabaena* are able to fix atmospheric nitrogen

and persist through periods of N-limitation. In a recent paper (Brookes *et al.*, *in prep.*) discusses the range of options available for cyanobacterial control including artificial mixing and manipulation of flow. Although flow can prevent the establishment of surface scums (Mitrovic *et al.*, 2003), the nutrient status of source water must be known. In early 2000, hypolimnetic water was released from the Kangaroo Creek Reservoir to flush a *Microcystis* bloom from the lake. Since the hypolimnetic water contained high concentrations of nutrients and due to density differences, the cooler water flowed under the Torrens Lake water and over the weir. There was dilution of the population, but the replenishment of nutrients augmented the *Microcystis* bloom that lasted for an additional 3 weeks. The most appropriate measure to control cyanobacteria in the Torrens Lake is any technique, which is able to reduce or 'strip' phosphorus concentrations. These techniques would need to be applied quickly after any summer rain events.

7.4.5 Conclusions

In conclusion, autogenic selection processes predominantly govern phytoplankton composition within the Torrens Lake during Summer and Autumn. The coexistence of species representing C-S-R functional strategies implies that there were no competitive exclusions, although inter-specific competition was evident at selected sites. The summed difference index and cluster analysis of data revealed that the phytoplankton community was highly dynamic at all sites and displayed a large degree of heterogeneity both temporally and spatially. Although no single factor was identified to control any species the major allogenic factors influencing the changes in composition were summer storm events, which acted to temporarily dilute populations, replenish nutrients and reduce water column stability. Water column stability was also affected by afternoon wind mixing. The storm water runoff associated with the summer rainfall acted as a disturbance consistent with the intermediate disturbance hypothesis. Phytoplankton and subsequently diversity generally recovered and reached high levels approximately 7 days after a disturbance. It is difficult to predict and manage phytoplankton in small-shallow urban lakes such as the Torrens Lake due to the unpredictability of summer rainfall and the short time scale of events such as storm water pulses from the surrounding catchment. As stated by Tilman (1996) "the forces controlling species composition, diversity, dynamics, and stability of an ecosystem remain one of the major mysteries of modern science".

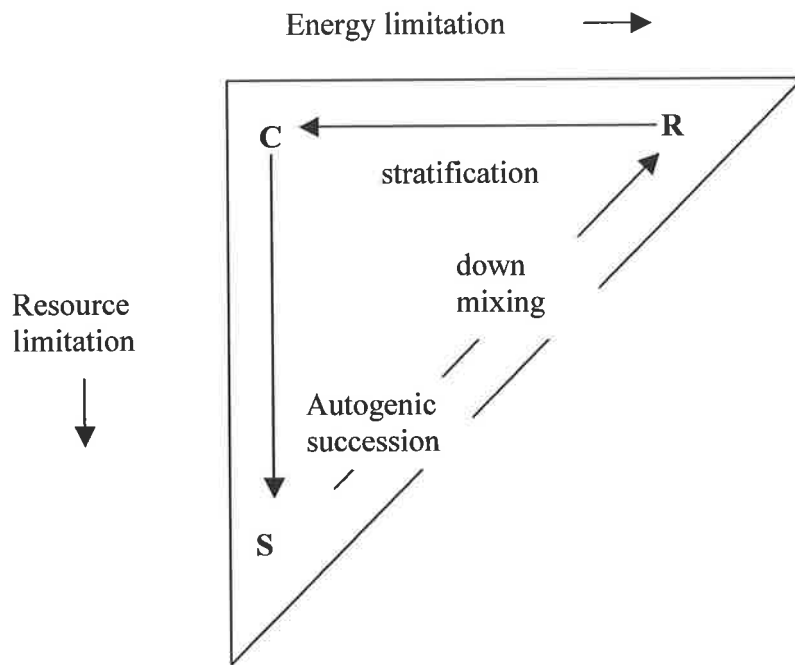


Figure 7.1 Selective tracking habitat templates and phytoplankton C-S-R life history strategies after Reynolds (1997)-figure 49c. C-S-R represents the morphological preadaptations of phytoplankton to invasive (-C), acquisitive (-S) or acclimative (-R) life styles, respectively.

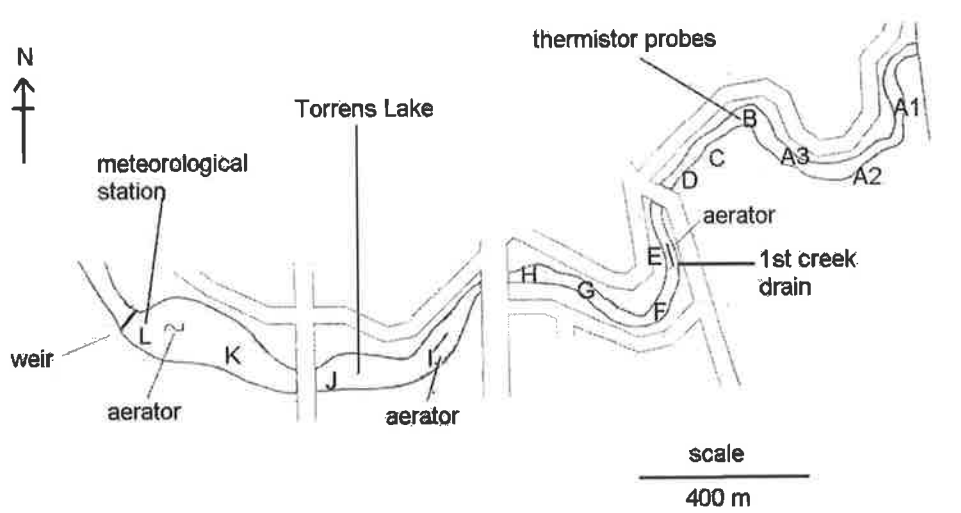


Figure 7.2 Map of lower Torrens Lake showing the sample sites A₁ to L, locations of 3 bubble plume aerators and the 1st creek drain.



Figure 7.3 Photographs of the upper section of the Torrens Lake showing sampling sites A₂ (a) and B (b), highlighting the narrowness of the river and overhanging trees, which may prevent wind-induced mixing of the water column.



Figure 7.3 Photographs of the middle section of the Torrens Lake showing sampling sites E (c) and I (d) highlighting the surrounding land use broader reaches of the middle section of the lake.



(e)



(f)

Figure 7.3 Photographs of the lower sections of the Torrens Lake showing sampling sites H (e) and L (f). The weir monitoring location is in the distance of photograph f.

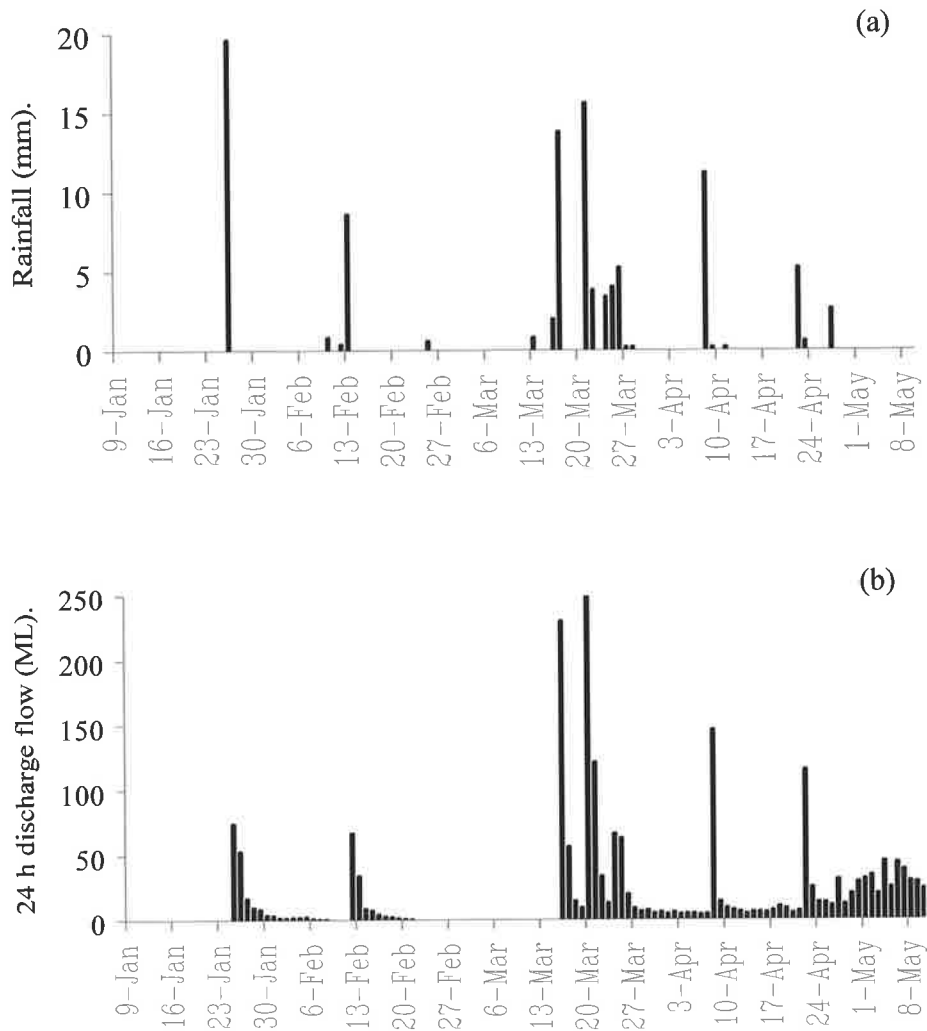


Figure 7.4 24-h rainfall (a) and discharge at Holbrookes Road (b) during the study period. Rainfall was measured at Kent Town 2 km east of the Torrens Lake, while discharge at Holbrookes Road is indicative of flow over the city weir near site L. Note: the discharge in early May was related not to rainfall but water release from the Kangaroo Creek Reservoir associated with maintenance.

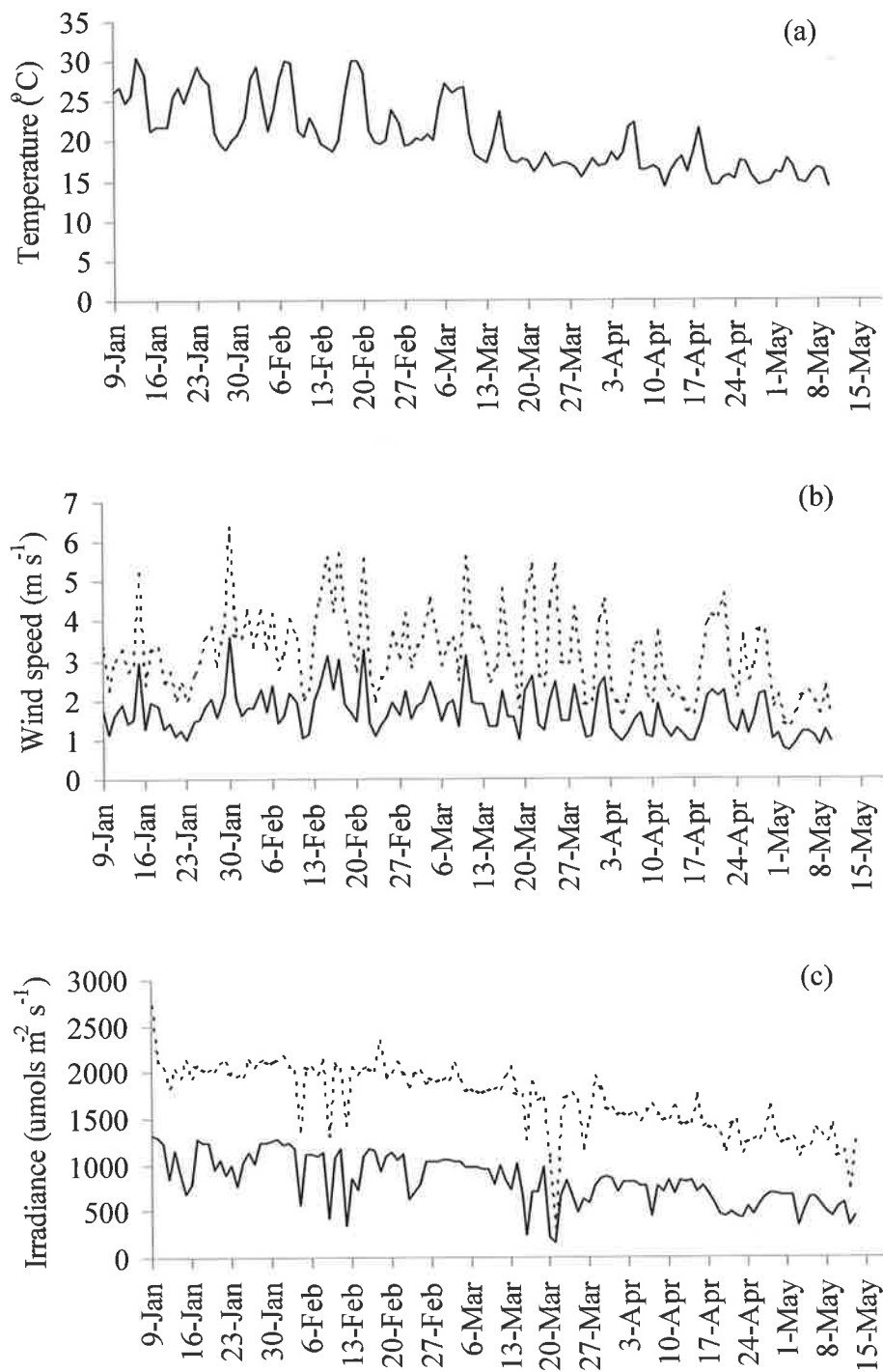


Figure 7.5 Meteorological conditions at site L including daily average air temperature (a), daily average and maximum wind speed (b) and daily average and maximum instantaneous surface irradiance (c). Note: with the exception of irradiance (day length) all data was average over 24 hours.

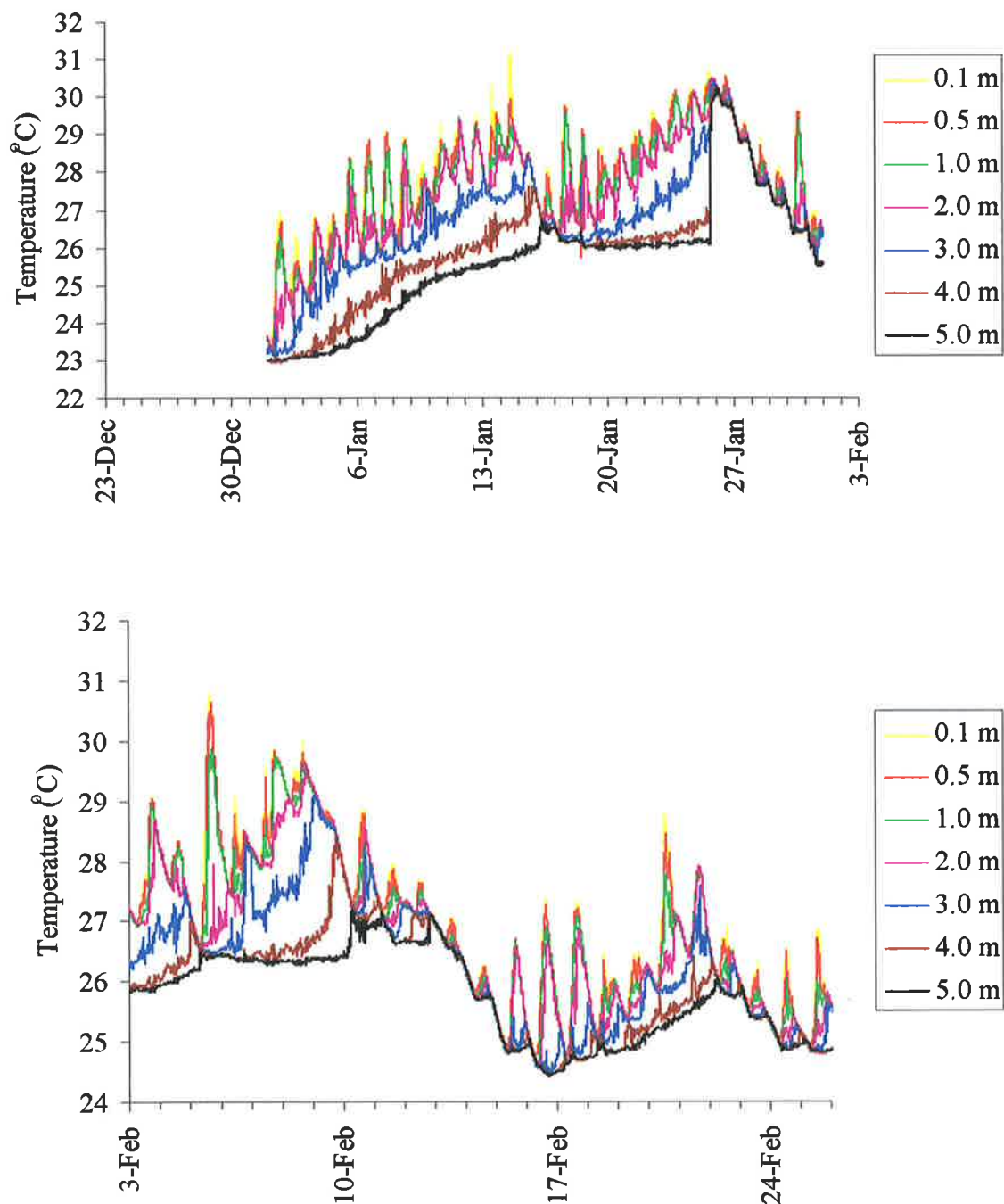


Figure 7.6 Vertical temperature structure at site L in the lower Torrens Lake during January-February.

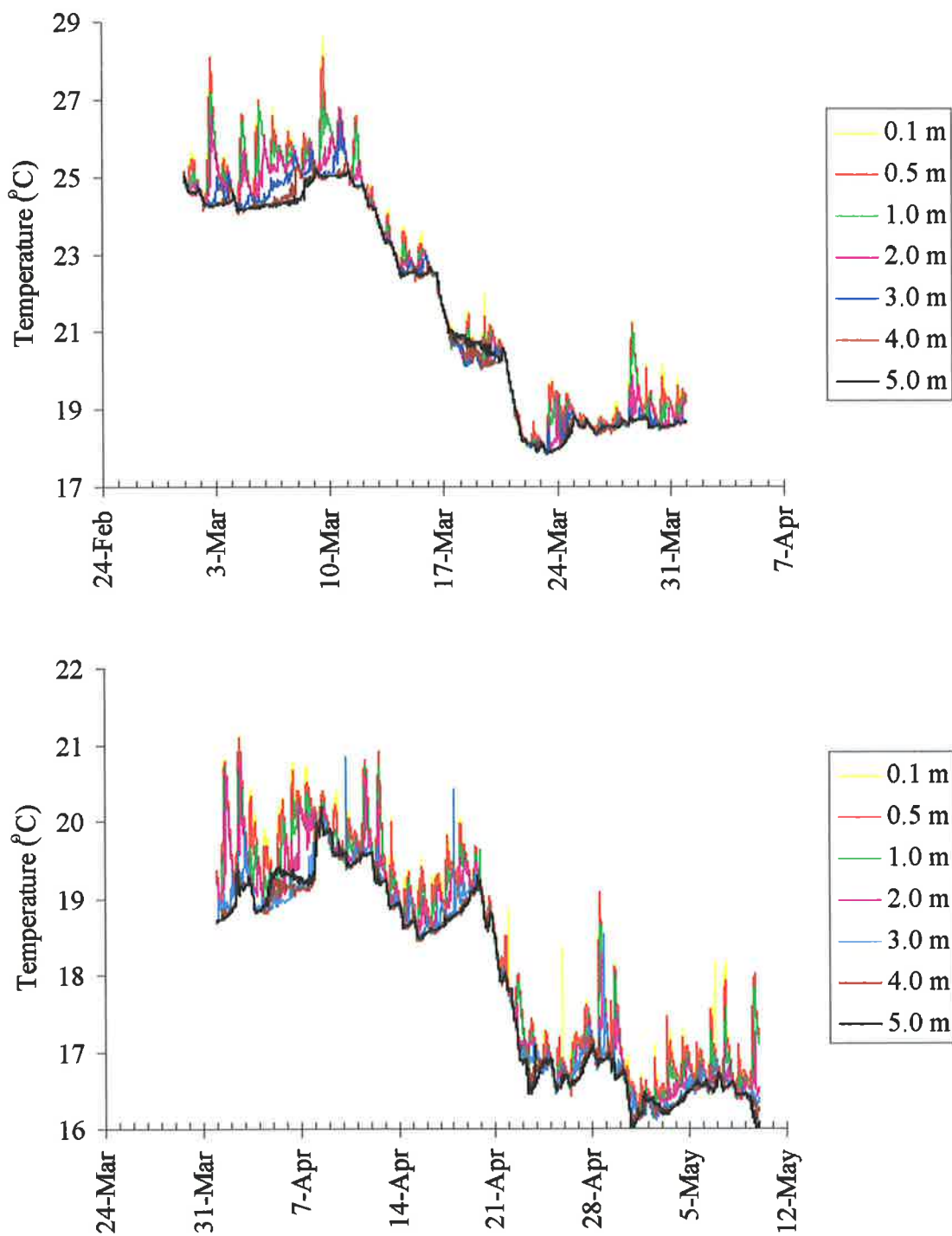


Figure 7.6 Vertical temperature structure at site L in the lower Torrens Lake during March-May.

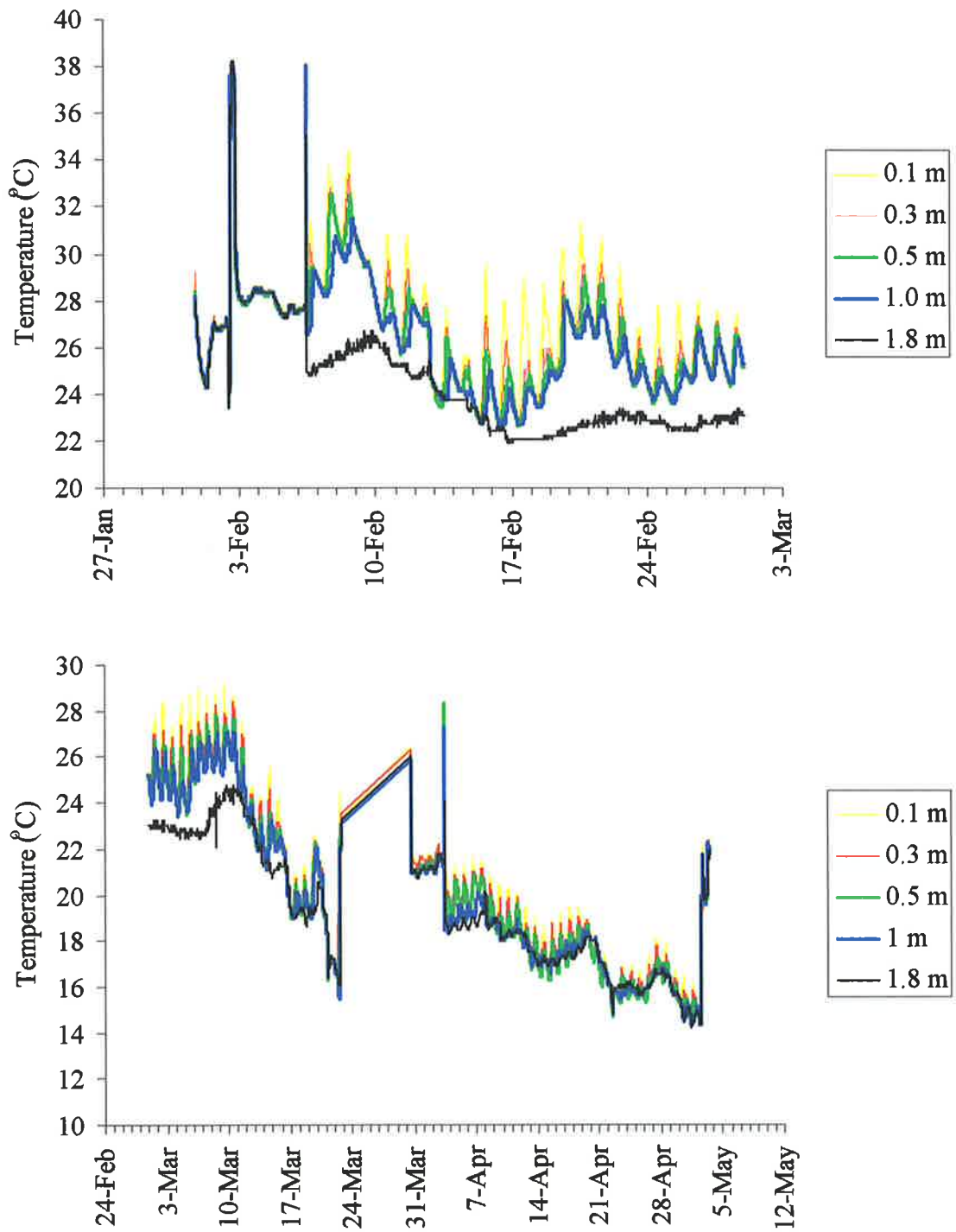


Figure 7.7 Vertical temperature structure at site B in the upper Torrens Lake during February-May. Note: no data was available for January.

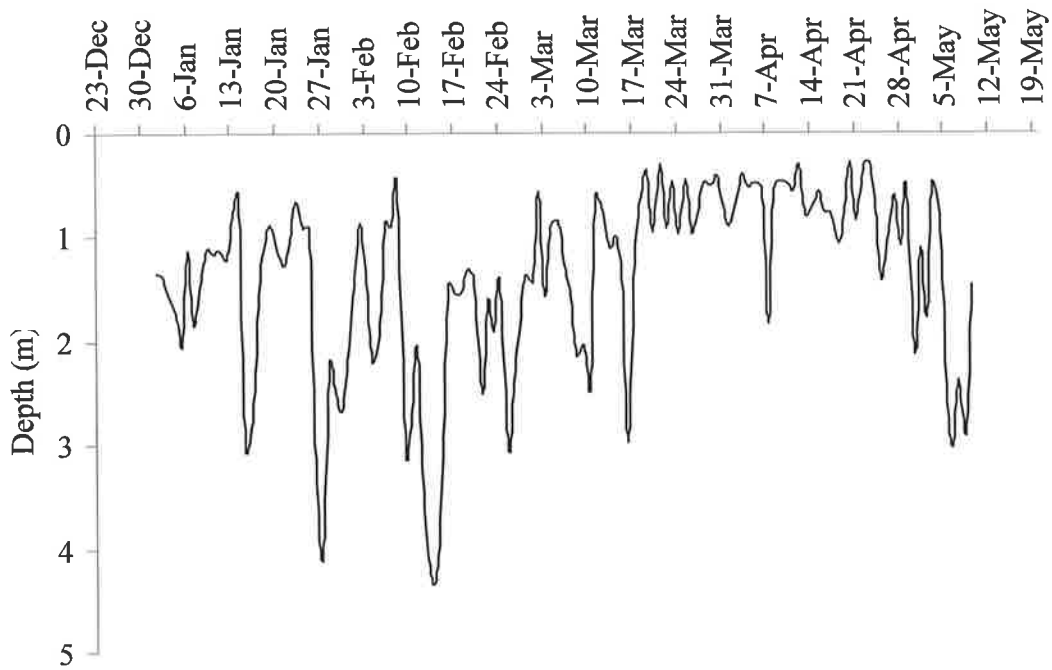


Figure 7.8 Calculated daily average surface mixed layer depth at site L in the lower Torrens Lake over the study period.

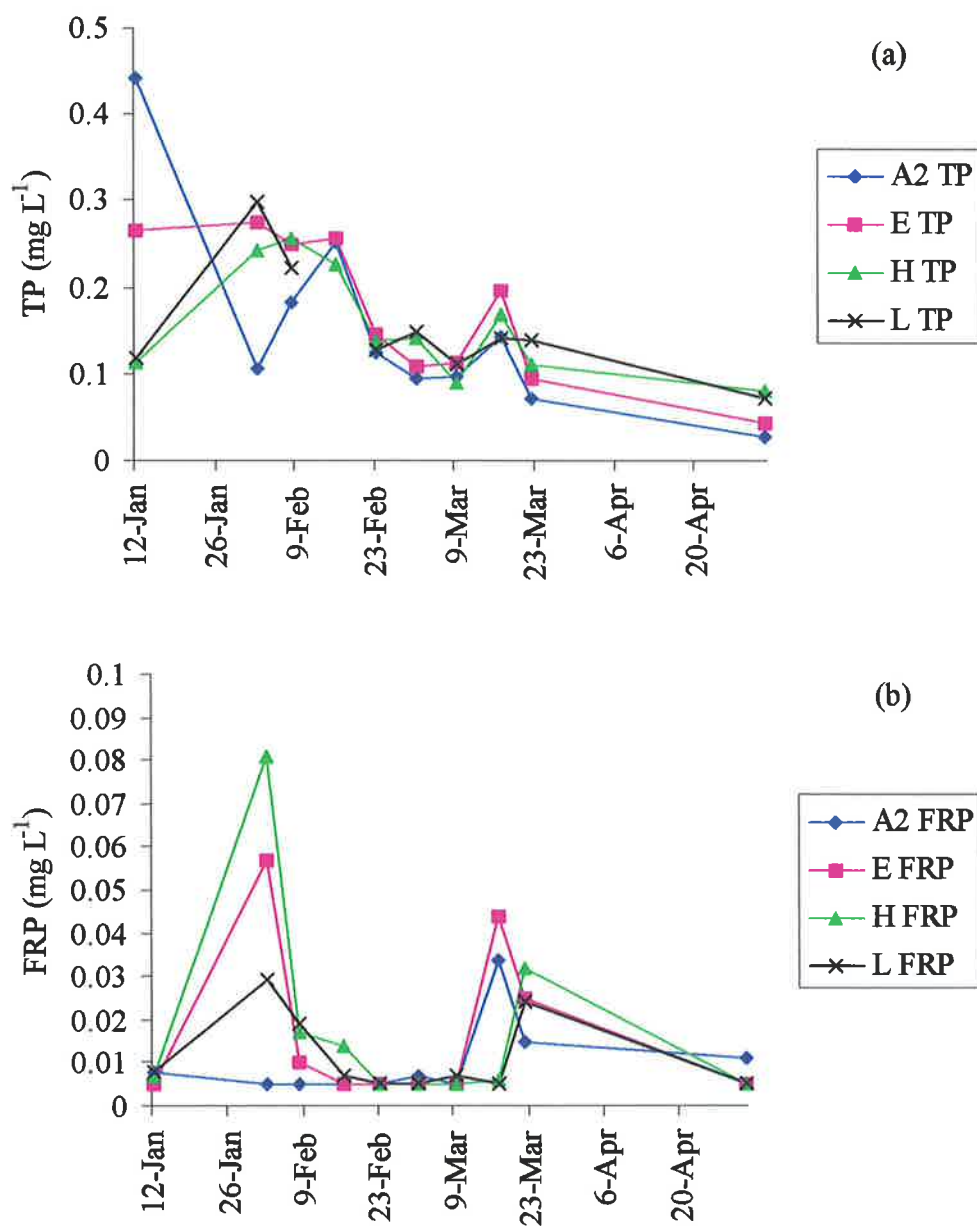


Figure 7.9 Total phosphorus (a) and filterable reactive phosphorus concentrations (b) at sites A₂, E, H and L in the Torrens Lake.

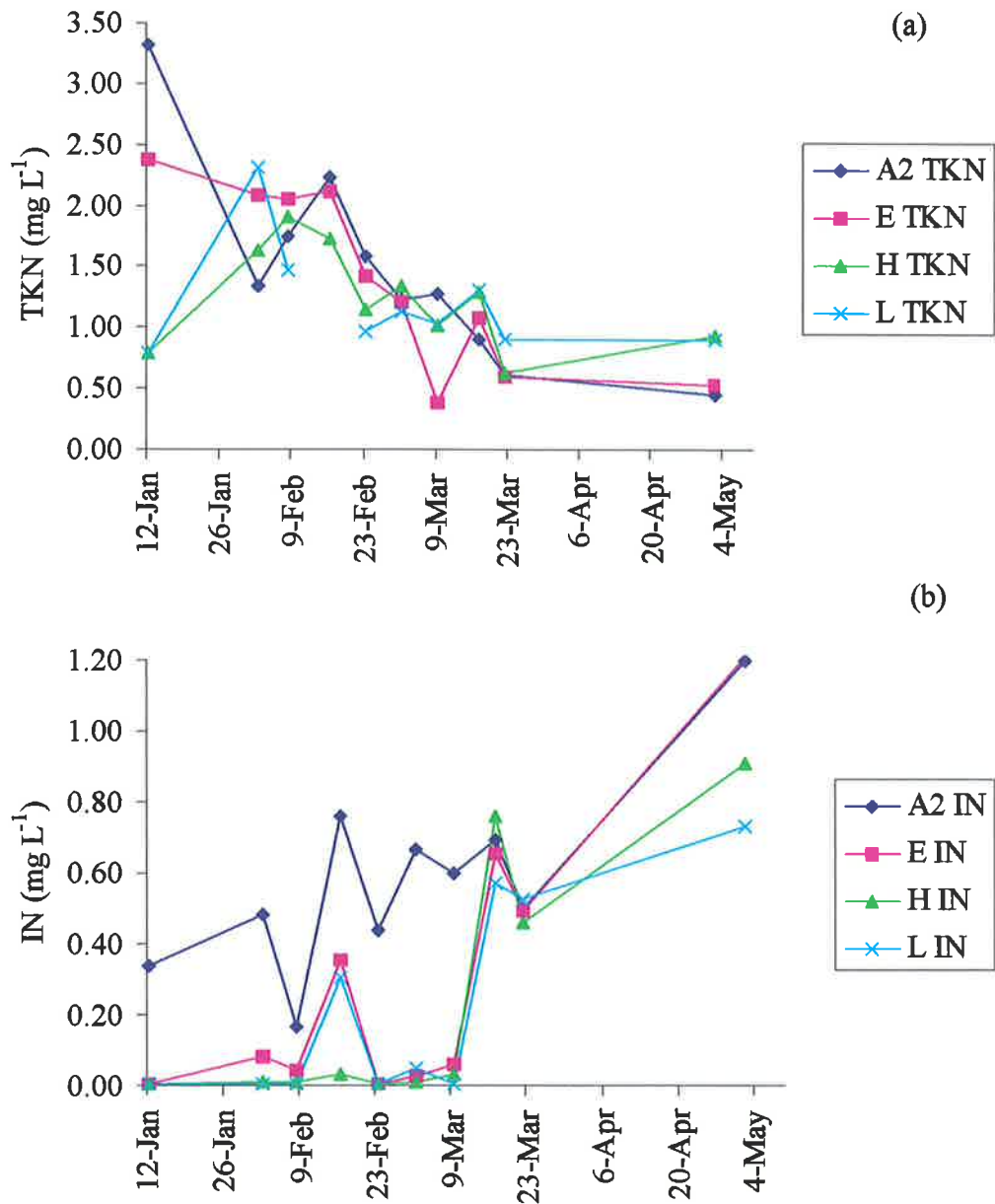


Figure 7.10 Total Kjeldahl nitrogen (a) and inorganic nitrogen concentrations, NO_x (b) at sites A₂, E, H and L in the Torrens Lake.

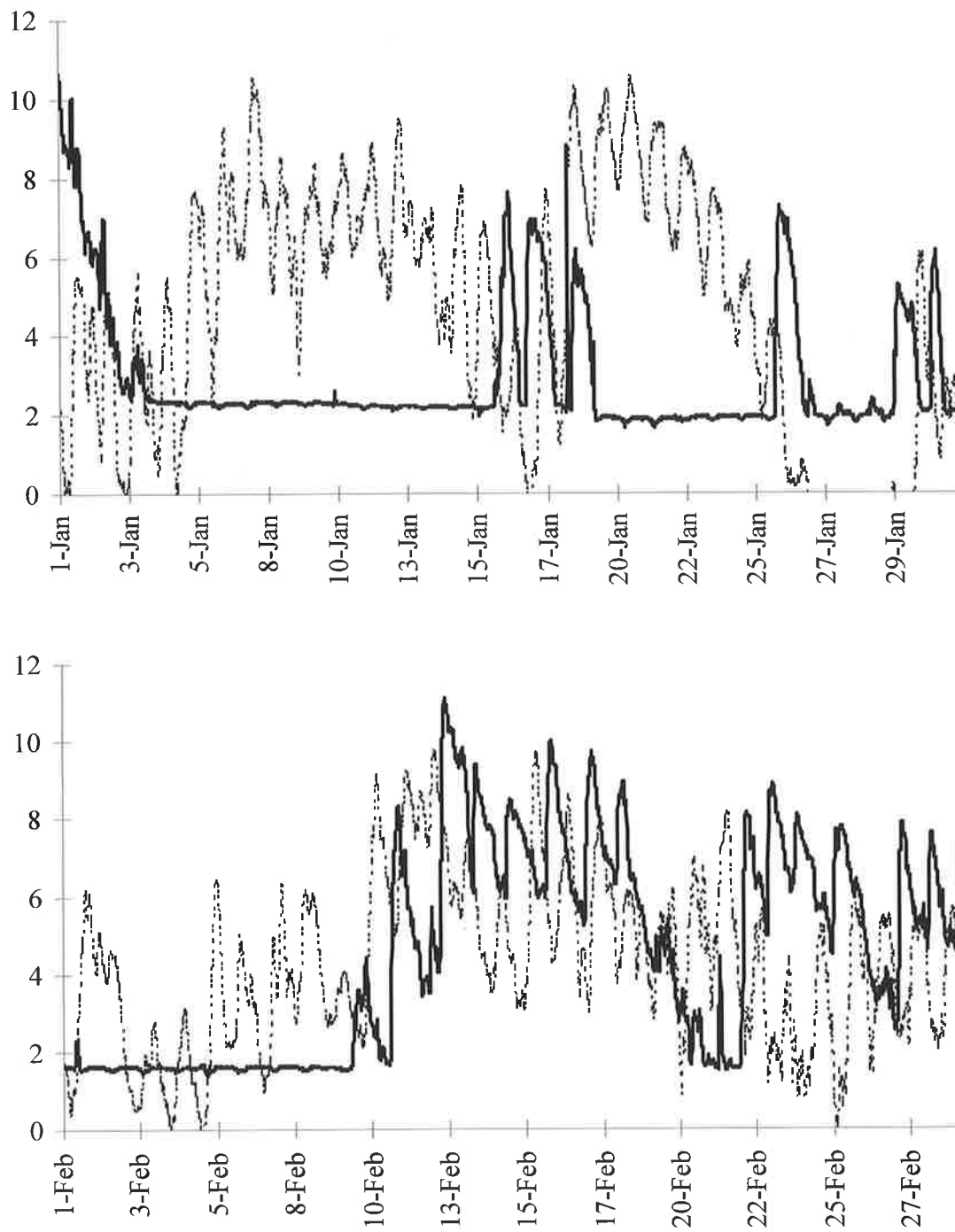


Figure 7.11 Dissolved oxygen concentration (mg L^{-1}) at 0.5 m (broken line) and 4.5 m (solid line) depth at site L for January-February.

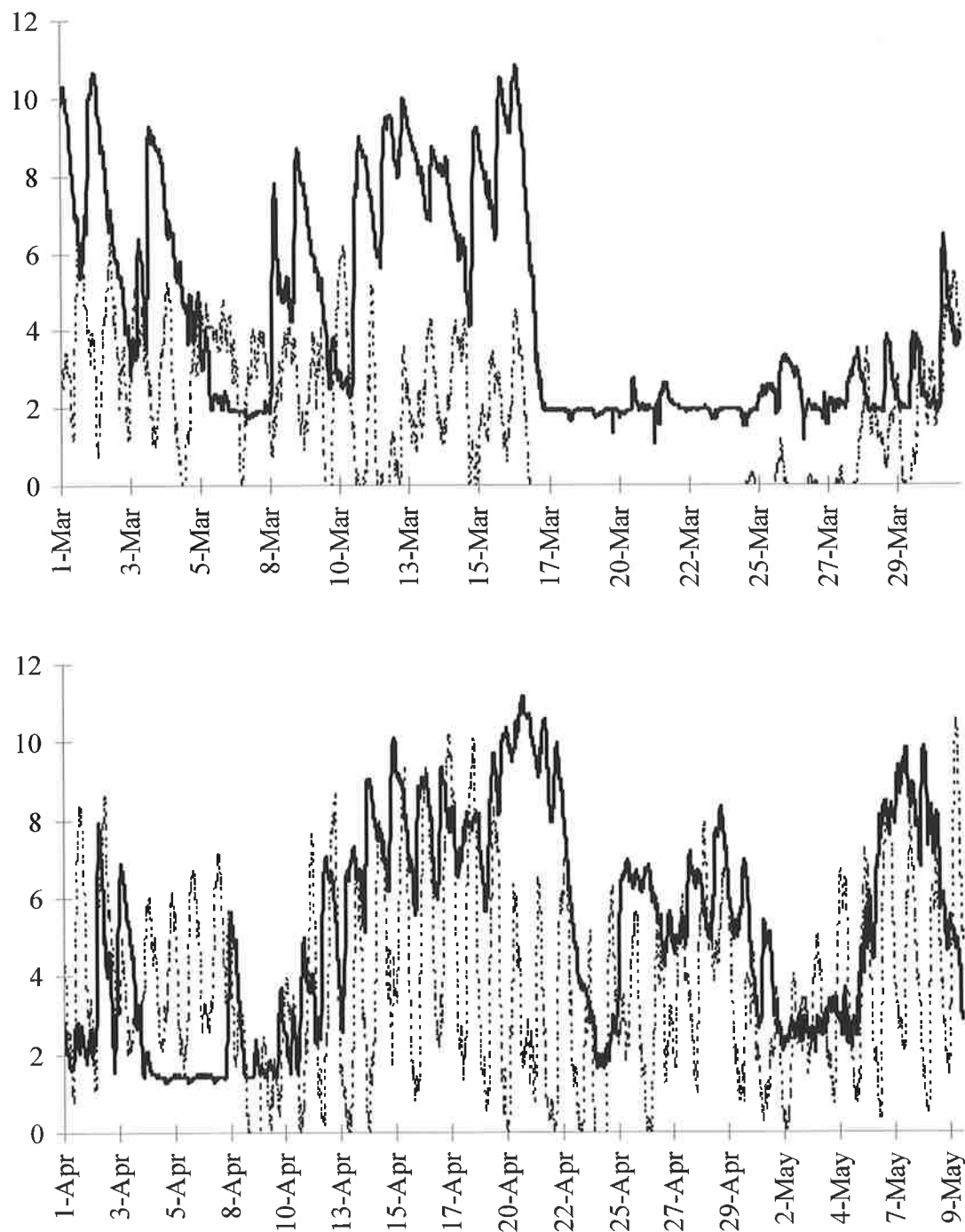


Figure 7.11 Dissolved oxygen concentration (mg L^{-1}) at 0.5 m (broken line) and 4.5 m (solid line) depth at site L for March-May.

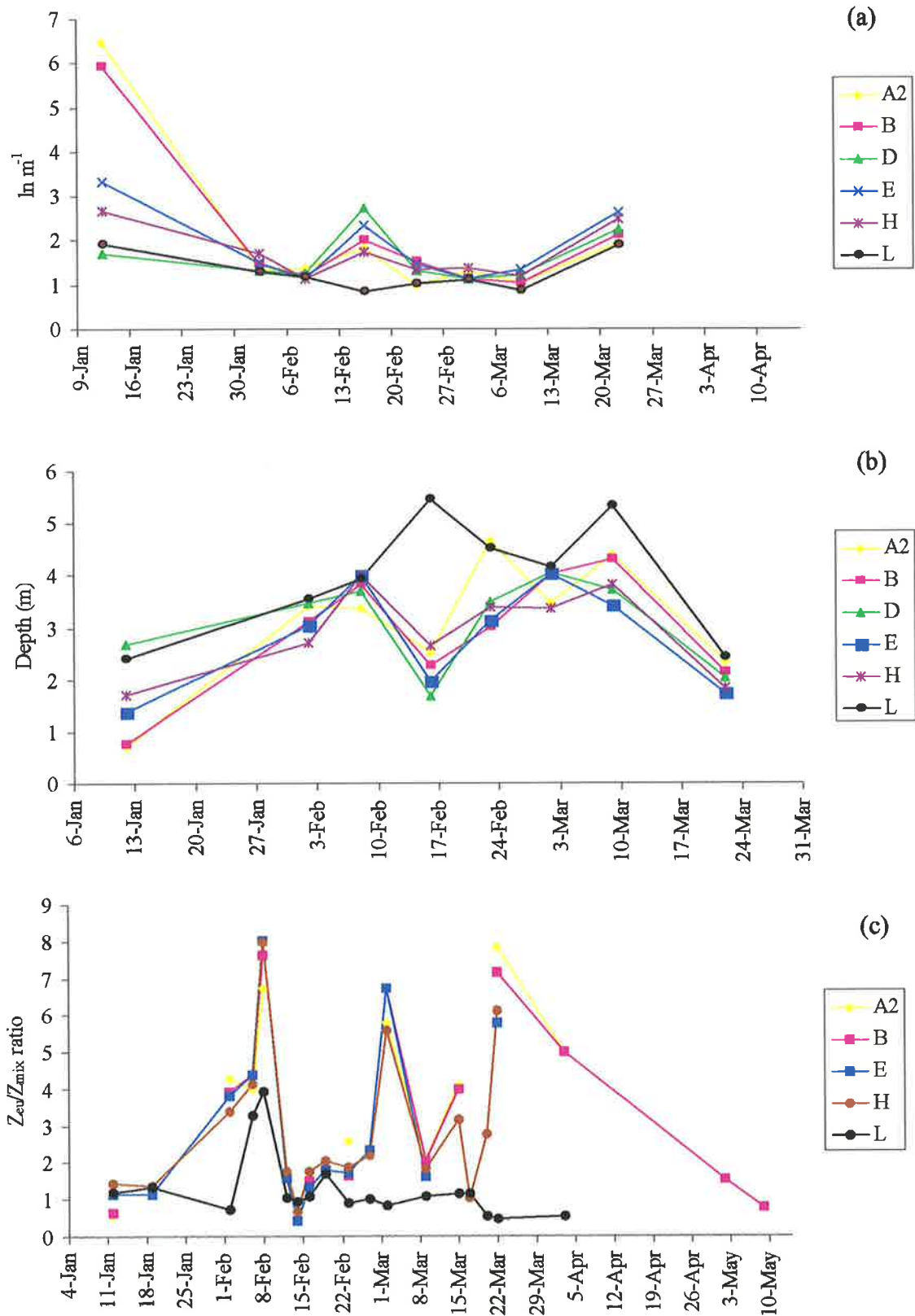


Figure 7.12 Temporal changes in light attenuation coefficient (a), euphotic depth (b) and the euphotic depth: mixed depth ratio (c) at selected sites within the Torrens Lake.

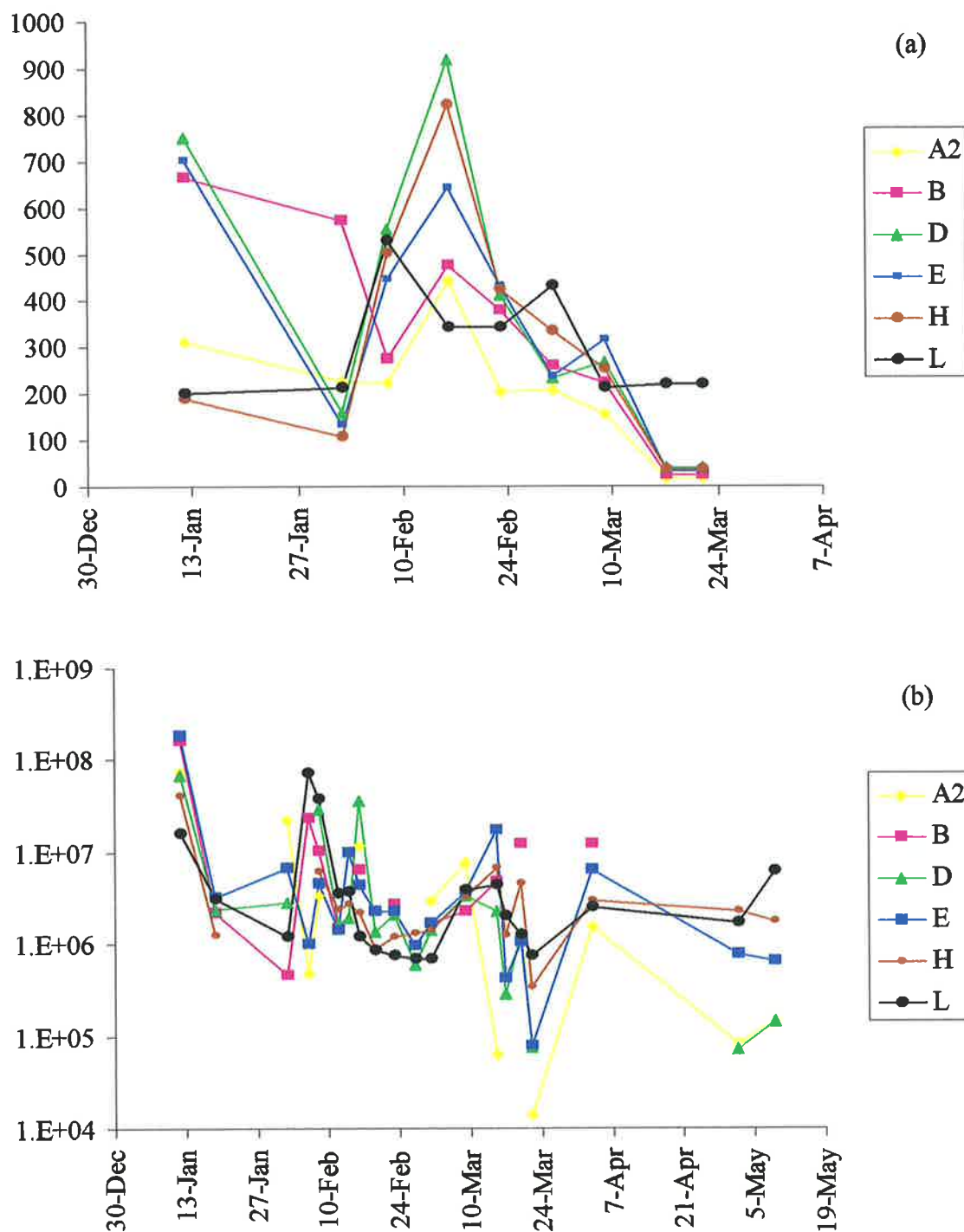


Figure 7.13 Temporal changes in chlorophyll *a* concentration- mg m^{-2} (a) and biovolume- $\mu\text{m}^3 \text{mL}^{-1}$ (b) at selected sites within the Torrens Lake.

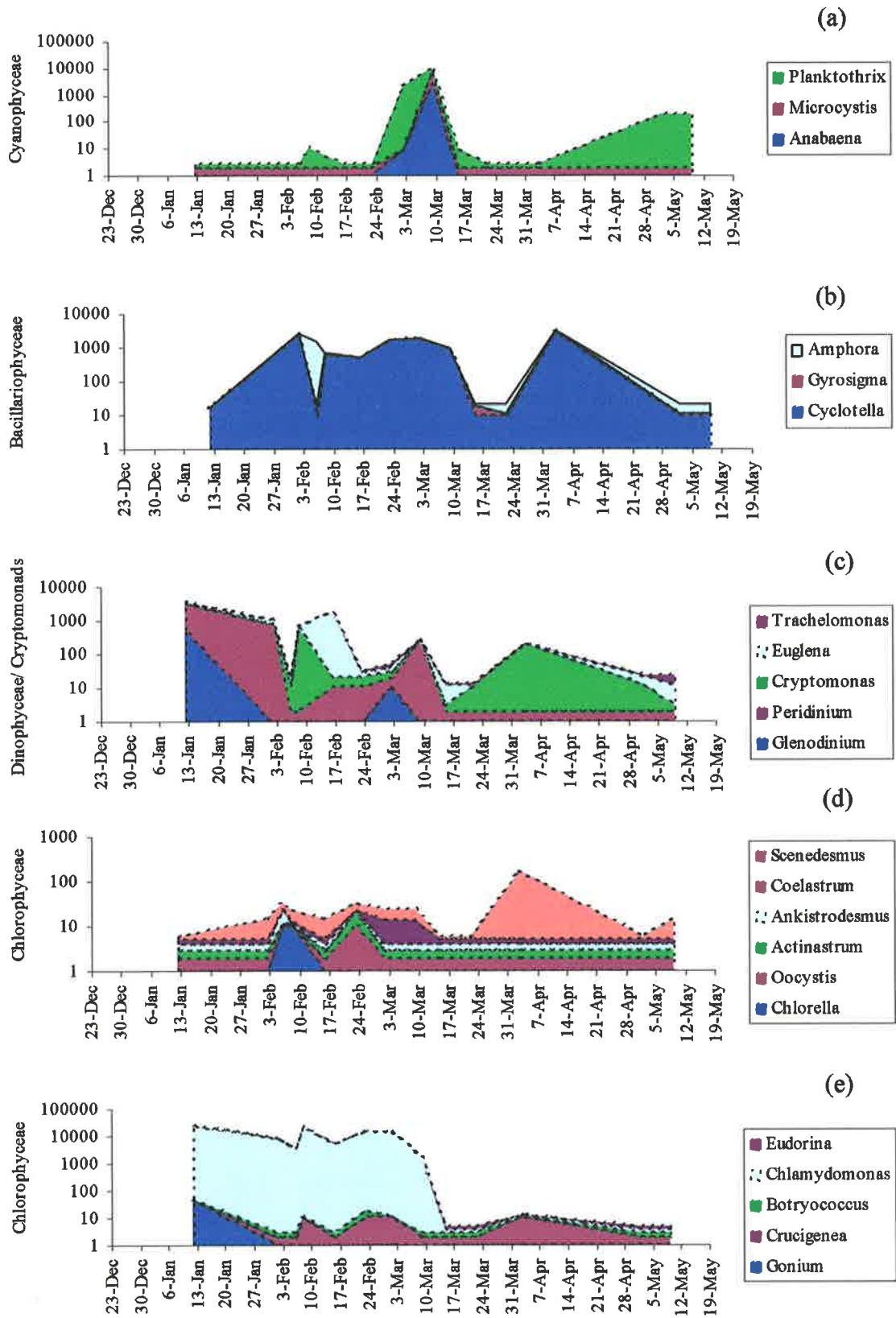


Figure 7.14 Species composition at site A₂. Cells numbers are expressed as cells mL⁻¹.

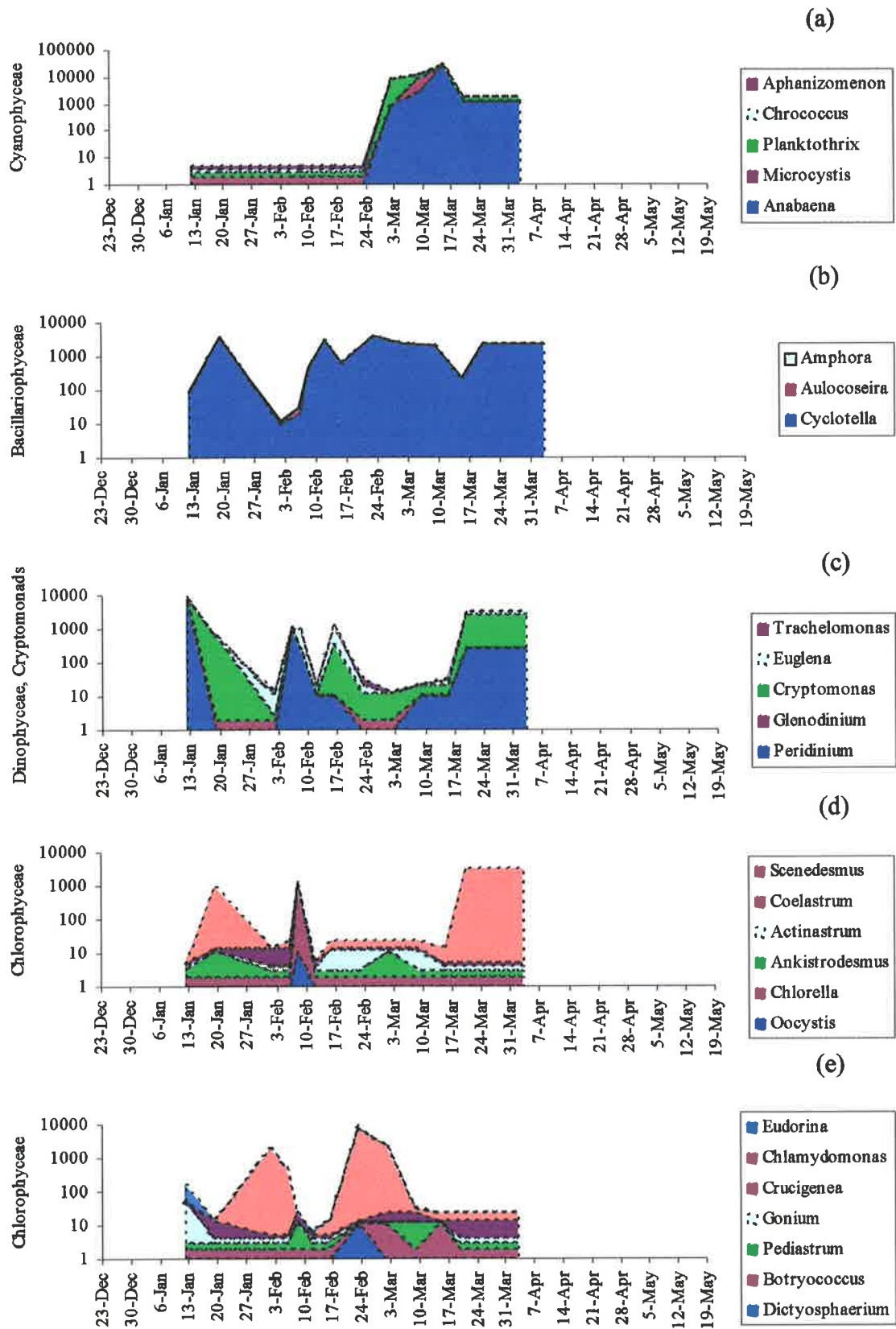


Figure 7.15 Species composition at site B. Cells numbers are expressed as cells mL⁻¹.

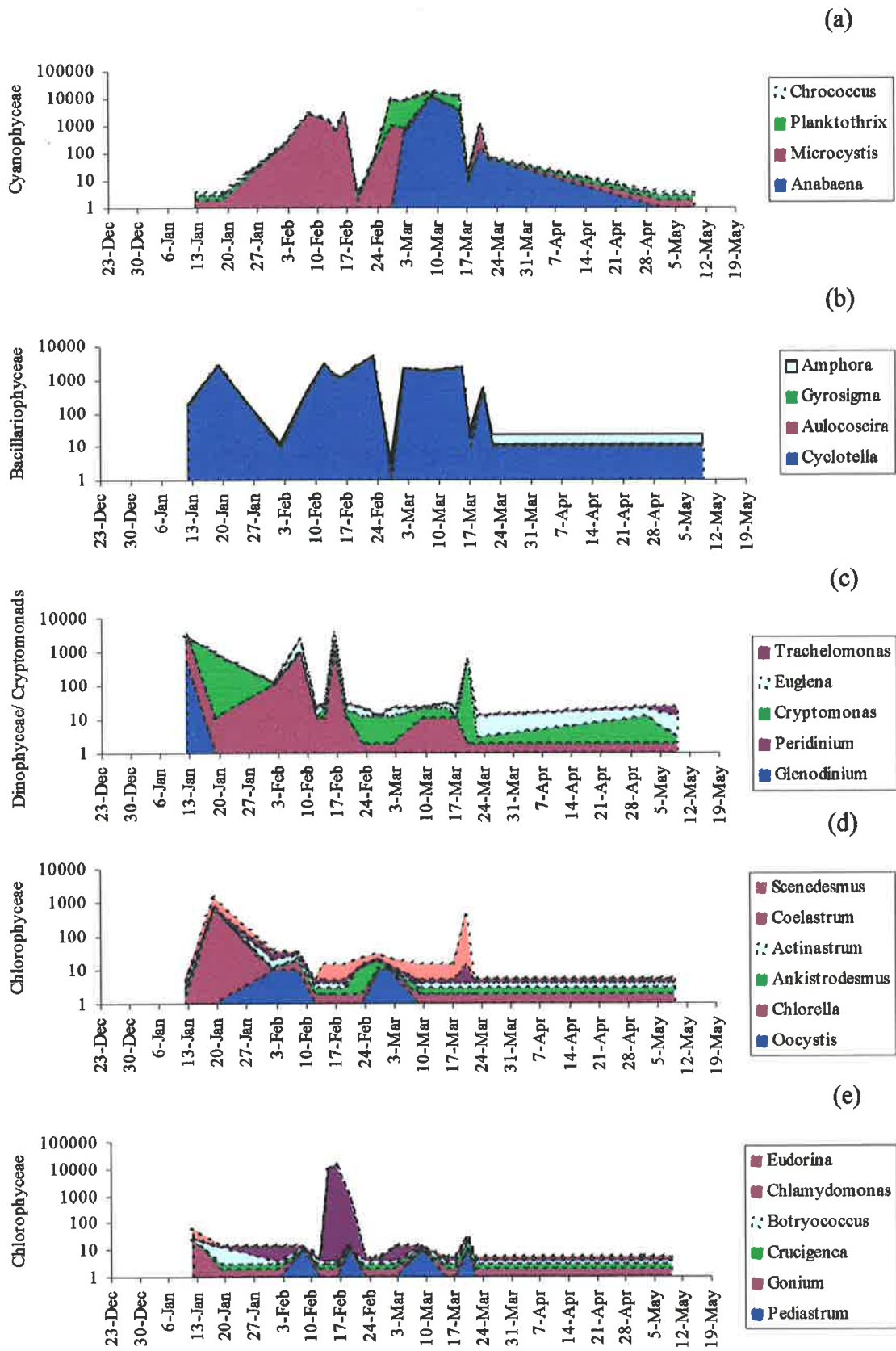


Figure 7.16 Species composition at site D. Cell numbers are expressed as cells mL⁻¹.

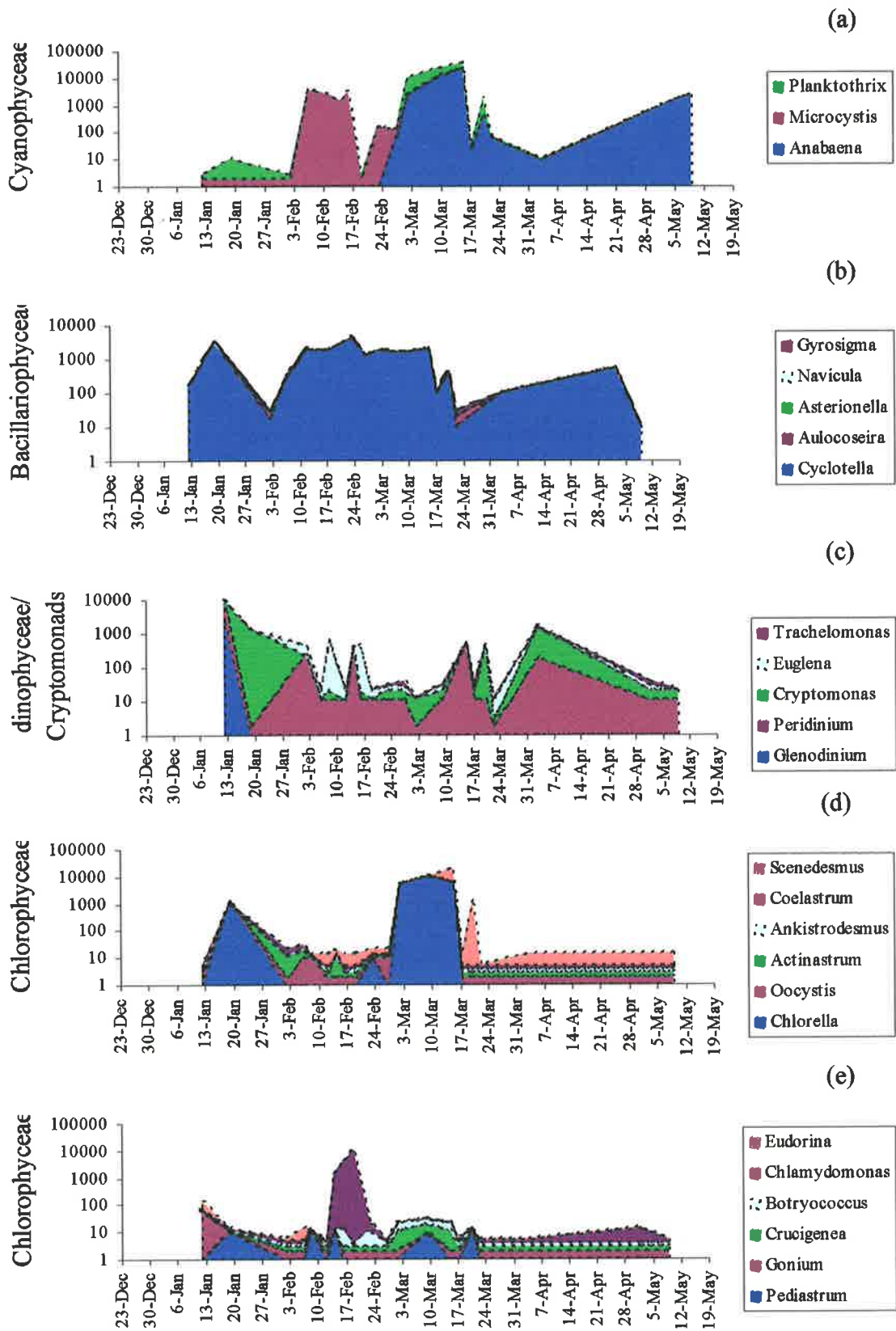


Figure 7.17 Species composition at site E. Cells are expressed as cells mL⁻¹.

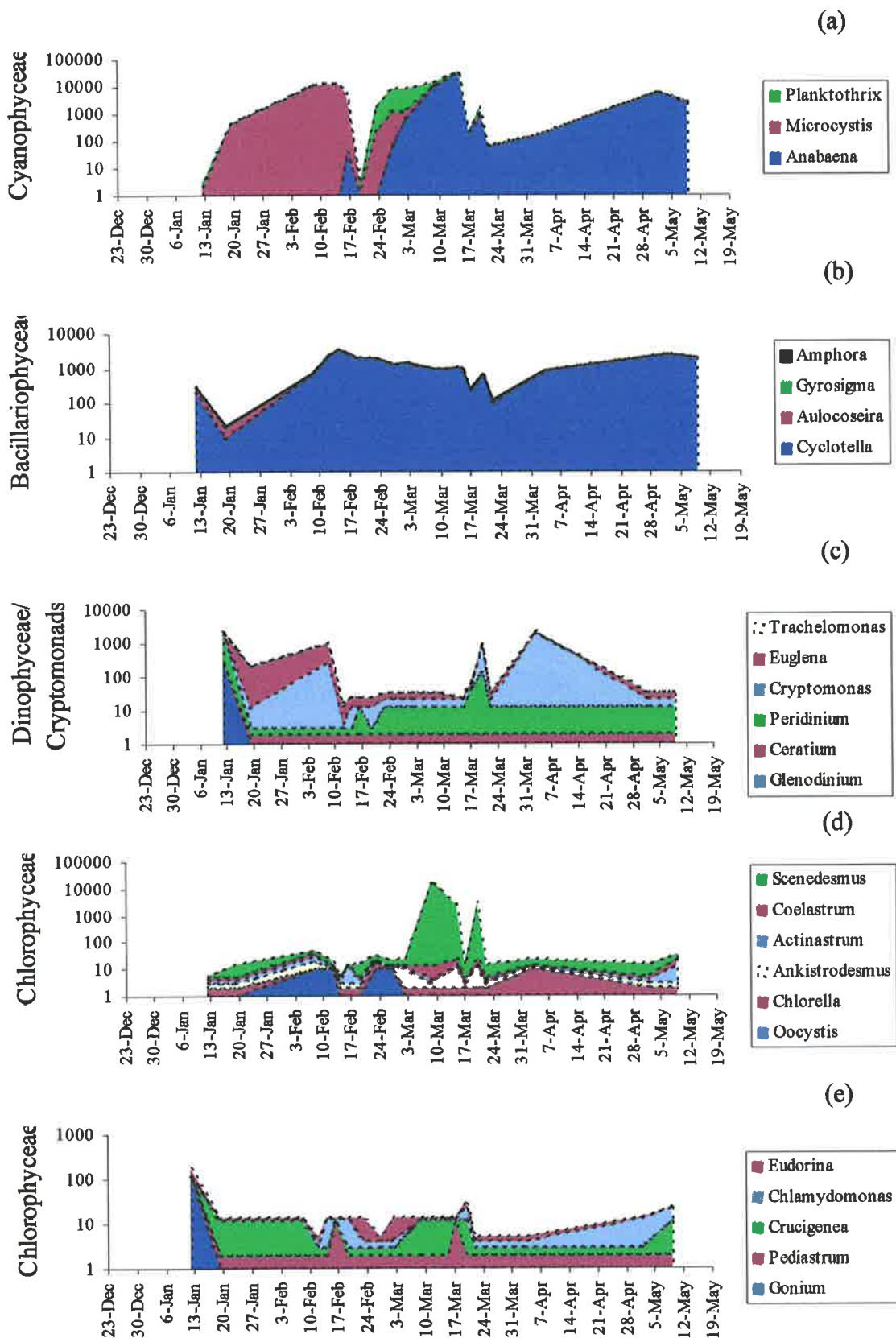


Figure 7.18 Species composition at site H. Cell numbers are expressed as cells mL⁻¹.

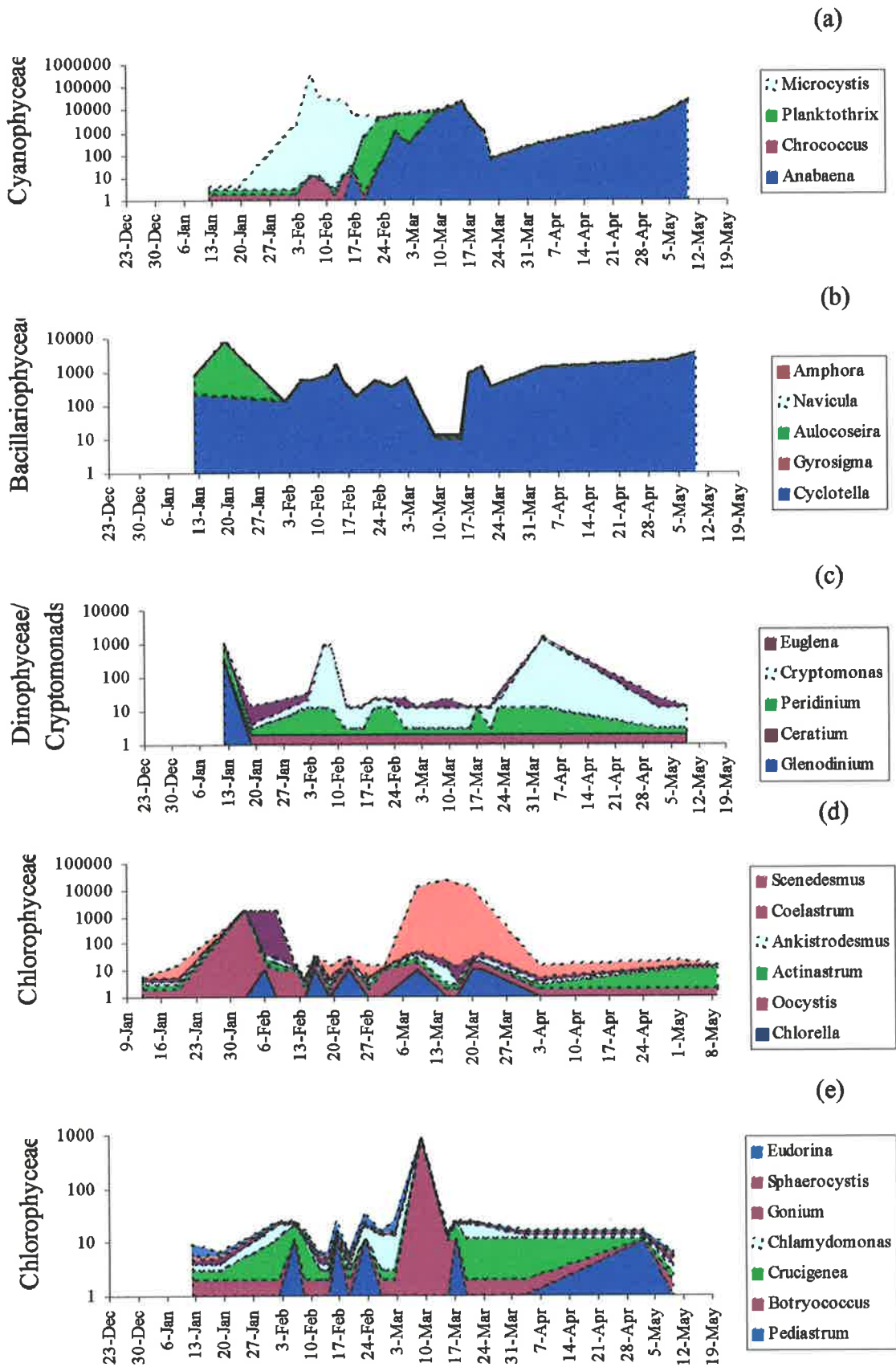


Figure 7.19 Species composition at site L. Cell numbers are expressed as cells mL⁻¹.

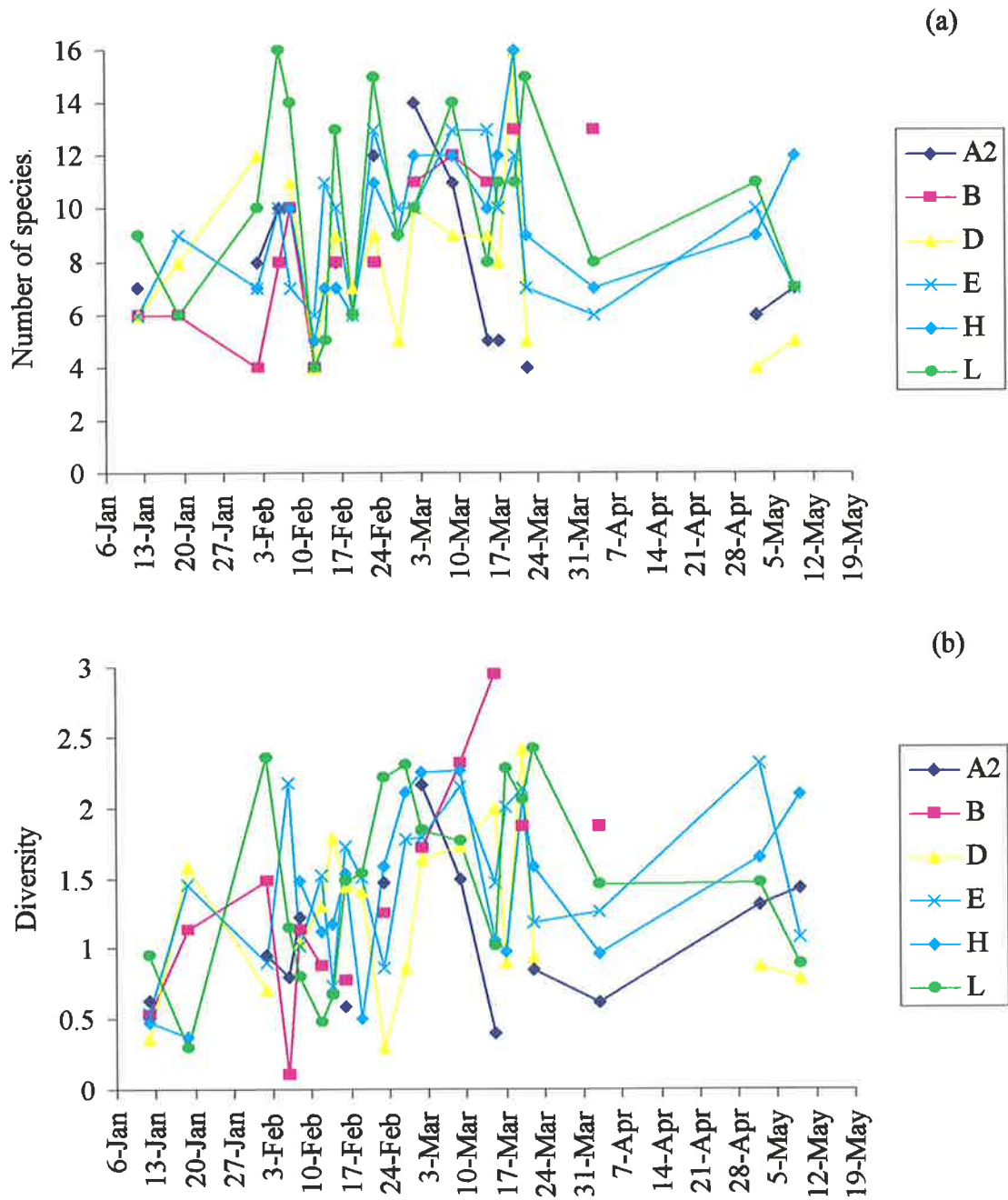


Figure 7.20 Variation in phytoplankton species number (a) and diversity (b) at selected sites within the Torrens Lake in 2001. Diversity was calculated according to the Shannon-Weaver index.

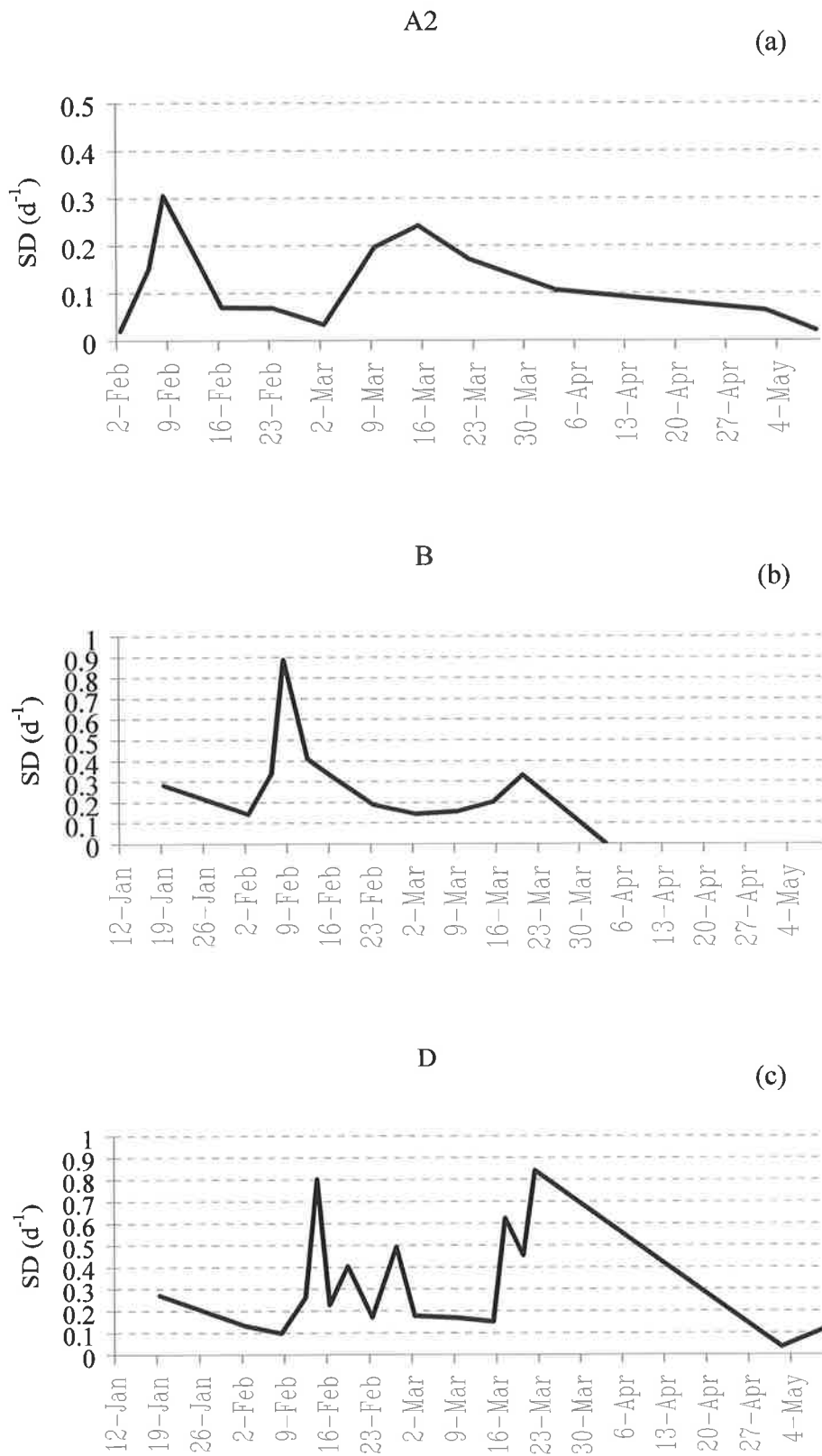


Figure 7.21 Summed difference index [SD] (d^{-1}) for the phytoplankton community at sites A₂, B and D in the Torrens Lake.

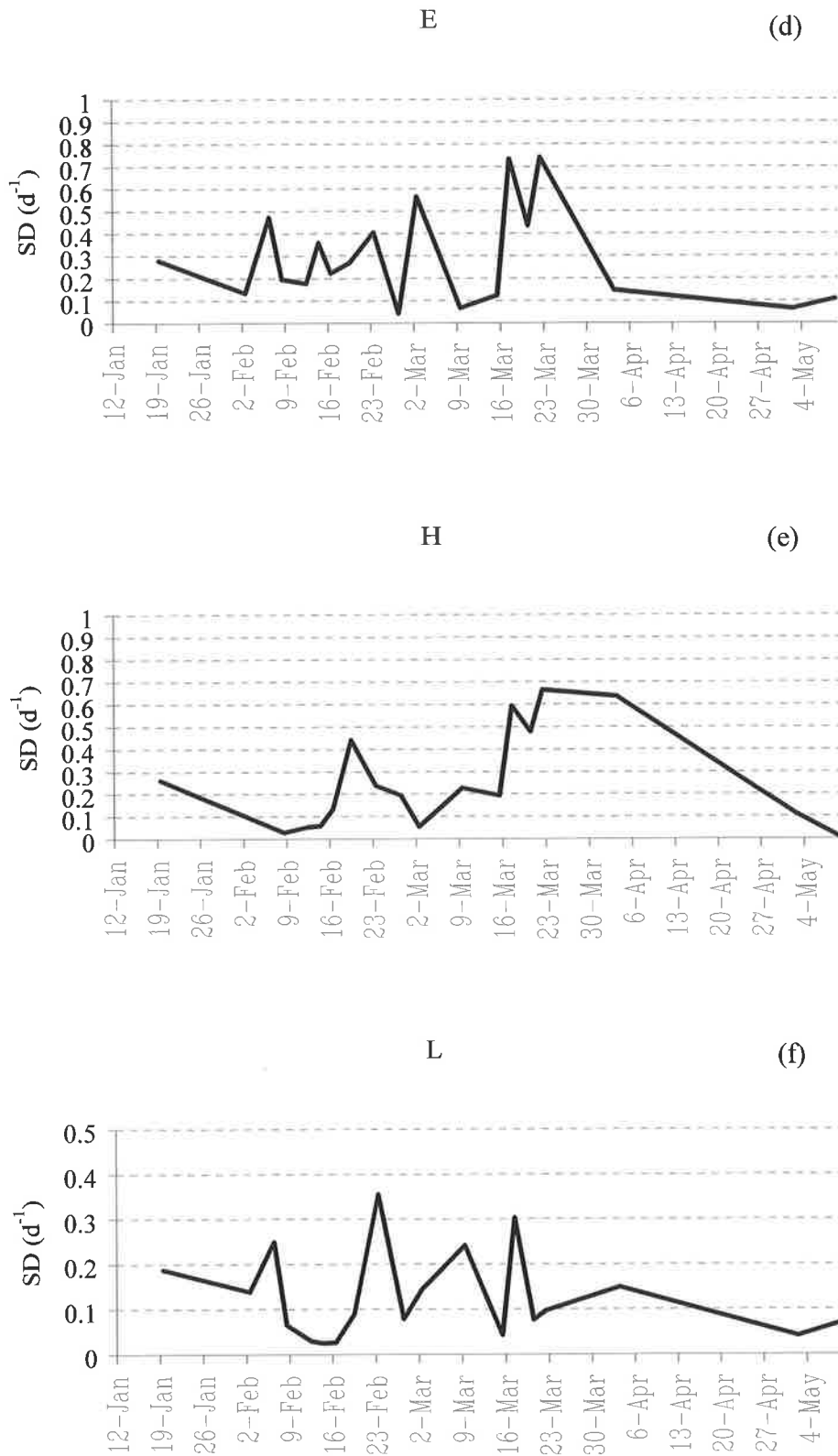


Figure 7.21 Summed difference index [SD] (d⁻¹) for the phytoplankton community at sites, E, H and L.

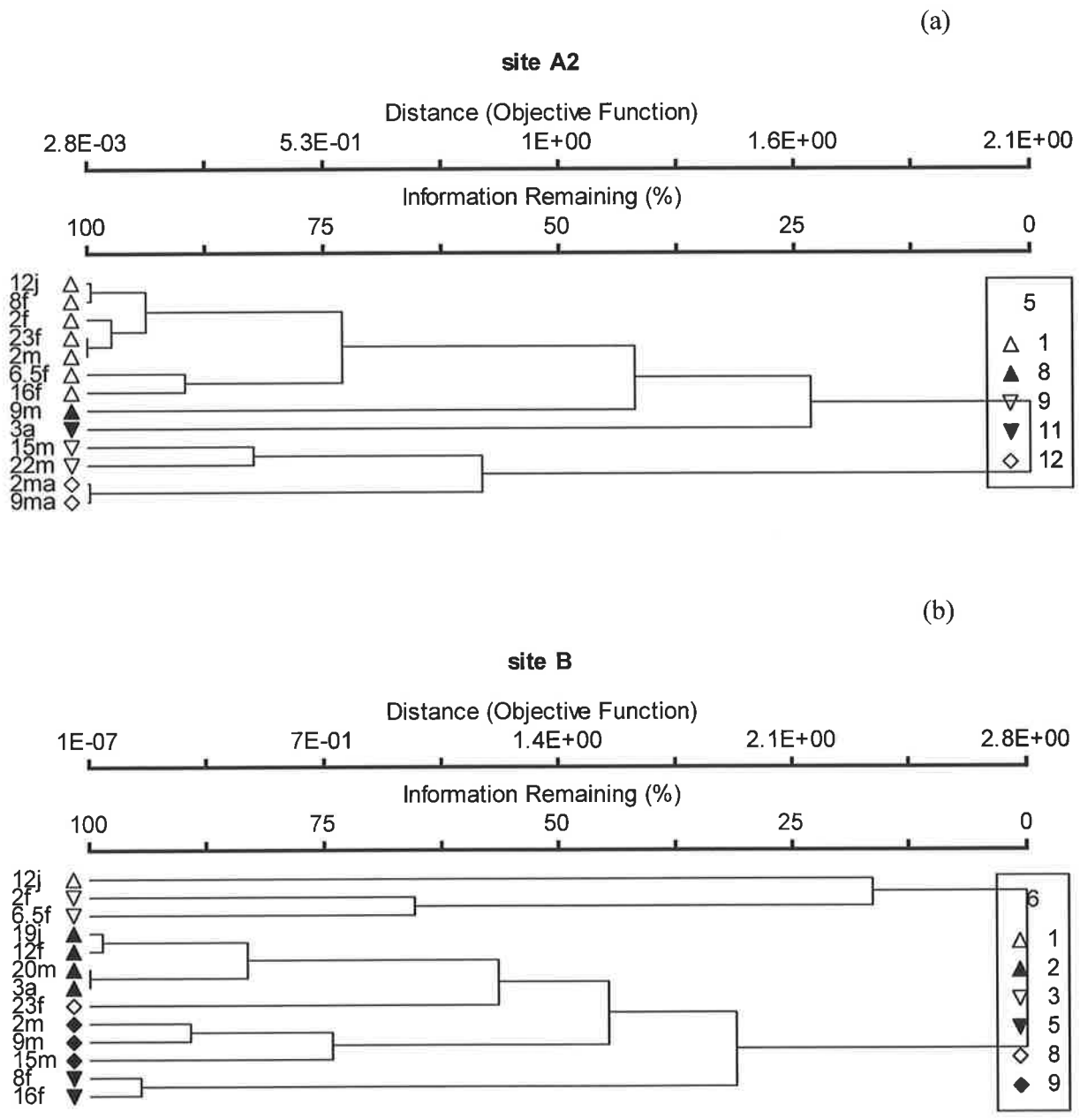


Figure 7.22 Dendrogram date groupings based upon species composition at sites A₂ (a) and B (b). At site A₂, 5 groups were identified and the mrpp = 0.0004684. At site B, 6 groups were identified and the mrpp = 0.0004058.

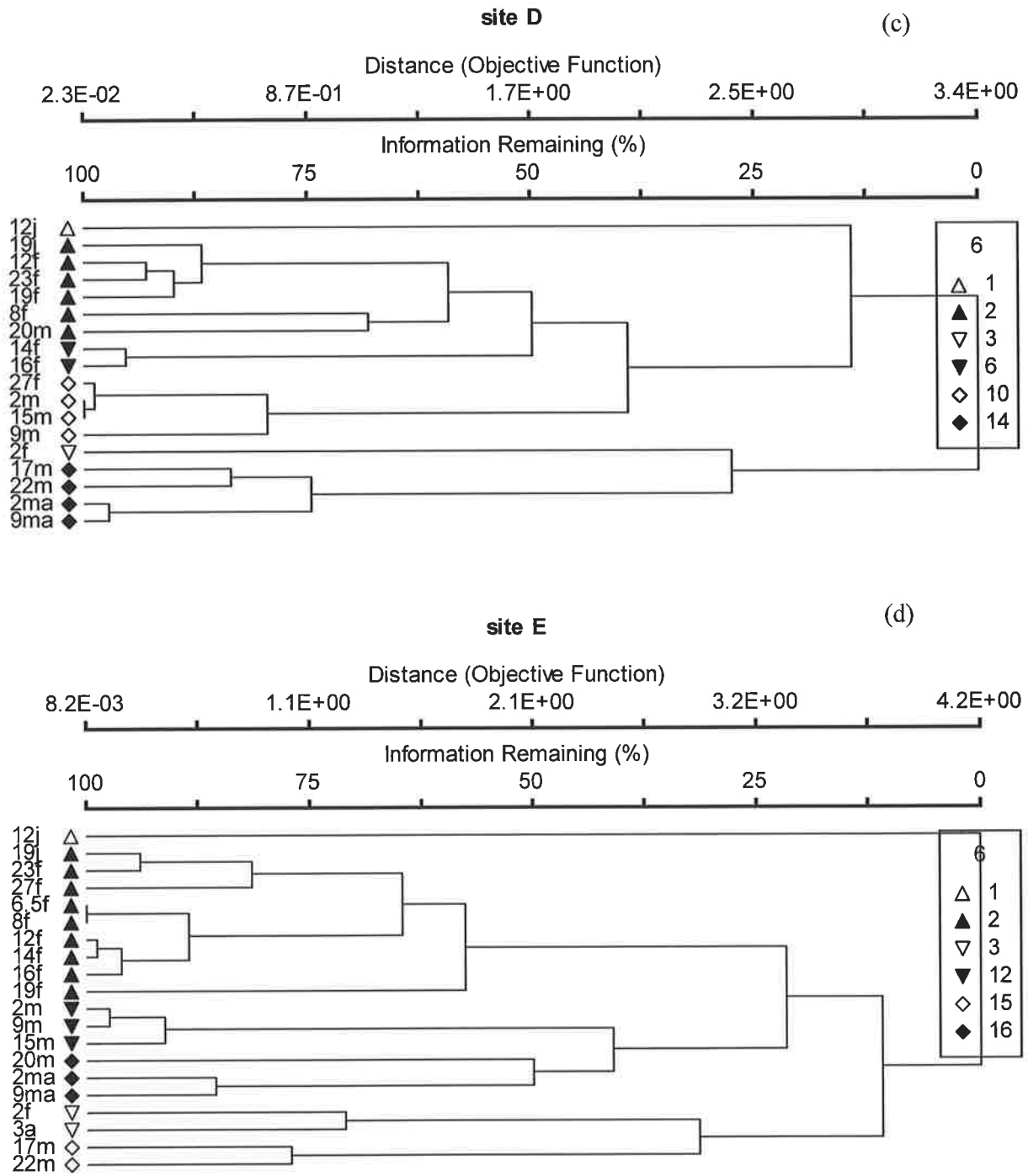


Figure 7.22 Dendrogram date groupings based upon species composition at sites D (c) and E (d). At site D, 6 groups were identified and the $mrpp = 0.0005124$. At site E, 6 groups were identified and the $mrpp = 0.0000016$.

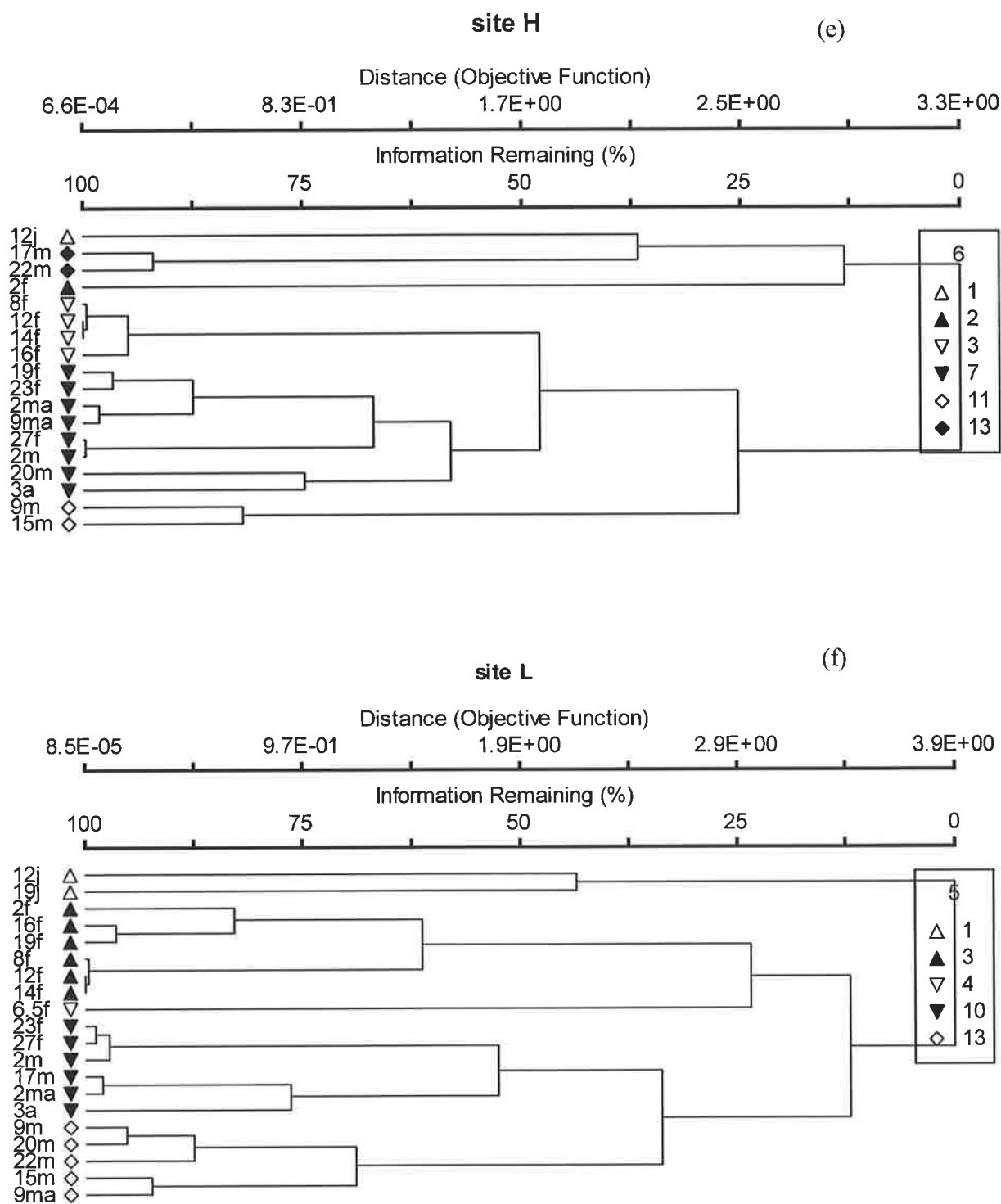


Figure 7.22 Dendrogram date groupings based upon species composition at sites H (e) and L (f). At site H, 6 groups were identified and the mrpp = 0.0000238. At site L, 5 groups were identified and the mrpp = 0.0000140.

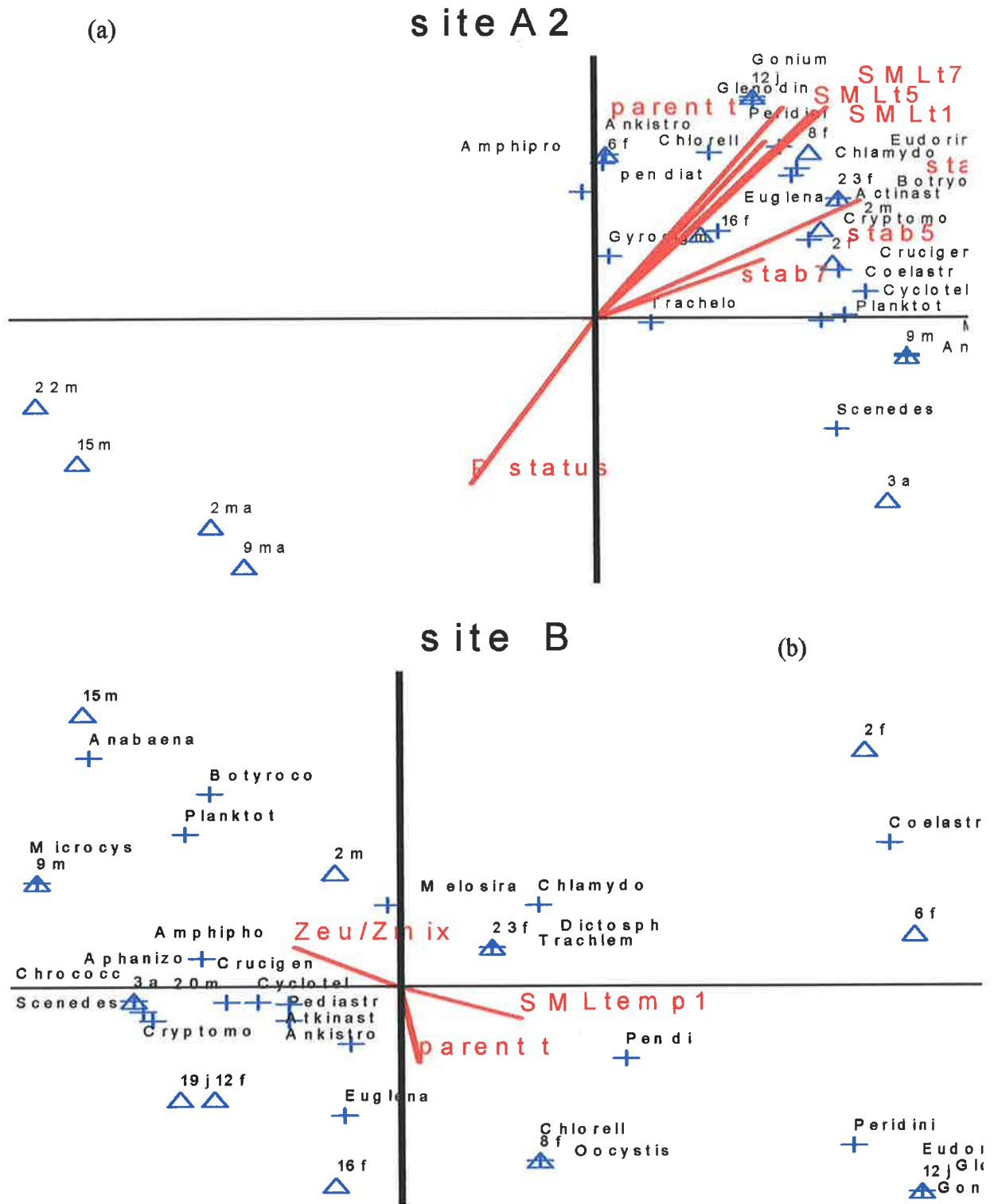


Figure 7.23 Ordination of phytoplankton community composition and cardinal points for sites A₂ (a) and B (b). At site A₂, $r^2 = 0.3$, final stress for 2-D solution = 9.32, final stability = 0.0029 (42 iterations). At site B, $r^2 = 0.25$, final stress for 2-D solution = 13.85, final stability = 0.0049 (40 iterations). Note: triangles = dates, where j = January, f = February, m = March, a = April and ma = May and crosses = species.

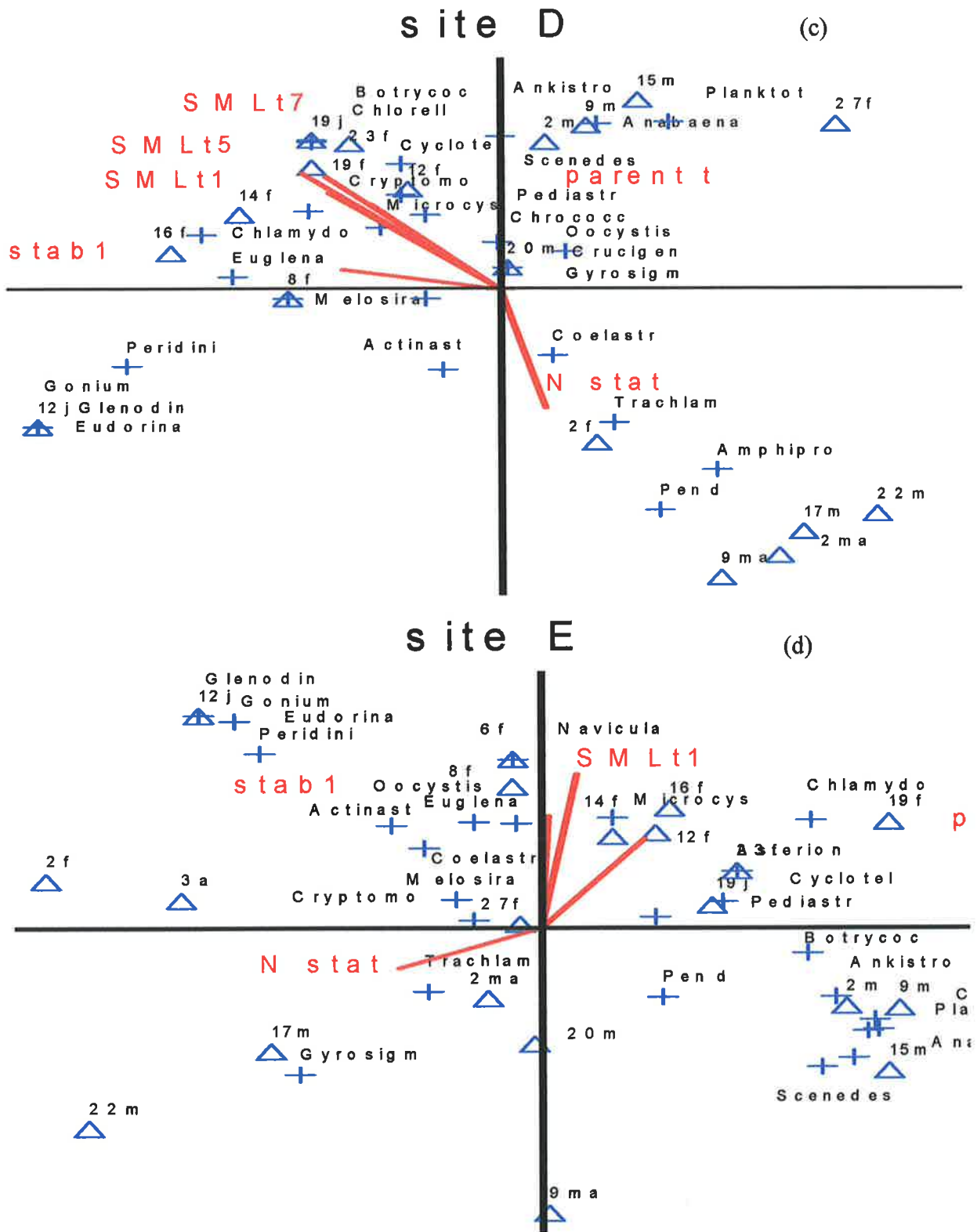


Figure 7.23 Ordination of phytoplankton community composition and cardinal points for sites D (c) and E (d). At site D, $r^2 = 0.3$, final stress for 2-D solution = 13.7, final stability = 0.0037 (21 iterations). At site E, $r^2 = 0.3$, final stress for 2-D solution = 13.7, final stability = 0.0047 (37 iterations). Note: triangles = dates, where j = January, f = February, m = March, a = April and ma = May and crosses = species.

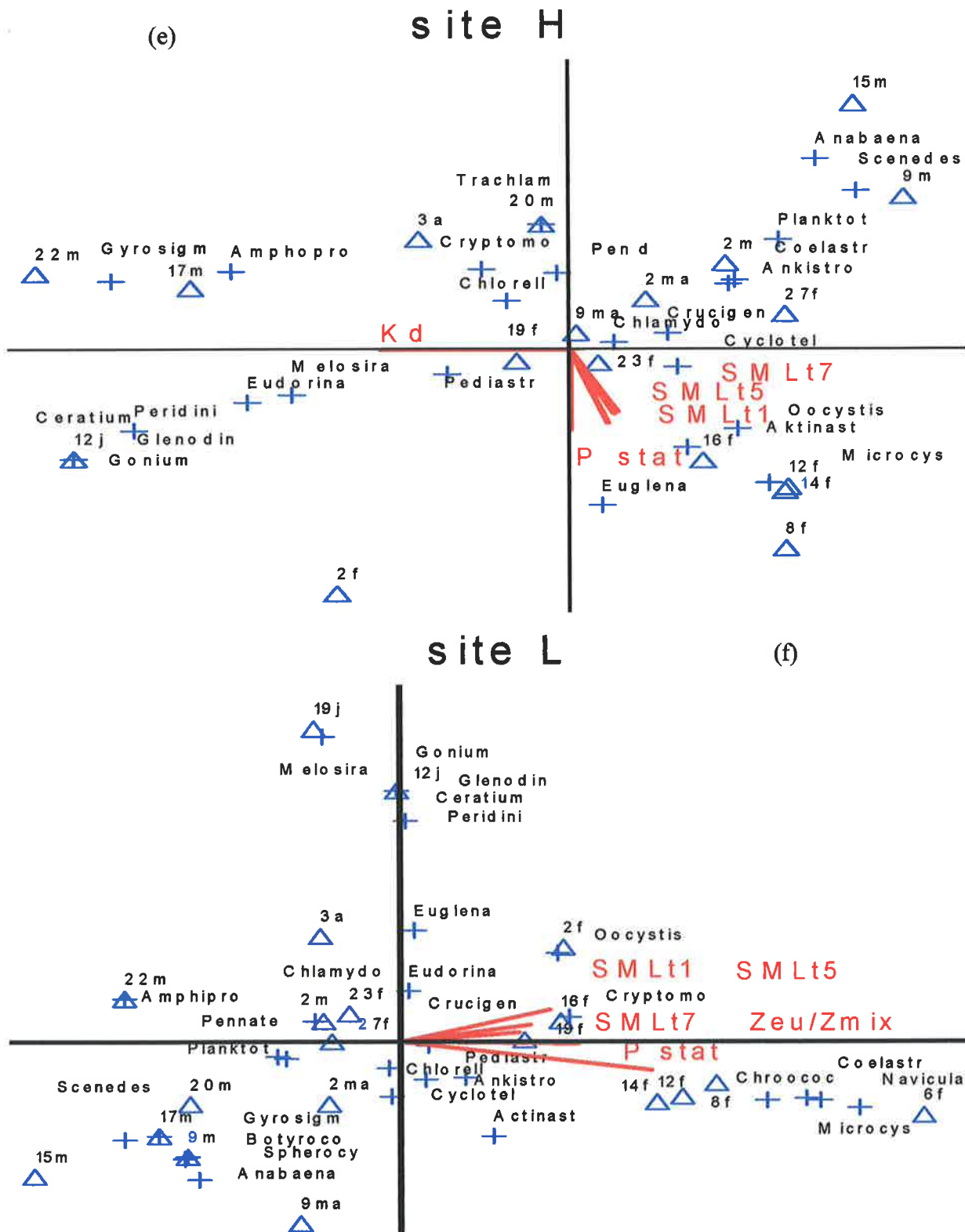


Figure 7.23 Ordination of phytoplankton community composition and cardinal points for sites H (e) and L (f). At site H, $r^2 = 0.25$, final stress for 2-D solution = 13.3, final stability = 0.0033 (19 iterations). At site L, $r^2 = 0.25$, final stress for 2-D solution = 13.19, final stability = 0.0033 (57 iterations). Note: triangles = dates, where j = January, f = February, m = march, a = April and ma = May and crosses = species.

Chapter 8

General summary and discussion

8.1 Phytoplankton and turbulence

This thesis investigated the influence of turbulence and disturbance on phytoplankton, at the physiological, population and community scales. Physical forcing governs the shape of the pelagic environment, the extent and duration of mixing or stratification and generates the motions that transport organisms and substances both vertically and horizontally. The transport (or lack of it) influences the access of phytoplankton to resources and consequently affects the rate of biological processes. The generation time of phytoplankton in relation to the scales of physical variability means that phytoplankton respond at all levels from the physiological to the assemblage.

The aims of the thesis were to firstly widen the application of flow cytometry and fluorometry in freshwater phytoplankton ecology. Secondly, to use this technology to explore the impact of large scale physical processes including wind-induced mixing on cell photo-physiology, entrainment and distribution and also discern the significance of small-scale shear on cell activity and viability. Physical processes often constitute major disturbances and the thesis investigated phytoplankton spatial and temporal heterogeneity of an urban lake to explore the applicability of the intermediate disturbance hypothesis.

8.2 Biological techniques and field studies

A major requirement in studying the relationship between environmental variability and physiological processes is the ability to sample and analyse biological components at appropriate

temporal and spatial scales. Biological techniques need to address time scales similar to the scales of physical processes (minutes to hours). Moreover, the greater the speed of measurement, the greater the number of possible sampling sites, which results in an increase in spatial resolution. The first component examined the reliability of flow cytometry in combination with fluorescent stains (FDA, Sytox) to detect the response of phytoplankton to environmental variability. The staining protocols of FDA and Sytox were optimized for several freshwater phytoplankton, for their ability to quantify cell metabolic activity and viability, respectively. The magnitude of stain fluorescence was dependent upon the species, the stain concentration and loading time. Sytox staining time was less species-dependent. 'Activity' and 'viability' states were established and enabled a comparison between the two stains to quantify cell viability. Using *M. aeruginosa*, Sytox stain was found to be more accurate than FDA in determining the number of nonviable cells.

Preliminary experiments involving nutrient limitation/ repletion and copper toxicity demonstrated that the two stains could be used to measure phytoplankton metabolic activity and viability in bioassays. The techniques were applied to natural phytoplankton in the Myponga Reservoir, to determine whether turbulence below the surface mixer or away at depth (i.e. 70 m) caused any deleterious impacts on phytoplankton in the short term. No discernible affect was detected, which is consistent with the fact that the reservoir is exposed to wind mixing and consequently the phytoplankton community is composed of species that are tolerant to turbulent mixing and associated factors (e.g. shear, light). A finding that is consistent with the modeling approach adopted by Lewis *et al.* (*in press*) who demonstrated that artificial mixing using surface mixers had no significant affect on phytoplankton composition within Myponga Reservoir.

Flow cytometry enables the measurement of metabolic activity of individual cells and consequently is an ideal tool to discern small-scale shear effects on phytoplankton. The oscillating grid study involving *M. aeruginosa* (chapter 6), revealed that small-scale shear affected cell metabolic activity and viability. At low turbulent intensities, metabolic activity was stimulated whereas at high intensities, metabolic activity and cell viability decreased. The use of fluorescent stains for selective physiological processes and flow cytometry hold great potential in assessing the role and significance of small-scale shear in phytoplankton ecology. Specific areas

include the assessment of the species sensitively to turbulence hypothesis of Thomas and Gibson (1990) and the role of turbulence in facilitating nutrient uptake.

The bench flow cytometer used in this study restricted its application in field studies. However, as new technologies such as Cytobuoy (Dubelaar and Gerritzen, 2000) become more readily available, the influence of turbulence and artificial mixing systems on phytoplankton activity and cell size (or filament length) will become more accurately gauged. In chapter 4, modeling demonstrated that colony size (and similarly filament length) influenced *M. aeruginosa* entrainment and distribution, which has implications for artificial mixing strategies (discussed below). Moreover, the incorporation of stains which measure N-fixation with flow cytometry will enable further testing of the theory that the presence of heterocystic cyanobacteria is inversely related to turbulent mixing (e.g. Paerl 2000).

The second component of biological techniques explored involved active PAM fluorometry. Preliminary experiments demonstrated that the photo-physiology parameters of photochemical quenching, maximum quantum yield of PS2 and absorption cross-section responded to light intensity, duration of exposure to illumination and nutrient status of phytoplankton. In particular, the magnitude of F_v/F_m was dependent upon light intensity and dose and provided a feature of phytoplankton that could be traced to assess the impacts of turbulent mixing and or thermal stratification on cell entrainment and distribution. Light intensities $> 400 \mu\text{mol m}^{-2} \text{s}^{-1}$ and nitrogen and phosphorus deficiency decreased F_v/F_m , while the absorption cross-section also decreased with nitrogen deficiency as reported earlier (Kolber *et al.*, 1988). The ultimate test of a technique involves its application to field populations under natural conditions. Fluorometry enabled the determination of photosynthesis integrated over depth and time for a Myponga field population. The technique in combination with the Walsby (1997) model, enabled measurement of the productivity of the reservoir. Such measurements allow water supply authorities to determine reservoir carbon budgets and deduce the influence of carbon compounds on water treatment processes (Bertilsson and Jones, 2003; Linden, 2003).

The Torrens Lake studies used fluorometry to provide a link between the interplay of wind mixing, thermal stratification, cell motility, distribution and photosynthesis. In chapter 3, the

Peridinium cinctum study revealed that this species migrates vertically within a shallow lake, ascending in the morning and descending in the afternoon at swimming velocities ranging between $1.48 \times 10^{-4} \text{ m s}^{-1}$ and $5.37 \times 10^{-4} \text{ m s}^{-1}$. Cell vertical distribution was a function of wind speed and swimming velocity. Measurements of F_v/F_m of *P. cinctum* cells through time and depth showed minimal photoinhibition, despite cells actively avoiding high irradiance at the surface of the lake. The minor depression of F_v/F_m in surface samples and recovery to initial values later in the day, contrasts with the results in chapter 2 and *M. aeruginosa* in chapter 4, which generally displayed major depressions with high light intensities. A comparison between modeled daily photosynthetic rates of the *in situ* migrating population ($2.6 \text{ g O}_2 \text{ m}^{-2}$) and a theoretical homogenous population under isothermal conditions ($3.1 \text{ g O}_2 \text{ m}^{-2}$) revealed that migration did not increase photosynthetic production. Consequently, it was postulated that although phototaxis plays a major role in vertical migration, dinoflagellates move deeper in the water column to avoid small-scale shear stress generated in the surface mixed layer. Moreover, the Torrens Lake monitoring study (chapter 7) revealed that *Peridinium* and *Glenodinium* were aligned to the presence of a persistent parent thermocline and higher surface mixed layer water temperatures (figure 7.23).

In chapter 4, the photosynthetic capacity of cells was also used to determine the previous light history of *M. aeruginosa* colonies. As insolation increased the Torrens Lake stratified and colonies displayed a depression in F_v/F_m , which became less severe with depth. In the afternoon, wind speed increased entraining colonies and disrupting the discrete depth variable F_v/F_m response. The point where the photochemical response became homogenized enabled the determination of the shear velocity necessary to entrain colonies. Rates of F'_v/F'_m depression were light intensity dependent whereas recovery was dependent upon light dose. Modeling the response of F'_v/F'_m to different mixing scenarios demonstrated the importance of factors such as colony size, wind speed, mixed layer depth and transport time in cyanobacterial ecology. Simulations revealed that as the surface mixed layer is deepened, F'_v/F'_m recovers compared to a shallow surface mixed layer. Similarly, in the case of nocturnal mixing and stratification at dawn, the shallower the starting depth of a colony, the greater the depression in F'_v/F'_m , compared to cells deeper in the water column. If colony size is increased, heterogeneity in F'_v/F'_m responses is decreased, due to the faster floating velocities of larger colonies. In turbulent water where the euphotic depth is less than the mixed depth and transport rates are high, there is insignificant

depression in F'_v/F'_m . But as transport rates decrease as may occur as a water body receives more heat, cells or colonies at the surface will display greater depression. Moreover, this depression in near surface colonies will be exacerbated, if the mixed depth increases relative to the transport rate as occurs in the ocean or highly attenuated inland waters.

The two field studies involving active fluorometry demonstrated the usefulness of the technique to increase the temporal resolution between physical mixing and biological processes (e.g. photosynthesis, entrainment). The technique is fast, non-invasive and can be readily applied in field studies. With faster measurements, more accurate assessments of photosynthesis and productivity can be made and at the same time take into account the influence of wind mixing or stratification on cell distribution and subsequently availability to light. Such resolution is particularly useful for hydrodynamic-phytoplankton models.

Fluorometry and flow cytometry are powerful tools in marine research. However, their application and potential in inland waters and estuaries has yet to be reached. An immediate useful application of fluorometry includes the influence of 'disturbance' and storm water nutrient replenishment on productivity in the Torrens Lake. Bergmann *et al.* (2002) used active fluorometry to study the influence of light and nutrients on the photosynthetic efficiency of phytoplankton in the Neuse River Estuary. The measurement of F'_v/F'_m detected nutrient limitation during periods of prolonged stratification. As also discussed by Beardall *et al.* (2001b), photochemical efficiency is useful to assess nutrient limitation and may assist in Torrens Lake studies to rapidly assess the limiting nutrient (s) in relation to catchment rainfall. A second domestic application involves the role of flow in the lower Murray River and the development and or productivity of problematic phytoplankton such as *Nodularia*. As river flow decreases, salinity levels increase and thermal stratification develops which may favour the growth of *Nodularia*. As reported elsewhere (Brookes *et al.*, 2002), flow cytometry and fluorescent stains have applicability to other research areas including ecotoxicology (e.g. Regel *et al.*, 2002), measurement of cyanobacterial buoyancy (Brookes *et al.*, 2000b) and dark survivorship studies (Jochem, 1999) which may be useful in artificial mixing trials involving intrusions and phytoplankton.

8.3 Phytoplankton entrainment and implications

Much of the ecology of phytoplankton is between the two extremes of being fully entrained in a deep turbulent mixed layer to disentrained under stratified conditions. The high degree of variability in meteorological forcing ensures that phytoplankton composition is liable to change as a result of the suspension characteristics of individual species. Whether the cell sinks, floats or swims, its position is constantly liable to readjustment and access to resources. The entrainment criterion determines the relationship between intrinsic velocity of the species and the mean velocity of the shear. It plays a major role in the population dynamics of phytoplankton in water bodies, which are subject to intermittent stratification and mixing, experience patchy meteorological forcing or in the case of rivers, high and low flows. Non-motile species, which require mixing for suspension, may incur significant losses under abrupt periods of stratification. Conversely, the advantages afforded to motile species such as *Peridinium* and *Microcystis* may be negated when lake stability decreases. The entrainment model, detailed in Reynolds (1994a) was investigated for both *Peridinium* and *Microcystis*. *Peridinium* cell distribution was a function of wind speed and associated shear velocity and swimming velocity. When, $\psi < 1$, distribution was dominated by wind speed and when $\psi > 1$, distribution was dominated by swimming velocity. The field observations verified the threshold of one within the model and a shear velocity of $>8.1 \times 10^{-3} \text{ m s}^{-1}$ to entrain *Peridinium*. In contrast to *Peridinium*, the shear velocity necessary to entrain *Microcystis* colonies was determined by the homogeneity in F_v/F_m response. The point where the photochemical response became homogenized under the set of wind conditions revealed that a shear velocity of $3.0 \times 10^{-3} \text{ m s}^{-1}$ was sufficient to entrain colonies with a mean radius of $53.6 \mu\text{m}$. Increasingly, the quantification of current and shear velocity is useful to explain community dynamics (Mitrovic *et al.*, 2003; Kawara *et al.*, 2001) and also has implications for management of cyanobacteria using artificial mixing. Interestingly, Mitrovic *et al.* (2003) report that a shear velocity of between $2.66\text{--}2.91 \times 10^{-3} \text{ m s}^{-1}$ coincided with the absence of *Anabaena* in the Murray River, which is of the same order to entrain *Peridinium* and *Microcystis*. As discussed in chapter 4, strategies that increase entrainment of cyanobacteria from the water surface and deepen the surface mixed layer may offer an additional management tool to complement traditional bubble plume aerator devices. Furthermore, research by O'Brien *et al.* (in review) shows that the degree of disaggregation of *Microcystis* colonies is a function of turbulent dissipation which may influence the entrainment and vertical distribution of colonial species

under different mixing regimes. Specifically, if a *Microcystis* colony or *Anabaena* filament disaggregates, the smaller colonies/ filaments/ cells may be entrained at a lower shear velocity and may take longer to recover from a deep mixing event (chapter 4). Factors such as colony/ filament strength, vulnerability to shear stress, entrainment, the depth of the surface mixed layer, and in combination with hydrodynamic modeling need to be further explored.

8.4 Turbulent intensity and phytoplankton

In natural systems, the effects of small-scale shear cannot be separated from those of other factors such as light and nutrients, which makes it difficult to investigate or determine the significance of direct effects on phytoplankton. Reynolds (1994a) states, "It is not the intensity of turbulence, but rather its extent and duration which affects algae". The extent or depth of mixing and duration or intermittency to mixing stratification strongly influences phytoplankton physiology and community composition. But, the degree of uncertainty of turbulent intensity in the field, and the lack of studies involving small-scale shear and freshwater phytoplankton led to the quantification of turbulent intensity around artificial mixing devices (chapter 5) and exposure of *M. aeruginosa* to grid-generated turbulence (chapter 6). Flow velocity sampling using an acoustic Doppler velocimeter around the Myponga Reservoir surface mixers and the Torrens Lake aeration systems, not only assisted in determining their operation characteristics, but also the shear velocities and turbulent kinetic energy dissipation rates generated. Shear velocities and turbulent kinetic energy dissipation rates were found to be high and ranged from $5.9 \times 10^{-3} \text{ m s}^{-1}$ to $7.9 \times 10^{-2} \text{ m s}^{-1}$ and $5 \times 10^{-7} \text{ m}^2 \text{ s}^{-3}$ to $3.6 \times 10^{-3} \text{ m}^2 \text{ s}^{-3}$, respectively (table 5.4). Exposing *M. aeruginosa* to high turbulent intensities ($> 3 \text{ Hz}$) within the oscillating grid tank, deleteriously affected metabolic activity and viability. The long exposure time of 96 hours to cause an effect and the likely short exposure times around artificial mixing systems in freshwaters verifies Reynolds's statement, and suggests that despite the inhibitory effects, small-scale shear is not likely to be a major factor controlling the development of blooms. Phytoplankton ecology can be better explained as a result of large-scale mixing processes and the physiological responses of the phytoplankton.

8.5 Lake management

Water supply and the health of aquatic systems are increasingly being recognized as crucial, immediate and inexplicitly linked global issues. To ensure long-term water supplies and ecosystem health, requires an understanding of the biological, chemical and physical processes and the temporal and spatial scales of their interaction. The Torrens Lake has similar problems to many lakes in the world, with development in its upper catchment, clearance of vegetation and hard surfacing, concentration of nutrients into storm water, flow regulation and cyanobacterial blooms. The management of lakes such as the Torrens, is complicated by the time scales over which physical, chemical and biological processes occur. Time-scales can range from sub-daily, such as large rain events, to seasonal changes in stratification, temperature and chemical concentrations. In chapter 7, the Torrens Lake monitoring study, demonstrated firstly the high degree of spatial and temporal heterogeneity in phytoplankton composition and secondly the difficulty in managing water body, which is prone to stochastic meteorological forcing and associated storm water runoff.

The phytoplankton community consisted of a diverse number of genera composing of C-S-R strategists. Although, there is no single factor controlling phytoplankton dynamics, summer storm events comprising of increased wind mixing and nutrient replenishment with rainfall acted to disturb the phytoplankton community. After a lag of approximately 7-10 days, such events increased diversity and the number of genera. Nutrient replenishment also enabled problematic cyanobacterial species to develop. Allogenic selection processes were more important than autogenic selection processes as the community was highly dynamic. The response of the phytoplankton community to disturbances was consistent with the intermediate disturbance hypothesis of Connell (1978). Despite the study being limited by not evaluating zooplankton grazing pressure or internal nutrient recycling, it does suggest that the brief summer rainfall events 'trigger' cyanobacterial blooms. This indicates that cyanobacteria are limited by nutrients as opposed to light conditions, and due to the shallowness of the lake, artificial mixing strategies are inappropriate.

The role of hydrodynamics and specifically turbulence in controlling biochemical and ecosystem activity has long been recognized. However, a recent discussion paper by the American Society of Limnology and Oceanography (ASLO, 2003) has identified that future research needs to further couple hydrodynamics with limnology. This thesis has concentrated on the primary producers of the aquatic ecosystem. The development, wider and co-occurring application of technologies such as flow cytometry, fluorometry, current velocity meters and meteorological instrumentation will further improve our understanding of aquatic systems.

Bibliography

- Aguilera J, Jimenez C, Rodriguez-Maroto JM and Niell FX (1994) Influence of subsidiary energy on growth of *Dunaliella viridis* Teodoresco: the role of extra energy in algal growth. *Journal of Applied Phycology* **6**, 323-330.
- Agusti S, Satta MP, Mura MP and Benavent E (1998) Dissolved esterase activity as a tracer of phytoplankton lysis: Evidence of high phytoplankton lysis rates in the northwestern Mediterranean. *Limnology and Oceanography* **43**, 1836-1849.
- Agusti S and Durarte CM (2000) Strong seasonality in phytoplankton cell lysis in the NW Mediterranean littoral. *Limnology and Oceanography* **45**, 940-947.
- Agusti S and Sanchez MC (2002) Cell viability in natural phytoplankton communities quantified by a membrane permeability probe. *Limnology and Oceanography* **47**, 818-828.
- American Society for Limnology and Oceanography, ASLO (2003) *Emerging research issues for limnology: The study of inland waters*. Draft proceedings of the NSF/ASLO workshop, February 2003.
- Arsenault G, Cvetkovic AD and Popovic R (1993) Toxic effects of copper on *Selenastrum capricornutum* measured by a flow cytometry-based method. *Water Pollution Research Journal of Canada* **28**, 757-765.
- Ault TR (2000) Vertical migration by the marine dinoflagellate *Prorocentrum triestinum* maximises photosynthetic yield. *Oecologia* **125**, 466-475.
- Barbiero RP, James WF and Barko JW (1999) The effects of disturbance events on phytoplankton community structure in a small temperate reservoir. *Freshwater Biology* **42**, 503-512.
- Batchelor GK (1967) *The Theory of Homogeneous Turbulence* (5th edn.). Cambridge University Press, Cambridge.
- Bazzaz FA (1996) *Plants in Changing Environments: linking Physiological, Population, and Community Ecology*. Cambridge University Press, Cambridge.
- Beardall J, Berman T, Heraud P, Kadiri MO, Light BR, Patterson G, Roberts S, Sulzberger B, Sahan E, Uehlinger U and Wood B (2001a) A comparison of methods for detection of phosphate limitation in microalgae. *Aquatic Science* **63**, 107-121.
- Beardall J, Young E and Roberts S (2001b) Approaches for determining phytoplankton nutrient limitation. *Aquatic Science* **63**, 44-69.
- Bentley-Mowat JA (1982) Application of fluorescence microscopy to pollution studies on marine phytoplankton. *Botanica Marina* **25**, 203-204.
- Berdalet E (1992) Effects of turbulence on the marine dinoflagellate *Gymnodinium nelsonii*. *Journal of Phycology* **28**, 267-272.
- Berdalet E and Estrada M (1993) Effects of turbulence on several dinoflagellate species. *In Toxic Phytoplankton in the Sea*. Eds. Smayda TJ and Shimizu Y, Elsevier Science Publications, Amsterdam, pp. 737-741.

- Berges JA and Falkowski PG (1998) Physiological stress and cell death in marine phytoplankton: Induction of proteases in response to nitrogen or light limitation. *Limnology and Oceanography* **43**, 129-135.
- Berglund DL and Eversman S (1988) Flow cytometric measurement of pollutant stresses on algal cells. *Cytometry* **9**, 150-155.
- Bergmann T, Richardson TL, Paerl H, Pinckney JL and Schofield O (2002) Synergy of light and nutrients on the photosynthetic efficiency of phytoplankton populations from the Neuse River Estuary, North Carolina. *Journal of Plankton Research* **24(9)**, 923-933.
- Bertilsson, S and Jones, JB (2003) Supply of dissolved organic matter to aquatic ecosystems: autochthonous sources. In *Aquatic Ecosystems: Interactivity of Dissolved Organic Matter*. Eds. Findlay SEG and Sinsabaugh RL, Elsevier Science, New York, pp. 512.
- Beutel MW and Horne AJ (1999) A review of the effects of hypolimnetic oxygenation on lake and reservoir water quality. *Journal of Lake and Reservoir Management* **15**, 285-297.
- Blasco D (1978) Observations on the diel migration of marine dinoflagellates off the Baja California coast. *Marine Biology* **46**, 41-47.
- Brookes JD (1997) The influence of nutrients and light on the metabolic activity and buoyancy of *Microcystis aeruginosa* and *Anabaena circinalis*. PhD thesis, University of Adelaide, Adelaide.
- Brookes JD, Ganf GG and Burch MD (1998) Buoyancy regulation of *Microcystis aeruginosa*. *Verhandlungen Internationale Vereinigung for Theoretische und Angewandte Limnologie*. **26**, 1670-1673.
- Brookes JD, Ganf GG, Green D and Whittington J (1999) The influence of light and nutrients on buoyancy, filament aggregation and flotation of *Anabaena circinalis*. *Journal of Plankton Research* **21**, 327-341.
- Brookes JD, Geary SM, Ganf GG and Burch MD (2000a) Use of FDA and flow cytometry to assess metabolic activity as an indicator of nutrient status in phytoplankton. *Marine and Freshwater Research* **51**, 817-823.
- Brookes JD, Ganf GG and Oliver RL (2000b) Heterogeneity of cyanobacterial gas vesicle volume and metabolic activity: an explanation for differential buoyancy status of field populations. *Journal of Plankton Research* **22**, 1579-1589.
- Brookes J, Burch MD and Tarrant P (2000c) Artificial destratification: evidence for improved water quality. *Water* **27**, 18-22.
- Brookes JD and Ganf GG (2001) Variations in the buoyancy response of *Microcystis aeruginosa* to nitrogen, phosphorous and light. *Journal of Plankton Research* **32**, 1399-1411.
- Brookes JD, Regel RH, Ganf GG and Burch MD (2002) Applications of flow cytometry to phytoplankton research. *Verhandlungen Internationale Vereinigung for Theoretische und Angewandte Limnologie* **28**, 1-6. 1311-1316
- Brookes JD, Regel RH and Ganf GG (*in press*) Changes in the photochemistry of *Microcystis aeruginosa* in response to light and mixing. *New Phytologist*.
- Brookes JD, Baker P, Burch MD, Ganf GG, Lewis DL and Hartley K (*in preparation*). Management of cyanobacteria in a shallow urban lake: assessing the options.

- Brussard CPD, Marie D, Thyraug R and Bratbak G (2001) Flow cytometric analysis of phytoplankton viability. *Aquatic Microbial Ecology* **26**, 157-166.
- Brussard CPD, Riegman R, Noordeloos AAM, Cadee GC, Witte H, Kop AJ, Nieuwland G, Duyl FCV and Bak RPM (1995) Effects of grazing, sedimentation and phytoplankton cell lysis on the structure of a coastal pelagic food web. *Marine Ecology Progress Series* **123**, 259-271.
- Buranathanitt T, Cockrell DJ and John PH (1982) Some effects of Langmuir circulation on the quality of water resource systems. *Ecological Modelling* **15**, 49-74.
- Burch MD, Brookes JD, Tarrant P and Dellaverde P (2000) Mixing it up with blue-green algae. *Water* **27**, 21-24.
- Cachot J, Romana LA and Galgani F (1994) *In vivo* esterase activity in protoplasts as a bioassay of environmental quality. *Aquatic Botany* **48**, 297-312.
- Campbell D, Hurry V, Clarke AK, Gustafsson P and Oquist G (1998) Chlorophyll fluorescence analysis of cyanobacterial photosynthesis. *Microbiology and Molecular Biology Reviews* **62**, 667-683.
- Chorus I and Schlag G (1993) Importance of intermediate disturbances for the species composition and diversity of phytoplankton in two very different Berlin lakes. *Hydrobiologia* **249**, 67-92.
- Connell JH (1978) Diversity in tropical rain forests and coral reefs. *Science* **199**, 1302-1310.
- Cox JD, Padley MB and Hannon J (1998) Use of computational fluid dynamics to model reservoir mixing and destratification. *Water Science and Technology* **37**, 227-234.
- Daldorph PWG (1998) Management and treatment of algae in lowland reservoirs in Eastern England. *Water Science and Technology* **37**, 57-63.
- Demmig-Adams B and Adams WW (1992) Photoprotection and other responses of plants to high light stress. *Plant Physiology and Plant Molecular Biology* **43**, 599-626.
- Denman KL and Gargett AE (1983) Time and space scales of vertical mixing and advection of phytoplankton in the upper ocean. *Limnology and Oceanography* **28**, 801-815.
- Dorsey J, Yentsch CM, Mayo S and McKenna C (1989) Rapid analytical technique for the assessment of cell metabolic activity in marine microalgae. *Cytometry* **10**, 622-628.
- Dubelaar GBJ and Gerritzen PL (2000) Cytobuoy: a step forward towards using flow cytometry in operational oceanography. *Scientia Marina* **64(2)**, 255-265.
- Dubinsky Z (1992) The functional and optical absorption cross-section of phytoplankton photosynthesis. In *Primary Productivity and Biochemical Cycles in the Sea*. Eds. Falkowski PG and Woodhead AD, Plenum Press, New York.
- Edson JJ and Jones RC (1988) spatial, temporal, and storm runoff-related variations in phytoplankton community structure in a small, suburban reservoir. *Hydrobiologia* **169**, 353-362.
- Elliot JA, Irish AE and Reynolds CS (2001) The effects of vertical mixing on a phytoplankton community: a modeling approach to the intermediate disturbance hypothesis. *Freshwater Biology* **46**, 1291-1297.

- Eloranta P and Raike A (1995) Light as a factor affecting the vertical distribution of *Gonyostomum semen* (Ehr) Diesing (Raphidophyceae) in lakes. *Aqua Fenn* **25**, 15-22.
- Eppley RW (1980) Estimating phytoplankton growth rates in the central oligotrophic oceans. In *Primary Productivity in the Sea*. Ed. Falkowski PG, Plenum Press, New York, pp. 231-242.
- Estrada M and Berdalet E (1997) Phytoplankton in a turbulent world. *Scientia Marina* **61**, 125-140.
- Estrada M and Berdalet E (1998) Effects of turbulence on phytoplankton. In *Physiological Ecology of Harmful Algal Blooms*. Eds. Anderson DM, Cembella AD and Hallegraeef GM, Springer-Verlag Berlin, Heidelberg, NATI AS1 Series G41, pp. 601-618.
- Falconer IR, Burch MD, Steffenson DA, Choice M and Coverdale OR (1994) Toxicity of the blue-green alga (cyanobacterium) *Microcystis aeruginosa* in drinking water to growing pigs, as an animal model for human injury and risk assessment. *Journal of Environmental Toxicology and Water Quality* **9**, 131-139.
- Falkowski PG and Kolber Z (1995) Variations in chlorophyll fluorescence yields in phytoplankton in the world oceans. *Australian Journal of Plant Physiology* **22**, 341-355.
- Faller AJ (1971) Oceanic turbulence and the Langmuir circulation. *Annual Review of Ecological Systems* **2**, 201-236.
- Ferris JM and Christian R (1991) Aquatic primary production in relation to microalgal responses to changing light: a review. *Aquatic Sciences* **53**, 187-217.
- Flameling A and Kromkamp J (1997) Photoacclimation of *Scenedesmus proturbans* (Chlorophyceae) to fluctuating irradiances simulating vertical mixing. *Journal of Plankton Research* **19**, 1011-1024.
- Fogg GE (1991) Tansley review No. 30: the phytoplankton ways of life. *New Phytologist* **118**, 191-232.
- Fogg GE and Than-Tun (1960) Interrelations of photosynthesis and assimilation of elementary nitrogen in a blue green alga. *Proceedings of Royal Society of London B* **153**, 111-127.
- Franklin NM, Adams MS, Stauber JL and Lim RP (2001) Development of an improved rapid enzyme inhibition bioassay with marine and freshwater microalgae using flow cytometry. *Archives of Environmental Contamination and Toxicology* **40**, 469-480.
- Frisch U (1996) *Turbulence*. Cambridge University Press, Cambridge.
- Gala WR and Giesey JP (1994) Flow cytometric determination of the photoinduced toxicity of anthracene to the green alga *Selenastrum capricornutum*. *Environmental Toxicology and Chemistry* **13**, 831-840.
- Galleron C (1976) Synchronization of the marine dinoflagellate *Amphidinium carterae* in dense cultures. *Journal of Phycology* **12**, 69-73.
- Ganf GG (1974) Diurnal mixing and the vertical distribution of phytoplankton in a shallow equatorial lake (Lake George, Uganda). *Journal of Ecology* **62**, 611-629.
- Ganf GG, Brookes JD, Linden L, Hodgson C and Burch MD (*in preparation*) Luxury nutrient uptake sustains a *Microcystis* bloom in a shallow urban lake (the Torrens Lake, South Australia).

- Ganf GG and Oliver RL (1982) Vertical separation of light and available nutrients as a factor causing replacement of green algae by blue-green algae in the plankton of a stratified lake. *Journal of Ecology* **70**, 829-844.
- Gargett AE (1997) "Theories" and techniques for observing turbulence in the ocean euphotic zone. *Scientia Marina* **61**, 25-45.
- Gargett AE, Sanford TB and Osborn TR (1979) Surface mixing layers in the Sargasso Sea. *Journal of Physical Oceanography* **9**, 1090-1111.
- Geary S, Ganf GG and Brookes JD (1997) The use of FDA and flow cytometry to measure the metabolic activity of the cyanobacteria *Microcystis aeruginosa*. *Verhandlungen der Internationale Vereinigung für Theoretische und Angewandte Limnologie* **26**, 2367-2369.
- Geider RJ, La Roche J, Greene RM and Olaizola M (1993) Response of the photosynthetic apparatus of *Phaeodactylum tricoratum* (Bacillariophyceae) to nitrate, phosphate, or iron starvation. *Journal of Phycology* **29**, 755-766.
- Genty B, Briantais JM and Baker NR (1989) The relationship between the quantum yield of photosynthetic electron transport and quenching of chlorophyll fluorescence. *Biochimica et Biophysica Acta* **990**, 87-92.
- George R, Flick RE and Guza RT (1994) Observations of turbulence in the surf zone. *Journal of Geophysical Research* **99**, 801-810.
- Gibson CH and Thomas WH (1995) Effects of turbulence intermittency on growth inhibition of a red tide dinoflagellate, *Gonyaulax polyedra* Stein. *Journal of Geophysical Research* **100**, 841-846.
- Greene RM, Kolber ZS, Swift DG, Tindale NW and Falkowski PG (1994) Physiological limitation of phytoplankton photosynthesis in eastern equatorial Pacific determined from variability in the quantum yield of fluorescence. *Limnology and Oceanography* **39**, 1061-1074.
- Grime JP (1979) *Plant Strategies and Vegetation Processes*. Wiley-Interscience, Chichester.
- Gross TF, Williams AJ and Terray EA (1994) Bottom boundary layer spectral dissipation estimates in the presence of wave motions. *Continental Shelf Research* **14**, 1239-1256.
- Grover JP (1988) Dynamics of competition in a variable environment: experiments with two diatom species. *Ecology* **69**, 408-417.
- Guanzon NG, Nakahara H and Yoshida Y (1994) Inhibitory effects of heavy metals on growth and photosynthesis of three freshwater microalgae. *Fisheries Science* **60**, 379-384.
- Guillard RL and Lorenzen CJ (1972) Yellow-green algae with chlorophyllide C^{1,2}. *Journal of Phycology* **29**, 729-739.
- Harris GP (1980) The relationship between chlorophyll a fluorescence, diffuse attenuation changes and photosynthesis in natural phytoplankton populations. *Journal of Plankton Research* **2**, 109-127.
- Harris GP (1986) *Phytoplankton Ecology*. Chapman and Hall, London.
- Harris GP, Heaney SI and Talling JF (1979) Physiological and environmental constraints in the ecology of the planktonic dinoflagellate *Ceratium hirundinella*. *Freshwater Biology* **9**, 413-428.

- Hawkins PR and Griffiths DJ (1993) Artificial destratification of a small tropical reservoir: effects upon the phytoplankton. *Hydrobiologia* **43**, 463-504.
- Heathershaw AD (1976) Measurements of turbulence in the Irish Sea benthic boundary layer. In *The Benthic Boundary Layer*. Ed. McCave IN, Plenum Press, New York, pp. 11-32.
- Herath G (1997) Freshwater algal blooms and their control: comparison of the European and Australian experience. *Journal of Environmental Management* **51**, 217-227.
- Holzmann R (1993) Seasonal fluctuations in the diversity and compositional stability of phytoplankton communities in shallow lakes in upper Bavaria. *Hydrobiologia* **249**, 101-109.
- Hondzo MM, Kapur A and Lembi CA (1998) The effect of small-scale fluid motion on the green alga *Scenedesmus quadricauda*. *Hydrobiologia* **364**, 225-235.
- Hondzo MM and Lyn D (1999) Quantified small-scale inhibits the growth of a green alga. *Freshwater Biology* **41**, 51-61.
- Howarth RW, Butler T and Lunde K (1993) Turbulence and planktonic nitrogen fixation: a mesocosm experiment. *Limnology and Oceanography* **38**, 1696-1711.
- Humphries SE and Imberger J (1982) *The influence of the internal structure and dynamics of Burrinjuck Reservoir on phytoplankton blooms*. University of Western Australia, Nedlands, ED 82-023.
- Humphries SE and Lyne VD (1988) Cyanophyte blooms: the role of cell buoyancy. *Limnology and Oceanography* **33**, 79-81.
- Ibelings BW (1996) Changes in photosynthesis in response to combined irradiance and temperature stress in cyanobacterial waterblooms. *Journal of Phycology* **32**, 549-557.
- Ibelings BW and de Windner B (1994) Stress caused by irradiance, temperature and dehydration in cyanobacterial surface water blooms, induced by exposure to a sinusoidal light regime. In *Proceedings of the NATO Workshop*. pp. 311-318.
- Ibelings BW, Kroon BMA and Mur LR (1994) Acclimation of photosystem 2 in a cyanobacterium and a eukaryotic green alga to high and fluctuating photosynthetic photon flux densities, simulating light regimes induced by mixing in lakes. *New Phytologist* **128**, 407-424.
- Ibelings BW and Mur LR (1992) Microprofiles of photosynthesis and oxygen concentration in *Microcystis* scums. *FEMS Microbiology Ecology* **86**, 195-202.
- Imberger J (1985) The diurnal mixed layer. *Limnology and Oceanography* **30**, 737-770.
- Imberger J, Patterson JC, Hebbert B and Loh I (1978) Dynamics of reservoirs of medium size. *Journal of Hydrological Divisions ASCE* **104**, 725-743.
- Imteaz MA and Asaeda T (2000) Artificial mixing of lake water by bubble plume and effects of bubbling operations on algal bloom. *Water Research* **34**, 1919-1929.
- Jacobsen BA and Simonsen P (1993) Disturbance events affecting phytoplankton biomass, composition and species diversity in a shallow, eutrophic, temperate lake. *Hydrobiologia* **249**, 9-14.

- Jochem FJ (1999) Dark survival strategies in marine phytoplankton assessed by cytometric measurement of metabolic activity with fluorescein diacetate. *Marine Biology* **135**, 721-728.
- Jochimsen EM and Carmichael WW (1998) Liver failure and death after exposure to microcystins at a haemodialysis center in Brazil. *New England Journal of Medicine* **338**, 873-878.
- Jones RI (1988) Vertical distribution and diel migration of flagellated phytoplankton in a small humic lake. *Hydrobiologia* **161**, 75-87.
- Juhl AR, Trainer VL and Latz MI (2001) Effect of fluid shear and irradiance on population growth and cellular toxin content of the dinoflagellate *Alexandrium fundyense*. *Limnology and Oceanography* **46**, 758-764.
- Juhl AR, Velazquez V and Latz MI (2000) Effect of growth conditions on flow-induced inhibition of population growth of a red-tide dinoflagellate. *Limnology and Oceanography* **45**, 905-915.
- Jungo E, Visser PM, Stroom J and Mur LR (2001) Artificial mixing to reduce growth of the blue-green alga *Microcystis* in Lake Nieuwe Meer, Amsterdam: an evaluation of 7 years of experience. *Water Science and Technology* **1**, 17-23.
- Kawara O, Li J and Ono Y (2001) A study on influence of current velocity on growth of phytoplankton. *2nd World Water Congress*, International Water Association, Berlin, poster presentation, pp. 127.
- Kiorboe T (1993) Turbulence, phytoplankton cell size, and the structure of pelagic food webs. In *Advances in Marine Biology*. Eds. Blaxter JHS and Southward AJ, Academic Press Limited, London, pp. 2-61.
- Kiorboe T, Andersen KP and Dam HG (1990) Coagulation efficiency and aggregate formation in marine phytoplankton. *Marine Biology* **107**, 235-245.
- Kirke BK (2000) Circulation, destratification, mixing and aeration: why and how? *Water* **27**, 24-30.
- Kit E, Fernando HJS and Brown JA (1995) Experimental examination of Eulerian frequency spectra in zero-mean-shear turbulence. *Physical Fluids* **7**, 1168-1170.
- Kit E, Strang E and Fernando H (1997) Measurements of turbulence near shear-free interfaces. *Journal of Fluid Mechanics* **334**, 293-314.
- Kohler J (1993) Growth, production and losses of phytoplankton in the lowland River Spree. I. Population dynamics. *Journal of Plankton Research* **15**, 335-349.
- Kolber Z and Falkowski PG (1993) Use of active fluorescence to estimate phytoplankton photosynthesis *in situ*. *Limnology and Oceanography* **38**, 1646-1665.
- Kolber Z, Zehr J and Falkowski P (1988) Effects of growth irradiance and nitrogen limitation on photosynthetic energy conversion in photosystem II. *Plant Physiology* **88**, 923-929.
- Kolmogorov AN (1941) The local structure of turbulence in incompressible viscous fluid for very large Reynolds numbers. *Doklady Akademia Nauk SSSR* **30**, 301-305.
- Koseff JR, Holen JK, Monismith SG and Cloern JE (1993) Coupled effects of vertical mixing and benthic grazing on phytoplankton populations in shallow, turbid estuaries. *Journal of Marine Research* **51**, 843-868.

- Krause GH, Weis E (1991) Chlorophyll fluorescence and photosynthesis: the basics. *Annual Review of Plant Physiology and Plant Molecular Biology* **42**, 313-349.
- Kromkamp J and Limbeek M (1993) Effect of short variations in irradiance on light harvesting and photosynthesis of the marine diatom *Skeletonema costatum*: a laboratory study simulating vertical mixing. *Journal of General Microbiology* **139**, 2277-2284.
- Kromkamp J and Walsby AE (1990) A computer model of buoyancy and vertical migration in cyanobacteria. *Journal of Plankton Research* **12**, 191-183.
- Kroon BMA (1992) *Photosynthesis in algal mass cultures*. PhD thesis. University of Amsterdam, Amsterdam.
- Kroon BMA, Latasa M, Ibelings BW and Mur LR (1992) The effect of dynamic light regimes on *Chlorella*. *Hydrobiologia* **238**, 71-78.
- Kucera S (1996) *Effects of small-scale shear forces on N₂ fixing cyanobacteria*. Masters thesis, University of North Carolina, North Carolina.
- La Roche J, Geider RJ, Graziano LM, Murray H and Lewis K (1993) Induction of specific proteins in eukaryotic algae grown under iron-, phosphorus-, or nitrogen-deficient conditions. *Journal of Phycology* **29**, 767-777.
- Lampert W (1987) Further studies on the inhibitory effect of the toxic blue-green *Microcystis aeruginosa* on the filtering rate of zooplankton. *Archiv fur Hydrobiologie* **95**, 207-220.
- Langmuir I (1938) Surface motions of water induced by winds. *Science* **87**, 119-123.
- Langsrud S and Sundheim G (1996) Flow cytometry for rapid assessment of viability after exposure to a quaternary ammonium compound. *Journal of Applied Bacteriology* **81**, 411-418.
- Lazier JRN and Mann KH (1989) Turbulence and the diffusive layers around small organisms. *Deep-Sea Research* **36**, 1721-1733.
- Lebaron P, Catala P and Parthuisot N (1998) Effectiveness of SYTOX green stain for bacterial viability assessment. *Applied Environmental Microbiology* **64**, 2697-2700.
- Legendre L (1981) Hydrodynamic control of marine phytoplankton production: the paradox of stability. In *Ecohydrodynamics*. Ed. Nihoul JCJ, Elsevier Scientific, Amsterdam, pp. 191-208.
- Leszczynska M and Oleszkiewicz JA (1996) Application of the fluorescein diacetate hydrolysis as an acute toxicity test. *Environmental Toxicology* **17**, 79-85.
- Levin SA (1992) The problem of scale and pattern in ecology. *Ecology* **73**, 1943-1967.
- Lewis MR, Cullen JJ and Platt T (1984a) Relationships between vertical mixing and photoadaptation of phytoplankton: similarity criteria. *Marine Ecology Progress Series* **15**, 141-149.
- Lewis MR, Horne EP, Cullen JJ, Oakey NS and Platt T (1984b) Turbulent motions may control phytoplankton photosynthesis in the upper ocean. *Nature* **311**, 49-50.
- Lewis WM (1978) Analysis of succession in a tropical phytoplankton community and a new measure of succession rate. *American Naturalist* **112**, 401-414.

- Lewis DM (2000) Turbulent transport of phytoplankton in artificially destratified reservoirs. *In Proceedings of the CRC for Water Quality and Treatment Second Postgraduate Student Conference*. Ed. CRCWQT, Daylesford, pp. 17-22.
- Lewis DM, Brookes JD, Antenucci JP and Lambert MF (2002) Surface mixing for destratification: simulating the impact. *Water* **29**, 27-29.
- Lewis DM (2003) *Destratification and control of cyanobacterial growth in reservoirs*. PhD thesis, University of Adelaide, Adelaide.
- Lewis DM, Elliot AJ, Brookes JD, Lambert MF, Irish AE and Reynolds CS (*in press*) The effects of artificial mixing and copper sulphate dosing on phytoplankton in a simulated Australian reservoir. *Lakes and Reservoirs: Research and Management* **8**.
- Linden L (2000) *Cell lysis and bloom decline of phytoplankton in the Torrens Lake*. Honours thesis, University of Adelaide, Adelaide.
- Linden L (2003) *Detrital carbon cycling in lentic freshwater ecosystems* (and its relevance to the water industry). PhD seminar, Department of Environmental Biology, University of Adelaide, 3 February 2003.
- Lippemeier S, Hartig P and Colijn F (1999) Direct impact of silicate on the photosynthetic performance of the diatom *Thalassiosira weissflogii* assessed by on- and off-line PAM fluorescence measurements. *Journal of Plankton Research* **21**, 269-283.
- MacIntyre S (1993) Vertical mixing in a shallow, eutrophic lake: possible consequences for the light climate of phytoplankton. *Limnology and Oceanography* **38**, 798-817.
- MacIntyre S and Melack JM (1995) Vertical and horizontal transport in lakes: linking littoral, benthic, and pelagic habitats. *Journal of North American Benthological Society* **14**, 599-615.
- MacIntyre S (1996) Turbulent eddies and their implications for phytoplankton within the euphotic zone of Lake Biwa, Japan. *Japanese Journal of Limnology* **57**, 395-410.
- MacIntyre S (1998) Turbulent mixing and resource supply to phytoplankton. *In Physical Processes in Lakes and Oceans*. Ed. Imberger J, American Geophysical Union, Washington DC, pp. 539-567.
- MacKenzie BR and Leggett WC (1993) Wind-based models for estimating the dissipation rates of turbulent energy in aquatic environments: empirical comparisons. *Marine Ecology Progress Series* **94**, 207-216.
- MacKenzie BR (2001). Senior Research Scientist. Danish Institute for Fisheries and Marine Research, Charlottenlund Castle.
- Maftah A, Huet O, Gallet PF and Ratinaud MH (1994) Flow cytometry's contribution to the measurement of cell functions. *Biology of the Cell* **78**, 85-93.
- Mann KH and Lazier JRN (1991) *Dynamics of Marine Ecosystems: Biological-Physical Interactions in the Oceans*. Blackwell Scientific Publications, Boston.
- Margalef R (1978) Life-forms of phytoplankton as survival alternatives in an unstable environment. *Oceanologica Acta* **1**, 493-509.
- Marmorino GO and Caldwell DR (1978) Temperature finestructure and microstructure observations in a coastal upwelling region during a period of variable winds (Oregon, summer 1974). *Deep-Sea Research* **25**, 1073-1106.

- Marra J (1978) Phytoplankton response to vertical movement in a mixed layer. *Marine Biology* **46**, 203-208.
- Matsato Y, Isao S, Nozomu Y and Yoshiro O (1995) Research on phototactic swimming velocity of the dinoflagellate *Peridinium*. *Japanese Journal of Limnology* **56(20)**, 125-135.
- Matveev V, Matveeva L and Jones G (1994) Study of the ability of *Daphnia carinata* King to control phytoplankton and resist cyanobacterial toxicity: implications for biomanipulation in Australia. *Australian Journal of Marine and Freshwater Research* **45**, 889-904.
- McAuliffe TF and Rosich RS (1990) The triumphs and tribulations of artificial mixing in Australian water bodies. *Water Aug*, 22-23.
- Minier C, Galgani F and Robert JM (1993) *In vivo* characterization of esterase activity in *Calothrix* PCC 7601, *Haslea ostrearia* and *Prorocentrum micans*. *Botanica Marina* **36**, 245-252.
- Mitrovic SM, Bowling LC and Buckney RT (2001) Vertical disentrainment of *Anabaena circinalis* in the turbid, freshwater Darling River, Australia: quantifying potential benefits from buoyancy. *Journal of Plankton Research* **23**, 47-55.
- Mitrovic SM, Oliver RL, Rees C, Bowling LC and Buckney RT (2003) Critical flow velocities for the growth and dominance of *Anabaena circinalis* in some turbid freshwater rivers. *Freshwater Biology* **48**, 164-174.
- Moffat BD and Snell TW (1995) Rapid toxicity assessment using *in vivo* enzyme test for *Brachionus plicatilis* (Rotifera). *Ecotoxicology and Environmental Safety* **30**, 47-53.
- Moisander PH, Hench JL, Kononen K and Paerl HW (2002) Small-scale shear effects on heterocystous cyanobacteria. *Limnology and Oceanography* **47**, 108-119.
- Monismith SG, Imberger J and Morison ML (1990) Convective motions in the sidearm of a small reservoir. *Limnology and Oceanography* **35**, 1676-1702.
- Morgan P and Elliot SL (2002) Mechanical destratification for reservoir management. *Water* **29**, 30-35.
- Morse GK, Lester JN and Perry R (1993) *The economic and environmental impact of phosphate removal from wastewater in the European Community*. Great Britain Centre for European D'Etudes des Polyphosphates.
- Nicholls KH, Kennedy W and Hammett C (1980) A fish kill in Heart Lake, Ontario, associated with the collapse of a massive population of *Ceratium hirundinella* (Dinophyceae). *Freshwater Biology* **10**, 553-561.
- Nicklisch A (1998) Growth and light absorption of some planktonic cyanobacteria, diatoms and Chlorophyceae under simulated natural light fluctuations. *Journal of Plankton Research* **20**, 105-119.
- Nixon, SW (1988) Physical energy inputs and the comparative ecology of lake and marine ecosystems. *Limnology and Oceanography* **36**, 751-760.
- Nyholm N and Kallqvist T (1989) Methods for growth inhibition toxicity tests with freshwater algae. *Environmental Toxicology and Chemistry* **8**, 689-703.
- O'Brien KR, Meyer DL, Waite AM, Ivey GN and Hamilton DP (*in review*). Disaggregation of *Microcystis* colonies under turbulent mixing: laboratory experiments in a grid-stirred tank. Submitted to the *Journal of Plankton Research*.

- Obukhov AM (1941) On the distribution of energy in the spectrum of turbulent flow. *Doklady. Akademia Nauk SSSR* **32(1)**, 22-24.
- Oliver RL (1982) *Factors controlling phytoplankton seasonal succession in Mt Bold Reservoir, South Australia*. PhD thesis, University of Adelaide, Adelaide.
- Oliver RL and Ganf GG (2000) Freshwater blooms. In *The Ecology of Cyanobacteria: Their Diversity in Time and Space*. Eds. Whitton BA and Potts M, Kluwer Academic Publishers, Dordrecht, pp. 150-194.
- Oliver RL and Whittington J (1998) Using measurements of variable chlorophyll-*a* fluorescence to investigate the influence of water movement on the photochemistry of phytoplankton. In *Physical Processes in Lakes and Oceans*. Ed. Imberger J, American Geophysical Union, Washington DC, pp. 517-534.
- Osborn T (1996) The role of turbulent diffusion for copepods with feeding currents. *Journal of Plankton Research* **18**, 185-195.
- Osborn TR (1980) Estimates of the local rate of vertical diffusion from dissipation measurements. *Journal of Physical Oceanography* **10**, 83-89.
- Owens TG (1991) Energy transformation and fluorescence in photosynthesis. In *Particle analysis in oceanography*. Ed. Demers S, Springer-Verlag, Berlin, pp. 101-137.
- Ozmidov RV (1965) On the turbulent exchange in a stably stratified ocean. *Izvestia, Atmospheric and Oceanic Physical Sciences* **1**, 853-860.
- Padisak J (1993) The influence of different disturbance frequencies on the species richness, diversity and equitability of phytoplankton in shallow urban lakes. *Hydrobiologia* **249**, 135-156.
- Paerl HW (1988) Nuisance phytoplankton blooms in coastal, estuarine, and inland waters. *Limnology and Oceanography* **33**, 823-847.
- Paerl HW (2000) Marine plankton. In *The Ecology of Cyanobacteria: Their Diversity in Time and Space*. Eds. Whitton BA and Potts M, Kluwer Academic Publishers, Dordrecht, pp. 140-143.
- Parkhill JP, Maillet G and Cullen JJ (2001) Fluorescence-based maximal quantum yield for PSII as a diagnostic of nutrient stress. *Journal of Phycology* **37**, 517-529.
- Pasciak WJ and Gavis J (1975) Transport limited nutrient uptake rates in *Ditylum brightwellii*. *Limnology and Oceanography* **20**, 604-617.
- Pastorok RA, Ginn TC and Lorenzen MW (1980) Review of aeration/ circulation for lake management. In *Restoration of Lakes and Inland Waters*. US EPA, Washington DC, pp. 124-133.
- Peters F and Marrase C (2000) Effects of turbulence on plankton: an overview of experimental evidence and some theoretical considerations. *Marine Ecology Progress Series* **205**, 291-306.
- Peters F (2001). Senior Research Scientist. Institut de Ciències del Mar, Barcelona.
- Peters F and Redondo JM (1997) Turbulence generation and measurement: application to studies on plankton. *Scientia Marina* **61**, 205-228.
- Pielou EC (1975) *Ecological Diversity*. Wiley and Sons Inc., New York.

- Plueddemann AJ, Smith JA, Farmer DM, Weller RA, Crawford WA, Pinkel R, Vagle S and Gnanadesikan A (1996) Structure and variability of Langmuir circulation during the Surface Waves Processes Program. *Journal of Geophysical Research* **101**, 3525-3543.
- Pollinger U and Zemel E (1981) *In situ* and experimental evidence of the influence of turbulence on cell division processes of *Peridinium cinctum* forma *westii* (Lemm.) Lefevre. *British Phycology Journal* **16**, 281-287.
- Premazzi G, Buonaccorsi G and Zilio P (1989) Flow cytometry for algal studies. *Water Research* **23**, 431-442.
- Prezelin BB, Tilzer MM, Schofield O and Haese C (1991) The control of the production process of phytoplankton by the physical structure of the aquatic environment with special reference to its optical properties. *Aquatic Sciences* **53**, 136-185.
- Reckermann M and Colijn F (1998) Aquatic flow cytometry: achievements and prospects. In *Proceedings of the Aquatic Flow Cytometry: Achievements and Prospects*. Eds. Reckermann M and Colijn F, Busum, Germany. *Scientia Marina*.
- Regel RH (1997) *The response of Microcystis aeruginosa (Cyanophyceae) to heavy metals and stormwater*. Honours thesis, University of Adelaide, Adelaide.
- Regel RH, Brookes JD, Lewis D, Ganf GG and Burch MD (2001) Time scales of 'events' and threats to water quality within lakes and reservoirs. *2nd World Water Congress*, International Water Association, Berlin, poster presentation, pp. 139.
- Regel RH, Ferris JM, Ganf GG and Brookes JD (2002) Algal esterase activity as a biomeasure of environmental degradation in a freshwater creek. *Aquatic Toxicology* **59**, 209-223.
- Reynolds CS and Walsby AE (1975) Water Blooms. *Biological Reviews* **50**, 437-481.
- Reynolds CS (1980) Phytoplankton assemblages and their periodicity in stratifying lake systems. *Holarctic Ecology* **3**, 141-159.
- Reynolds CS (1982) Phytoplankton periodicity: its motivation, mechanism and manipulation. *Annual Report Freshwater Biological Association* **50**, 60-75.
- Reynolds CS, Wiseman SW, Godfrey BM and Butterwick C (1983) Some effects of artificial mixing on the dynamics of phytoplankton populations in large limnetic enclosures. *Journal of Plankton Research* **5**, 203-234.
- Reynolds CS (1984a) *The Ecology of Freshwater Phytoplankton*. Cambridge University Press, Cambridge.
- Reynolds CS (1984b) Phytoplankton periodicity: the interactions of form, function and environmental variability. *Freshwater Biology* **14**, 111-142.
- Reynolds CS and Reynolds JB (1985) The atypical seasonality of phytoplankton in Crose Mere, 1972: an independent test of the hypothesis that variability in the physical environment regulates community dynamics and structure. *British Phycology Journal* **20**, 227-242.
- Reynolds CS (1986) Experimental manipulations of the phytoplankton periodicity in large limnetic enclosures in Blelham Tarn, English Lake District. *Hydrobiologia* **138**, 43-64.
- Reynolds CS (1987) Community organisation in the freshwater phytoplankton. In *Organisation of Communities, Past and Present*. Eds. Gee M and Giller PS, Blackwell Scientific Publications, Oxford, pp. 297-325.

- Reynolds CS (1988a) Functional morphology and the adaptive strategies of freshwater phytoplankton. *In Growth and Reproductive Strategies of Freshwater Phytoplankton*. Ed. Sandgren CD, Cambridge University Press, New York, pp. 388-433.
- Reynolds CS (1988b) Potomoplankton: paradigms, paradoxes and prognoses. *In Algae and the Aquatic Environment*. Ed. Round FE, Biopress, Bristol, pp. 285-311.
- Reynolds CS (1988c) The theory of ecological succession applied to the freshwater phytoplankton. *Verhandlungen Internationale Vereinigung fur Theoretische und Angewandte Limnologie* **23**, 683-691.
- Reynolds CS (1988d) The concept of ecological succession applied to seasonal periodicity of freshwater phytoplankton. *Verhandlungen Internationale Vereinigung fur Theoretische und Angewandte Limnologie*, **23**, 683-691.
- Reynolds CS and West JR (1988) *Stratification in the Severn Estuary - Physical Aspects and Biological Consequences*. Report to Severn Tidal Power Group, Freshwater Biological Association, Ambleside.
- Reynolds CS (1989) Physical determinants of phytoplankton succession. *In Plankton Ecology*. Ed. Sommer U, Brock-Springer, Madison, pp. 9-56.
- Reynolds CS (1993) Scales of disturbance and their role in plankton ecology. *Hydrobiologia* **249**, 151-171.
- Reynolds CS, Padiak J and Sommer U (1993) Intermediate disturbance hypothesis in the ecology of phytoplankton and the maintenance of species diversity: a synthesis. *Hydrobiologia* **249**, 183-188.
- Reynolds CS (1994a) The role of fluid motion in the dynamics of phytoplankton in lakes and rivers. *In Aquatic Ecology: Scale, Pattern and Processes*. Eds. Giller PS, Hildrew AG and Raffaelli DG, Blackwell Scientific Publications, Oxford, pp. 141-187.
- Reynolds CS (1994b) The long, the short and the stalled: on the attributes of phytoplankton selected by physical mixing in lakes and rivers. *Hydrobiologia* **289**, 9-21.
- Reynolds CS (1997) *Vegetation Processes in the Pelagic: A Model for Ecosystem Theory*. Ecology Institute, Oldendorf/ Luhe.
- Reynolds CS (1998) Plants in motion: physical-biological interaction in the plankton. *In Physical Processes in Lakes and Oceans*. Ed. Imberger J, American Geophysical Union, Washington DC, pp. 535-560.
- Richardson LF (1922) *Weather Prediction by Numerical Process*. Cambridge University Press, Cambridge.
- Richmond A and Vonshak A (1978) *Spirulina* culture in Israel. *Archives Hydrobiolgy* **11**, 274-280.
- Rothschild BJ and Osborn TR (1988) Small-scale turbulence and plankton contact rates. *Journal of Plankton Research* **10**, 465-474.
- Rotman B and Papermaster BW (1966) Membrane properties of living mammalian cells as studied by enzymatic hydrolysis of fluorogenic esters. *Proceedings of National Academy of Sciences* **55**, 134-141.
- Round FE (1971) The growth and succession of algal populations in freshwaters. *Mitteilungen Internationale Vereinigung fur Theoretische und Angewandte Limnologie* **19**, 70-99.

- Rybak M (1985) Some ecological effects of artificial circulation on the phytoplankton. *Hydrobiologia* **122**, 89-96.
- Sabater S and Munoz I (1990) Successional dynamics of the phytoplankton in the lower part of the river Ebro. *Journal of Plankton Research* **12**, 573-592.
- Sanford LP (1997) Turbulent mixing in experimental ecosystem studies. *Marine Ecology Progress Series* **161**, 265-293.
- Sas H (1989) *Lake Restoration via Reduction of Nutrient Loading: Expectations, Experiences, Extrapolations*. Academia Verlag Richarz, St. Augustin.
- Savidge G (1981) Studies of the effects of small-scale turbulence on phytoplankton. *Journal of Marine Biological Association, U.K.* **61**, 477-488.
- Schreiber U, Bilger W and Schliwa U (1986) Continuous recording of photochemical and non-photochemical quenching with a new type of modulation fluorometer. *Photosynthesis Research* **10**, 51-62.
- Schreiber U, Neubauer C and Schliwa U (1994) PAM fluorometer based on medium-frequency pulsed Xe-flash measuring light: A highly sensitive new tool in basic and applied photosynthesis research. *Photosynthesis Research* **36**, 65-72.
- Schubert H, Matthijs HCP, Mur LR and Schiewer U (1995) Blooming of cyanobacteria in turbulent water with steep light gradients: the effect of intermittent light and dark periods on the oxygen evolution capacity of *Synechocystis* sp. PCC 6803. *FEMS Microbiology Ecology* **18**, 237-245.
- Selvin R, Reguera B, Bravo I and Yentsch CM (1989) Use of fluorescein diacetate (FDA) as a single-cell probe of metabolic activity in dinoflagellate cultures. *Biological Oceanography* **6**, 505-511.
- Shannon CE (1948) A mathematical theory of communities. *Bell Systems Technology Journal* **27**, 623-656.
- Shay TJ and Gregg MC (1986) Convectively driven mixing in the upper ocean. *Journal of Physical Oceanography* **16**, 1777-1798.
- Sherman BS and Webster IT (1994) A model for the light-limited growth of buoyant phytoplankton in a shallow, turbid water body. *Australian Journal of Marine and Freshwater Research* **45**, 847-862.
- Simmons J (1998) Algal control and destratification at Hanningford Reservoir. *Water Science and Technology* **37**, 309-316.
- Simpson JH, Crawford WR, Rippeth TR, Campbell AR and Cheok JVS (1996) The vertical structure of turbulent dissipation in shelf seas. *Journal of Physical Oceanography* **26**, 1759-1590.
- Smayda TJ (1997) Harmful algal blooms: their ecophysiology and general relevance to phytoplankton blooms in the sea. *Limnology and Oceanography* **42**, 1137-1153.
- Sommer U (1981) The role of r- and K-selection in the succession of phytoplankton in Lake Constance. *Acta Oecologia* **2**, 327-342.
- Sommer U (1993) Disturbance-diversity relationships in two lakes of similar nutrient chemistry but contrasting disturbance regimes. *Hydrobiologia* **249**, 59-65.

- Sommer U, Padisak J, Reynolds CS and Juhasz-Nagy (1993) Hutchinson's heritage: the diversity-disturbance relationship in phytoplankton. *Hydrobiologia* **249**, 1-7.
- Sommer U (1995) An experimental test of the intermediate disturbance hypothesis using cultures of marine phytoplankton. *Limnology and Oceanography* **40**, 1271-1277.
- Spigel RH and Imberger J (1987) Mixing processes relevant to phytoplankton dynamics in lakes. *New Zealand Journal of Marine and Freshwater Research* **21**, 361-377.
- Steinberg C (1983) Effects of artificial destratification on the phytoplankton populations in a small lake. *Journal of Plankton Research* **5**, 855-864.
- Steinberg C and Zimmerman GM (1988) Intermittent destratification: a therapy against cyanobacteria in lakes. *Environmental Technology Letters* **9**, 337-350.
- Steinberg C and Tille-Backhaus R (1990) Re-occurrence of filamentous planktonic cyanobacteria during permanent artificial destratification. *Journal of Plankton Research* **12**, 661-664.
- Stiansen JE (2001) *Small-scale turbulence in relation to plankton ecology; sources, measurements and analysis - with focus on energy dissipation rates and turbulent scales*. PhD thesis, University of Bergen, Bergen.
- Stiansen JE and Sundby S (2001) Improved methods for generating and estimating turbulence in tanks suitable for fish larvae experiments. *Scientia Marina* **65**, 151-167.
- Straskraba M (1998) Coupling hydrobiology and hydrodynamics: lakes and reservoirs. In *Physical Processes in Lakes and Oceans*. Ed. Imberger J, American Geophysical Union, Washington DC, pp. 623-644.
- Sullivan JM and Swift E (2003) Effects of small-scale turbulence on net growth rate and size of ten species of marine dinoflagellates. *Journal of Phycology* **39**, 83-94.
- Talling JF and Driver (1963) Some problems in the estimation of chlorophyll *a* in phytoplankton. In *Proceedings of the Conference on Primary Productivity Measurements, Marine and Fresh-water*. Ed. Do TI, U.S. Atomic Energy Commission, pp. 142-146.
- Talling JF (1971) The underwater light climate as a controlling factor in the production ecology of freshwater phytoplankton. *Mitteilungen Internationale Vereinigung für Theoretische und Angewandte Limnologie* **19**, 214-243.
- Taylor AH and Stephens JA (1993) Diurnal variations of convective mixing and the spring bloom of phytoplankton. *Deep-Sea Research* **40**, 389-408.
- Teixera MGLC, Costa MCN, Carvalho VLP, Pereira MS and Hage E (1993) *Bulletin of the PAM American Health Organization* **27**, 244-253.
- Tennekes H and Lumley JL (1972) *A First Course in Turbulence*. MIT Press, Cambridge, MA.
- Terray EA, Donelan MA, Agrawal YC, Drennan WM, Kahma KK, Williams AJ, Hwang PA, and Kitaigorodskii SA (1996) Estimates of kinetic energy dissipation under breaking waves. *Journal Physical Oceanography* **26**, 792-807.
- Thomas WH and Gibson CH (1990) Effects of small-scale turbulence on microalgae. *Journal of Applied Phycology* **2**, 71-77.
- Thomas WH, Vernet M and Gibson CH (1995) Effects of small-scale turbulence on photosynthesis, pigmentation, cell division and cell size in the marine dinoflagellate *Gonyaulax polyedra* (Dinophyceae). *Journal of Phycology* **31**, 50-59.

- Thomas WH, Tynan CT and Gibson CH (1997) Turbulence-phytoplankton interrelationships. In *Progress in Phycological Research*. Eds. Round FE and Chapman DJ, Biopress, Bristol, pp. 284-318.
- Thompson FM and Turner JS (1975) Mixing across an interface due to turbulence generated by an oscillating grid. *Journal of Fluid Mechanics* **67**, 349-368.
- Tilman D (1996) In *Limnology*. Kalf J, Prentice Hall Inc., New Jersey (2002), pp, 312.
- Toetz DW (1981) Effects of whole lake mixing on water quality and phytoplankton. *Water Research* **15**, 1205-1210.
- Turner JS (1973) *Buoyancy Effects in Fluids*. Cambridge University Press, Cambridge.
- Tuttle RC and Loeblich AR (1975) An optimal growth medium for the dinoflagellate *Cryptothecodinium cohnii*. *Phycologia* **14**, 1-8.
- Tynan CT (1993) *Effects of small-scale turbulence on dinoflagellates*. PhD thesis, University of California, California.
- Van Bleijswijk JDL, Kempers RS, Wal PVD, Westbroek P, Egge JK and Lukk T (1994) Standing stocks of PIC, POC, PON and *Emiliania huxleyi* coccospheres and liths in sea water enclosures with different phosphate loadings. *Sarsia* **79**, 307-317.
- Van Kooten O and Snel JFH (1990) The use of chlorophyll fluorescence nomenclature in plant stress physiology. *Photosynthesis Research* **25**, 147-150.
- Veldhuis MJW, Cucci TL and Sieracki ME (1997) Cellular DNA content of marine phytoplankton using two new fluorochromes: taxonomic and ecological implications. *Journal of Phycology* **33**, 527-541.
- Veldhuis MJW and Kraay GW (2000) Application of flow cytometry in marine phytoplankton research: current applications and future perspective. *Scientia Marina* **64**, 121-134.
- Veldhuis MJW, Kraay GW and Timmermans KR (2001) Cell death in phytoplankton: correlation between changes in membrane permeability, photosynthetic activity, pigmentation and growth. *European Journal of Phycology* **36**, 167-177.
- Veron F and Melville WK (1999) Pulse-to-pulse coherent doppler measurements of waves and turbulence. *Journal of Atmospheric and Oceanic Technology* **16**, 1580-1593.
- Villareal TA and Morton SL (2002) Use of cell-specific PAM-fluorometry to characterise host shading in the epiphytic dinoflagellate *Gambierdiscus toxicus*. *Marine Ecology* **23**, 127-140.
- Villarino ML, Figueias FG, Jones KJ, Alvarez-Salgado XA, Richard J and Edwards A (1995) Evidence of *in situ* diel vertical migration of a red-tide microplankton species in Ria de Vigo (NW Spain). *Marine Biology* **123**, 607-617.
- Vincent WF, Neale PJ and Richerson PJ (1984) Photoinhibition: algal responses to bright light during diel stratification and mixing in a tropical alpine lake. *Journal of Phycology* **20**, 201-211.
- Visser PM (1995) *Growth and vertical movement of the cyanobacterium Microcystis in stable and artificially mixed water columns*. PhD thesis, University of Amsterdam, Amsterdam.

- Visser PM, Ibelings BW, Van der Veer B, Koedods J and Mur LR (1996) Artificial mixing prevents nuisance blooms of the cyanobacterium *Microcystis* in Lake Nieuwe Meer, The Netherlands. *Freshwater Biology* **36**, 435-450.
- Wahl TL (2001) *WinADV*, US Bureau of Reclamation.
- Wallace BB and Hamilton DP (1999) The effects of variations in irradiance on buoyancy regulation in *Microcystis aeruginosa*. *Limnology and Oceanography* **44**, 273-281.
depth in a water column. *New Phytologist* **136**, 189-209.
- Walsby AE, Kinsman R, Ibelings BW and Reynolds CS (1991) Highly buoyant colonies of the cyanobacterium *Anabaena lemmermanii* form persistent surface waterblooms. *Archiv fur Hydrobiologie* **121**, 261-280.
- Walsby AE (1994) Gas vesicles. *Microbiological Reviews* **58**, 94-144.
- Walsby AE (1997) Numerical simulation of phytoplankton photosynthesis through time and depth in a water column. *New Phytologist* **136**, 189-209.
- Wells MG and Sherman BS (2001) Stratification produced by surface cooling in lakes with significant shallow regions. *Limnology and Oceanography* **46**, 1747-1759.
- White AW (1976) Growth inhibition caused by turbulence in the toxic marine dinoflagellate *Gonyaulax excavata*. *Journal of Fisheries Research Board Canada* **33**, 2598-2602.
- White PS and Pickett STA (1985) Natural disturbance and patch dynamics: an introduction. *In The Ecology of Natural Disturbance and Patch Dynamics*. Eds. Pickett STA and White PS, Academic Press, Orlando, pp. 3-13.
- Whittington J, Sherman B, Green D and Oliver RL (2000) Growth of *Ceratium hirundinella* in a sub-tropical Australian reservoir: the role of vertical migration. *Journal of Plankton Research* **22**, 1025-1045.
- Williams SC, Hong Y, Danavall DCA, Howard-Jones MH, Gibson D, Frischer ME and Verity PG (1998) Distinguishing between living and nonliving bacteria: evaluation of the vital stain propidium iodide and its combined use with molecular probes in aquatic samples. *Journal of Microbiological Methods* **32**, 225-236.
- Xu C, Auger J and Govindjee (1990) Chlorophyll *a* fluorescence measurements of isolated spinach thylakoids obtained by using single-laser-based flow cytometry. *Cytometry* **11**, 349-358.
- Xue HB and Sigg L (1990) Binding of Cu(II) to algae in a metal buffer. *Water Research* **24**, 1129-1136.
- Yamazaki H, Osborn TR and Squires KD (1991) Direct numerical simulation of planktonic contact in turbulent flow. *Journal of Plankton Research* **13**, 629-643.
- Yarmolinsky MB (1995) Programmed cell death in bacterial populations. *Science* **267**, 836-837.
- Yentsch CM, Campbell JW and Gucci TL (1988) Is only a fraction of natural phytoplankton populations metabolically active? Evidence via the FDA staining protocol. *Transactions of the American Geophysical Union, EOS*, **69**, 1133.
- Yentsch CM and Horan PK (1983) Flow cytometry and cell sorting: A technique for analysis and sorting of aquatic particles. *Limnology and Oceanography* **28**, 1275-1280.

- Zevenboom W and Mur LR (1984) Growth and photosynthetic response of the cyanobacterium *Microcystis aeruginosa* in relation to photoperiodicity and irradiance. *Archive Microbiology* **139**, 232-239.

Appendix 1

Turbulent kinetic energy dissipation rate Fortran program

```
C /Variables\
C alpha = alpha from Kit et al. (1995) -0.5 or Sanford (1997)- 1.5.
C dt = sampling period.
C E(w) = Eulerian frequency spectrum.
C Fr(k) = real part of Fourier transform.
C Fi(k) = imaginary part of Fourier tranform.
C fN = Nyquist frequency.
C KEDR = kinetic energy dissipation rate.
C Nmax = maximum number of velocity data points.
C Nu = number of velocity data points.
C pi = 3.14159265358979323846.
C R(i) = ith autocorrelation.
C U(i) = ith velocity.
C Um(i) = mean velocity.
C Urms = root mean square velocity.
C w0 = fundamental angular frequency.
C
C /Input File\
C dt Nu
C U(1)
C U(2)
C .
C .
C .
C U(Nu)
C
C /Program TurbSpec\
=====
Program TurbSpec
implicit none

integer Nmax
parameter (Nmax=5000)

integer i,k,n,Nu,Ei,Uwin
character*20 Finp,Fout
real sum,dt,angle,pi,w0,fN,f,Um(Nmax),Urms
real logw,alpha,Emax,Ec,Etrans,KEDR,log10
real U(Nmax),R(Nmax),Fr(Nmax),Fi(Nmax),E(Nmax)

print *, 'Turbulence characteristics program:'
Uwin=50

!Read in velocity data from file:
print *, 'Input filename?'
read(*,*) Finp
open(UNIT=1,FILE=Finp,STATUS='OLD')
read(1,*) dt,Nu
if (Nu.GT.Nmax) then
print *, 'Too many data points, increase Nmax.'
stop
endif
```

```

do i=1,Nu
  read(1,*) U(i)
enddo
close(1)

!Calculate mean velocity:
do i=(1+Uwin),(Nu-Uwin)
  sum=0.0
  do k=-Uwin,Uwin
    sum=sum+U(i+k)
  enddo
  Um(i)=sum/(2.0*Uwin+1.0)
  enddo
do i=1,Uwin
  Um(i)=Um(Uwin+1)
  Um(Nu-i+1)=Um(Nu-Uwin)
enddo

!Calculate RMS velocity:
sum=0.0
do i=1,Nu
  sum=sum+(Um(i)-U(i))**2.0
enddo
Urms=sqrt(sum/Nu)

!Perform discrete autocorrelation:
do k=1,Nu
  sum=0.0
  do i=1,(Nu-k)
    sum=sum+(U(i)-Um(i))*(U(i+k)-Um(i+k))
  enddo
  R(k)=sum/(Urms*Urms*Nu)
enddo

!Calculate useful quantities:
pi=acos(-1.0)
w0=2.0*pi/Nu
fN=1/(2.0*dt)

!Perform discrete Fourier transform:
do k=0,(Nu-1)
  Fr(k+1)=0.0
  Fi(k+1)=0.0
  do n=0,(Nu-1)
    angle=k*w0*n
    Fr(k+1)=Fr(k+1)+R(n+1)*cos(angle)/Nu
    Fi(k+1)=Fi(k+1)-R(n+1)*sin(angle)/Nu
  enddo
enddo

!Calculate spectral energy:
do i=1,Nu
  E(i)=Fr(i)**2.0+Fi(i)**2.0
enddo

!Find first spectral energy point on -5/3 line.
Emax=-100.0
i=0
f=0.0

```

```

dowhile (f.LT.fN)
i=i+1
f=i*fN/(0.5*Nu)
logw=log10(2.0*pi*f)
Etrans=log10(E(i+1))+5.0/3.0*logw
if (Etrans.GT.Emax) then
  Ei=i
  Emax=Etrans
endif
enddo

!Calculate the kinetic energy dissipation rate:
Ec=log10(E(Ei+1))+5.0/3.0*log10(2.0*pi*Ei/(Nu*dt))
alpha=0.8
KEDR=1.0/Urms*((10.0**Ec)/alpha)**1.5

!Print out results:
print *, 'Output filename?'
read(*,*) Fout
open(UNIT=2,FILE=Fout,STATUS='UNKNOWN')
write(2,*) 'Turbulence Characteristics:'
write(2,*)
write(2,*) 'Sampling period =',dt,' (s)'
write(2,*) 'Number of velocity data points =',Nu
write(2,*) 'RMS velocity =',Urms,' (m/s)'
write(2,*) 'Kinetic energy dissipation rate =',KEDR,' (m2/s3)'
write(2,*)
write(2,*) 'Velocity data:'
write(2,*) 't U(t) Um(t) U'(t) R(t)'
write(2,*) '(s) (m/s) (m/s) (m/s) (-)'
do i=0,(N-1)
  write(2,*) i*dt,U(i+1),Um(i+1),(U(i+1)-Um(i+1)),R(i+1)
enddo
write(2,*)
write(2,*) 'Turbulence spectrum data:'
write(2,*) 'f w Fr(w) Fi(w) E(w)'
write(2,*) '(Hz) (rad/s) (-) (-) (m2/s)'
i=-1
f=0.0
dowhile (f.LT.fN)
i=i+1
f=i*fN/(0.5*Nu)
write(2,*) f,(2.0*pi*f),Fr(i+1),Fi(i+1),E(i+1)
enddo
close(2)

print *, 'Program Completed.'
End

```

C

C /Function Log10\

C Calculate the base 10 logarithm.

C

```

Function log10(x)
implicit none
real x,log10
log10=log(x)/log(10.0)
return
End

```

C